2006

A micromechanical approach for predicting the complex shear modulus and accumulated shear strain of asphalt mixtures from binder and mastics

Cristian Druta
Louisiana State University and Agricultural and Mechanical College

A MICROMECHANICAL APPROACH FOR PREDICTING THE COMPLEX SHEAR MODULUS AND ACCUMULATED SHEAR STRAIN OF ASPHALT MIXTURES FROM BINDER AND MASTICS

A Dissertation

Submitted to the Graduate Faculty of the
Louisiana State University and
Agricultural and Mechanical College
in partial fulfillment of the
requirements for the degree of
Doctor of Philosophy

in

The Interdepartmental Program in Engineering Sciences

by

Cristian Druta
B.S., Polytechnic University of Bucharest, 1995
M.S., Louisiana State University, 2003
December 2006

ACKNOWLEDGMENTS

I am indebted to many people for their kindness and effort on my behalf. Foremost among them is Dr. Linbing Wang, my advisor, whom I wish to thank for his kind advice and patient mentorship. The constancy of his support has allowed me to fulfill my objectives in graduate school, and without him, this program would not have been accomplished.

It is also a pleasure to express my gratitude to the individuals whose guidance, support and encouragement assisted the development and completion of this dissertation. In this respect, I would like to thank Dr. Voyiadjis, my co-advisor and co-chair, for being in my doctoral committee and for his expert guidance.

Extended appreciation goes to the professors who served on my doctoral committee, Dr. Suresh Moorthy, Dr. Su-Seng Pang, and Dr. Darrell Henry, whose support helped me in finishing my doctoral program.

Special thanks to Dr. John B. Metcalf for his encouragement, guidance and patience over the past five years, and the assumption that I would do fine, which helped me tremendously in completing this dissertation.

I would also like to express my gratitude to all the people from Louisiana Transportation Research Center who helped me with my research: Dr. Louay Mohammad, Chris Abadie, Willie Gueho, Amar Raghavendra, Codrin Daranga, and Keith Beard. I have learned a tremendous amount about research from their experience.

Finally, I would like to thank my parents and my sister for their love and support which have always encouraged me to pursue. This work was possible because of their dedication and strong commitment to our education and because of their high expectations and belief in me to achieve this goal.

TABLE OF CONTENTS

Acknowledgments ---------- ii

List of Tables ---------- vi

List of Figures ---------- vii

List of Abbreviations ---------- xii

Abstract ---------- xiii

CHAPTER 1. INTRODUCTION ---------- 1
1.1 Flexible Pavement Composition and Structure ---------- 1
1.2 Asphalt Binders and Mastics ---------- 3
1.3 Distresses in Asphalt Pavements - ---------- 6
1.4 Strategic Highway Research Program (SHRP) ---------- 8
1.5 Dynamic Shear Complex Modulus (G*) - ---------- 10
1.6 Problem Statement ---------- 10
1.7 Objectives of Study ---------- 13
1.8 Organization of Dissertation ---------- 14

CHAPTER 2. LITERATURE REVIEW ---------- 17
2.1 Asphalt Binders and Mastics Characterization ---------- 17
2.2 Effect of Mineral Fillers on Asphalt Binders and Mixtures ---------- 28
2.3 Asphalt Mixtures Characterization ---------- 34

CHAPTER 3. ASPHALT BINDER AND MASTICS EXPERIMENTAL PROGRAM ------- 46
3.1 Usage of Asphalt Binders in the United States ---------- 46
3.2 Performance Graded (PG) Binder Specifications ---------- 47
3.3 Asphalt Binder Used in the Study (PG64-22) ---------- 48
3.4 Asphalt Rheology ---------- 50
3.5 Asphalt Modifiers (Mineral Fillers) ---------- 52
3.6 Asphalt Mastics ---------- 54
3.7 Dynamic Shear Rheometer (DSR) ---------- 54
3.7.1 General Presentation ---------- 54
3.7.2 Summary of Method ---------- 55
3.7.3 Testing Equipment ---------- 56
3.7.4 Asphalt Binder and Mastic Specimen Preparation ---------- 59
3.7.5 Testing Procedure ---------- 60
3.7.6 DSR Analysis Theory ---------- 62
3.8 Dynamic Shear Rheometer (DSR) Testing ---------- 68
3.8.1 DSR Oscillation at Single Frequency - ---------- 69
3.8.2 DSR Shear Frequency Sweep at Constant Stress ---------- 70
3.8.3 Repeated Shear Creep Loading and Recovery Testing ---------- 72

CHAPTER 4. SUMMARY AND ANALISYS OF DSR TEST RESULTS ---------- 76
4.1 DSR Oscillation at Single Frequency ---------- 76
4.2 DSR Frequency Sweep Oscillation Test Results ---------- 82
4.3 Repeated Shear Creep Loading and Recovery Testing ---------- 93
4.4 Estimation of Complex Shear Modulus G* Using the Hirsch Model ---------- 102

CHAPTER 5. LABORATORY SUPERPAVE ASPHALT MIXTURES DESIGN ---------- 109
5.1 Asphalt Mixture or Hot Mix Asphalt (HMA) ---------- 109
5.2 Asphalt Binder ---------- 110
5.3 Mineral Aggregate ---------- 110
5.4 Aggregate Gradation ---------- 112
5.5 Asphalt Mixture Behavior ---------- 114
5.6 Wheel Path Rutting ---------- 116
5.7 Asphalt Mixture Volumetrics ---------- 117

CHAPTER 6. ASPHALT CONCRETE (HMA) SPECIMEN PREPARATION ---------- 122
6.1 Procedure Overview ---------- 122
6.2 Superpave Gyratory Compactor ---------- 124
6.3 Specimens Compaction and Cutting ---------- 128
6.4 Analyzing Compacted Paving Mixtures ---------- 130
6.4.1 Maximum Specific Gravity of Compacted Mixtures G_{mm} ---------- 131
6.4.2 Bulk Specific Gravity of Compacted Mixtures G_{mb} ---------- 132
6.4.3 Percent VMA in Compacted Mixtures ---------- 132
6.4.4 Bulk Specific Gravity of Aggregate (G_{sb}) ---------- 133
6.4.5 Percent Air Voids in Compacted Mixture (V_a) ---------- 134
6.4.6 Percent VFA in Compacted Mixtures ---------- 134

CHAPTER 7. ASPHALT MIXTURES TESTING METHODOLOGY ---------- 135
7.1 Specimen Preparation ---------- 135
7.2 Superpave Shear Tester (SST) ---------- 136
7.3 Tests Performed with the Superpave Shear Tester (SST) ---------- 139
7.3.1 SST Frequency Sweep at Constant Height (FSCH) ---------- 139
7.3.2 SST Repeated Shear at Constant Height (RSCH) ---------- 145

CHAPTER 8. SUMMARY AND ANALISYS OF SST TEST RESULTS ---------- 150
8.1 Shear Frequency Sweep at Constant Height (FSCH) Tests Results ---------- 150
8.2 Repeated Shear Loading at Constant Height (RSCH) Tests Results ---------- 155
8.3 Estimation of Complex Shear Modulus G* Using the Hirsch Model ---------- 157
8.4 Estimation of Permanent Shear Strain in Asphalt Mixtures using Shenoy Equation 158

CHAPTER 9. CONCLUSIONS AND RECOMMENDATIONS ---------- 161
9.1 Research Summary ---------- 161
9.2 Conclusions ---------- 162
9.3 Recommendations ---------- 164

REFERENCES ---------- 165

APPENDIX
A: DSR SINGLE FREQUENCY OSCILLATION TEST RESULTS ---------- 171

B: DSR FREQUENCY SWEEP OSCILLATION AT CONSTANT SHEAR STRESS TEST RESULTS ---------- 177

C: PHASE ANGLE DEPENDENCY ON LOADING FREQUENCY ---------- 193

D: DSR MASTER CURVES ---------- 198

E: DSR REPEATED SHEAR CREEP LOADING AND RECOVERY TEST RESULTS ---------- 202

F: PREDICTION OF COMPLEX SHEAR MODULUS G* USING THE HIRSCH MODEL ---------- 210

G: DEFINITIONS OF VOLUMETRIC COMPONENTS OF ASPHALT MIXTURES - 216

H: SST FREQUENCY SWEEP AT CONSTANT HEIGHT (FSCH) TEST RESULTS - 221

J: SST REPEATED SHEAR AT CONSTANT HEIGHT (RSCH) TEST RESULTS ---- 231

VITA ---------- 236

LIST OF TABLES

Table 3.1 Summary of AASHTO MP1 Requirements ---------- 49

Table 3.2. Properties of fillers ---------- 53

Table 4.1 Average values for the rut-controlling term ($|G^*|/\sin\delta$) ---------- 80

Table 4.2 Shift factors for asphalt binder and mastics ---------- 89

Table 4.3 Maximum accumulated shear strain (γ_{acc}) values for limestone mastics ---------- 95

Table 5.1 Properties of granite ---------- 111

Table 5.2 Granite aggregate gradation for HMA (6% air voids) mix design ---------- 113

Table 5.3 Superpave asphalt mix design requirements ---------- 120

Table 6.1 Number of gyrations function of design ESALs ---------- 130

Table 6.2 Data for sample of asphalt mixture ---------- 133

Table 7.1 Testing schedule for frequency sweep at constant height ---------- 141

Table 7.2 Data collection during an RSCH test ---------- 148

Table 8.1 Maximum accumulated shear strain (γ_{acc}) values for asphalt mixtures ---------- 157

LIST OF FIGURES

Figure 1.1 Typical flexible pavement structure ---------- 1

Figure 1.2 Asphalt concrete (Hot Mix Asphalt) structure ---------- 2

Figure 1.3 Distribution of load stress in flexible pavement ---------- 3

Figure 1.4 Asphalt binder nomenclature ---------- 4

Figure 1.5 Rutting in asphalt pavement ---------- 7

Figure 1.6 Superpave asphalt testing methods and equipment ---------- 10

Figure 2.1 Creep compliance curves for all aging levels ---------- 18

Figure 2.2 Relationship between mixture stiffness and binder stiffness ---------- 19

Figure 2.3 Durability potential of mixtures versus filler activity at different periods of immersion, using resilient modulus criterion ---------- 29

Figure 3.1 Mechanical responses of elastic, viscous, and viscoelastic materials ---------- 51

Figure 3.2 Gradation of the mineral fillers ---------- 53

Figure 3.3 Schematic configuration and loading mode of DSR ---------- 56

Figure 3.4 Automated Dynamic Shear Rheometer (ADSR) ---------- 57

Figure 3.5 Preparing asphalt specimens for the DSR testing ---------- 59

Figure 3.6 Asphalt binder sample placed on the fixed platen of the ADSR ---------- 60

Figure 3.7 Trimmed asphalt binder specimen ---------- 61

Figure 3.8 Proper asphalt binder bulge between the platens ---------- 62

Figure 3.9 Dynamic load induced by the DSR ---------- 63

Figure 3.10 Complete cycle of the DSR “spindle” ---------- 63

Figure 3.11 Elastic response of the asphalt binder ($\delta = 0$ deg) ---------- 65

Figure 3.12 Viscous response of the asphalt binder ($\delta = 90$ deg) ---------- 65

Figure 3.13 Viscoelastic behavior of the asphalt binder ($0 < \delta < 90°$) ---------- 66

Figure 3.14 Relationship between shear complex modulus (G*) and phase angle (δ) ---------- 67

Figure 3.15 Linear viscoelastic region of asphalt binder ---------- 69

Figure 3.16 Applying strains or stresses in dynamic testing ---------- 70

Figure 3.17 Stepwise increase in frequency sweep testing using DSR ---------- 71

Figure 3.18 Stress and strain responses of several typical samples ---------- 72

Figure 3.19 Strain and compliance curves for viscoelastic samples subjected to variable stresses within the boundaries of linear viscoelasticity ---------- 74

Figure 3.20 Accumulated permanent strain in repeated shear creep loading and recovery ----- 75

Figure 4.1 Stiffening of asphalt binder by the addition of various filler volume fractions at 46 °C ---------- 78

Figure 4.2 Stiffening of asphalt binder by the addition of various filler volume fractions at 55 °C ---------- 79

Figure 4.3 Stiffening of asphalt binder by the addition of various filler volume fractions at 64 °C ---------- 79

Figure 4.4 Dependency of phase angle on temperature when tested by DSR ---------- 81

Figure 4.5 Dependency of phase angle on volume fractions of fillers when tested by DSR --- 81

Figure 4.6 Shear complex moduli for pure binder (PG64-22) ---------- 83

Figure 4.7 Shear complex moduli for donna fill (10%) mastic ---------- 83

Figure 4.8 Shear complex moduli for limestone (10%) mastic ---------- 84

Figure 4.9 Shear complex moduli for granite (10%) mastic ---------- 84

Figure 4.10 Shear stiffness variation function of filler volume fraction for donna fill mastics - 85

Figure 4.11 Shear stiffness variation function of filler volume fraction for limestone mastics - 86

Figure 4.12 Shear stiffness variation function of filler volume fraction for granite mastics --- 86

Figure 4.13 Phase angle variation function of frequency loading for donna fill (20%) mastic -- 87

Figure 4.14 Phase angle variation function of frequency loading for limestone (20%) mastic -- 87

Figure 4.15 Phase angle variation function of frequency loading for granite (20%) mastic ---- 88

Figure 4.16 Stiffness master curve for donna fill mastic ---------- 89

Figure 4.17 Stiffness master curve for limestone mastic ---------- 90

Figure 4.18 Stiffness master curve for granite mastic ---------- 90

Figure 4.19 Shear stiffness variation function of (10%) mineral filler type ---------- 91

Figure 4.20 Shear stiffness variation function of (20%) mineral filler type ---------- 92

Figure 4.21 Shear stiffness variation function of (30%) mineral filler type ---------- 92

Figure 4.22 Limestone mastics after 100 cycles of creep loading and recovery @ 46 °C ------ 94

Figure 4.23 Creep loading and recovery of limestone mastics after 10 cycles @ 55 °C -------- 95

Figure 4.24 Creep loading and recovery of limestone mastics after 20 cycles @ 64 °C -------- 96

Figure 4.25 Dependency of accumulated strain against time ---------- 100

Figure 4.26 Predicted and measured accumulated strain values after 100 cycles ---------- 102

Figure 4.27 Hirsch arrangement of phases for asphalt concrete ---------- 103

Figure 4.28 Alternate version of the modified Hirsch model ---------- 104

Figure 4.29 Estimated versus measured complex shear modulus for donna fill mastics at 46 °C ---------- 107

Figure 4.30 Estimated versus measured complex shear modulus for donna fill mastics at 55 °C ---------- 107

Figure 4.31 Estimated versus measured complex shear modulus for donna fill mastics at 64 °C ---------- 108

Figure 5.1 Schematic of asphalt mixture material ---------- 109

Figure 5.2 Example of Superpave aggregate gradation ---------- 112

Figure 5.3 Granite gradation used in the study ---------- 114

Figure 5.4 Critical stresses transmitted in flexible pavement ---------- 115

Figure 5.5 Deformation of the flexible pavement due to weak structure ---------- 116

Figure 5.6 Deformation of the flexible pavement due to poor HMA design ---------- 117

Figure 5.7 Mass and volume relationships in asphalt mixtures ---------- 118

Figure 5.8 Types of ESALs used by the Superpave system ---------- 120

Figure 6.1 Adding the appropriate quantity of asphalt binder to the aggregate ---------- 123

Figure 6.2 Mechanical mixer used for preparing the batch ---------- 123

Figure 6.3 Pouring the asphalt mixture in the mold in order to be compacted ---------- 124

Figure 6.4 Schematic of a gyratory compactor proposed by Superpave ---------- 126

Figure 6.5 Schematic of the compaction process in the SGC ---------- 126

Figure 6.6 Actual Superpave Gyratory Compactor ---------- 127

Figure 6.7 Compacting asphalt mixture in the gyratory compactor ---------- 128

Figure 6.8 Demolding and cooling of asphalt concrete specimens ---------- 129

Figure 6.9 Cutting compacted specimen at required dimensions for testing ---------- 129

Figure 7.1 Compression device used for gluing asphalt specimens and platens together ---- 135

Figure 7.2 Asphalt mixture specimen with two platens and horizontal LVDT attached to it -- 136

Figure 7.3 Schematic of the Superpave Shear Tester Equipment ---------- 137

Figure 7.4 COX 7000 Superpave Shear Tester ---------- 138

Figure 7.5 Asphalt mixture specimen prepared for SST testing ---------- 140

Figure 7.6 Shear strain and axial stress applications in frequency sweep test at constant height (FSCH) ---------- 141

Figure 7.7 Example frequency sweep shear load and deformation curves (5 Hz) ---------- 142

Figure 7.8 Example frequency sweep axial load and deformation curves (5 Hz) ---------- 143

Figure 7.9 Poor example of frequency sweep axial and shear load curves (5 Hz) ---------- 144

Figure 7.10 Poor example of frequency sweep axial and shear deformation curves (5 Hz) -- 144

Figure 7.11 Plot of permanent deformation vs. load applications showing three parts ------- 145

Figure 7.12 Haversian stress applications in the repeated shear test at constant height ------- 146

Figure 7.13 Example of axial and shear load curves of RSCH test ---------- 148

Figure 7.14 Plot of cumulative shear strain vs. number of shear load cycles ---------- 149

Figure 8.1 Shear complex modulus dependency on temperature and loading frequency of asphalt mixtures ---------- 151

Figure 8.2 Phase angle dependency on frequency and temperature of asphalt mixture ------- 152

Figure 8.3 Variation of G* components with the loading frequency at 3% asphalt content - 153

Figure 8.4 G*/sinϕ versus frequency for different asphalt mixtures at 6% air voids ---------- 154

Figure 8.5 Single master curve at 3% asphalt content mixture ---------- 155

Figure 8.6 SST RSCH test results for asphalt mixtures at 55° and 64 °C ---------- 156

Figure 8.7 Estimated versus measured complex shear modulus for asphalt mixtures --------- 158

Figure 8.8 Estimated versus measured accumulated shear strain values for 3% asphalt content mixture at 55 °C ---------- 159

Figure 8.9 Estimated versus measured accumulated shear strain values for 3% asphalt content mixture at 64 °C ---------- 160

Figure 9.1 Asphalt concrete 3-D X-ray tomography image ---------- 164

LIST OF ABBREVIATIONS

AASHTO	American Association of State Highway and Transportation Officials
AC	Asphalt Concrete
DOT	Department of Transportation
DSR	Dynamic Shear Rheometer
ESAL	Equivalent Single Axle Load
FHWA	Federal Highway Administration
FSCH	Frequency Sweep at Constant Height
HMA	Hot Mix Asphalt
IDT	Indirect Tensile Tester
LTRC	Louisiana Transportation Research Center
LVDT	Linear Variable Displacement Transducer
μm	Micrometer (micron)
RSCH	Repeated Shear at Constant Height
SHRP	Strategic Highway Research Program
SST	Superpave Shear Tester
Superpave	Superior Performing Asphalt Pavements

ABSTRACT

Asphalt mixtures are particulate composite materials consisting of uniformly distributed mineral aggregates, asphalt binder and air voids. Mixtures of asphalt binder and filler, also called mastics, are often assumed to behave as simple viscoelastic materials, where the binders are stiffened by the filler. Because the workability and performance of bituminous mixes are known to be affected by the filler-asphalt mixture (or mastic) properties, this study is intended for performing rheological tests on asphalt binder and mastics and use the results in order to estimate performance parameters of asphalt mixture.

The present work uses the PG64-22 asphalt binder test data initially to predict mastics' performance parameters - shear modulus (G*) and accumulated permanent shear strain (γ_{acc}) and then same properties for asphalt mixtures, in order to find a correlation between the three materials. Mastics were obtained by mixing the PG64-22 asphalt with three types of filler - donna fill, limestone, and granite - in five different percentages by volume - 5, 10, 15, 20, and 30%. The asphalt mixtures contained granite aggregate, 6% air voids content and five asphalt contents - 3% through 7%. Binder and mastics were tested at three temperatures (46°, 55°, and 64 °C) using a dynamic shear rheometer (DSR), while the mixtures were tested at two temperatures (55° and 64 °C) using the Superpave shear tester. Newly developed Hirsch model was used for estimating the shear moduli of asphalt mastics and mixtures, while for estimating the accumulated permanent shear strain a semi-empirical equation developed by Shenoy was used. Both estimations have been performed by using the shear modulus of the binder obtained from the DSR. The binder, mastics, and mixtures rheological data were generated using the appropriate equipment for each material, under identical conditions of measurement, thus

making it possible to identify a correlation between the materials. There was a good agreement between the measured and estimated values using the two methods (Hirsch and Shenoy), with Pearson correlation parameters (R^2) being over 0.90 or better.

CHAPTER 1. INTRODUCTION

1.1 Flexible Pavement Composition and Structure

The United States road network has approximately 4 million miles of roadway, of which almost 70 percent are paved (Buttlar et al., 1998; Derucher et al., 1998). Hot mix asphalt (HMA) pavements are an extensive part of this roadway. Flexible pavements support loads through bearing rather than flexural action, as rigid pavements do (Weissman et al., 2000). They comprise several layers of carefully selected materials designed to gradually distribute loads from the pavement surface to the layers underneath. The design ensures the load transmitted to each successive layer does not exceed the layer's load bearing capacity. A typical flexible pavement section is shown in Figure 1.1, presenting the various layers composing it. This study will only concentrate on the top layer (surface), i.e., the hot mix asphalt layer or the asphalt concrete layer.

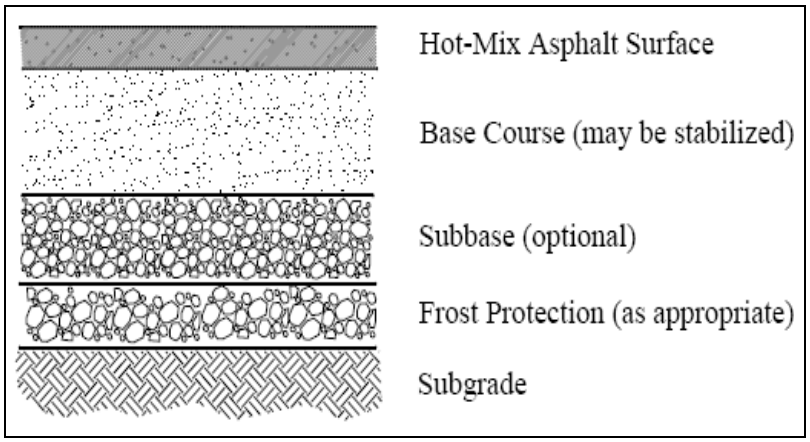

Figure 1.1 Typical flexible pavement structure (Atkins, 2003).

Bituminous surface (or wearing course), also known as the hot mix asphalt (HMA) surface, is made up of a mixture of various selected aggregates bound together with asphalt cement or other bituminous binders and different percentages of air voids, as shown in Figure 1.2.

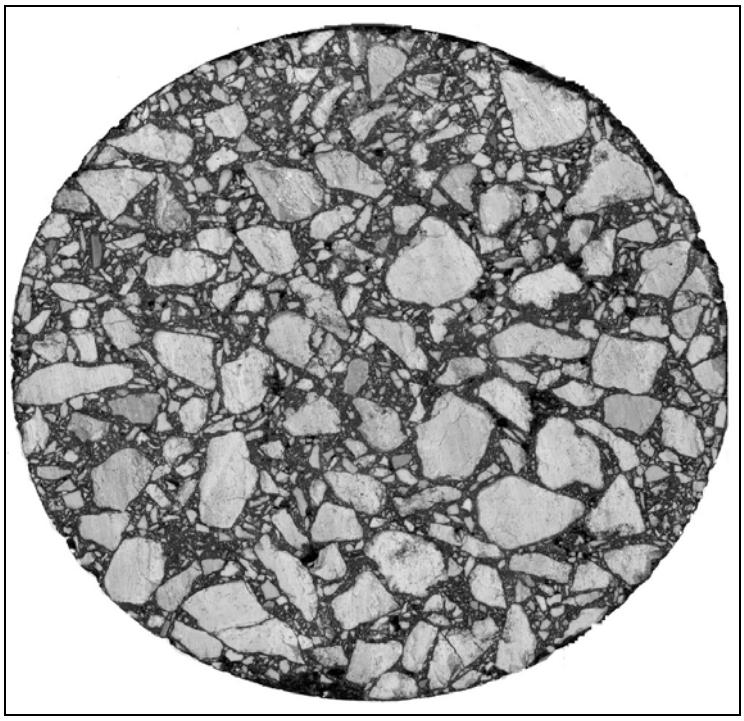

Figure 1.2 Asphalt concrete (Hot Mix Asphalt) structure.

This surface prevents the penetration of surface water to the base course and provides a smooth, well-bonded surface free from loose particles, which might endanger motor vehicles or people. It also resists the stresses caused by vehicle loads and supplies a skid-resistant surface without causing undue wear on tires.

Figure 1.3 depicts the distribution of the imposed load to the subgrade in a typical flexible pavement section. It can be seen that the base course serves as the principal structural component of the flexible pavement and it distributes the imposed wheel load to the pavement foundation, the subbase and the subgrade. The quality of the base course is a function of its

composition, physical properties, and compaction of the material (Roque et al., 2004). This layer is used in areas where frost action is severe or the subgrade soil is extremely weak. The subbase course functions like the base course, but the material requirements for the subbase are not as strict as those for the base course since the subbase is subjected to lower load stresses. The subbase consists of stabilized or properly compacted granular material, while the subgrade is the compacted soil layer that forms the foundation of the pavement system. Subgrade soils are subjected to lower stresses than the surface, base, and subbase courses (Anderson et al., 2000).

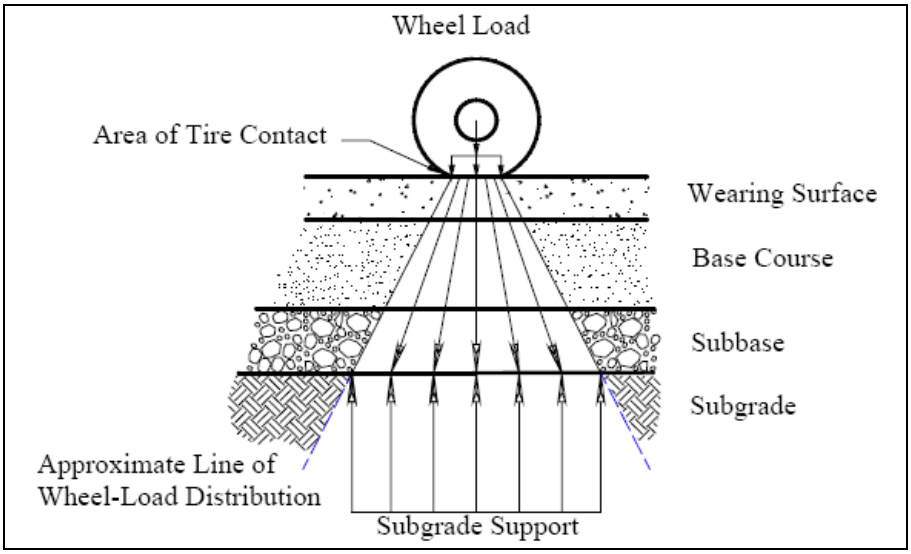

Figure 1.3 Distribution of load stress in flexible pavement (Buttlar, 1998).

1.2 Asphalt Binders and Mastics

Asphalt binder (or cement) is a dark-brown to black viscoelastic material that is produced by petroleum distillation. The "viscoelastic" term means that asphalt has the properties of both a viscous material, such as motor oil, or more realistically, water, and an elastic material, such as a rubber (Shenoy and Romero, 2001). However, the property that asphalt exhibits, whether viscous, elastic, or most often, a combination of both, depends on temperature and time of

loading. Before Superpave design in 1992, asphalt binder specifications were mainly developed around physical property test (penetration, viscosity, ductility) at standard test temperatures. The difficulty of these types of specifications was determining the relationship between the test result and actual performance of the asphalt binder over the range of temperatures that a pavement will experience. The Superpave asphalt binder specification addresses physical properties that can be related directly to field performance of the pavement. Asphalt binder properties are tested at temperatures that are encountered by in-service pavements. The Superpave asphalt binder specification is intended to improve performance by limiting the potential for the asphalt binder to contribute towards permanent deformation, low temperature cracking and fatigue cracking in HMA pavements. The important distinction between "before" Superpave asphalt binder specifications and the Superpave asphalt binder specifications are the overall format of the requirements. The required physical properties remain constant for all of the performance grades (PG) (Rowe et al., 2004). However, the temperatures at which these properties must be reached vary depending on the climate (Pellinen et al., 2004) in which the asphalt binder is expected to be used as shown in Figure 1.4.

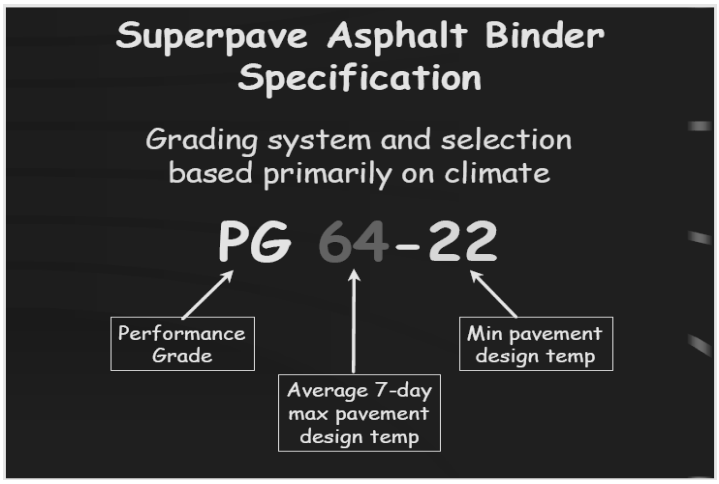

Figure 1.4 Asphalt binder nomenclature (FHWA - Superpave Implementation, 2003)

The Superpave performance graded (PG) binder specification makes use of these tendencies to test the asphalt under a project's expected climatic and aging conditions to help reduce pavement distress. Strategic Highway Research Program (SHRP) researchers developed new equipment standards as well as incorporated equipment used by other industries to develop binder and mixture tests. In this study, the testing equipment used was the Dynamic Shear Rheometer (DSR) for binder and mastics and the Superpave Shear Tester (SST) for asphalt mixtures. Both pieces of equipment were developed under SHRP as a way to measure the shear characteristics of binders and asphalt mixtures. They measure the shear dynamic modulus, which is the absolute value of the complex modulus in shear, and the phase angle, parameters that are used to characterize the viscoelastic properties of binders and evaluate the permanent deformation of asphalt pavements.

Aside from the binders, mastics play an important role in the compaction and performance of bituminous mixtures (Daniel and Kim, 1998). The addition of mineral fillers, very fine material, to asphalt binder is known to stiffen the asphalt binder, transforming it in a new material called ***mastic***. This new material is known to affect the workability of the asphalt mix and, therefore, play an important role in the compaction and performance of bituminous mixtures. In fact, if a core of asphalt concrete is observed in cross section, three components can be visually observed - mineral aggregates, air voids, and mastic. The asphalt cement occurs not as asphalt alone, but is intimately mixed with mineral fillers forming the mastic (Kandhal et al., 1998).

Many different views and definitions of stiffening or reinforcement mechanisms are found in the literature, but before continuing, it is necessary to establish some consistent definitions for the following reinforcement mechanisms:

Volume-Filling Reinforcement: The stiffening caused by the presence of rigid inclusions in a less rigid matrix. This stiffening level was assumed to be adequately described by the generalized self-consistent scheme (GSCS) model, or by the simplified GSCS-based prediction equations (Buttlar et al., 1998).

Physiochemical Reinforcement: The stiffening caused by interfacial effects between asphalt and filler particles, including absorption, adsorption, and selective sorption. This reinforcement mechanism is taken as the difference between measured mastic moduli at very low volume concentrations (below the onset of particle-interaction reinforcement) and those predicted by the GSCS model (volume filling reinforcement) (Meegoda and Chang, 1997). Thus, physiochemical reinforcement is assumed to be independent of filler volume concentration. This includes stiffening effects caused by layers of asphalt rigidly adhered to filler particles and partially altered asphalt layers somewhat further away from the particle. Other departures from micromechanics assumptions causing differences between measured and predicted results, such as non-spherical particles and imperfect blending of filler and asphalt, are also included in this category by the present definition.

Particle-Interaction Reinforcement: The stiffening that takes place beyond volume filling and physiochemical reinforcement caused by interactions between particles of filler/altered asphalt. This effect increases with increasing filler content, as rigid matter comes into contact and forms a skeletal framework (Roberts et al., 1996).

1.3 Distresses in Asphalt Pavements

Two major elements contribute to asphalt pavement deterioration: the gradual effects of weathering and the action of vehicle traffic (Huang, 1993). Early detection and repair of pavement defects is the most important preventive maintenance procedure. Failure to perform

routine maintenance during the early stages of deterioration may eventually result in serious pavement distresses that require extensive repairs that will be costly in terms of dollars and closure time. There are five areas of distress for which guidance is needed: fatigue cracking, (wheel path) rutting, thermal cracking, friction, and moisture susceptibility (Dongre et al., 2003). All of these distresses can result in loss of performance, but rutting or permanent deformation, presented in Figure 1.5, is the one distress that is most likely to be a sudden failure as a result of unsatisfactory hot mix asphalt or asphalt mixture (Ishai and Craus, 1996). Other distresses are typically long term failures that show up after a few years of traffic.

Figure 1.5 Rutting in asphalt pavement (Bahia, 2003).

Rutting results from the accumulation of small amounts of unrecoverable strain as a result of repeated loads applied to the pavement. This permanent deformation in HMA is caused by consolidation and/or lateral movement of the HMA under traffic or by a combination of densification (decrease in volume and, hence, increase in density) and shear deformation and

can occur in any one or more of the HMA layers as well as in the unbound materials underneath the HMA. Shear failure (lateral movement) of the HMA courses generally occurs in the top 100 mm of the pavement surface (Schwartz et al., 2002), however, it can occur deeper if satisfactory materials are not used. Wheel path rutting in asphalt pavements usually develops gradually with increasing numbers of load applications, typically appearing as longitudinal depressions in the wheel paths sometimes accompanied by small upheavals to the sides (Smith and Hesp, 2000).

1.4 Strategic Highway Research Program (SHRP)

Building and maintaining HMA highways is an expensive task, therefore, it is vital that a quality product be consistently produced. Efforts are continually being made to increase the quality and performance of the asphalt concrete pavements. Asphalt concrete pavements usually consist of mineral aggregates held together by asphalt cement binders. Mineral aggregates are distributed throughout the mixture in sizes ranging from coarse to fine (Anderson and Marasteanu, 1999; Chang and Meegoda, 1999). The overall performance of the mixture is largely dependent on the type of asphalt cement binder and mineral filler. The testing and grading of asphalt cement binders has progressively changed to meet the demanding needs for quality HMA pavements.

In order to improve the performance, durability, and safety of the road system, the **Strategic Highway Research Program** (SHRP) was established by Congress in 1987 as a five year research program. Fifty million dollars of the one hundred and fifty million dollars of the SHRP research funds were used for the development of asphalt specifications to directly relate laboratory analysis with field performance.

The goal of the SHRP asphalt research was the development of a system that would relate the material characteristics of hot mix asphalt to pavement performance (Chowdhury et al.,

2001). Asphalt materials have typically been tested and designed with empirical laboratory procedures, meaning that field experience was still required to determine if the laboratory analysis implied good pavement performance. However, even with proper adherence to these procedures and the development of mix design criteria, asphalt technologists have had various degrees of success in overcoming the three main asphalt pavement distresses: permanent deformation or rutting; fatigue cracking, which leads to alligator cracking; and low temperature cracking.

A final product of the SHRP asphalt research was the Superpave asphalt mixture design and analysis system. Superpave is an acronym for Superior Performing Asphalt Pavements. Superpave represents an improved, performance-based system for specifying asphalt binders and mineral aggregates, performing asphalt mixture design, and analyzing pavement performance. The system includes an asphalt binder specification that uses new binder physical property tests; a series of aggregate tests and specifications; a hot mix asphalt (HMA) design and analysis system; and computer software to integrate the system components. As with any design process, field control measurements are still necessary to ensure the field produced mixtures match the laboratory design (Wright and Dixon, 2004). The Superpave binder specification and mix design procedures incorporate various test equipment, test methods, and design criteria as shown in Figure 1.6.

A unique feature of the Superpave system is that its tests are performed at temperatures and aging conditions that more realistically represent those encountered by in-service pavements (Uddin, 1999). If the pavement distresses addressed by Superpave (rutting, fatigue cracking, and low temperature cracking) do occur in the pavement, they do so at relatively typical stages in a pavement's life and under relatively common temperature conditions.

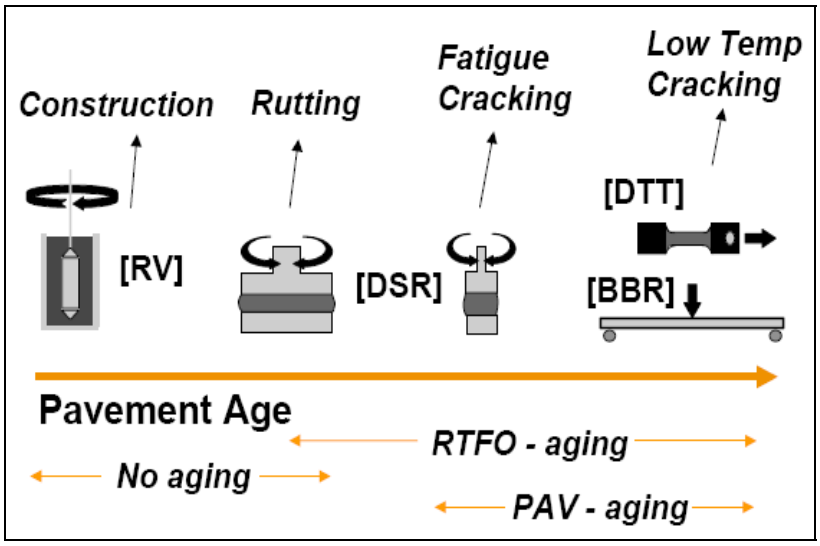

Figure 1.6 Superpave asphalt testing methods and equipment (SHRP Implementation, 2003).

1.5 Dynamic Shear Complex Modulus (G*)

The Dynamic Shear Rheometer (DSR) and Superpave Shear Tester (SST) developed under SHRP are used to characterize the visco-elastic properties of the binder (mastics) and asphalt mixtures or HMAs (Zaniewski and Pumphrey, 2004). The DSR measures the complex shear modulus G* and phase angle δ - which indicates the visco-elastic behavior of material - by subjecting a small sample of binder or mastic to oscillatory shear stress while sandwiched between two parallel plates. The DSR is used to determine G* and δ by measuring the shear strain response of a specimen to a fixed torque. In the case of the SST, samples of asphalt mixtures, having larger dimensions, are subjected to much larger oscillatory stresses in order to evaluate their resistance to rutting. A detailed description of these two pieces of equipment along with the testing results will be presented in the next chapters.

1.6 Problem Statement

The micromechanical behavior of asphalt concrete has attracted considerable recent attention, due to the fact that consists of a combination of mineral aggregates, asphalt binder,

mineral filler, and air voids; all the materials being held together by the asphalt binder (Vacin et al., 2003). Mineral aggregates used in the mixtures are uniformly distributed and range in size from coarse (> 4.75 mm) to fine (< 4.75 mm). Each material, as well as the asphalt binder-aggregate interface, contributes to the hot mix asphalt's (HMA) resistance to permanent deformation and other pavement distresses. However, it is well understood that the HMA is affected by both temperature and rate of loading (Smith and Hesp, 2000). The asphalt mastic, or the combination of the asphalt binder (cement) and mineral filler in an asphalt paving mixture, has long been known to influence the overall performance of asphalt paving mixtures (Anderson et al., 2001). The behavior of the asphalt mastic bears influence on nearly every aspect of asphalt mixture design, construction, and performance. In the design of asphaltic paving mixtures, the mastic influences the lubrication of the larger aggregate particles, and thus affects voids in the mineral aggregate (VMA), compaction characteristics, and optimum asphalt content. During construction of hot-mix asphalt pavements (HMA), the mastic must have enough stiffness to prevent drain-down, or the downward migration of the mastic mainly due to gravitational forces during storage and handling. This is particularly important in open- or gap-graded mixtures, such as stone mastic asphalt (SMA) mixtures. Finally, the stiffness of the mastic in the field impacts the ability of the mixture to resist permanent deformation at higher temperatures, influences stress development and fatigue resistance at intermediate temperatures, and influences stress development and fracture resistance at low temperatures (Chen, 1996). Although considerable work has been conducted to measure and even predict empirical and fundamental properties of asphalt mastics, very little work has been reported where rigorous mechanics based models have been used to explain the complicated behavior of asphalt mastics.

Mineral fillers have commonly been used in asphalt mixtures to fill the voids between the coarse aggregate particles (Gubler, 1999). Generally, the aggregate material passing the No. 200 sieve (0.075 μm) has been called filler and was used in percentages by volume in the mixture designs. Mineral fillers are known to affect the workability of the mix and, therefore, play an important role in the compaction and performance of bituminous mixtures, due to the fact that the asphalt cement occurs not as asphalt alone, but is intimately mixed with mineral fillers forming the mastic.

Although several studies have been reported in the asphalt literature, a good correlation between any measured physical property and the stiffening of asphalt by mineral fillers has not been reported (Coree, 1999) yet. This may be attributed to the fact that the stiffening potential of mineral fillers is a complex function of several factors such as average particle size, gradation, shape of the particles, presence of agglomerates, degree of dispersion, and asphalt-filler interface properties. Also, some of these properties interact with each other in complex ways - for example, the degree of dispersion is related to asphalt-filler interface properties, and the presence of agglomerates is dependent upon the average particle size and the asphalt-filler interface properties (Dongre, 2002).

Micromechanical models (Buttlar et al., 1998) can predict fundamental material properties of a composite based upon the properties of the individual constituents at different temperatures. In addition, the models also consider the relative proportions of each constituent and often require geometric information about the various constituent phases. However, the models provide a fundamental baseline that allows one to separate basic mechanical reinforcing from other more complicated, material dependent stiffening mechanisms. In this study, the Hirsch micromechanical model developed by Christensen et al. (2003), has been used in order to

predict the complex modulus of asphalt mixtures and mastics from binder and mastics, while for the accumulated strain, estimation was done using a semi-empirical equation developed by Shenoy (2002) and based on binder shear complex modulus and phase angle (δ). Using micromechanics methods, the macro behavior of asphalt concrete could be predicted from its microstructure and the properties of its constituents. Also, by understanding the various stiffening mechanisms in asphalt mastics, it might be possible to more accurately identify mixture design targets and to set quality control limits in a manner which will ensure that the mastic stiffness stays within a range that will lead to a good performing mixture.

1.7 Objectives of Study

The main objectives of this research study are to estimate the shear complex moduli and accumulated shear strain of asphalt mastics and mixtures using the binder complex moduli through testing by Dynamic Shear Rheometer (DSR) and Superpave Shear Tester (SST). This study tries to link the shear complex moduli of binder with the ones of mastics and asphalt mixtures using the "master curve" technique and modified Hirsch and Shenoy models based on volumetric composition of asphalt mastics and mixtures. A good correlation between asphalt mastics and mixtures using only one model for predicting the shear complex moduli and one model for estimating the accumulated strains will diminish the researchers' work in the future regarding the improvement of asphalt pavements in order to drastically decrease or eliminate the permanent deformation or rutting.

The experimental research consists of two distinct parts. First part is dedicated to the testing of asphalt binder and mastics using the DSR, while the second part is focused on the testing of asphalt concrete mixtures using the SST. The goals of this study will be achieved through the following specific tasks:

1. Review the literature pertinent to asphalt binder reinforcing mechanisms, effect of fillers on binders and mixtures, and mastics and mixtures testing;
2. Employ Hirsch and Shenoy micromechanical models in order to predict asphalt mastic and mixtures shear moduli and accumulated permanent strains;
3. Describe a series of experimental tests and analyses conducted to illustrate the usefulness of micromechanics in understanding reinforcing mechanisms in asphalt mastics and mixtures;
4. Discuss how the present work can be employed in mixture design and control in a practical manner;

For the first part of the study asphalt binder PG64-22 and three types of fillers - Donna Fill, Limestone, and Granite - in five volume fractions were investigated under different testing conditions. For the interpretation of the DSR data at frequency sweep, "master curves" technique was employed in order to determine a correlation between the binder and the mastics using test results at different temperatures and frequencies. By knowing the characteristic parameters of the master curve, one can estimate the shear complex modulus and phase angle at any given frequency using SHRP equations.

The Hirsch model employed is usually used for estimating the asphalt concrete complex modulus from binder modulus, voids in mineral aggregate (VMA), and voids filled with asphalt (VFA). The proposed model was verified by comparing the predicted moduli to values obtained from DSR testing.

The repeated shear creep load and recovery test for binders was used as a possible means to estimate the rate of accumulation of permanent strain in the mastics and compare the results to those obtained for the pure binder. Shenoy (2002) model is used to predict the accumulated strain by using asphalt binder shear complex modulus (G^*) and phase angle (δ) parameters given by Dynamic Shear Rheometer (DSR).

1.8 Organization of Dissertation

This dissertation is organized into eight chapters, as follows:

Chapter 1 serves as an introduction, stating the nature of the problem to be addressed, objectives of the research, and scope of work accomplished.

Chapter 2 summarizes the literature review on asphalt binders, mastics and mixtures testing in order to improve the permanent deformation in asphalt pavements. It covers aspects regarding permanent deformation, its different types and causes, and previous research work on asphalt mastics and mixtures. Selected studies conducted since the initiation of SHRP program related to the effect of aggregate gradation, focusing especially on mineral fillers, types of asphalts, and temperature, are also described in this chapter.

Chapter 3 describes the testing procedure and data acquisition using the Dynamic Shear Rheometer (DSR) when testing the asphalt binder and mastics at different temperatures and frequencies. It also describes various testing parameters used for evaluating the behavior of the two materials in order to predict the future deformation of asphalt pavements.

Chapter 4 shows information on summary and analyses of dynamic rheometer test results and estimation of complex shear modulus G* using the Hirsch model. It also shows information on the estimation of permanent strain using the Shenoy semi empirical equation.

Chapter 5 describes the Superpave asphalt mixture design, including information on asphalt binder, mineral aggregate gradation, asphalt mixture behavior, wheel path rutting, and asphalt mixture volumetrics.

Chapter 6 provides information on asphalt mixtures materials and testing using the Superpave Shear Tester (SST), a mechanical equipment developed under the SHRP. The information obtained from the SST is utilized to compare generated data for any proposed mixture of unknown performance with another mixture with known performance under the same conditions at identical temperatures.

Chapter 7 is a description of the theoretical methodology applied to the testing data in order to construct the master curves and predict the shear complex modulus and accumulated strain for mastics and asphalt mixtures.

Chapter 8 covers analysis of the results from different tests which have been conducted to evaluate SHRP parameters of asphalt mastics and mixtures: repeated shear at constant stress ratio, frequency sweep at constant height, and repeated shear at constant height.

Chapter 9 presents the conclusions and recommendations that arise from the asphalt mastics and mixtures study.

CHAPTER 2. LITERATURE REVIEW

Asphalt binders and mastics, as well as mineral aggregates, play a critical role in the quality and performance of flexible pavements, therefore, asphalt pavement engineers must have a thorough understanding of their behavior (Shenoy et al., 2003). Proven testing equipment and test specifications are necessary to accurately evaluate and select the appropriate materials for a pavement structure, in this case the HMA surface (wearing) course. The purpose of this chapter therefore, is to review various research papers that characterize the rheological behavior of asphalt binders and mixtures. It will contain aspects about how important are the asphalt binders for the mixtures, how mineral fillers affect the overall behavior of mastics and mixture, and how researchers seek ways to predict different mixtures properties by using the properties of the ingredients. It is also the intent of this chapter to indicate the fact that only few studies have been focused on doing research related to binder-mastic and mixture correlation, most of the research being concentrated on improving the properties of the binders or changing some of the asphalt concrete design parameters, such as asphalt content, air voids content or filler content.

2.1 Asphalt Binders and Mastics Characterization

Daniel et al. (1998) have studied the effects of aging on viscoelastic properties of asphalt-aggregate mixtures. Of special interest was how the fatigue performance of asphalt concrete mixtures changes with time because of changing material properties, due to the fact that they are related. They found out that aging of the asphalt concrete mixture results in a decrease in the slope of the linear portions of the creep and relaxation curves as shown in Figure 2.1. Also, the dynamic modulus increased and phase angles decreased with higher levels of aging. Values of dynamic moduli at all aging levels decreased with frequency and higher temperatures. STA stands for short-term aging, while LTA for long-term aging. The relative changes in dynamic

modulus and phase angle between aging levels were not as prominent as those seen in the creep and relaxation curves because of excessive background noise in deflection measurements during the complex modulus testing.

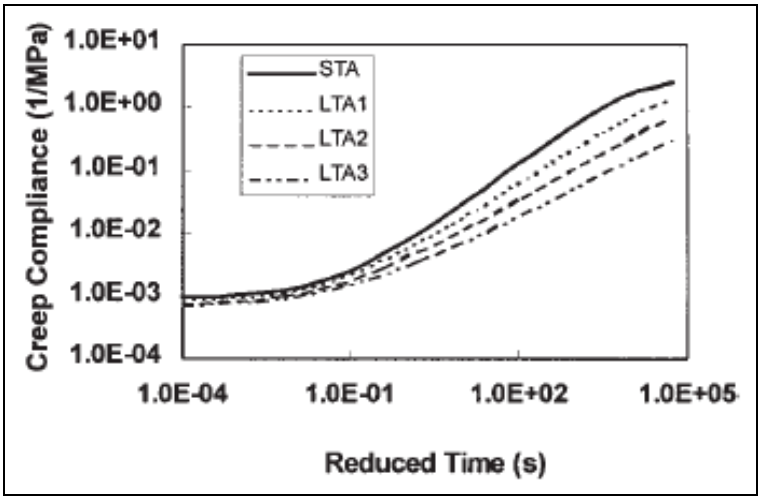

Figure 2.1 Creep compliance curves for all aging levels (Daniel et al., 1998).

A research study was initiated by Anderson et al. (1999) to ascertain if all PG 70-22 binders would perform the same in an asphalt mixture in Kentucky, regardless of method of manufacture of the binder. Five PG 70-22 binders and one PG 64-22 binder (control) were incorporated into an asphalt mixture through a hot-mix asphalt plant and test sections were placed for each binder. Asphalt mixtures were sampled at the plant and taken to the laboratory for mechanical property testing that included repeated shear test at constant height (RSCH), frequency sweep test at constant height (FSCH), and indirect tensile creep test (ITC). These tests were chosen to evaluate the properties (creep compliance, stiffness) of the asphalt mixtures at low temperatures (between -12 and -30 °C). Thermal stress analysis techniques permitted the critical mixture temperature for single-event thermal cracking to be compared to critical binder temperatures. While the critical binder temperature, calculated from BBR stiffness, matched

reasonably well with the critical mixture temperature, the critical binder temperature calculated from BBR m-value (parameter which controls the low temperature grade of the asphalt binder) did not match as well. The m-value critical temperature was generally higher than that indicated by the low temperature indirect tensile creep testing. While not all PG 70-22 performed the same in mixture testing, the research did not clarify if differences in mixture properties for the PG 70-22 binders are related to differences in binder stiffness, differences in method of manufacture, or both. There was also a weak relationship ($R^2 = 0.39$) between low temperature binder stiffness and mixture stiffness at -12°C and 60 seconds loading as can be seen from Figure 2.2.

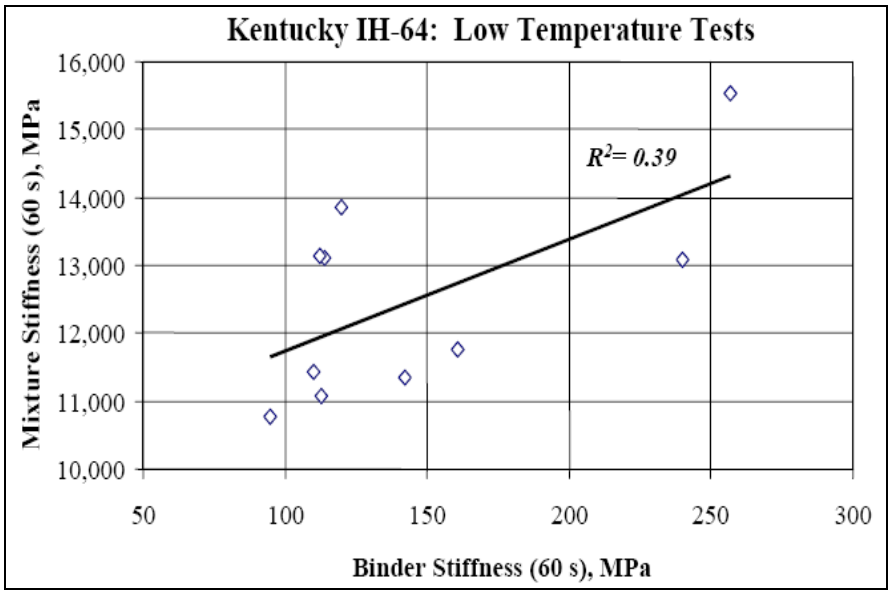

Figure 2.2 Relationship between mixture stiffness and binder stiffness (Anderson et al., 1999)

SHRP researchers Peterson et al. (1999) have studied the extraction and recovery of asphalt cement (binder) from mixtures, which is a routine task in most asphalt laboratories. Characterization of extracted asphalt binder and aggregate is important for design, quality control, performance prediction and research purposes. Different methods, equipment and solvents for extraction of asphalt binders have significant effects on the properties of the

extracted asphalt binder and aggregate. Peterson's (1999) study was conducted under NCHRP 9-12 project, *Incorporation of Reclaimed Asphalt Pavement in the Superpave System,* in order to review the variables in extraction and recovery methods. One objective of their study was to evaluate different extraction and recovery methods and determine the best to use for the NCHRP 9-12 study, while the second objective was to determine if additional aging of recovered binders is necessary when conducting mix designs in the laboratory. The experimental matrix developed included two different extraction procedures, two recovery methods and three different solvents. Properties (stiffness, m-value, and G*/sinδ) of extracted aggregates and asphalt binders from two different Reclaimed Asphalt Pavements (RAP) were studied. The results demonstrated significant variability on properties of extracted asphalt binder with different solvents, extraction and recovery methods. However, the extracted RAP aggregate gradation was not significantly different with different methods and solvents, while the aging of the recovered binders demonstrated insignificant changes (G*/sinδ did not have a significant increase) for the blending of RAP binders.

Kern and Carpenter (1999) have used the Superpave binder grading system in order to relate a measure of rutting behavior of asphalt mixtures with actual temperature data to show that it is more fundamentally correct and relatively easy to obtain a relationship between the frequency distribution of high temperatures with traffic levels when selecting performance-graded binders. The Performance Grading (PG) system provides a selection process based on the potential performance characteristics of the binder as related to the climatic considerations of the area, principally the temperature. The selection criterion for the high-temperature grade uses the average of the maximum consecutive 7-day high pavement temperatures at a 20-mm depth with requisite grade bumps. This selection criterion is examined as to how well it actually relates to

the performance of the asphalt concrete under high temperatures, principally permanent deformations in the mixtures, which is a fundamental connection that must be established before adjustments are made to the binder grade on the basis of the traffic using the pavement. The current temperature criterion is compared with the actual temperature distributions of a number of cities across the United States to demonstrate the disconnected nature of this value in relation to the actual pavement temperatures. They found out that cities with the same PG temperatures may have very different pavement temperature distributions and the percentage of time that the pavements are subjected to temperatures higher than a given PG grade may be different. Thus, different rutting potentials may occur when the binders suggested by the Superpave criterion are used. Also, modified binders showed different stiffness characteristics than unmodified binders. This result suggests that a general specification may not consistently characterize and classify the field performance of modified binders. According to the Georgia loaded wheel (GLW) rut depth prediction model, two cities with the same PG temperature may have very different GLW predicted rut depths. This result suggests that the performance of a given binder in these cities would be different, the difference being caused by the actual temperature distributions. The GLW rutting model, also suggests that two cities with the same PG temperatures may actually need different PG binders to provide similar performance.

Anderson et al. (2000) have done some research regarding the improvement of the repeatability of the AASHTO and ASTM test methods used to grade Superpave asphalt binders, due to the fact, that the test methods in themselves are not sufficient to ensure uniformity in testing practice from one laboratory to another. Through a series of workshops conducted in the Northeast Center for Paving Technology, it was concluded that practices in many of the laboratories varied sufficiently to warrant further training and the development of a manual of

testing practice. They developed a manual of practice which incorporated issues grouped into four main categories: handling, sampling, and sample preparation; temperature measurements; equipment calibration; and testing procedures.

Shenoy (2001) proposed a refinement of the Superpave specification parameter for performance grading of asphalt binder, by showing that the semi-empirical approach involving curve-fitting of experimental data is not necessary if the derivations are based on fundamental concepts. He concluded that the Superpave specification parameter $G^*/\sin\delta$ (also known as the rutting parameter) for high temperature performance grading of paving asphalts has not been found to be adequate in rating various binders, especially some polymer-modified ones, for their rutting resistance. This has led researchers to seek other possible parameters that may better relate to rutting resistance and also to search for ways to improve the existing parameter $|G^*|/\sin\delta$, so that it is more sensitive to pavement performance. Some researchers have suggested the repeated creep and recovery test, while others have used a semi-empirical approach as a means to refine the existing Superpave specification parameter. The final equations obtained by Shenoy (2001) through a theoretical development were verified using part of the same experimental data that were used by the earlier researchers.

Anderson et al. (2002) have focused their research in the use of zero shear viscosity (ZSV) as a specification criterion for asphalt binders, which can be determined directly from long-term creep tests. Their interest was precipitated by the apparent inability of the current Superpave criterion, $G^*/\sin\delta$, to capture the contribution to rutting resistance afforded by polymer modification. Laboratory test data for ten different unmodified and modified binders were obtained through a series of creep and dynamic experiments. ZSV values obtained from two of the more promising methods were compared along with a comparison of the ZSV ranking

with the Superpave grading temperature. The authors concluded that two of the methods provided very similar values for the ZSV when applied over a considerable range in test temperatures and that the results from the two methods can be used interchangeably for the materials that were tested. The asphalt binders ranked quite differently when ranking according to their Superpave grading temperature or their ZSV.

In their research on Zero Shear Viscosity (ZSV), Rowe (2002) et al. have come to the conclusion that this parameter can be estimated by performing a frequency sweep test at a single temperature by using a Dynamic Shear Rheometer (DSR). Because the ZSV can be computed from isotherms of stiffness data generated by a DSR, thus eliminating the need to perform the repetitive creep test, the authors then computed the ZSV from binder master curves and compared the derived results to performance of pavement test sections evaluated under controlled conditions. They concluded that, since the ZSV is measured at conditions close to the current specification requirement for $G^*/\sin\delta$, the existing test equipment (DSR) can be used to determine the necessary input data for the calculations.

Due to the fact that a new specification for determining the critical cracking temperature, T_{cr}, of asphalt binders was introduced by AASHTO - MP1a, Dongre et al. (2002) have focused their research on calculating this temperature based on the stiffness data from the Bending Beam Rheometer (BBR) and the tensile strength from the Direct Tension Test (DTT). The researchers also conducted experiments to compare the AASHTO protocol with a new one developed by the University of Calgary. They concluded that there was no significant difference found in the DTT tensile strength results obtained using the two sample preparation protocols and that the variability of the strength values did not significantly affect the MP1a critical cracking temperature.

Also, Dongre and D'Angelo (2002) have evaluated different parameters for Superpave high temperature binder specification based on rutting performance in the Accelerated Loading Facility (ALF). They have tested five asphalt binders used in the Federal Highway Administration's Accelerated Loading Facility (FHWA ALF) and additionally, two binders used by Nevada Department of Transportation (DOT) in construction of highway I-80. Results showed that the zero-shear viscosity (ZSV) correlated reasonably well with performance and was the best parameter among all evaluated. It was also found that to obtain the zero-shear viscosity of asphalt binders with reasonable accuracy, two conditions must be met. The first condition is that the shear stress must be in the Newtonian region and the second requirement is that steady state must be achieved. Multiple cycles of creep-recovery test do not achieve steady state unless each creep portion is carried out to steady state.

Basu et al. (2002) in an effort to propose practical laboratory tests that require less time to perform, have used the time-temperature superposition principle to show that the stiffness after 2 hours loading at the Performance Graded (PG) low temperature can be approximated by the stiffness after 60 seconds loading at 10ºC above the PG low temperature. This equivalence principle was developed based on test results from the eight core asphalts and the effect of physical hardening on time-temperature superposition was not taken into account either. The comparison of the stiffnesses at 60 seconds loading and at 2 hours loading showed significant differences for all asphalts investigated, in that the 60 seconds stiffness values were significantly higher than the 2-hour values and differences ranged from 32% to 66%. Researchers found out that these differences were much reduced for the tests performed after conditioning for 3 days that were less affected by physical hardening, thus it appears that the equivalence factor is asphalt specific and conditioning time specific.

Shenoy et al. (2003) have studied the relationships between the mechanical properties of the asphalt mixtures and the rheological properties of the binders/mastics when assessing the resistance of the mixtures/binders to permanent deformation. Based on the data analyzed in their work, using the Superpave Shear Tester (SST), the French Pavement Rutting Tester (PRT), and the Hamburg Wheel-Tracking Device (WTD), it can be said that the properties of the mixtures (rut depth and cumulative shear strain) for evaluating permanent deformation seemed to have not a good correlation with the rheological properties of the binder/mastics for the French tester and Hamburg wheel, but correlated better with the results from the dynamic shear rheometer regarding rut controlling parameter $G^*/\sin\delta$. However, the observations in their work were system-specific and may not be applicable in other circumstances involving different aggregate-binder combinations or some other specific design parameters.

Uddin (2003) research has concentrated on viscoelastic characterization of polymer-modified asphalt binders of pavement applications, regarding rutting as primary reason of premature deterioration of asphalt highway pavements. In his study the virgin asphalt and modified asphalt binders and mixes used on several test sections of the I-55 highway rehabilitation project in northern Mississippi were compared. The laboratory creep compliance data for these binders were measured at low temperatures using a modified test procedure adapted for the Bending Beam Rheometer (BBR) device. The creep compliance data of the binder was used as an input to simulate creep compliance behavior of the mix using a micromechanical model. The field evaluation confirmed the relatively poor performance of the virgin asphalt section with respect to rutting, compared to modified binder sections. Also, the mix creep compliance and relaxation moduli values predicted using the micromechanics

approach also indicated poor performance of the control asphalt section compared to other modified binder sections.

Dongre et al. (2003) have conducted a study to determine a new binder parameter that may replace the existing Superpave high temperature specification parameter ($G^*/\sin\delta$), which they consider inadequate due to increasing concerns of its applicability to polymer and other modified asphalt binders (PMA). In their study several parameters were calculated from rheological test data generated on four asphalt binders of different grades at four test temperatures. Two of the binders were unmodified and the other two were modified binders. Laboratory hot-mix rutting tests were also conducted at three temperatures on the Asphalt Pavement Analyzer (APA) and the Dry Hamburg rut testers. It was found that the APA overestimated the rutting potential of modified binders, while the Dry Hamburg produced reasonable results. From the correlation between Dry Hamburg data and binder parameters, the storage viscosity, η', was found to be the most promising binder parameter that can adequately characterize the rutting resistance of both unmodified and modified asphalt binders, because out of all the other parameters it is the easiest to measure with minimal change in existing instrumentation and software. A new specification criterion for η' was also determined, according with which the η' has a value of 220 Pa·s for RTFOT aged asphalt binders and could reasonably replace the current Superpave high PG grade temperature parameter $G^*/\sin\delta$. Researchers consider that it should be further evaluated to determine its repeatability and reproducibility.

Neubauer and Partl (2004) investigated the behaviour of stone mastic asphalts SMA 11 and SMA 16 with standard and polymer-modified binders combinations in order to find out whether Marshall and Gyratory methods provide the same optimum binder content. The

investigations were complemented by determinations of rutting at relatively high temperatures (60°C) using the wheel tracking test. The polymer-modified binders mixes resulted in lower deformation values than in mixes containing the standard binder.

Vacin (2004) thought that further laboratory investigations have to be done in the field of loading time and temperature from the perspective of rutting, fatigue and low temperature cracking. One possible method of investigation with the advantage of providing more insight into the material structure is to characterize materials on larger time and frequency domains by using the Time Temperature Superposition (TTS) principle. His goal was to test two polymer modified binders (PMA) of different performance grades (PG's) by the dynamic shear and bending beam rheometers (DSR and BBR). Binder results were then compared with the results of mastics and hot mix asphalt (HMA). By applying the TTS principle to the obtained master curves from the three of the tested materials (PMA, mastic and HMA), preliminary results showed that the performance of shear compliance of the HMA was similar to binder and mastic at short loading (and/or low temperatures), but exhibited different behavior at long time loading (and/or high temperatures). Vacin (2004) also found out a good correlation between the bending beam and the dynamic shear rheometers data for the given materials, in that, the DSR data can be used to predict the low temperature behavior of materials, if TTS is applied correctly (log D = log J/3).

Delgadillo et al. (2004) offered a revised system for testing and evaluating asphalt binders based on damage behavior by conducting binder rutting tests that would allow a more direct qualification of binders for specific climate and traffic conditions. Their research has shown how a mechanistic system based on damage behavior can be transformed in a new rutting specification, by developing a new parameter, called viscous component of the creep stiffness G_v, which is intended to replace $G^*/\sin\delta$.

2.2 Effect of Mineral Fillers on Asphalt Binders and Mixtures

Chen (1996) used Nielsen's micromechanical model and the time-temperature superposition principle to characterize the stiffness of asphalt mastics, after the data obtained from the Bending Beam Rheometer (BBR) and the Dynamic Shear Rheometer (DSR) were converted to the same unit. According to the data, the stiffening effects of the filler were relatively small at shorter loading times or low temperatures, but larger at higher temperatures or long loading times, thus stiffening effect was found to be asphalt dependent, as well as filler dependent. Also, the validity of the micromechanical model was confirmed in his study for two types of mineral filler.

In their study, Jiang et al. (1996) have discussed the rheology of asphaltic binders and their effects on asphalt concrete with the intention of improving the correlation between conventional mix design results and pavement performance. Their test results showed that mineral filler can increase the viscosity and decrease the shear index of asphalt, except apparently at a lower frequency or a higher temperature, all these effects becoming more pronounced with a continuously increasing filler to asphalt (F/A) ratio. They also discovered that mineral fillers of small particle size, lower bulk density, and higher compressibility are more effective, but more difficult to quick mix homogeneously into the asphalt. The use of these fillers will be limited to the lower F/A range unless working temperatures are adjusted properly according to the binder's consistency. Some modification methods of the binders (air-blown, polymer addition) can effectively improve the rheology of asphalt, but whether these changes are always good for the pavement will depend on environmental conditions, mix design, and rheology.

Ishai and Craus (1996) research focused on the effects of some aggregate and filler characteristics on behavior and durability of asphalt paving mixture. It was found that for most filler types tested, there is a unified trend for all physico-chemical effects toward the combination of higher geometric irregularity with higher intensity of adsorption. This combined effect causes a strengthening of the filler-bitumen bonds and a relative increase in the amount of fixed bitumen. The outcome is mastics with higher consistency or mixtures with higher strength. Exceptions to this general trend could be found for some filler types that have relatively high geometric irregularity (limestone) but very low surface activity (crushed glass). The adsorption intensity (as can be evaluated by the heat of the filler-bitumen interaction) is a significant factor for characterizing the physicochemical capacity of the filler and its influence on the behavior and durability of bituminous mixtures as shown in Figure 2.3.

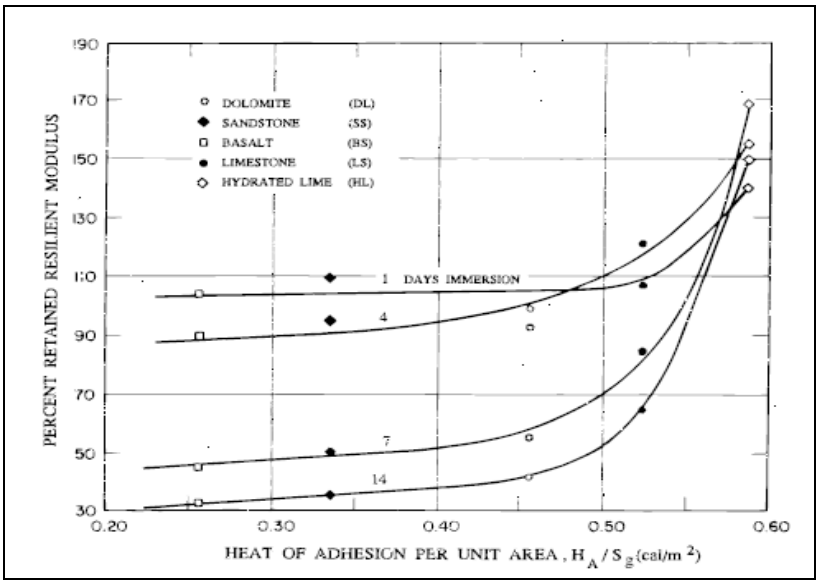

Figure 2.3 Durability potential of mixtures versus filler activity at different periods of immersion, using resilient modulus criterion (Ishai and Craus, 1996).

In this context, the durability index, which is a one-point characterization of the entire durability curve (retained strength versus immersion time), was highly correlated with the specific heat of adsorption of the various filler types, indicating the high durability potential of active fillers and the low durability potential of nonactive ones. The effect of the filler was usually manifested after long periods of immersion; mixtures with nonactive fillers deteriorate rapidly after 4 or 7 days of immersion. Those with active fillers usually maintained a proper retained strength for a long immersion time at optimum bitumen content and above. The durability potential of the mixture usually increased with the incremental increase in bitumen content above the optimum content, and in this respect, mixtures with nonactive fillers were found to be much more sensitive to bitumen content than were mixtures with active fillers.

Shashidhar and Romero (1998) studied the workability and performance of bituminous mixes which are known to be affected by the filler-asphalt mixture (or mastic) properties. The addition of fillers is known to stiffen asphalt, but the degree of stiffening is a function of several filler and asphalt properties, which are not well understood. This complex problem was simplified by introducing two intermediate measurable parameters, the maximum packing fraction, ϕ_m, and the generalized Einstein coefficient, K_E. This enabled a better understanding of the influence of various factors such as average particle size, gradation, particle shape, presence of agglomerates, degree of dispersion, and the asphalt-filler interface on the stiffening potential of asphalt. Maximum packing fraction (ϕ_m) represents the maximum amount of fillers that can be added to asphalt without prompting the emergence of air voids, which are formed when the value of ϕ_m is lower than that of ϕ_2 (filler volume fraction). When these values are equal, however, the stiffness of the mastic is infinite compared to that of the binder. The generalized Einstein coefficient K_E is the stiffening rate of the mastics as a function of filler addition. They concluded

that the stiffening effect of the fillers increased with decreasing particle sizes below 10 μm. Above 10 μm, such dependencies were not significant. The asphalt-filler interface was shown to have a significant effect on stiffening, while the interface properties changed from asphalt to asphalt, but it can be engineered to yield desired properties. Fillers in asphalts with low ϕ_m, indicated that they were poorly dispersed, while agglomerates shown to increase K_E, decrease ϕ_m, and therefore increase stiffening power. Asphalts with agglomerated fillers showed to have stiffnesses greater than those with unagglomerated fillers.

Kandhal et al. (1998) have concentrated their studies on the characterization tests for mineral fillers related to performance of asphalt paving mixtures. Because fine aggregates passing 0.075 mm (No. 200) sieve (generally called P200 material) have a significant effect on the performance of asphalt paving mixtures in terms of permanent deformation, fatigue cracking, and moisture susceptibility, their study was undertaken to determine which P200 characterization tests are most related to the performance of asphalt paving mixtures. For this purpose six P200 materials representing a wide range of mineralogical composition and particle sizes were used and were characterized by six tests including Rigden voids, particle size analysis, and methylene blue test. It has been found that the particle sizes, in microns, corresponding to 60 and 10 percent passing and the methylene blue test were related to the performance of asphalt paving mixtures, in that the permanent deformation and stiffness of asphalt mixtures have improved with the decrease in particle size of the mineral filler (P200 material).

Tayebali et al. (1998) investigated the possibility of increasing the amount of fines in asphalt mixtures, based on the washed sieve analysis, from a maximum of about 8 percent as currently specified, without adversely affecting the performance of the mixture. At the same time, it was also of interest to investigate the influence of the mineral filler type (crushed versus

natural river sands, or combinations thereof) on asphalt (Marshall) mix design and on the shear permanent deformation performance. They found out that by increasing the amount of mineral filler the Marshall stability and unit weight increased. This procedure led to a higher shear resilient modulus due to increased unit weight, without adversely affecting its rutting during the repeated shear testing by SST.

Gubler et al. (1999) have studied the influence of three mineral fillers on the aging mechanism of asphalt binders. They have found out that the complex modulus G* as well as the phase angle varied with magnitude and time of loading, thus the mechanical properties of mastics depended not only on the conditions at the time of measurement, but also on sample history prior to the measurement. Therefore fillers might influence the aging of a binder by promoting oxidation or side reactions, such as dehydration or polymerization, fact that leads to a hardening of asphalt mixture. At the same time, the filler has a hindrance effect on diffusion of oxygen into the mastic, due to the fact that the filler fraction is completely impermeable to oxygen, thus its presence may retard the aging process. Researchers defined the catalytic effect of filler as changes in the aging index and the phase angle caused by aging of binder (PAV) in the presence and the absence of mineral filler.

Kim et al. (2003) have done a mechanistic evaluation of mineral fillers on fatigue resistance and fundamental material characteristics by using two mineral fillers: limestone and hydrated lime. Their test results were analyzed using viscoealstic theory, a fatigue prediction model based on continuum damage mechanics, and a rheological composite model. Based on the test results they concluded that dynamic mechanical analysis can be effectively used to characterize basic material properties and the fatigue behavior of asphalt binders and mastics. Also, fillers provided better resistance to microcracking due to a lower rate of damage evolution

and higher capability for total damage accumulation. The hydrated lime mixtures, generally showed higher moduli than limestone filled mixtures and was more effective than limestone filler regarding the fatigue life, which infers that mechanisms other than a volume filling effect occurred. The improvement in fatigue life due to hydrated lime was much greater in one of the asphalt mixes, fact which indicated that the physico-chemical interaction between bitumen and filler was dependent on the type of materials.

Neubauer and Partl (2004) investigated the behaviour of stone mastic asphalts SMA 11 and SMA 16 with different filler/binder combinations in order to find out whether Marshall and Gyratory methods provide the same optimum binder content. They found out that none of the optimum binder content values determined by the Marshall and the Gyratory compactor method were identical for any of the filler/binder combinations used, the optimum binder contents determined using the Marshall compactor were distinctly higher than those using the Gyratory compactor. From the values of air void contents, voids of mineral aggregate (VMA) and volume of voids filled with binder (VFA) for all the mixes could be seen that stone mastic asphalt was more efficiently compacted with the Gyratory compactor than with the Marshall compactor. The kneading-type compaction of the bituminous composition achieved with the Gyratory compactor allows aggregate grains to move, as a result of which air voids are more readily filled than it is the case with the impact compaction with the Marshall hammer. Also, the wheel tracking test revealed no excessive permanent deformation values for any of the filler/binder combinations under consideration.

Lackner et al. (2005) research focused on the effect of filler shape and mineralogy on the low-temperature creep of asphalt mastic, process that provides the stress relaxation capacity in flexible pavements required to avoid cracking as a consequence of thermal shrinkage during

winter periods. Based on the experimental results obtained from Bending Beam Rheometer (BBR) for both, asphalt and mastic, a multiscale model was employed for the prediction of low-temperature creep properties of the bitumen-filler composite. Accounting for the distinct matrix-inclusion morphology present at the mastic-scale, a homogenization scheme (Mori-Tanaka) was employed in order to be applied to the bitumen-filler composite, giving insight into the effect of filler on the low-temperature behavior of mastic. Hereby, the filler particles were considered as rigid inclusions with spherical shape, resulting in excellent agreement between the creep parameters of the homogenized material and the respective experimental BBR result. This agreement indicated that only the volume fraction of the filler, entering the Mori-Tanaka scheme, and neither the filler geometry nor the chemical composition of the filler influenced low-temperature creep of asphalt mastic.

2.3 Asphalt Mixtures Characterization

Chang and Meegoda (1997) research was related to the mechanical behavior and internal structure of hot mix asphalt concrete (HMA) due to the change in temperature. They used a modified micro mechanical model, ASBAL, based on the Discrete Element Method (DEM) to simulate the stress-strain behavior and variation of internal structure of HMA. The Burger's element was added to ASBAL to describe the viscoelastic behavior of asphalt cement, while the master curves of asphalt binder at different temperatures were used to describe the stress-strain behavior. Behavior of HMA at four different temperatures subjected to constant stress and unconfined compression tests were simulated and the simulation showed the ability of the ASBAL model to predict the temperature susceptibility of HMA assembly. Therefore, this micro mechanical model could be used as a tool to understand the mechanism of high temperature rutting.

Daniel and Kim (1998) have looked for relationships among rate-dependent stiffnesses of asphalt concrete using laboratory and field test methods. Once a relationship can be established, field measured stiffnesses can be converted to appropriate laboratory values, reducing the need for costly and destructive cores from the pavements and the laboratory values can then be used in design or to evaluate pavement condition. In their research, five testing methods were examined to develop a relationship between the measured stiffnesses, and they included three laboratory tests (creep compliance, complex modulus, and impact resonance method), and two field tests (falling weight deflectometer and surface wave method). Theoretical relationships using linear viscoelasticity were used to relate laboratory and field measured stiffnesses. A comparison of creep stiffness, S(t), and relaxation modulus, E(t), calculated from creep compliance, D(t), revealed large differences of E(t) at intermediate times. The relationship between creep compliance and dynamic modulus was extended to successfully predict high frequency stiffnesses such as those from the impact resonance and surface wave methods. Using stiffnesses from the laboratory and field measured at different frequencies, a linear relationship was discovered in three separate cases. Knowing the relationship between frequency and stiffness (as measured by the different methods) is linear on a log-log scale, laboratory stiffnesses may be predicted from field testing.

Buttlar et al. (1998) have studied particulate composite micromechanics models in order to investigate three reinforcement regimes in asphalt mastics: volume filling, physiochemical, and particle interaction. Among them, the generalized self-consistent scheme (GSCS) model was found to produce very reasonable baseline reinforcement levels based upon volume-filling a soft asphaltic matrix with rigid filler particles. The fundamental nature of the modeling approach allowed the examination of physiochemical stiffening effects, through a new equivalent rigid

layer modeling technique. This technique illustrated that the development of rigidly adsorbed layers of just 2-10 angstroms can account for differences between the volume filling reinforcement prediction and measured values at lower volume concentrations. Some of the stiffening effects that were originally thought to be a result of particle interaction reinforcement were shown to be largely explained by physiochemical reinforcement. Also, viscosity-based stiffening ratios were found to be much larger that, but apparently related to, modulus-based stiffening ratios.

Uddin (1998) has carried out research related to micromechanical analysis method for calculating the creep compliance of asphaltic mixes on a microscopic level using laboratory viscoelastic characterization of the binder and elastic material properties of the aggregates at a given temperature. The micromechanical model was based upon the "method of cells" (MOC) previously developed in order to predict viscoelastic response of resin matrix composites. The properties of the aggregate were assumed to be linear elastic and could be described by the elastic constitutive relationship. The above micromechanical model has been incorporated in a microcomputer program ASPHALT which calculates the viscoelastic response of the mix and predicts the mix stiffness. The asphalt and polymer-modified asphalt mixes used on the I-55 rehabilitation project in northern Mississippi were analyzed and reasonably good agreement was found between the predicted modulus and measured modulus of the mix if proper percent air voids (4.4 to 6) are considered in the micromechanical model.

Deshpande and Cebon (1999) have developed a simple constitutive model using the "shear box" analogy from soil mechanics and theories for the deformation of nonlinear viscous composites, to characterize the steady-state deformation of idealized asphalt mixes under compressive stress loads by conducting triaxial compression tests, where both volumetric and

deviatoric strains were measured. The specimens were observed to dilate under compressive stresses and the deformation behavior was seen to be dependent on the mean as well as the deviatoric stresses. Also, predictions of the model were found to agree well with experimental measurements.

Weissman et al. (1999) studied rutting of asphalt concrete pavements, a critical distress mechanism, that typically occurs at elevated temperatures and slow loading rates under the action of heavy trucks. They proposed a concept called Representative Volume Element (RVE) that determines the minimum specimen dimensions required in laboratory testing (triaxial and shear) to obtain reliable and repeatable laboratory test data.

Smith and Hesp (2000) conducted research on crack pinning (fatigue) in asphalt mastic and concrete at relatively low temperature by using a series of model binder systems containing glass spheres with narrow particle size distributions and two mastic systems containing ground limestone fillers, which possessed significantly different gradations. Testing at various strain levels allowed the relationship between fatigue life and strain to be determined for the different systems. The results indicated that as the particle size of the filler decreases, the fatigue life of the asphalt mastic increases, while for asphalt concrete (limestone fillers) fatigue tests on both dense- and gap-graded systems the particle size did not significantly affect the fatigue life of the mixes. The results also confirmed that crack pinning is the major mechanism responsible for improved fatigue performance, as well as the interfacial bonding of polymer-modified bitumen to the surface of filler particles.

Anderson and Marasteanu (1999) performed a study on the physical hardening (aging) of asphalt binders, a reversible process that occurs below room temperature and causes time-dependent isothermal changes in the rheological behavior and specific volume of these materials.

They observed that the physical hardening has taken place, both above and below T_g (glass transition temperature) by using three different techniques: dilatometry, differential scanning calorimetry, and rheological considerations (peak in the loss modulus G" versus temperature), techniques which gave roughly equivalent estimates of this temperature. The behavior of physical hardening was explained in terms of the presence of crystalline fractions (wax) in the asphalt binder. The researchers also proposed some ways to model physical hardening based on stiffness ratio and stiffening rate.

Coree (1999) has proposed two charts for asphalt concrete design. The first chart provides a universal and simultaneous representation of all the secondary volumetric parameters (V_a, VMA, VFA) in linear form, while the second chart provides a quick and robust means of displaying all the primary volumetric parameters (Vv, V_b, V_s) simultaneously and allows for a more logical way to identify a design binder content and secondary volumetric parameters under the Superpave system. He also developed a simple graphical method that may be used to analyze, volumetrically, both Marshall and Superpave mix designs and as a point-estimate method to identify the binder content that will yield any given air void content.

Kose et al. (2000) have expected that although aggregates in asphalt mixtures undergo small strains under loading, most of the strain will accumulate within the binder. Taking into account that there is a difference of several orders of magnitude between the stiffness of aggregate and that for binder, they investigated the induced deformation under loading in asphalt mixes, which can result in a wide distribution of stresses and strains within each of the components. In their study, imaging techniques and high optical resolution scanning were applied in order to understand the distribution of binder and air voids in selected HMAs. From the analysis of selected mixtures, the strain in the asphalt mastic (containing mineral filler 40 μm

in size or smaller) varied widely, being as high as 85 times the bulk strain of the mixture, with an average value approximately 4.3 times the mixture bulk strain for the evaluated mixtures. From the analysis of the idealized (simulated) mastics, the binder strain was as high as 6 times the mastic strain with the average value of the binder strain being approximately 1.8 times the mastic strain. Their analyses indicated that the strain in the binder could range between an average of 7.8 times and a maximum of 510 times the bulk strain of the mixture and by considering the air voids (3 to 4 percent level) in the analysis there would be a reduction in the mastic strain, as well as a reduction in the resistance of the mix.

Shenoy and Romero (2001) have provided a standardized method by which various mixtures can be compared and their expected performance can be assessed in a uniform manner using the Superpave Shear Tester (SST). Based on the their findings, it resulted that complete mixture evaluation could be done through the Frequency Sweep at Constant Height (FSCH) data from the SST, without the need to generate the Repeated Shear at Constant Height (RSCH) data, fact which would reduce the experimental time without compromising the information obtained. The shear moduli versus frequency data from the FSCH at different temperatures were unified to form a single curve for each mixture so that a specification parameter T_S (°C) can be determined and each unified curve was fitted with a constitutive equation from which model parameters were evaluated. The slope B_1 in the low frequency region of the unified curve, when normalized with the term (T/T_S), resulted in a parameter that relates to the permanent strain (D_T) after 5000 cycles in RSCH at any temperature T. There is a good possibility that the slope B_2 in the high frequency region of the unified curve may relate to distresses in the intermediate temperature range, such as fatigue. If this is proven true through future research, then the Superpave Shear Tester could be considered a “simple performance tester.”

Shenoy (2002) has studied the possibility of using a rut-controlling parameter C_R as an identification tag to grade binders and rank their expected field performance in order to match the expected behavior of the binder with that of the mixture and thus, relate it to field performance. The development of this parameter was based on the refined specification term $G^*/(1-(1/\tan\delta\sin\delta))$, estimated from the material's volumetric-flow rate (MVR) through the use of a unification technique, at a high specification temperature T_{HS}. Shenoy (2002) has also shown that the permanent deformation data from the SST tests can be related to the rutting control term C_R, which is obtained from frequency sweep data measured from the DSR. Thus, where precision is required, C_R should be used, while the MVR could be used routinely for verification purposes of performance-graded asphalts.

Zhang et al. (2002) have done a comparative study of two relatively fundamental tests, Repeated Shear at Constant Height test (RSCH) and Repeated Load Confined Creep test (RLCC), and one simulative test, Asphalt Pavement Analyzer (APA) rut test, which also included a comparison and correlation of various parameters (permanent deformation or strain, slopes and intercepts from linear or power law regressions) from the tests. The analysis data showed that the two fundamental tests, RSCH and RLCC, had significant correlation with APA rut tests, with the rut depth being dependent on the initial deformation. Based upon the relationships obtained from their research, preliminary guidelines were recommended for evaluating rut resistance on the basis of APA rut depth. Compared with the existing APA criteria developed by Georgia DOT, the acceptable rut depth criteria generated from their study was found reasonable and applicable.

Anderson et al. (2002) have tried to quantify the repeatability of the measurement of shear stiffness (frequency sweep) and the measurement of permanent shear strain (repeated-load,

constant-height testing) by using the Superpave Shear Tester (SST). According to their data single laboratory precision (repeatability) of both the frequency sweep and repeated shear tests at constant height were comparable and reasonable at approximately 10%. However, multi-laboratory (four labs) precision (reproducibility) was much higher for the repeated shear test at constant height (70%) compared to the shear frequency sweep test (approximately 38%). Labs measuring shear modulus with a side-mounted LVDT had slightly lower G* (at 10Hz) values and slightly higher variability than labs measuring shear modulus with a platen-to-platen mounted shear LVDT. Statistical analysis indicated that determination of a critical temperature by curve-shifting produced equivalent results among the four labs, while shear stiffness values and permanent shear strain values at different temperatures varied significantly in some cases.

Zhao and Kim's (2002) objective was to check the validity of the time-temperature superposition principle for hot-mix asphalt (HMA) with growing damage and viscoplastic strain in the compression state, which is essential for the permanent deformation characterization of HMA. Constant crosshead rate compression tests were conducted at temperatures between 25 and 55°C, and data were analyzed to construct the stress-log reduced time master curves for various strain levels. Research results indicated that HMA with growing damage remains thermo-rheologically simple (TRS) in the temperature range used in the study, and that the time-temperature shift factor is only a function of temperature and is independent of the strain level. Two types of tests, the repeated creep and recovery test and the cyclic sinusoidal loading test, were performed in their study to validate the time-temperature superposition in loading histories commonly used in asphalt mixture testing. The results further confirmed that the time temperature superposition was valid for HMA with growing damage and permanent deformation and that the response of HMA only depends on the reduced loading history.

Vacin et al. (2002) have used commercial rheometers for comprehensive testing of polymer modified asphalt binders, asphalt mastics and hot mix asphalts (HMA). Samples of each material were tested with the Dynamic Shear Rheometer (DSR) and the Bending Beam Rheometer (BBR) and were characterized by their discrete relaxation and retardation spectra (under the condition of small deformations). From the obtained relaxation and retardation spectra the shear compliance J(t) was calculated and compared with the tensile creep compliance, D(t), measured in BBR (both creep and recovery experiments were run). A simple relation between J(t) and D(t) was found for the asphalt binder and asphalt mastic. In the case of HMA the bulk compliance, B(t), contributed to D(t) at short and long times. Both the Boltzmann superposition principle and the time temperature superposition principle held for all tested materials, at low temperatures, very well, but qualitative differences were found, in the rheological behavior of the asphalt binder and asphalt mastic on one side, and the HMA on the other, both in dynamic (DSR) as well as in transient (BBR) experiments.

Antes et al. (2003) research has focused on the determination and the modeling of the stress dependent behavior of asphalt mixtures at high temperatures. It is known that most of the road engineering materials have a stress dependent behavior, their behavior being especially influenced by the magnitude of the confining stresses. For their study five different types of asphalt mixtures were subjected to a triaxial testing program in which the specimens were tested at various stress conditions, temperatures and loading frequencies. The results of the testing program were used to model a resilient modulus - M_r - of the mixtures as a function of the applied stresses. It appeared that a simple model could be developed that showed the dependency of the resilient modulus on the confining stress and was determined that the effects were not negligible since the M_r values obtained from the experimental program were significantly

different from the values determined using well known nomographs and equations to predict the M_r, or stiffness, value. Also ample attention was paid to the stress dependency of the Burger model parameters, which is often used to describe the viscoelastic behavior of asphalt mixtures for design analyses. Axial strains calculated by means of the Burger model were fitted to the measured axial strains and when the best fit was obtained, the values for the Burger's parameters that were used to obtain that fit were taken as the true values for those parameters. The analyses showed that most of the Burger's parameters were stress dependent and also some unexpected frequency dependency was observed. The results of the Antes et al. (2003) experimental program are now used to predict the permanent deformation of some accelerated pavement test sections which were already tested and which were made of the same asphalt mixtures.

Bahia et al. (2003) have considered the Superpave Gyratory Compactor (SGC) as one of the best means to capture performance related properties of mixtures or aggregate blends for mixture design. Their research was an attempt to utilize the gyratory compactor to measure the mixture resistance to densification and distortion, measurements that were used to estimate quality of aggregate structure. They also used the gyratory compactor to evaluate the potential of an aggregate blend to resist traffic loading, as well as to resist compaction during construction, approach that allows the volumetric properties to play only a partial role in selecting components and adds mechanical properties to the selection of the design blend and asphalt content. The study also covered the matter of using the DSR results to compliment the mixture design procedure by using the Creep and Recovery binder testing and the binder fatigue testing results as recommended by the NCHRP 9-10 project. Unfortunately, their criteria were not validated, but were proposed as a starting point for a new conceptual mixture design approach.

Christensen et al. (2003) have proposed to present a new, rational and effective model for

estimating the modulus of asphalt concrete using binder modulus and volumetric composition. Their model was based upon an existing version of the law of mixtures, called the Hirsch model, which combines series and parallel elements of phases. In applying the Hirsch model to asphalt concrete, the relative proportion of material in parallel arrangement, called the contact volume, is not constant but varies with time and temperature. Several versions of the Hirsch model were evaluated, included ones using mastic as the binder, and one in which the effect of film thickness on asphalt binder modulus was incorporated into the equation. The most effective model was the simplest, in which the modulus of the asphalt concrete is directly estimated from binder modulus, VMA, and VFA. Models were presented for both dynamic complex shear modulus (G*) and dynamic complex extensional modulus (E*), along with semi-empirical equations for estimating phase angle in shear and in extensional loading. Their proposed model was verified by comparing predicted modulus and phase angles to values reported in the literature for a range of mixtures.

Pellinen et al. (2004) investigated existing fatigue models (originally developed for predicting crack initiation) and how they relate to mixture volumetrics, and which of several fatigue transfer functions predict the failure of mixtures and expected fatigue life most accurately. Their work was done by employing layered elastic analysis to obtain stresses and strains in the pavement under monthly temperature variations and the calculated tensile strains were used in the fatigue transfer functions to predict the fatigue life of the pavement. The mix and distress data was obtained from the WesTrack project (Nevada) and all fatigue model predictions were poor to fair, with the SHRP model showing highest accuracy (72%) and the Shell models showing lowest accuracy (28%). This analysis indicated that there was a trade-off in predicting failing or surviving mixtures correctly and the accuracy of predicting fatigue life

(N_f) compared to the applied traffic loading. For several reasons, Pellinen (2004) recommended using the Asphalt Institute fatigue transfer equation in Layered Elastic analysis to evaluate the fatigue cracking potential of asphalt mixtures.

Christensen and Bonaquist (2005) investigated recent research providing guidelines for establishing the design of voids in mineral aggregate (VMA) values, high enough to ensure good durability while still achieving superior rut resistance. Because of the perceived increase in surface cracking and raveling, many pavement engineers feel that asphalt concrete mixtures have become too lean, that is, the voids in mineral aggregate (VMA) and effective binder content by volume (VBE) are too low for adequate fatigue resistance and durability. Unfortunately, there is substantial evidence that increasing VMA and VBE can decrease the rut resistance of asphalt concrete pavements. Researchers found out that to ensure adequate fatigue resistance, the minimum VMA values for mixtures designed according to the Superpave system should be increased by 1 % over current recommended minimums, while in cases where design air void content is allowed to vary from 4 %, the implied minimum effective binder content (VBE) should also be increased 1 % and enforced in addition to minimum VMA values. Because of severe exposure to the effects of traffic loading and the elements, wearing course mixtures and rich base course mixtures should have a minimum VMA of 16 % and a minimum VBE of 12 %, regardless of nominal maximum aggregate size. Also, adequate rut resistance can be achieved regardless of VMA by making certain that the proper binder grade is selected for a given application and that the aggregate blend contains sufficient fines relative to the mix design. Adequate fineness will also help keep the permeability of in-place mixtures low. Although some variability in VMA is inevitable during field production, plant personnel should strive to keep overall VMA levels close to design values.

CHAPTER 3. ASPHALT BINDER AND MASTICS EXPERIMENTAL PROGRAM

This chapter provides information on the materials and procedures used for the production of asphalt mastics in the laboratory, and a detailed description of the testing procedures and instrumentation.

3.1 Usage of Asphalt Binders in the United States

Construction and maintenance costs for the U.S. roadway infrastructure are approximately $100 billion/year, about 1 percent of the U.S. gross domestic product, and asphalt paving is the largest component of this cost, representing about 20 percent of the total (Zhang et al., 2002). About 95 percent of the paved roads in the United States are surfaced with asphalt, and most are produced using hot-mix construction. The asphalt binder functions as an inexpensive (typically, $0.05/pound), waterproof, thermoplastic adhesive. In other words, it acts as the glue that holds the road together. In its most common form, asphalt binder is simply the residue from petroleum refining, which, in order to achieve the necessary properties for paving purposes, it must be produced from a carefully chosen crude oil blend, and processed to an appropriate grade (Atkins, 2003). For a few applications, additives (usually polymers) are blended or reacted with the binder to enhance its properties.

Asphalt binders are produced mainly by petroleum refiners and, to a lesser extent, by formulators who purchase blending stock from refiners. As a result of the new Superpave specifications, both phases of production require increased logistical control and greater attention to quality. Although changes in the refining phase have been relatively minor during the last years, changes in the formulation phase have been substantial and have been driven, in part, by the wide range of binder grades required by the Superpave system which enables binder

performance to be closely matched to climatic conditions (Bahia et al., 2003). For example, binders necessary for severe climate regions cannot be made from crude oil alone; they must be modified, modification which improves the properties and increases the cost of the binder. The implementation of the Superpave system has increased the use of unconventional binder additives, air blowing, blending, and chemical modification, changes that will challenge the asphalt pavement industry to show that binders produced by different means to similar specifications can perform equally well. As the relationship between binder properties and mixture performance is better understood, the specifications will continue to evolve. New and more cost-effective modification technologies will be developed, and the use of custom blending and modification will increase. In return, these trends will cause additional supply changes, as binder producers seek to match their strategic resources and interests with the most appropriate demands in the asphalt market.

3.2 Performance Graded (PG) Binder Specifications

The new system (PG) for specifying asphalt binders is unique in that it is a performance based specification. It specifies binders on the basis of the climate and attendant pavement temperatures in which the binder is expected to serve (Dongre et al., 2004). Physical property requirements remain the same for the different grades, but the temperature at which the binder must attain the properties changes. Performance graded (PG) binders are graded for the high end and low end temperatures for example PG 64-22. The first number, 64, is often called the "high temperature grade." This means that the binder would possess adequate physical properties to resist rutting at least up to 64°C. This would be the high pavement temperature corresponding to the climate in which the binder is actually expected to serve. Likewise, the second number (-22) is often called the "low temperature grade" and means that the binder would possess adequate

physical properties to resist thermal cracking at least down to -22°C. Another key feature to binder evaluation in the Superpave system is that physical properties are measured on binders that have been laboratory aged to simulate their aged condition in the field. Some binder physical property measurements are performed on unaged binder. Physical properties are also measured on binders that have been aged in the Rolling Thin Film Oven (RTFO) to simulate oxidative hardening that occurs during hot mixing and placing and in the Pressure Aging Vessel (PAV) to simulate hardening in service that could be expected after a few years in place (Jiang et al., 1996).

3.3 Asphalt Binder Used in the Study (PG64-22)

Asphalt binder PG64-22 was selected for this study, which is a commonly used binder in Louisiana. PG64-22 is a Performance Grade (PG) asphalt cement based on two factors: traffic and pavement temperature, and has to conform to the requirements of AASHTO MP-1 (Standard Specification for Performance Graded Asphalt Binder). A summary of the AASHTO MP-1 specification is given in Table 3.1. Adjustments are made to the PG grade of asphalt cement based on traffic conditions and traffic volumes which are intended to enhance the design life of the pavement, all adjustments being made in six (6) degree increments. The high temperature of the asphalt binder relates to the effects of rutting while the low temperature relates to the fatigue cracking.

Personnel must be trained in the proper handling of PG64-22 and provided the information contained in the Material Safety Data Sheet (MSDS). The LADOT specifications state PG64-22 asphalt at hot mix plants may be heated to a maximum temperature of 177°C (350°F). However, the preferred storage temperatures for PG64-22 are 140°C to 168°C (285°F to

335°F), whilst unnecessarily high temperatures result in increased hardening and heating costs. More characteristics of the binder are to be found in **Appendix A**.

Table 3.1 Summary of AASHTO MP1 Requirements (Zaniewski and Pumphrey, 2004)

Test	Performance Parameter	Asphalt Binder Condition State	Specification	Specification Limit	Test Temp.[1] °C
RV	Flow ability	Neat	Viscosity	3 Pa.s	135
DSR	Rutting resistance	Neat	G*/sinδ @ 10 rad/sec	1.0 kPa (Min)	High
DSR	Rutting resistance	RTFO-aged	G*/sinδ @ 10 rad/sec	2.2 kPa (Min)	High
DSR	Fatigue cracking resistance	PAV aged[2]	G*sinδ @ 10 rad/sec	5000 kPa (Max)	Intermediate
BBR	Thermal cracking resistance	PAV aged[2]	Creep Stiffness, S @ 60 sec.	300 Mpa	Low+10°C
			m-value @ 60 secv.	0.300	Low+10°C
DTT	Thermal cracking resistance	PAV aged[2]	Failure Strain @ 1.0mm/min	1.0%	Low+10°C

PG64-22 is primarily used in paving for both new construction and pavement rehabilitation and in both dense-graded and open graded Hot Mix Asphalt (HMA). This product could also be used for sealing of edges of new to old paving and crack sealing. Other uses include spray applications for bridge deck and pavement protective membraning with fabrics. It has been reported that with proper aggregate characteristics and asphalt content, HMAs with PG64-22 as the binder may exhibit less tenderness than a similar mixture with a lower viscosity/softer asphalt. The typical tenderness problems of mixture shoving and checking during rolling and pavement surface scuffing and marking by traffic immediately after paving may be noticeably reduced. The use of proper mixing temperatures for a PG asphalt like PG64-22 is not only important to achieving adequate asphalt coating and mix compaction, but also to the asphalt

hardening and pavement properties. Therefore, it is important to consider the mixing temperatures recommended in the mix design or by the asphalt supplier.

3.4 Asphalt Rheology

Asphalt binders deform when subjected to loads and their properties also change with varying temperatures. The deformation is a combination of elastic response and viscous flow (Lay, 1990). The magnitude of deformation, or mechanical response, is dependent on load magnitude, duration, and rate of application and the temperature state of the material (Peterson et al., 1999). Since asphalt binders display both elastic and viscous response properties, they are classified as viscoelastic materials. The typical elastic, viscous, and viscoelastic responses to an applied stress is shown in Figure 3.1. An elastic material experiences recoverable deformation when subjected to a constant (or creep) load, Figure 3.1a, and will immediately deform and maintain a constant strain when loaded, as in Figure 3.1b. Also, the material will immediately return to its initial shape when the creep load is removed. A viscous Newtonian material, when subjected to a constant load, will deform at a constant rate until the load is removed, like in Figure 3.1c. The deformation of the viscous material, however, will remain after the load is removed; hence, a viscous material experiences non-recoverable deformation.

A viscoelastic material, when subjected to a creep load, experiences an immediate deformation followed by a continued time-dependent deformation (Kim et al., 2003), as shown in Figure 3.1d. The immediate deformation corresponds to the material's elastic response and the time-dependent deformation corresponds to the material's viscous response. Once the load is removed, the viscous deformation component immediately ceases, but this deformation is not recovered. The delayed elastic deformation component is slowly recovered at a decreasing rate. Thus, a viscoelastic material experiences only a partial recovery of the deformation resulting

from creep loading (Roberts et al., 2002). The viscoelastic behavior of asphalt can be characterized by its deformation resistance and the relative distribution of that resistance between the elastic component and the viscous component within the linear range (Kern and Carpenter, 1999). The relative distribution of the resistance between the elastic component and the viscous component is dependent on the asphalt cement characteristics and temperature and loading rate. The previous loading-response descriptions are for responses within the linear range, which is characterized by the deformation being directly proportional to the applied load at any time and temperature. Nonlinear loading responses are difficult to model for viscoelastic materials such as asphalt. Linear response models, however, are sufficient for the engineering analysis of asphalt binder response to the loading conditions and environmental stresses encountered in the field.

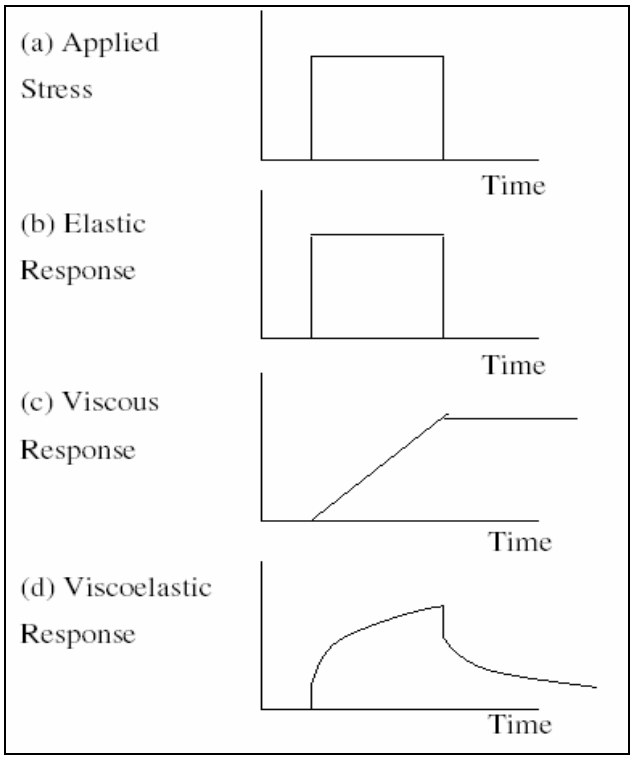

Figure 3.1 Mechanical responses of elastic, viscous, and viscoelastic materials (FHWA, 1995).

3.5 Asphalt Modifiers (Mineral Fillers)

Generally, the aggregate material passing the 0.075 mm (No. 200) sieve, also called P200 material, has been called filler (Smith and Hesp, 1998; Kim and Little, 2003). The filler, as one of the bituminous mixture ingredients, plays a major role in determining the properties and the behavior of the mixture. On one hand, the filler serves as an inertic material for filling the voids between coarser aggregate particles in the mixture. Conversely, because of its fineness and surface characteristics, the filler also serves as an active material. The activity of the filler is expressed in the physicochemical properties at the interface between the filler and the bitumen. Most research and practical knowledge on the effect of the filler in bituminous mixtures are mainly based on engineering properties of the filler: gradation, filler content, weight-volume relationships, and so forth, while most expressed relationships between these properties and the behavior of the mixture are basically empirical. On the other hand, only a few research works have been dedicated to investigating the physicochemical properties at the filler-bitumen interface: geometric characteristics, surface properties, adsorption, adhesion, and so forth. These properties have direct and significant influence on the interface properties in filler-bitumen systems and on the behavior and durability of the bituminous mixture.

For this study, three mineral fillers were selected: Donna Fill, Limestone and Granite, and they all were obtained from the Louisiana Transportation Research Center (LTRC), which uses them in various asphalt concrete projects. They can be found abundantly in aggregates used for hot mix asphalt. Usually, the effects of Donna Fill and granite as compared to natural sands for fine aggregate in asphalt mixtures demonstrated an increase in mixture stability, thicker film thickness retained and a reduction in rutting and stripping susceptibility.

Modifications made to hot mix asphalt with limestone might add years to its life, because these modifications can reduce stripping, rutting, cracking, and aging (Hand et al., 2001). Limestone substantially improves each of these properties when used alone, and also works well in conjunction with polymer additives, helping to create pavement systems that will perform to the highest expectations for many years. Life cycle cost analysis demonstrated that limestone is also cost-effective.

Some properties of the above mentioned materials are presented in Table 3.2.

Table 3.2. Properties of fillers (Waltham, 2002)

Type of Filler	Donna Fill	Limestone	Granite
Specific Gravity	2.67	2.76	2.85
Plasticity Index	Non-plastic	Non-plastic	Non-plastic
Specific Surface Area (cm^2/ml)	NA	6768	7206
Angularity Index	0.624	NA	NA
Bulk Density (kg/m^3)	1080	1116	1215
Modulus of Elasticity E (GPa)	57	65	75

Also, the gradations of the mineral fillers, based on the use of the bag-house, used in this study are presented in Figure 3.2.

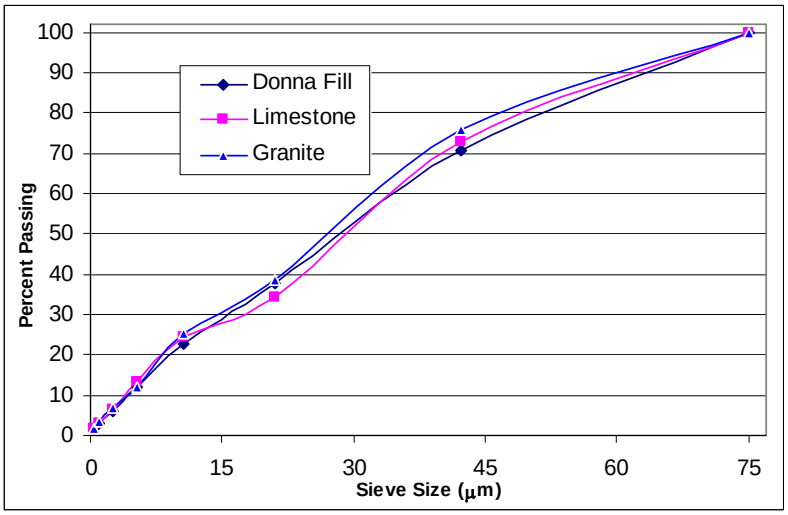

Figure 3.2 Gradation of the mineral fillers (Chen, 1996).

3.6 Asphalt Mastics

In asphalt mixtures, the asphalt cement (binder) occurs not as asphalt alone, but is intimately mixed with mineral fillers forming a new material called asphalt **mastic**. Such a distribution points to the important role played by the mastic in the workability and performance of asphalt concrete (Deshpande and Cebon, 1998). Mixtures of asphalt binder and filler or mastics are often assumed to behave as simple viscoelastic materials or simply, binders stiffened by filler. Stiffening of asphalt binder is only one way in which the addition of mineral filler changes the properties of this material.

In fact, mastics behave quite differently than simply stiffer binder. Asphalt filler mastics are time dependent - they flow with time - hence, they are considered rheological materials. The properties of these materials are also temperature dependent, thus, both loading times and test temperatures must be taken into account when characterizing the flow behavior of asphalt filler mastics. In this research, mastics were obtained by combining the asphalt binder PG64-22 with the three mineral fillers enumerated above - Donna Fill, Limestone, and Granite in five percentages - 5, 10, 15, 20, and 30% by volume.

3.7 Dynamic Shear Rheometer (DSR)

3.7.1 General Presentation

As presented earlier, asphalt and mastic are viscoelastic materials, meaning that they simultaneously show the behavior of an elastic material (e.g. rubber band) and a viscous material (e.g. molasses). The relationship between these two properties is used to measure the ability of the binder/mastic to resist permanent deformation and fatigue cracking. To resist rutting, a binder/mastic needs to be stiff and elastic; to resist fatigue cracking, they need to be flexible and elastic. The balance between these two needs is a critical one.

Also, asphalt concrete pavements can be prone to wheel path rutting in the early stages of their life. Repeated traffic loads increase the consolidation of the pavement structure after construction, thus causing depressions in the traffic wheel paths. Traffic induced rutting can also result from the lateral flow of the asphalt concrete materials in the wheel paths. Although the rutting potential of asphalt concrete pavements is influenced primarily by the quality of construction (compaction), mix design, and aggregate angularity and texture, the consistency of the binder and/or mastic must still be considered. Rutting is more prevalent at high service temperatures due to the increased fluidity of the asphalt, and the rutting potential of HMA pavements decreases with time since the asphalt binder stiffens with age hardening.

For this research, the Dynamic Shear Rheometer (DSR) was used to characterize the viscous and elastic behavior of asphalt binder/mastics at intermediate and high service temperatures. This was done by measuring the viscous and elastic properties of thin asphalt binder and mastic samples sandwiched between an oscillating and a fixed plate. Operational details of the DSR will be presented later in this chapter.

3.7.2 Summary of Method

The viscoelastic properties of asphalt are determined by evaluating the behavior of an asphalt specimen when subjected to oscillatory (sinusoidal) stresses. The AASHTO TP5 standard test method requires that a thin asphalt specimen be sandwiched between two parallel metal plates held in a constant temperature medium. One plate remains fixed while the other oscillates, at different angular frequencies with respect to the other, like shown in Figure 3.3. The Dynamic Shear Rheometer evaluates the specimen's response to the sinusoidal stresses and calculates several parameters of the asphalt, such as complex shear modulus, dynamic viscosity, phase angle, accumulated strain, etc.

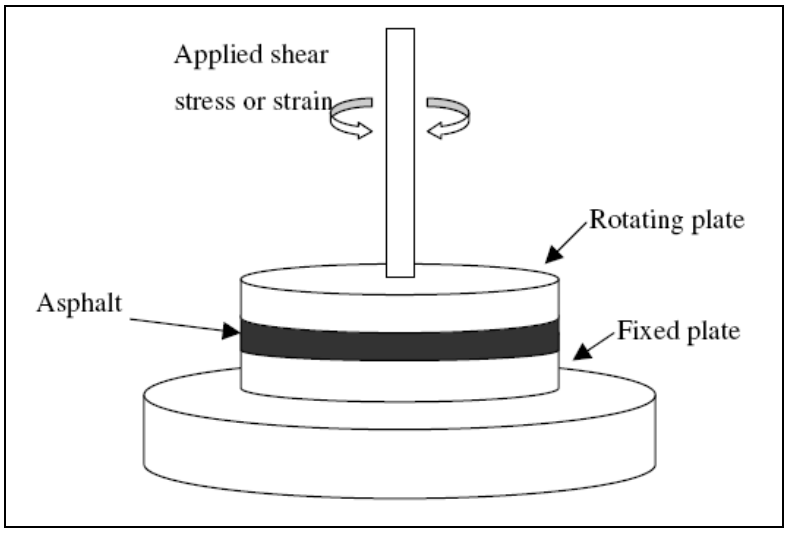

Figure 3.3 Schematic configuration and loading mode of DSR (Zaniewski, 2004).

The complex shear modulus, phase angle, and accumulated strain of a binder or mastic, which are indicators of the asphalt's resistance to shear deformation in the viscoelastic region, help predict the rutting potential and fatigue life of hot mix asphalt pavements (Kose et al., 2000).

3.7.3 Testing Equipment

The apparatus used for the testing of asphalt binder and mastics was a Bohlin Instruments® Automated Dynamic Shear Rheometer (ADSR) (Figure 3.4), a modular rheometer that offers users even greater flexibility than the common DSRs. This automated rheometer is capable of measuring asphalt response over a large range of temperatures, frequencies, and strain levels. However, G* (dynamic shear modulus, Pa) and δ (phase angle, degree), two important asphalt properties required by Superpave system, are calculated by the DSR software. Therefore, it is a simple matter of comparing results with requirements of the Superpave specification to determine compliance. The two parameters presented above will be described in detail later on in this chapter.

Figure 3.4 Automated Dynamic Shear Rheometer (ADSR) (Walton, 2000).

Some parameters that are reported by the apparatus (ADSR) include:

- G* to the nearest three significant figures,
- δ to the nearest 0.1 degrees,
- test plate size to the nearest 0.1 mm and gap to nearest 1μm,
- test temperature to the nearest 0.1° C,
- test frequency to the nearest 0.1 rad/sec, and
- strain amplitude to the nearest 0.001 percent.

The ADSR system includes the actual rheometer, temperature controller, data acquisition unit and a personal computer. The rheometer itself consists of a loading assembly, motor, load and strain transducer, parallel plates (an upper oscillatory spindle plate and a lower fixed plate) and an environmental control chamber with a Resistance Thermal Detector (RTD) mounted

inside. There are two types of dynamic shear rheometers: controlled stress and controlled strain. The controlled stress rheometers apply a sinusoidally varying stress and determine the resulting strain, while the controlled strain rheometers apply a sinusoidally varying strain and determine the resulting stress.

The ADSR uses two different sized parallel plate sets for evaluating asphalt binder: 8-mm diameter plates and 25-mm diameter plates. The 25-mm plates are used with unaged (unheated) or Rolling Thin Film Oven (RTFO) aged asphalt specimens when evaluating the rutting resistance parameter. The 8-mm plates are used with Pressure Aging Vessel (PAV) aged asphalt specimens when evaluating the fatigue cracking resistance parameter. Silicone molds are available for making asphalt test specimens for use with both the 25-mm plates and the 8-mm plates. The environmental chamber houses the parallel plates, a platinum resistance thermometer, the test specimen and the medium (water in this case) used for heating or cooling the asphalt specimen.

Because the properties of asphalt binders and mastics are so temperature dependent, rheometers have a precise means of controlling the temperature of the sample. This is normally accomplished by means of a circulating fluid (water) bath, which normally surrounds the test specimen. The water is circulated through a temperature controller that precisely adjusts and maintains the sample temperature uniformly at the desired value during the entire testing period.

The data acquisition unit records the test temperature, applied load, frequency and deflection angle during the entire testing and sends the test data to the personal computer. The computer software reduces the data and calculates the shear stress, shear strain, complex modulus, phase angle, dynamic viscosity, and other parameters required by a specific project.

3.7.4 Asphalt Binder and Mastic Specimen Preparation

In the case of asphalt binder, this is heated in the oven at around 150 °C until fluid enough to pour. Then the heated asphalt is poured into a silicone mold (25 mm in diameter) (Figure 3.5) and allowed to cool until solid enough to be removed from the mold.

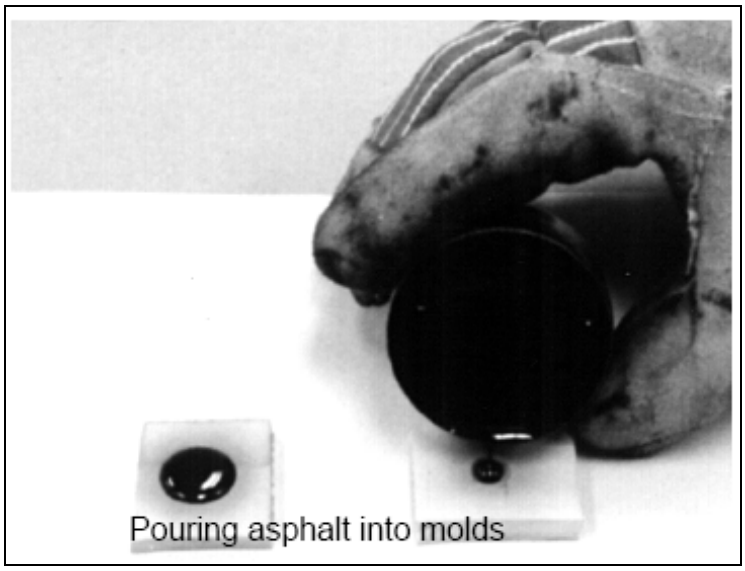

Figure 3.5 Preparing asphalt specimens for the DSR testing (FHWA, 1995).

After removal from the mold, the asphalt disk is placed between the fixed plate and the oscillating spindle of the DSR for testing, as shown in Figure 3.6.

In preparing the mastic samples, the fillers were heated for one hour in the oven at 150 °C in order to simulate the conditions during processing in the hot mix facility. Before mixing, the binders were also heated at 150 °C for 20 minutes in small containers, in order for both materials to be at the same temperature. Mixing was done for ten minutes by slowly adding the filler to the asphalt, while being stirred with a small mechanical mixer to ensure good homogeneity. Each filler was added in five volume fractions - 5, 10, 15, 20, and 30%, thus fifteen types of mastics being obtained for future testing.

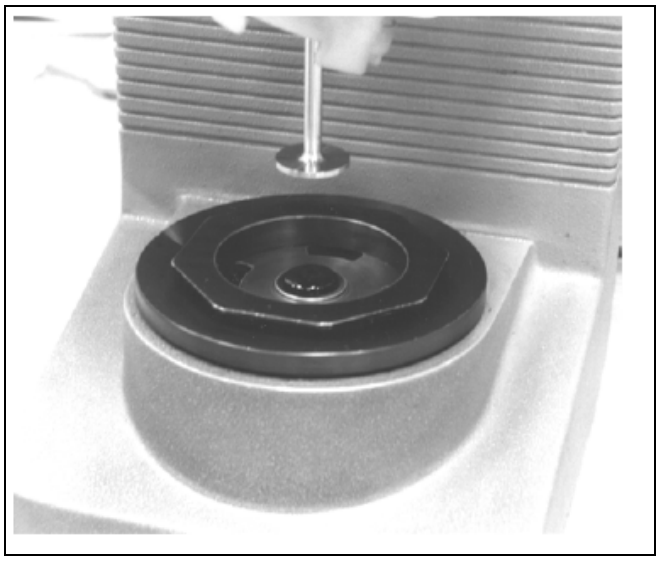

Figure 3.6 Asphalt binder sample placed on the fixed platen of the ADSR (FHWA Superpave, 1995).

In order to obtain mastic samples the hot mixture was poured into same silicone molds (25 mm in diameter) and allowed to cool until solid enough to be removed from the mold and tested with the DSR.

3.7.5 Testing Procedure

AASHTO TP5-98 "Standard Test Method for Determining the Rheological Properties of Asphalt Binder Using a Dynamic Shear Rheometer (DSR)" defines the protocol for conducting the dynamic shear rheometer test. The test temperature is set, as per AASHTO MP1 criteria, and depends on the asphalt type and the performance parameters that need to be measured. For rutting resistance evaluation - this research - neat and RTFO-aged asphalt binders are tested at high service temperatures. Test temperatures range, depending on the performance grade of asphalt, from 46 °C to 82 °C and the appropriate platen size selected is 25 mm in diameter. The gap between the upper and lower platens is then set, which represents a critical test parameter. The accuracy of the gap measurement is directly related to the accuracy of the asphalt/mastic

specimen evaluation. A micrometer wheel is used to measure the gap between platens (i.e. when the micrometer wheel is set on 1 mm and the upper platen is fully lowered, a 1-mm gap will be maintained between the platens). A gap measurement verification procedure, called setting the zero gap, must be conducted to ensure that the micrometer reading and the actual gap between the platens is the same. The zero gap is set by lowering the upper platen in small increments until the upper and lower plates just touch, or reach zero gap. The micrometer wheel is then set to zero, when zero gap between the platens have been achieved. Before setting the zero gap, the temperature controller is turned on and the environmental chamber is preheated, or cooled, to the desired test temperature. The zero gap is then set after the medium surrounding the platens stabilizes at that temperature.

The thickness of gap used depends on the test temperature and the aged condition of the asphalt binder. For this study, due to the fact that the binder was unaged and test temperatures were greater than 46 °C, the required gap was of 1000 microns (1 mm). With the asphalt specimen properly placed on the fixed platen, the upper platen is lowered to squeeze the asphalt specimen between them. The upper plate is lowered such that the gap between the two plates is 0.05 mm greater than the test gap (which is 1 mm).

The excess asphalt that is squeezed from between the platens is removed by trimming around the periphery of the platens, as shown in Figure 3.7.

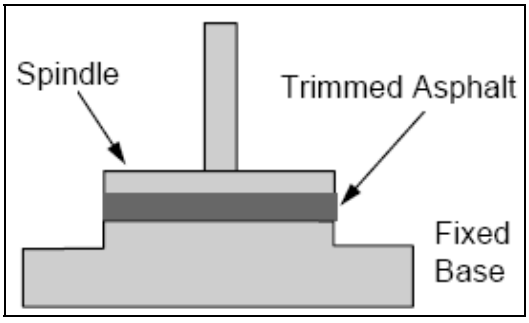

Figure 3.7 Trimmed asphalt binder specimen (Zaniewski, 2004).

The upper platen is then lowered to the test gap and the asphalt or mastic specimen should slightly bulge around the periphery of the plates like in Figure 3.8.

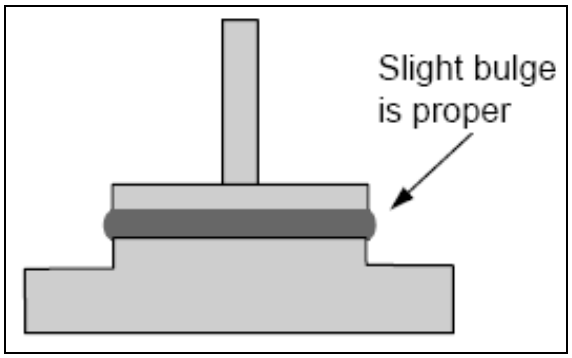

Figure 3.8 Proper asphalt binder bulge between the platens (Zaniewski, 2004).

3.7.6 DSR Analysis Theory

Due to the fact that the Dynamic Shear Rheometer (DSR) evaluates the asphalt binder properties at intermediate to high temperatures, its response has to be in the viscoelastic range, thus viscosity measurements alone are not sufficient to characterize its behavior (Shashidhar, 1998). Binder properties need to characterize its resistance to deformation and the relative distribution of the resistance between the elastic component and the viscous component. For this reason, dynamic, or oscillatory testing is a common technique for evaluating viscoelastic behavior.

The DSR evaluates the behavior of an asphalt specimen by subjecting it to oscillatory (sinusoidal) stresses. A thin asphalt specimen is sandwiched between two parallel metal plates held at a constant temperature medium, with one plate being fixed while the top one (spindle) oscillates, at different angular frequencies ω (rad/sec) with respect to each other. A DSR loading cycling is shown in Figure 3.9.

When torque from the DSR motor is applied, the oscillating platen moves from point A to point B.

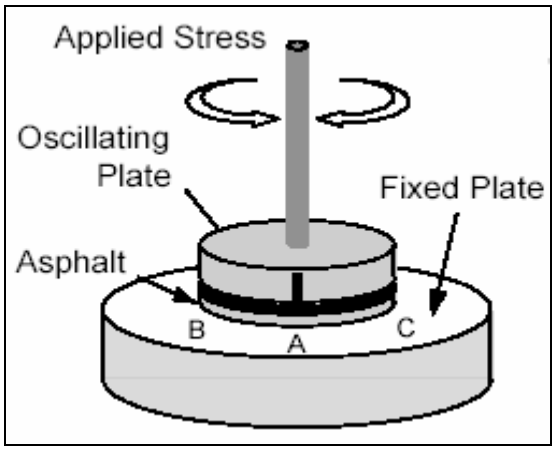

Figure 3.9 Dynamic load induced by the DSR (Walton, 2000).

The platen then moves back through point A to point C. The cycle of oscillation is completed as the platen goes back through point A again like in Figure 3.10 below.

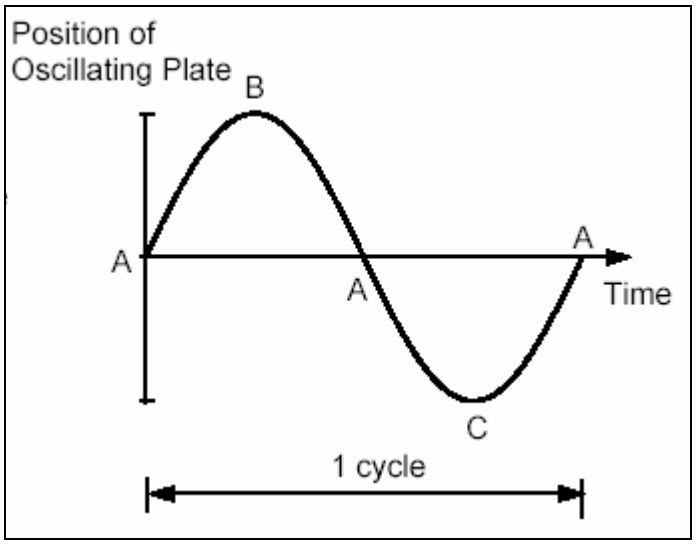

Figure 3.10 Complete cycle of the DSR "spindle" (Zaniewski, 2004).

Dynamic testing provides an indication of a binder's resistance to deformation and the elastic/viscous component distribution by determining the binder's complex modulus G* and phase angle (δ) (Anderson et al., 1999). The shear complex modulus, G*, commonly referred to as G star, represents the total deformation resistance when repeatedly sheared. The complex

modulus is defined as the ratio of the absolute value of the peak-to-peak shear stress to the absolute value of the peak-to-peak shear strain:

Complex Shear Modulus

$$G^* = \frac{|\tau_{max} - \tau_{min}|}{|\gamma_{max} - \gamma_{min}|} \quad [Pa] \tag{3.1}$$

with τ_{max} and γ_{max} having the following expressions:

$\tau_{max} = \frac{2T_{max}}{\pi r^3}$ [Pa]; $\gamma_{max} = \frac{\theta_{max} r}{h}$, where:

τ_{max} = absolute value of the peak-to-peak shear stress [Pa]

γ_{max} = absolute value of the peak-to-peak shear strain [%]

T_{max} = maximum applied torque (load) [Pa]

r = radius of specimen plate [mm]

θ_{max} = maximum deflection angle [rad]

h = specimen height [mm]

The phase angle, δ, represents the relative distribution between the elastic response and the viscous response to loading (Basu et al., 2003) of the asphalt binder and/or mastic. The phase angle indicates the delayed strain response, or lag, of the binder/mastic to the applied shear stress, during steady state conditions. A graphical description of the phase angle with respect to time, applied shear stress, and shear strain is shown in the following figures.

For the elastic response, Figure 3.11, the shear strain sinusoidal curve mirrors the applied shear stress sinusoidal curve at all points, and the time lag between the two parameters would be zero. It can be said that the shear strain is "in-phase" with the applied shear stress. For the viscous response, as shown in Figure 3.12, there is a gradual large strain response to the applied shear stress, due to the fact that the strain response has not yet reached steady state conditions.

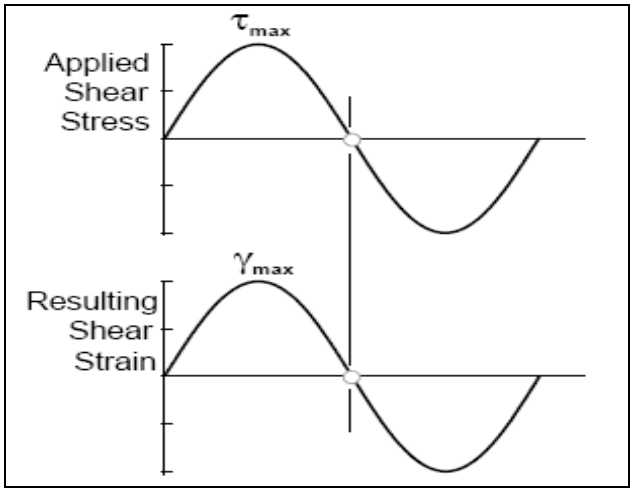

Figure 3.11 Elastic response of the asphalt binder (δ = 0 deg) (FHWA Superpave, 1995).

Hence, at all points from the steady state position the strain response has a consistent time lag of equal duration from the applied shear stress. Thus, the strain response has reached steady state conditions and is "out-of-phase" with the applied shear stress. Usually, very cold asphalt performs like an elastic material, while very hot asphalt performs like a viscous material.

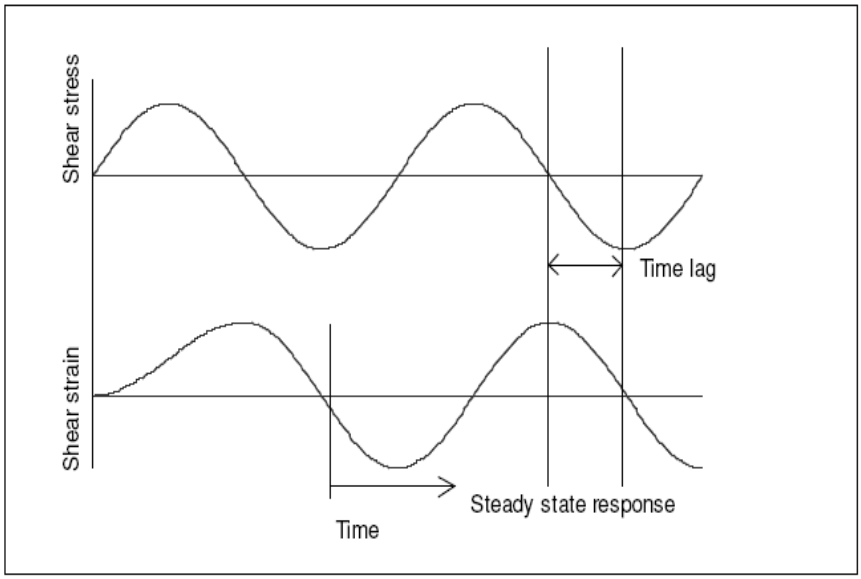

Figure 3.12 Viscous response of the asphalt binder (δ = 90 deg) (Zaniewski, 2004).

The time lag at steady state conditions can be represented graphically as a 90° shift between the maximum applied shear stress and the maximum shear strain. Thus, the strain response of a viscous material is 90° "out-of-phase" with the applied shear stress, Figure 3.12, therefore, the phase angle (δ) is 90 degrees. Conversely, there is no time lag between the applied shear stress and resultant strain response of an elastic material (Figure 3.11) therefore, the strain response is "in-phase" with the applied shear stress and the phase angle (δ) is zero degrees. We can say now that the phase angle δ is the product of the time lag and the frequency, as shown in the next equation.

$$\delta = \Delta t \times \omega \tag{3.2}$$

where:

Δt = time lag (s)

ω = angular frequency (rad/sec)

In the DSR, a viscoelastic material such as asphalt at normal service temperatures displays a stress-strain response between the two extremes, as shown in Figure 3.13 below.

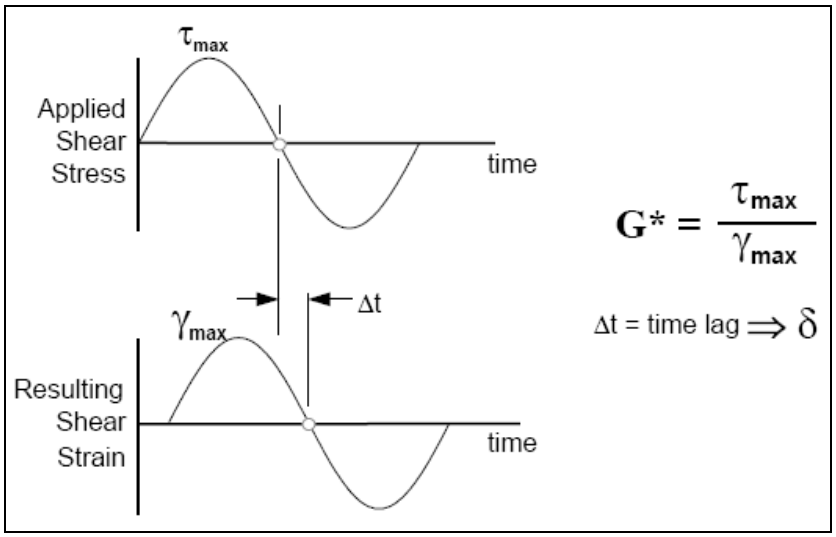

Figure 3.13 Viscoelastic behavior of the asphalt binder ($0 < \delta < 90°$) (FHWA, 1995).

The shear complex modulus (G*) consists of two components: one is the storage modulus, G' and the other is the loss modulus, G", as will be shown in Figure 3.14 below.

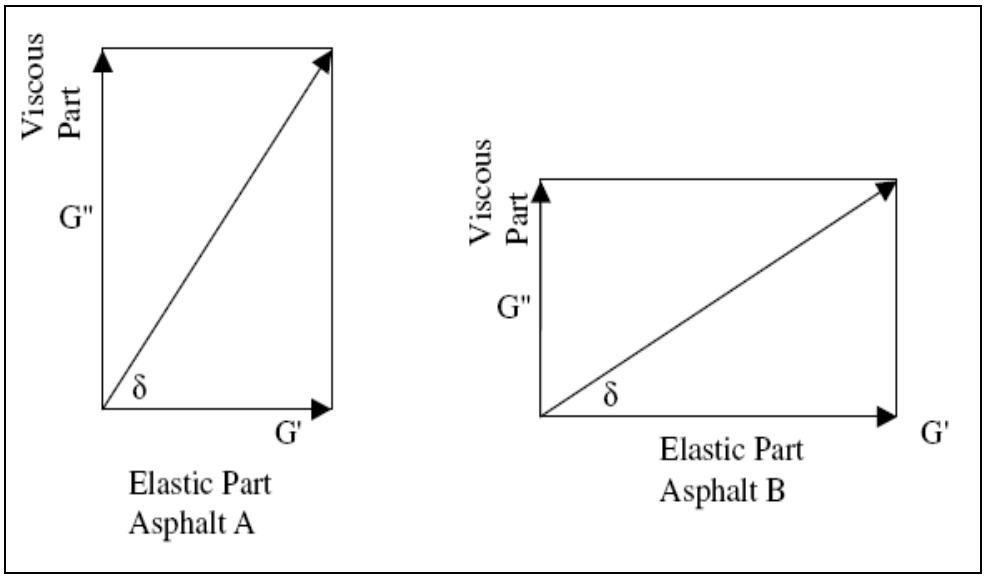

Figure 3.14 Relationship between shear complex modulus (G*) and phase angle (δ) (FHWA Superpave, 1995).

The storage modulus (G'), which is the elastic (recoverable) component, represents the amount of energy stored in the sample during each loading cycle. The loss modulus (G"), which is the viscous (non-recoverable) component, represents the amount of energy lost during each loading cycle. δ, the angle made with the horizontal axis, indicates the relative amounts of temporary and permanent deformation (Delgadillo et al., 2004). When the phase angle is zero degrees, elastic behavior, the complex modulus consists solely of the storage modulus (G'). Likewise, when the phase angle is 90 degrees, viscous behavior, the complex modulus consists solely of the loss modulus (G"). It is therefore necessary to determine both the complex modulus and the phase angle within the viscoelastic range of response to adequately characterize asphalt binders (Neubauer and Partl, 2004). In Figure 3.14 above, even though both asphalts are viscoelastic, asphalt **B** is more elastic than asphalt **A** because of its smaller δ.

In order to ensure repeatability, the complex modulus must be measured within the linear viscoelastic range, which is the region of behavior in which the shear modulus is independent of shear stress or strain. The limit of linear viscoelastic behavior is the point beyond which the complex modulus decreases to 95% of the measured value at zero-strain, as shown in Figure 3.15 (Peterson, et al., 1999).

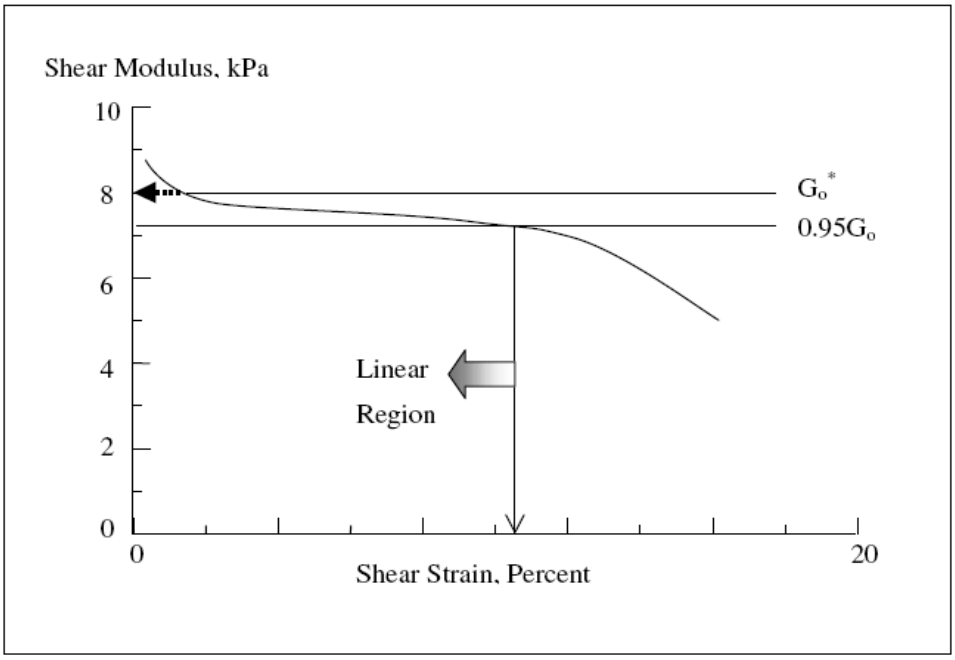

Figure 3.15 Linear viscoelastic region of asphalt binder (Peterson et al., 1999).

3.8 Dynamic Shear Rheometer (DSR) Testing

The rheological properties of the binder and mastics were measured using the Dynamic Shear Rheometer (DSR), by conducting three types of tests: dynamic shear oscillation at single frequency (1.596 Hz), dynamic frequency sweep oscillation (0.1, 1, 10, 50, and 100 Hz) and repeated shear creep loading and recovery at constant stress (300 Pa). The behavior of the materials was evaluated in terms of complex shear modulus - G*, rutting parameter - G*/sinδ, and phase angle - δ for the three types of tests. Samples were tested at three temperatures - 46°, 55°, and 64 °C with an automated dynamic shear rheometer - ADSR

(BOHLIN) that the Louisiana Transportation Research Center (LTRC) is currently using for its dynamic testing. All the results were obtained by taking the average of the tests values from two samples for each test performed.

3.8.1 DSR Oscillation at Single Frequency

After the asphalt sample is correctly placed in the DSR and the test temperature appears stable, the operator must allow about ten minutes for the temperature of the specimen to equilibrate to the test temperature. The actual temperature equilibration time is equipment and asphalt dependent and should be checked using a dummy specimen equipped with very accurate temperature sensing capabilities. A computer is also used with the DSR to control test parameters and record test results.

Testing consists of using the rheometer software to apply a constant oscillating shear strain (12%) and a single frequency (10 rad/sec or 1.596 Hz), in compliance with the Superpave recommendations (AASHTO T 315), and then recording the resulting complex modulus G*, rutting parameter G*/sinδ and phase angle δ. The 10 rad/sec angular frequency is equivalent to a frequency (*f*) of 1.59 cycles per second (1.59 Hz), as per the relationship $\omega = 2\pi f$ (Peterson et al., 1999; Uddin, 2003). The 10 rad/sec angular frequency corresponds, with sinusoidal loading, to a 0.1 second loading time, where loading time (t) is determined from the relationship $t = (2\pi f)^{-1}$. The 0.1-second loading time represents the loading time within a pavement structure resulting from the pass of a vehicle tire traveling at approximately 50 mph. Single frequency tests were performed on the asphalt binder PG64-22 and on all three mastics: Donna Fill, Limestone, and Granite in order to find out the influence of the mineral fillers on the rheological properties of the binder. All the materials were tested at three temperatures - 46°, 55°, 64 °C and at each temperature five volume fractions of each filler were used. A total of 96 samples were obtained

and were tested using 25-mm parallel plates with a 1.0 mm gap. The testing data is presented in **Appendix A**, while the data analysis is effectuated in the next chapter.

3.8.2 DSR Shear Frequency Sweep at Constant Stress

Shear dynamic tests performed with the DSR, provide data on complex modulus, viscosity and elasticity related to the frequency applied, meaning that these tests modes relates the assigned angular velocity or frequency to the resulting oscillating stress or strain (Schramm, 2000). Running an oscillatory test with a rotational rheometer means that the rotor - either the upper or the lower plate - is no longer turning continuously in one direction but it is made to deflect with a sinusoidal time function alternatively for a small angle φ (deflection angle) to the left and to the right, like shown in Figure 3.16. To stay within the realm of linear viscoelasticity, the angle of deflection of the rotor is almost always very small: often not more than 1°.

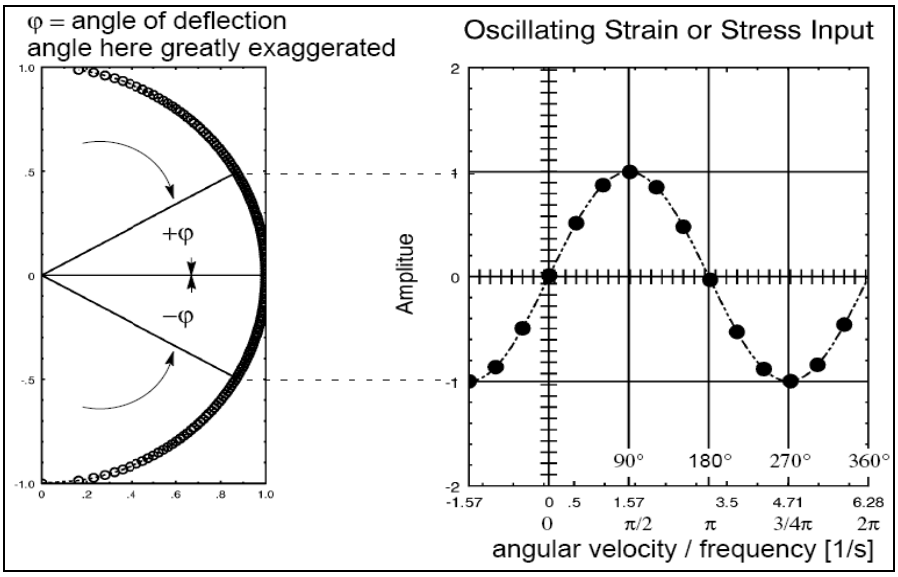

Figure 3.16 Applying strains or stresses in dynamic testing (Schramm, 2000).

The sample placed into that shearing gap is thus forced to strain in a similar sinusoidal function causing resisting stresses in the sample. Those stresses follow again a sinusoidal pattern, the

amplitude and the phase shift angle δ of which is related to the nature of the test sample. Basically, a frequency sweep means that the stress or strain frequency applied is stepwise increased and at any frequency step the two resulting values of G* and δ are measured, within an assigned frequency range. Figure 3.17 below shows a stepwise increase in frequencies while testing with the DSR. In general, frequency sweep tests results are used for the construction of the so-called "Master Curves" which are able to estimate the rheological properties of asphalt mastics and mixtures.

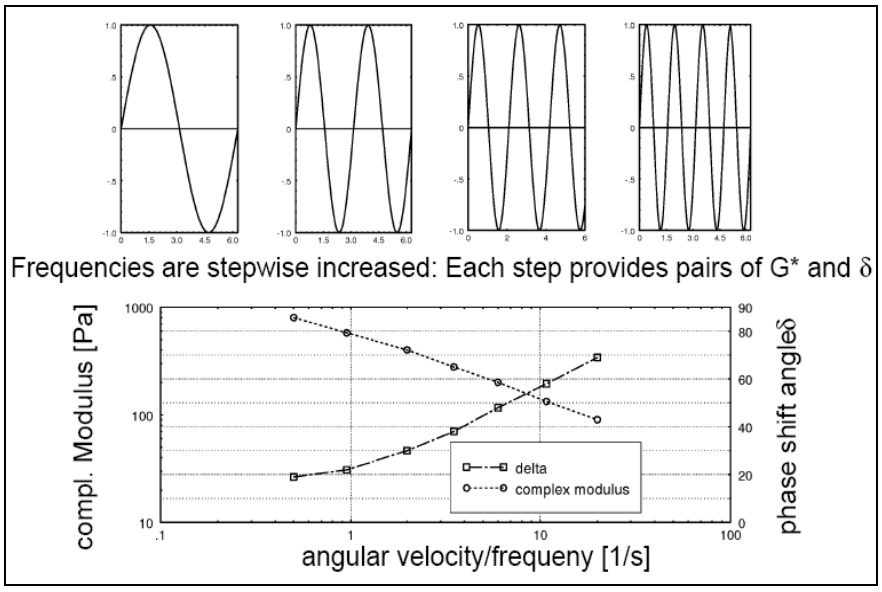

Figure 3.17 Stepwise increase in frequency sweep testing using DSR (Schramm, 2000).

In this study, frequency sweep tests were also performed on the same asphalt binder (PG64-22) and mastics at 46°, 55°, 64 °C. The tests were run on 25-mm parallel plates with a 1 mm gap after the samples were allowed to equilibrate for ten minutes at each temperature prior to testing. The shear stress applied was 2000 Pa and the frequencies used were the following: 0.1, 1, 10, 50, and 100 Hz. Frequency sweep tests results are presented in **Appendix B**.

3.8.3 Repeated Shear Creep Loading and Recovery Testing

Under this name a test method for viscoelasticity has been introduced, which allows one to differentiate well between the viscous and the elastic responses of a test specimen. This new high temperature test for asphalt binders was developed under the NCHRP Project 9-10, in order to address some concerns related to the testing of polymer modified binders. In comparison to the normal force measurement, which marks the shear rate dependency of viscosity and elasticity, the creep and recovery measurement introduces the additional parameter of "response time" to the stress-dependency of both the viscous and the elastic behavior of solids and fluids. Some types of responses of materials under loading are presented in Figure 3.18 below.

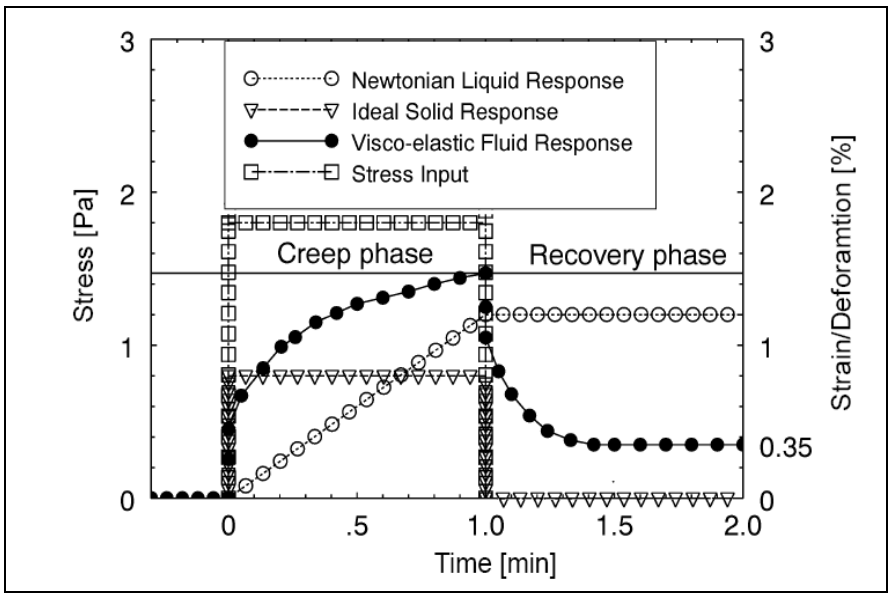

Figure 3.18 Stress and strain responses of several typical samples (Schramm, 2000).

Due to the fact that recovery, as well as the earlier creep phases are time-dependent, when a stress is applied instantaneously the fluid may react with several time-related phases of strain (see the black-dot line in Fig.3.18). While in the early phase of the creep test the elastic components can stretch to their mechanical limits, they will then float within the matrix mass

when the stress is maintained long-term: the sample shows now a viscous flow. By plotting the strain response as a function of time, the deformation shows initially a rapid often step-like increase which is followed by a gradually decreasing slope of the strain curve. This curve may finally lead within some minutes or even longer asymptotically into a tangent with a constant slope: the fluid is now showing a fully viscous response to the applied stress.

If the sample is a viscoelastic solid subjected to a stress below the yield value the strain curve will eventually approach asymptotically a constant strain level parallel to the time abscissa: under these conditions there is some elastic deformation but no flow. During the creep test of viscoelastic fluids the stress applied will cause a transient response which cannot be broken up clearly into the overlapping elastic and the viscous contribution. It is the advantage of the following recovery phase after the release of the applied stress that it separates the value of the total strain reached in the creep phase into the permanently maintained viscous part and the recovered elastic part (see also Fig. 3.18).

In creep tests a constant stress is assigned and the time-related strain is measured. The two can be mathematically interrelated by the following formula:

$$\gamma(t) = J(t)\tau \tag{3.3}$$

where:

$\gamma(t)$ = time-related strain

τ = applied shear stress [Pa]

$J(t)$ = time-related shear ,compliance [1/Pa]

This equation introduces the new term of the time-related shear compliance J(t), which is a material function similar to the viscosity η in steady-state-flow. It defines how compliant a

sample is: the higher the compliance the easier the sample can be deformed by a given stress. The compliance is defined as:

$$J(t) = \gamma(t)/\ \tau\ [1/Pa] \tag{3.4}$$

As long as the tested sample is subjected to test conditions which keep the stress/strain interaction in the linear viscoelastic region, the compliance will be independent of the applied stress, as shown in Figure 3.19.

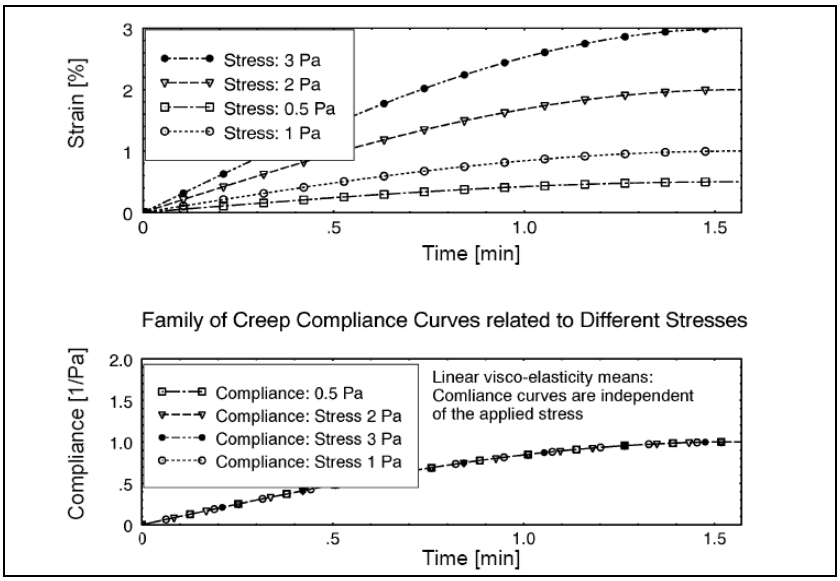

Figure 3.19 Strain and compliance curves for viscoelastic samples subjected to variable stresses within the boundaries of linear viscoelasticity (Schramm, 2000).

This fact is used for defining the limits for the proper creep and recovery testing of viscoelastic fluids within the limits of linear viscoelasticity.

The repeated shear creep loading test that was performed in this study was a controlled-stress test that applied a constant shear stress of 300 Pa to samples having 25-mm in diameter and using a 1-mm gap between the platens. The haversine shear loading and unloading were applied at a frequency of 1 Hz for 10 seconds: creep loading having a duration of one second

followed by a nine second recovery period to complete one creep-recovery cycle. During each cycle, the material (binder or mastic) reaches a peak strain and then recovers before the shear stress is applied again. The residual strain at the start of a new load cycle represents the permanent or accumulated strain, and is reported after one hundred cycles or 17 minutes (1000 seconds) period as shown in Figure 3.20.

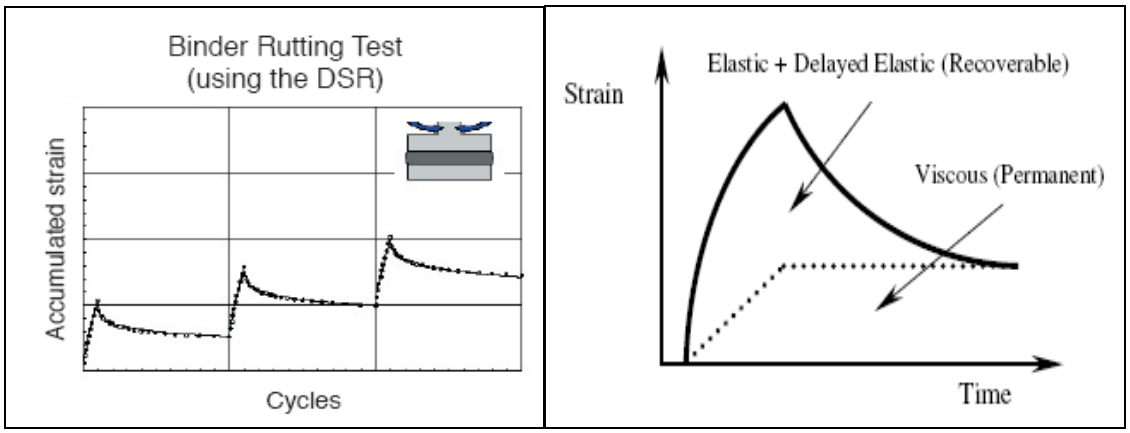

Figure 3.20 Accumulated permanent strain in repeated shear creep loading and recovery (Delgadillo et al., 2004).

For this study testing was conducted on limestone mastics at three temperatures - 46°, 55°, and 64 °C and three volume fractions of limestone filler - 5, 15, and 30%. Test results from the repeated shear creep loading and recovery are presented in **Appendix E**.

CHAPTER 4. SUMMARY AND ANALISYS OF DSR TEST RESULTS

This chapter presents a discussion on the asphalt binder and mastics tests results obtained in the laboratory by using a Dynamic Shear Rheometer (DSR). The tests results are used to draw conclusions on the performance of the two types of materials and their ability to meet the SHRP specifications and the AASHTO precision criteria.

4.1 DSR Oscillation at Single Frequency

The dynamic shear rheometer (DSR) is currently being used by the DOTs for determination of the viscoelastic properties of asphalts following the recommendations of the Strategic Highway Research Program (SHRP). The Superpave specification (rutting) parameter $G^*/\sin\delta$, was identified as the term to be used for high temperature performance grading, usually larger than 45 °C, of paving asphalts in rating the binders for their rutting resistance.

This study though, uses the dynamic shear rheometer (DSR) to, also, characterize the viscous and elastic behavior of asphalt mastics at high and intermediate service temperatures. Specification testing at single frequency recommended by SHRP was performed at 10 rad/sec (1.596 Hz), with the complex modulus G* and phase angle δ calculated automatically as part of the operation of the rheometer using proprietary computer software supplied by the equipment manufacturer. For this type of testing, both temperature and frequency of loading significantly affect the values of G* and δ for asphalt binders and mastics, as they behave like elastic solids at very low temperatures.

Basically, G*/sinδ was recommended as the Superpave specification parameter to give a measure of the rutting resistance of asphalts. The higher the G* value, the stiffer and thus the more resistant to rutting the asphalt binder, and implicitly the mastic, will be. The lower the δ value, the more elastic the asphalt binder (mastic), knowing that an increased elasticity makes

the asphalt binder (mastic) more resistant to permanent deformation. It has been found out that the rutting susceptibility should decrease with the increasing of the G*/sinδ values, thus the Superpave parameter is intended to control rutting by controlling the total energy dissipated per cycle. Antes et al (2003) suggested that rutting is a repeated creep mechanism developed under sinusoidal loading pulses. The pavement (HMA) layer subjected to traffic loading would recover some deformation due to elastic stored energy in the layer materials. The energy is dissipated in damping and in permanent flow. The damping energy is recoverable if given enough time, but the energy related to permanent flow is lost. The permanent portion of the dissipated energy is believed to be the main contributor to the rutting behavior of asphalt pavements.

SHRP researchers consider that, with each traffic load cycle, work is being done to deform the HMA pavement surface (Bennert et al., 2003). A part of this work is recovered by elastic rebound of the surface while some is dissipated in the form of permanent deformation and heat. In order to minimize permanent deformation (rutting), the amount of work dissipated during each loading cycle must be minimized. Mathematically, the work dissipated per loading cycle at a constant stress can be expressed as follows (Roberts et al., 1996):

$$W_i = \pi \cdot \tau_i(\gamma_i \cdot \sin\delta) = \pi\tau_i(\tau_i / G^*)\sin\delta = \pi\tau_i^2\left(\frac{1}{\frac{G^*}{\sin\delta}}\right) \quad (4.1)$$

where:

W_c = energy (work) dissipated per load cycle (i) per unit volume [N/m^2]

τ_i = shear stress applied during the load cycle (i) [Pa]

G* = shear complex modulus [Pa]

γ_ι = shear strain during the load cycle (i) (%)

δ = phase angle (° or rad)

This equation indicates that the work dissipated per loading cycle is inversely proportional to G*/sinδ and also shows that the work dissipated per loading cycle can be decreased by either increasing the value of G* and/or decreasing the value of δ.

Test results from the DSR single frequency are presented graphically in figures 4.1 through 4.3. Stiffening effects due to filler addition can be evaluated by plotting the dynamic shear moduli (or rutting parameter) of both, the binder and mastics, as a function of volume fraction of filler. It can be seen from these figures that the three mineral filler types influenced the rheological properties of asphalt binders differently. In fact, the figures show that different fillers have different effects on the same asphalt binder due to the filler properties and physical-chemical reactions between the two materials. The three figures below, show that the rutting parameters (G*/sinδ), and implicitly the dynamic shear moduli, of mastics obtained by adding granite are much larger than those where donna fill or limestone were used. This may be due to the fact that granite modulus of elasticity is higher than those of the other two types of filler used in this study (see Table 3.2).

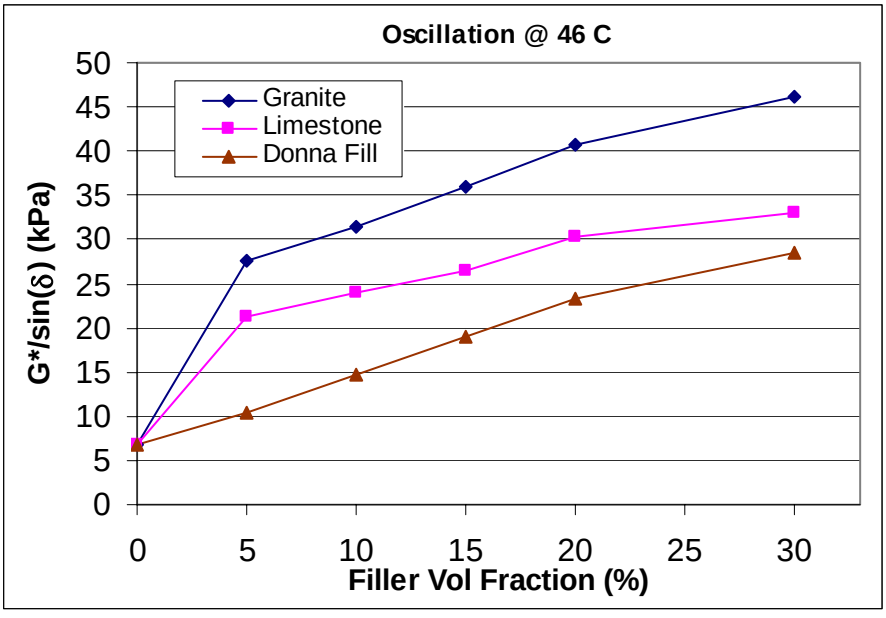

Figure 4.1 Stiffening of asphalt binder by the addition of various filler volume fractions at 46 °C.

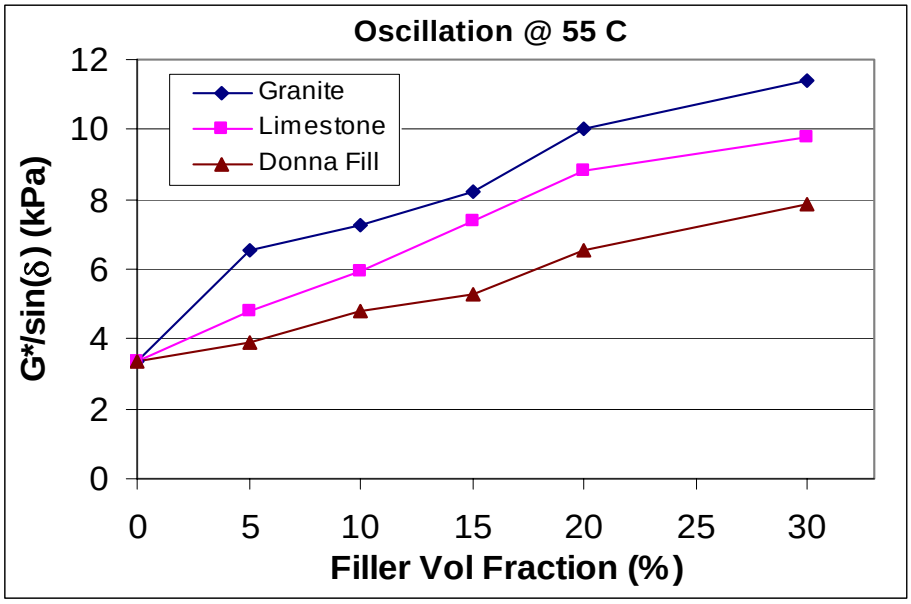

Figure 4.2 Stiffening of asphalt binder by the addition of various filler volume fractions at 55 °C.

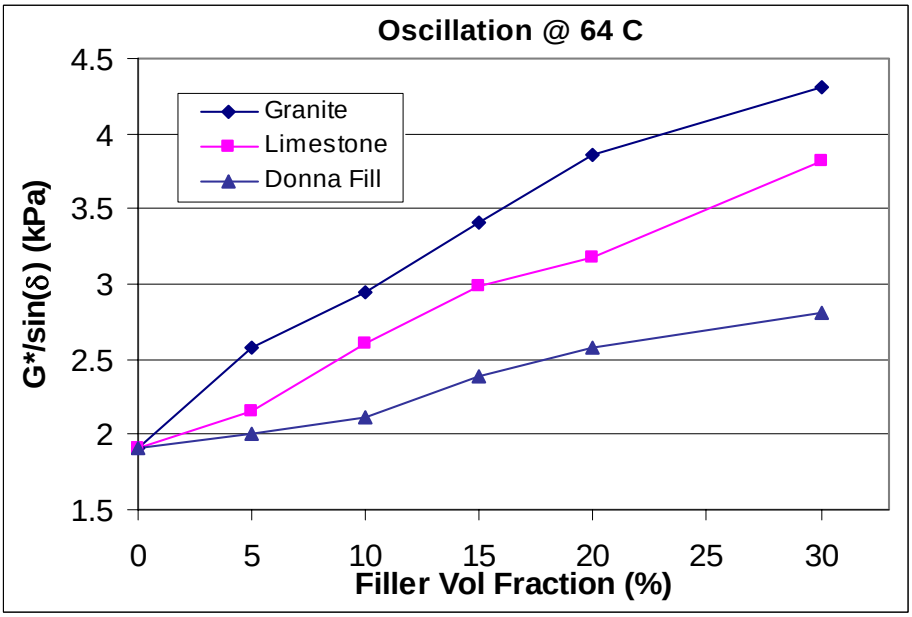

Figure 4.3 Stiffening of asphalt binder by the addition of various filler volume fractions at 64 °C.

Similar results were also observed for limestone mastics, i.e., their dynamic shear moduli are larger than those of donna fill, at all three temperatures. Thus, the fact that granite's elastic

modulus is larger than the other two mineral fillers' may lead to the result that the filling effect of this fine material is more pronounced in stiffening the asphalt binder. Even though, this does not mean that these two types of filler will perform better than Donna Fill in an actual asphalt mix. The values used in the graphs, for the (G*/sinδ) term, represent the averages of two values obtained for each test (see Table 4.1). For each mixture, the complex modulus G* and the phase angle δ were measured twice by DSR, at temperatures of 46°, 55°, and 64°C and at a frequency (ω) of 1.596 Hz (10 rad/s).

Table 4.1 Average values for the rut-controlling term (|G*|/sinδ) [kPa]

Rut-parameter	Filler (%)	0	5	10	15	20	30
G*/sin(δ) (46 °C)	Donna Fill	6.787	10.393	14.681	18.957	23.334	28.512
	Limestone		21.181	23.956	26.464	30.312	33.026
	Granite		27.645	31.429	35.960	40.811	46.182
G*/sin(δ) (55 °C)	Donna Fill	3.378	3.909	4.801	5.308	6.569	7.885
	Limestone		4.779	5.964	7.362	8.829	9.772
	Granite		6.516	7.232	8.206	9.992	11.376
G*/sin(δ) (64 °C)	Donna Fill	1.913	2.006	2.114	2.390	2.581	2.815
	Limestone		2.152	2.611	2.989	3.180	3.816
	Granite		2.578	2.944	3.406	3.860	4.305

Also, from the graphs it can be observed that the rut-parameter (G*/sinδ) requirement of the AASHTO MP1 of 1 kPa minimum was fulfilled (see **Appendix A**).

As expected, the phase angles for all materials increased with temperature (Figure 4.4), but remained almost constant regardless of the content of the mineral filler (Figure 4.5). This shows that both materials (asphalt and mastic) have a larger viscous component at higher temperatures, thus they both behave like viscoelastic materials at same temperatures. According to Kim and Little (2004), the phase angle of composite material is theoretically equal to that of the matrix material, when the matrix is incompressible and mixed with either voids or rigid particles. Therefore, this fact establishes that there is not a significant interaction at interfaces between matrix and fine particles.

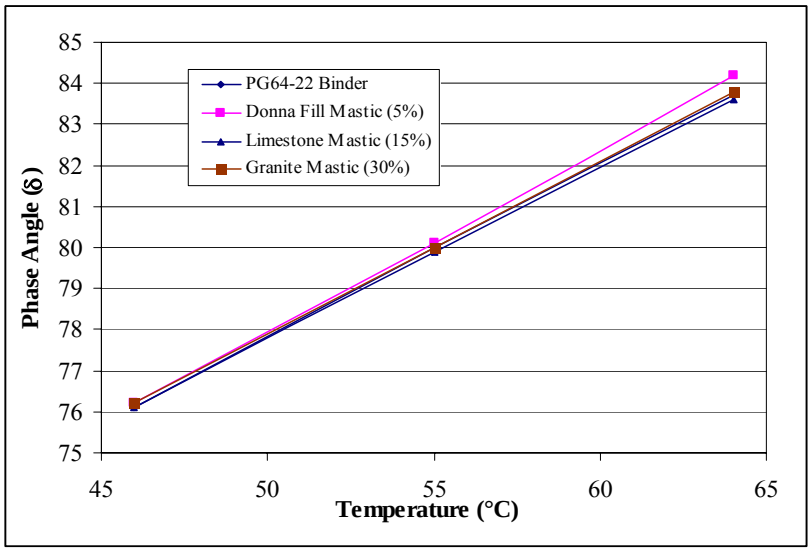

Figure 4.4 Dependency of phase angle on temperature when tested by DSR.

Phase angle dependency on temperatures, Figure 4.4, was plotted for pure binder and mastics having 5% donna fill, 15% limestone, and 30% granite (by volume) in order to emphasize the fact that it does not change significantly with the filler fraction addition. Same behavior can be observed in Figure 4.5, were the phase angle was plotted against filler volume fraction for all three testing temperatures.

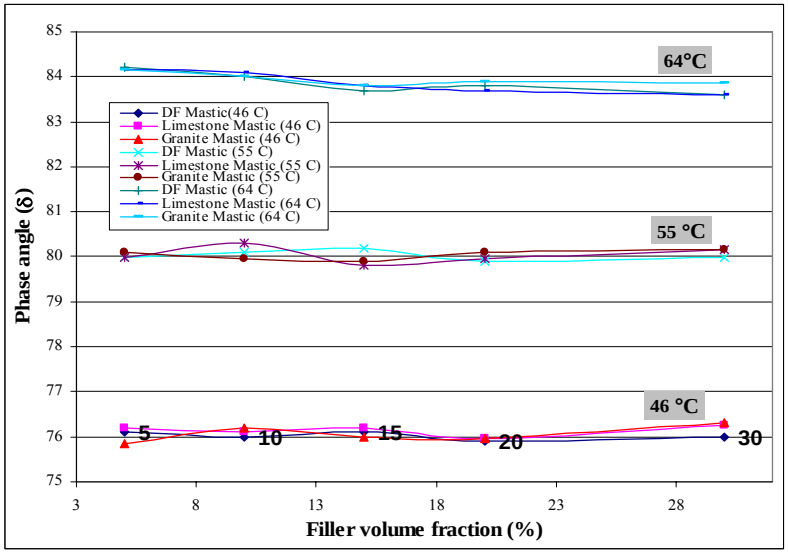

Figure 4.5 Dependency of phase angle on volume fractions of fillers when tested by DSR.

It can also be inferred (Kim and Little, 2004) that damping of composite materials is governed by the damping ability of the surrounding matrix, as long as the second phase represents air voids or rigid mineral particles without significant interaction at interfaces between matrix and particles.

4.2 DSR Frequency Sweep Oscillation Test Results

In general, multiple single frequencies or frequency sweep tests are performed in order to construct the master curves that will determine the rheological properties of mastics and mixes (Medani and Huurman, 2003). Dynamic shear complex moduli at different test temperatures and frequencies could be determined by using the time-temperature superposition principle. In constructing the master curves using the time-temperature superposition principle (Zhao and Kim, 2003), test data collected from the DSR at different temperatures and loading times, in terms of stiffness or shear complex modulus G*, are compared to a reference temperature, which usually is 25 °C. The data at any other temperatures are then shifted with respect to time until various curves overlap almost perfectly to form a single master curve. Typically, the shear complex modulus or stiffness modulus of asphaltic mixes increases with decreasing temperature and increasing loading frequency. Thus, the technique of the determination of the master curve is based on the principle of time-temperature correspondence, which uses the equivalence between frequency and temperature in order to determine the moduli of asphalt mastics and mixes.

DSR data from the three testing temperatures (46°, 55°, and 64°C) was used to construct the master curves for both binder and mastics. The shifting was conducted using Williams-Landel-Ferry equation, which will be presented in the following, normalized to the test temperature of 46 °C. Figures 4.6 to 4.9 below present the DSR frequency sweep test results for

asphalt binder, donna fill (10%), limestone (10%), and granite (10%) mastics at three temperatures - 46°, 55°, and 64°C.

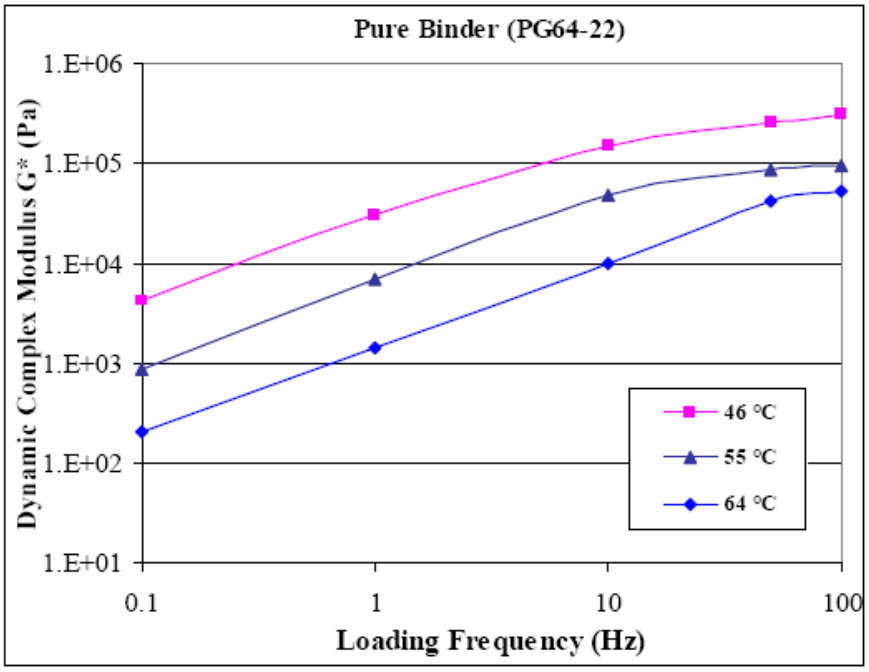

Figure 4.6 Shear complex moduli for pure binder (PG64-22).

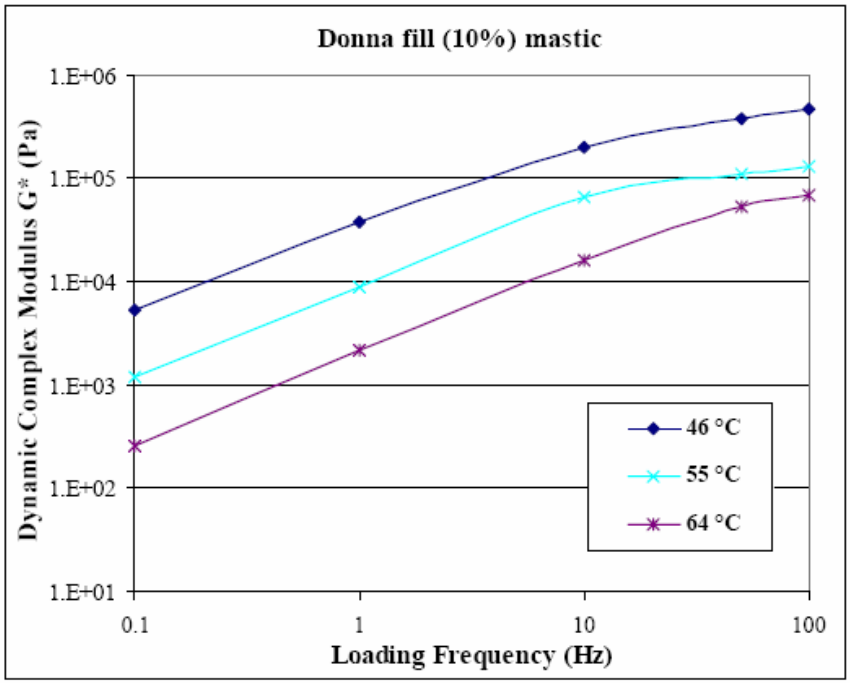

Figure 4.7 Shear complex moduli for donna fill mastic.

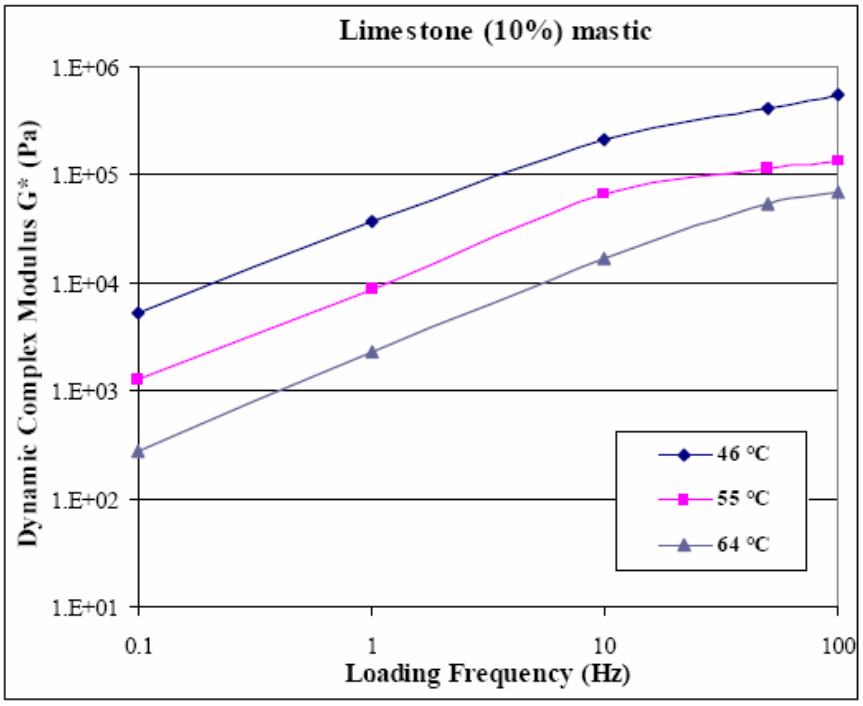

Figure 4.8 Shear complex moduli for limestone mastic.

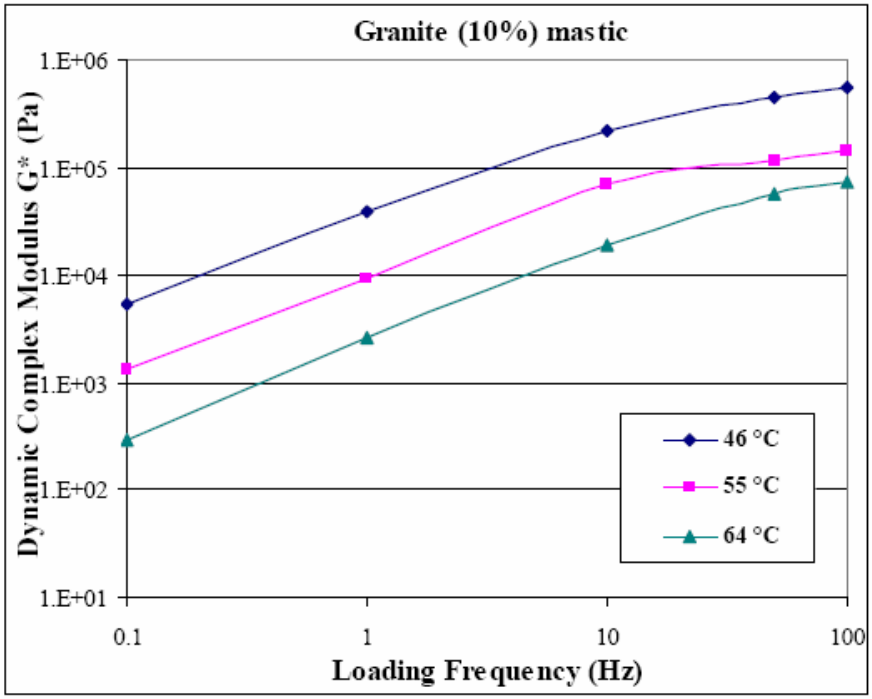

Figure 4.9 Shear complex moduli for donna fill mastic.

Also, in **Appendix B** are presented the rest test data from the DSR frequency sweep testing. As seen from the graphs, complex shear modulus (stiffness) values have increased with the increase in frequency, while they decreased with the increase of the temperature. The increase in the filler volume fraction, also increased the shear modulus values for all types of mastics, with granite filler showing the highest values among the mineral fillers. Figures 4.10 to 4.12 show the shear stiffness variation for asphalt mastics at three volume fractions (10%, 20%, and 30%) and three testing temperatures (46°, 55°, and 64°C).

In general, the increase in shear moduli due to the increase of the frequency is based on the fact that the material is in the plastic region at low frequencies (high values for phase angle), as shown in Figures 4.13 to 4.15, while for high frequencies the phase angle decreases, meaning that the material gets into the more elastic region. These figures show the rheological behavior of mastics at 20% volume fraction (phase angle variation) function of frequency sweep at all three testing temperatures.

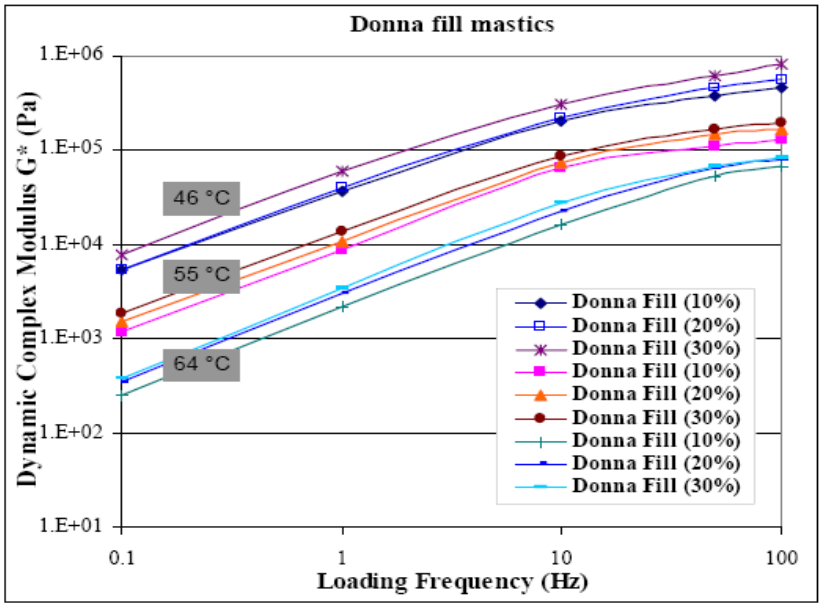

Figure 4.10 Shear stiffness variation function of filler volume fraction for donna fill mastics.

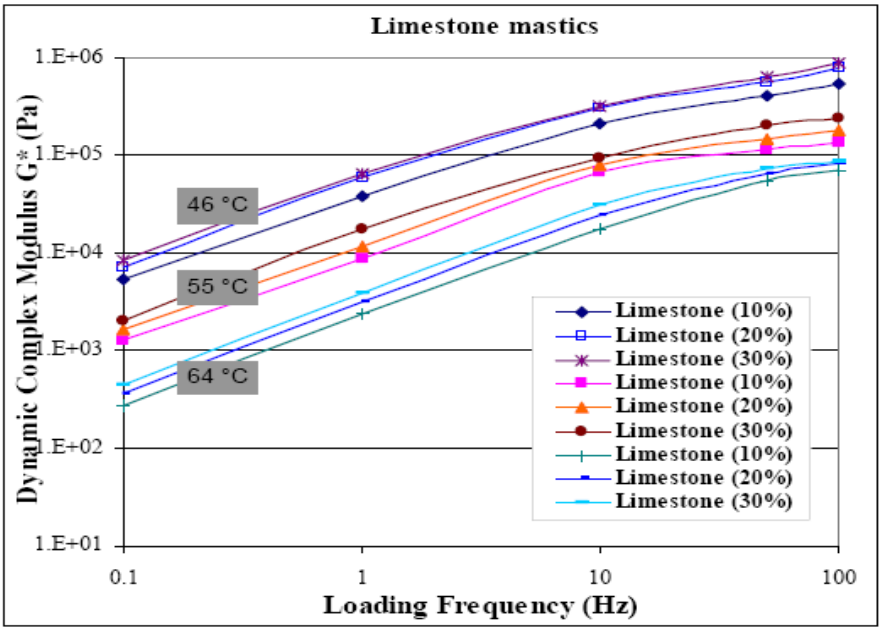

Figure 4.11 Shear stiffness variation function of filler volume fraction for limestone mastics.

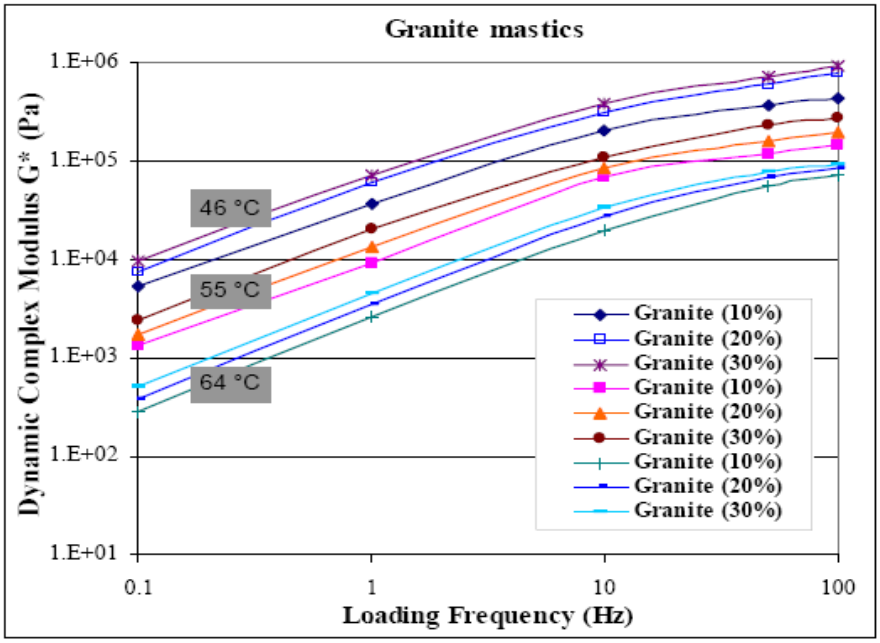

Figure 4.12 Shear stiffness variation function of filler volume fraction for granite mastics.

It can also be seen that the phase angle increased with the increase in temperature, as it did for single frequency (see Figure 4.4, Section 4.1). More figures related to phase angle variation function of frequency loading are presented in **Appendix C**.

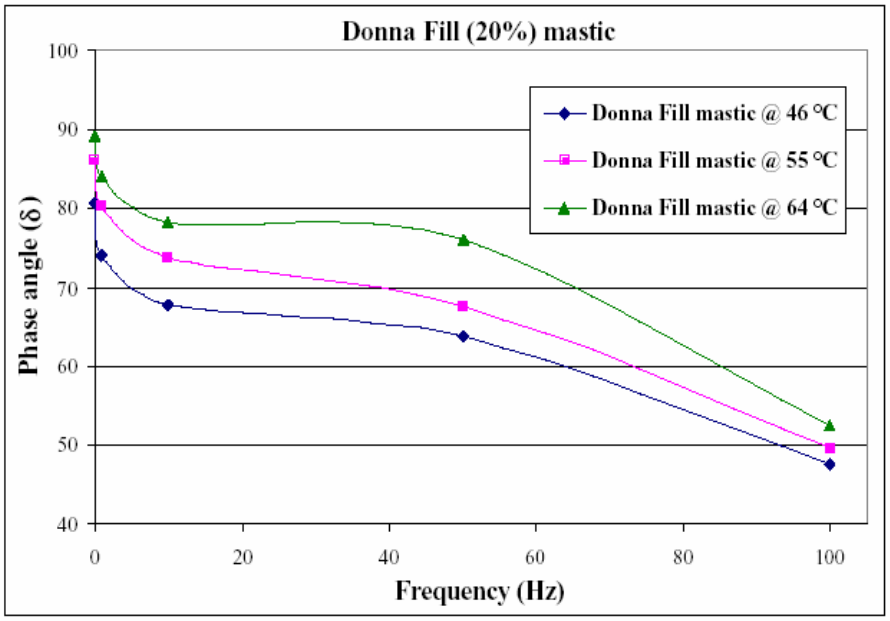

Figure 4.13 Phase angle variation function of frequency loading for donna fill (20%) mastic.

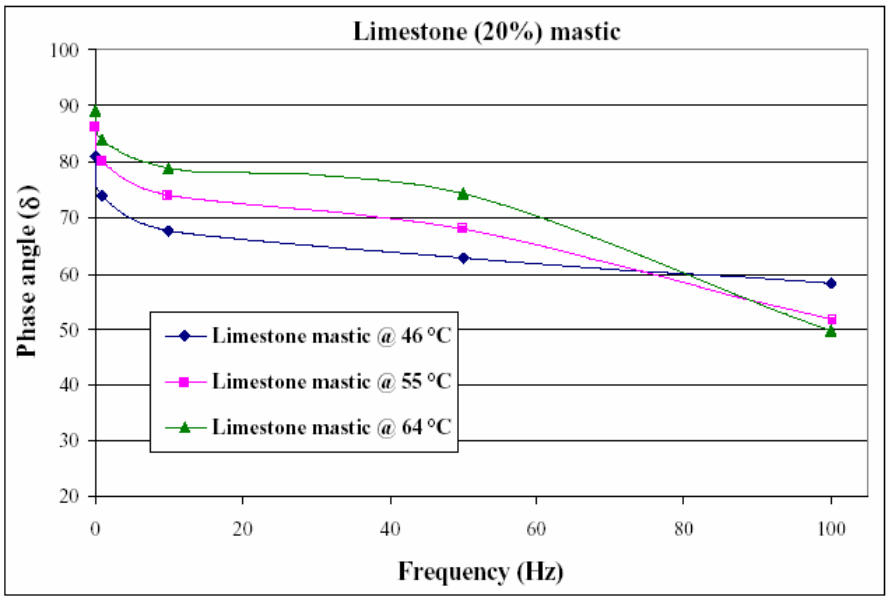

Figure 4.14 Phase angle variation function of frequency loading for limestone (20%) mastic.

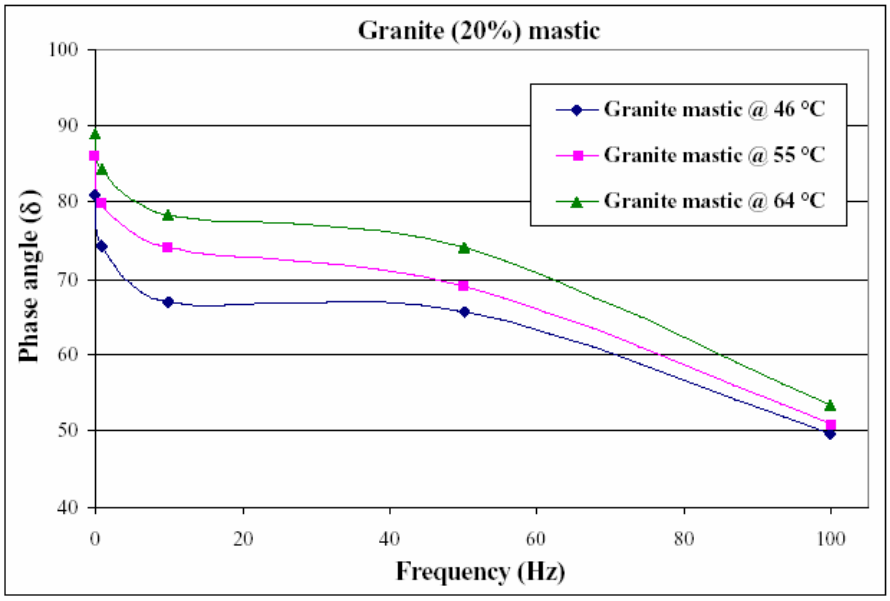

Figure 4.15 Phase angle variation function of frequency loading for granite (20%) mastic.

Using the above frequency sweep data, a horizontal shift factor a_T is produced. The shift factor defines the required shift at a given temperature, i.e., a constant by which the loading frequency ω must be divided to get a reduced frequency f_r for the master curve:

$$f_r = \omega / a_T \tag{4.2}$$

and it is only a function of temperature for a certain material. For temperatures larger than a reference temperature (T_{ref}) the Williams-Landel-Ferry (WLF) (Meegoda, 1999) equation has been widely used to calculate the shift factors for asphalt binders and mixes. In this study the reference temperature was taken as 46 °C. The formula for the calculation of the shift factor is represented by the following equation:

$$\log a_T = -\frac{C_1 \cdot (T - T_{ref})}{C_2 + T - T_{ref}} \tag{4.3}$$

where: a_T = horizontal shift factor

T = temperature, [°C]

T_{ref} = reference temperature, [°C]

C_1, C_2 = empirical constants (temperature dependent) (C_1 = 19 ; C_2 = 92)

Table 4.2 presents the calculated parameters for pure asphalt binder (PG64-22) and mastics containing 10% mineral fillers used in this study.

Table 4.2 Shift factors for asphalt binder PG64-22 and mastics

Material	Shift factor a(T)		
	46 °C	55 °C	64 °C
Pure binder PG64-22	1.0037	0.822	1.517
Donna fill (10%) mastic	1.0042	0.795	1.528
Limestone (10%) mastic	1.0036	0.824	1.514
Granite (10%) mastic	1.0021	0.819	1.497

Frequency sweep data from all mastics were used for the construction of shear dynamic modulus (stiffness) master curves at five frequencies: 0.1, 1, 10, 50, and 100 Hz. Shear stress applied was constant for all the tests and equal to 2500 Pa. Master curves for mastics containing 10% mineral filler are presented in the following, while those for 20% and 30% filler volume fractions are presented in **Appendix D**.

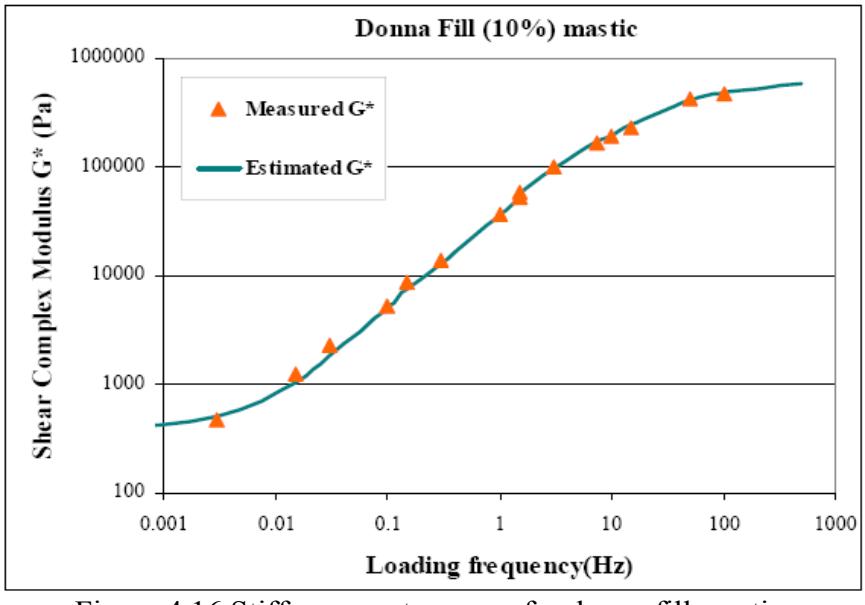

Figure 4.16 Stiffness master curve for donna fill mastic.

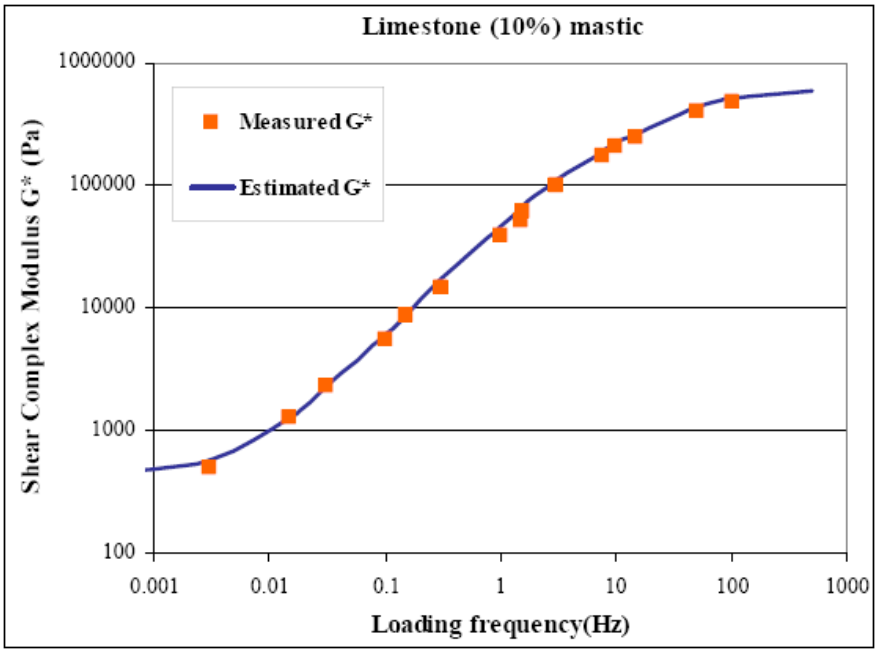

Figure 4.17 Stiffness master curve for limestone mastic.

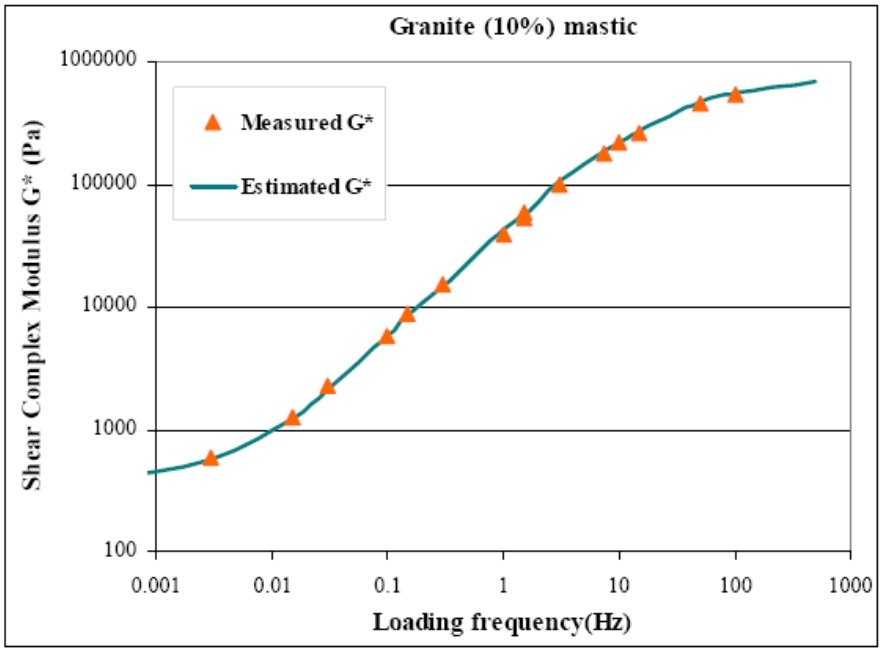

Figure 4.18 Stiffness master curve for granite mastic.

It can be seen from the above graphs that the mastics behaved the same way regardless of the filler volume fractions. From the data in **Appendix B**, the highest values of shear moduli were obtained for granite mastics, while the lowest values came from donna fill mastics, at same temperatures and frequencies. Again, this was possible due to the fact that the elastic moduli of granite are larger than those of the other two materials, thus the stiffening effect is more pronounced. Figures 4.19 through 4.21 below, show the shear stiffness variation, from the master curves, at 10%, 20%, and 30% filler volume fraction, for the three types of mastics.

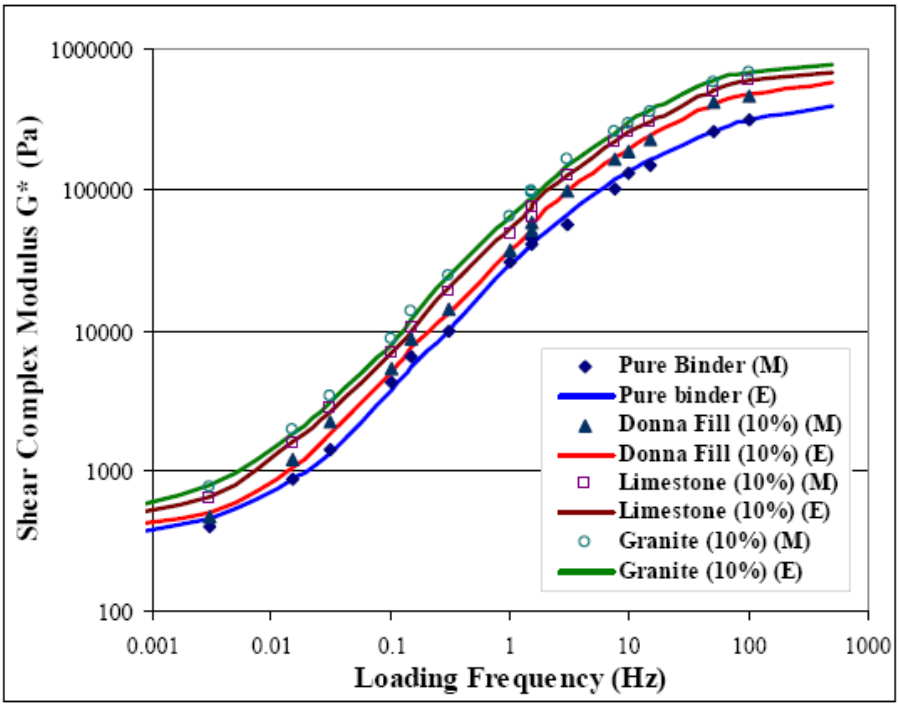

Figure 4.19 Shear stiffness variation function of (10%) mineral filler type.

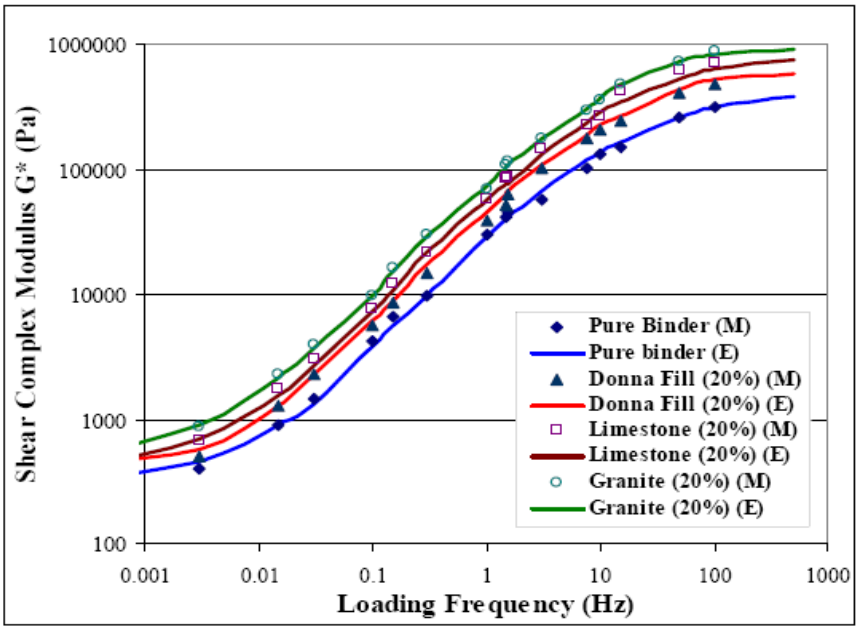

Figure 4.20 Shear stiffness variation function of (20%) mineral filler type.

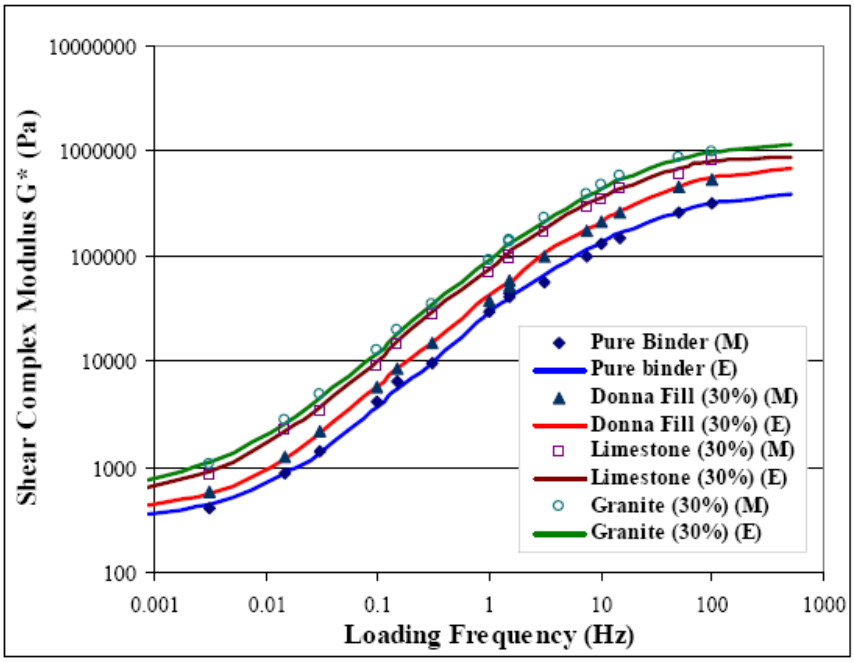

Figure 4.21 Shear stiffness variation function of (30%) mineral filler type.

4.3 Repeated Shear Creep Loading and Recovery Testing

Due to the fact that some of the asphalt pavement researchers discovered that the rut-parameter - G*/sinδ - did not necessarily reflect differences in asphalt binder modification, the NCHRP Project 9-10 which was initiated in order to address some of these concerns, included the development of a new high temperature test for asphalt binders called the repeated shear creep test. The repeated shear creep test is performed using the Dynamic Shear Rheometer (DSR) by applying a controlled shear stress (0.3 kPa) using a haversine load for 1 second followed by a 9-second rest period. During each cycle, the asphalt binder reaches a peak strain and then recovers before the shear stress is applied again. The permanent strain is then accumulated for 100 cycles (or 1000 seconds).

Repeated shear creep and recovery tests give extremely important practical information and, at the same time, useful data to one interested in the theory of the mechanical properties of asphalt binders or mastics. Since asphalt pavements are designed to be flexible, they must quickly return to their original configuration after loading. Rutting, pushing, and shoving are just a few of the failure mechanisms associated with inelastic or permanent deformation. Repeated loading without complete binder recovery is also a cause of fatigue cracking. Although the quality and gradation of the aggregate are important parts of the asphalt mix performance, the creep response of the binder/mastic is also a contributing factor. As creep is a time-dependent function, it is necessary to monitor recovery per unit time or to stipulate a time interval for an expected recovery. Since asphalt pavements are designed to be flexible, they must quickly return to their original configuration after loading.

For this study, repeated shear creep testing was conducted on limestone mastics at three temperatures - 46°, 55°, and 64 °C and three volume fractions of limestone - 5, 15, and 30%.

Figures 4.13 to 4.15 show that the total (accumulated) strain was influenced by the volume fraction of the mineral filler used, decreasing with the increase in the volume fraction of the filler. Smallest values of total strain were obtained for mastics with 30% filler, followed by the 15 and 5% filler. It can be inferred that larger volume filler fractions could improve better the resistance of asphalt pavements to rutting phenomenon compared to the smaller fractions of mineral filler. Test results presented in figures 4.14 and 4.15 are for 10 and 20 cycles, respectively, in order for the effect of the filler to be observed better. Figures containing complete test data for all temperatures and filler volume fraction are shown in **Appendix E**. It can be seen from these figures that the total strain was reduced by 10 ÷ 16%, with the highest reduction occurring for limestone (30%) mastic at 64 °C compared to the total strain of PG64-22 binder after 100 cycles of shear creep loading and recovery. Table 4.3 shows the maximum accumulated shear strain values for limestone mastics after one hundred loading cycles.

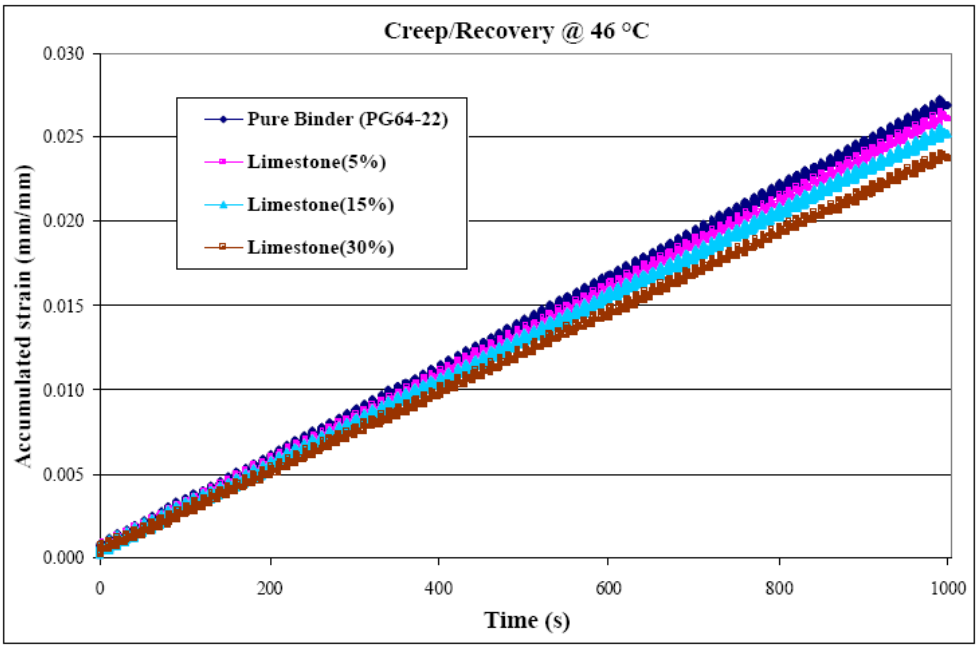

Figure 4.22 Limestone mastics after 100 cycles of creep loading and recovery @ 46 °C.

Table 4.3 Maximum accumulated shear strain (γ_{acc}) values for limestone mastics

Material	Maximum accumulated shear strain (γ_{acc})		
	46 °C	**55 °C**	**64 °C**
Pure binder PG64-22	0.0268	0.0331	0.0446
Limestone 5%	0.0261	0.0327	0.0437
Limestone 15%	0.0252	0.0315	0.0414
Limestone 30%	0.0237	0.0297	0.0374

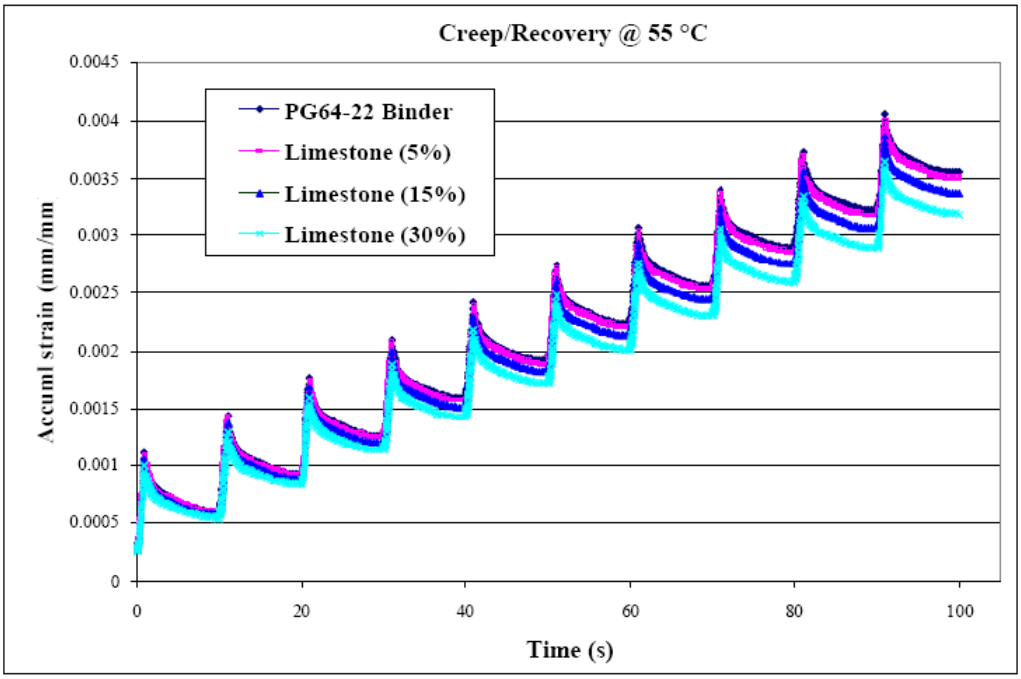

Figure 4.23 Creep loading and recovery of limestone mastics after 10 cycles @ 55 °C.

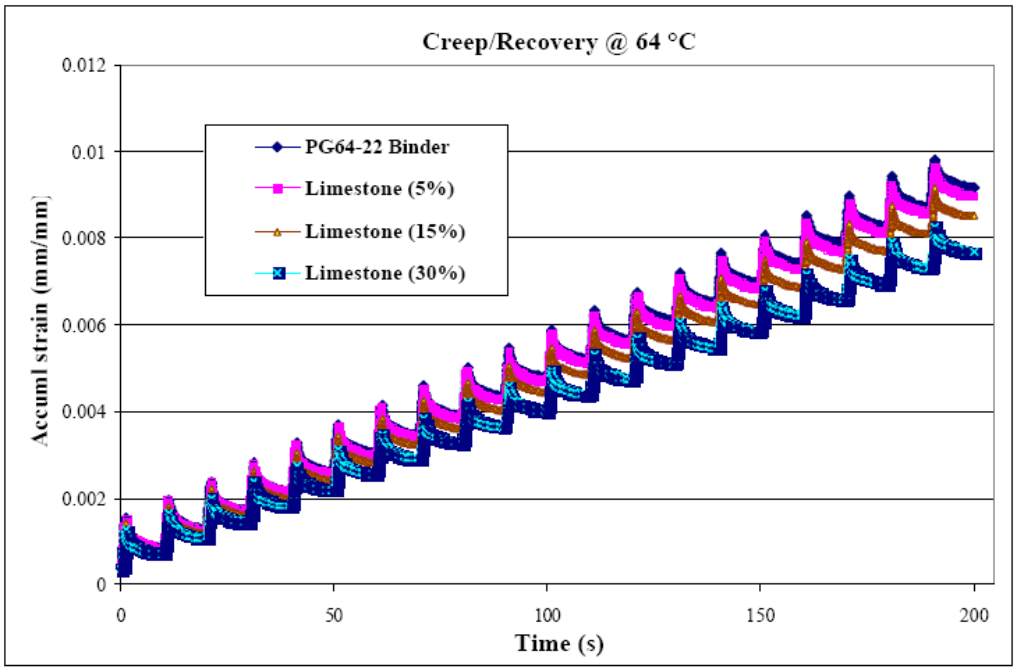

Figure 4.24 Creep loading and recovery of limestone mastics after 20 cycles @ 64 °C.

Rutting phenomena have led researchers to seek other possible parameters that may better relate to rutting resistance and also to search for ways to improve the existing parameter $|G^*|/\sin\delta$, so that it is more sensitive to pavement performance. Some researchers have suggested the repeated creep and recovery test, while others have used a semi-empirical approach as a means to refine the existing Superpave specification parameter.

Shenoy (2001) presents in his paper a refinement of the specification parameter $G^*/\sin\delta$ by using a semi-empirical model developed from the data generated by a conventional frequency sweep test using a DSR. It was believed by the researchers that this semi-empirical approach would better account for the increased influence of the phase angle δ on the accumulated strain (γ_{acc}) after a certain number of cycles (usually one hundred). This approach is based on the assumption that the strain accumulation rate depends upon the binder complex modulus (stiffness) and the viscoelasticity contribution $f(\delta)$ (at the appropriate rate and

temperature) and that these two contributions are independent. Thus, the equation for the rutting resistance would be:

$$R = \gamma_{unr}^{-1}(\%) = G^* \cdot f(\delta) \tag{4.4}$$

where:

R = rutting resistance [%]

γ_{unr} = unrecovered strain after one cycle

During the repeated creep recovery test, on applying a shear stress of τ_0 [Pa] for a duration of 't' seconds, the total deformation (or the maximum strain (γ_{max}) that the material undergoes must be the sum of the elastic deformation and the viscous deformation. From basic principles, the deformation behavior has to be mapped by the following equation relating the applied constant stress with the maximum strain:

$$\gamma_{max}(\%) = \frac{100\tau_0}{G^*} \tag{4.5}$$

where:

τ_0 = applied shear stress [Pa] in the creep experiment

G* = shear complex modulus obtained from DSR at matching time scale [Pa]

Substituting τ_0 = 300 [Pa], as required by NCHRP Project 9-10, in equation 4.6, the following equation results:

$$\gamma_{max}(\%) = \frac{30}{G^*} \tag{4.6}$$

Because the strain γ_{max} represents the value from the repeated creep experiment, while the complex modulus (stiffness) G* that is used in equation 4.6 is obtained from the frequency sweep or single frequency oscillatory measurement, in order to obtain a relationship between the

two parameters, comparisons must be made on a common platform, thereby requiring the time scales to be matched. For example, if the shear loading in the creep experiment is 1 second, then the G* value at oscillation frequency $\omega = 1$ rad/s must be used to match the time scale.

Having obtained the expression for the maximum strain per cycle from a creep loading experiment through basic principles, the next step is to focus on the recovery part of the creep experiment. In the linear range of response, under constant stress, the strain per unit stress is a unique function of time t referred to as the shear creep compliance function (Schramm, 2000), which can be described by the following equation:

$$J(t) = J_e + J_d\psi(t) + \frac{t}{\eta} = \frac{\gamma(t)[\%]}{100\tau_0} \tag{4.7}$$

where:

$J(t)$ = shear creep compliance [1/Pa]

J_e = elastic recoverable shear compliance [1/Pa]

J_d = delayed recoverable shear compliance [1/Pa]

$\psi(t)$ = normalized retardation function which ranges from zero at $t = 0$ to one when steady-state deformation is achieved;

η = steady-state viscosity [Pa·s] , and

t/η = contribution of the viscous deformation at time t that is unrecoverable.

Thus, the recoverable shear compliance $J_r(t)$, which can be measured directly from the recoverable deformation after removing the creep loading, is given by:

$$J_r(t) = J_e + J_d\psi(t) = \frac{\gamma(t)[\%]}{100\tau_0} \tag{4.8}$$

If it is assumed that sufficient time has elapsed for asymptotic conditions to be reached, then the steady-state recoverable creep compliance, J_r can be written as:

$$J_r = J_e + J_d \tag{4.9}$$

Shenoy (2001) also showed that:

$$J_r = \frac{G'}{G''^2} \tag{4.10}$$

where: G' = storage (elastic) modulus [Pa]

G" = loss (unrecovered) modulus [Pa], the two components of G* presented in Chapter 3. Therefore, from the previous definition of J_r, equation (4.8) we get:

$$\frac{\gamma(t)[\%]}{100\tau_0} = \frac{G'}{G''^2} \tag{4.11}$$

If sufficient time is given for the creep recovery, it is clear that all the elastic strain is recovered and the viscous strain is left unrecovered. It is often believed that the delayed elastic portion of the strain (see Figure 3.20) leaves remnants of the elastic strain, which then adds to the viscous strain if sufficient time for recovery has not elapsed.

If the elastic recovery is not complete, then every subsequent cycle would have its peak value slowly decreasing and its unrecoverable strain value also decreasing slowly, thereby showing nonlinear behavior. But, if the line joining the unrecoverable strain after every cycle is nearly a straight line, like in Figure 4.25, then, there is good evidence to suggest that the delayed elastic strain effect is minimal. In fact, Bahia et al. (1999) stated that in all of their observations the delayed elastic strain constituted less than 2% of the total strain.

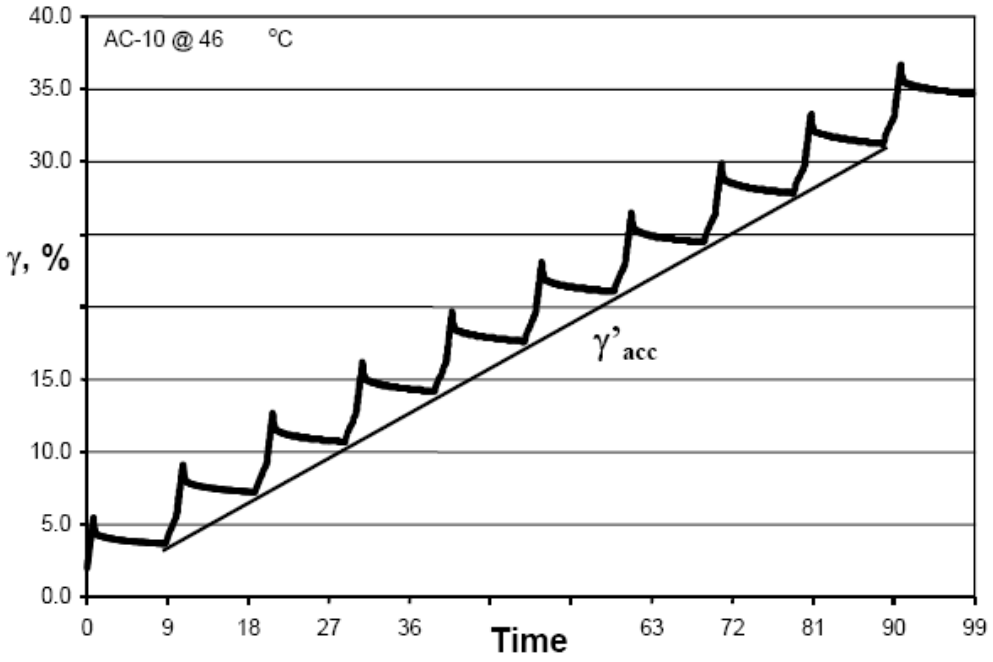

Figure 4.25 Dependency of accumulated strain against time (Dongre et al., 2002).

Nevertheless, the contribution of the delayed elastic strain effect must be taken into account if the intention is to develop a general relationship for viscoelastic systems, such that the derived expressions would be valid in situations when the recovery times are shorter or the temperatures of measurement are lower.

Hence, the percent recoverable strain can be written as:

$$\gamma_{rec}(\%) = \gamma_{max}(\%) - \gamma_{unr}(\%) \tag{4.12}$$

By combining equations (4.5), (4.11), and (4.12), the following equation is obtained with the rearrangement of the terms:

$$\frac{\gamma_{unr}(\%)}{\gamma_{max}(\%)} = 1 - \frac{G' \cdot G^*}{G''^2} \tag{4.13}$$

Using the fact that G' = G*cosδ and G" = G*sinδ, the two components of the shear complex modulus from Chapter 3, equation 4.14 can be simplified as:

$$\frac{\gamma_{unr}(\%)}{\gamma_{\max}(\%)} = 1 - \frac{1}{\tan\delta \sin\delta} \quad (4.14)$$

Equation (4.14) provides he refinement of the Superpave specification parameter G*/sinδ and it equals 1 when the phase angle δ is 90 degrees (totally unrecovered strain). By replacing γ_{max} from equation (4.5) the expression for the unrecovered strain is obtained:

$$\gamma_{unr}(\%) = \frac{100\tau_0}{G^*}\left(1 - \frac{1}{\tan\delta \sin\delta}\right) \quad (4.15)$$

Since G* and δ are function of frequency and temperature, the effect of traffic speed and pavement temperature are built into this equation. Thus, in order to minimize the unrecovered (or permanent) strain, the term $\frac{G^*}{\left(1 - \frac{1}{\tan\delta \sin\delta}\right)}$ needs to be maximized.

Figure 4.26 shows the accumulated strain of limestone (15%) mastic measured with the Dynamic Shear Rheometer (DSR) against the total strain obtained by using Shenoy's equation 4.15. Figures showing measured strains versus estimated strains at all three testing temperatures and filler volume fractions are presented in **Appendix E**. The graphs show a good correlation between the estimated values and the measured values, taking into account that all the R^2 values are greater than 0.95. The best estimation was obtained for 30% limestone mastics at 55° and 64 °C (0.998), while the poorest was for 15% limestone mastic at 55°C. Values for G^*_{binder} were

taken from the DSR single frequency oscillation tests at 1.6 Hz and 12% constant strain (SHRP requirements).

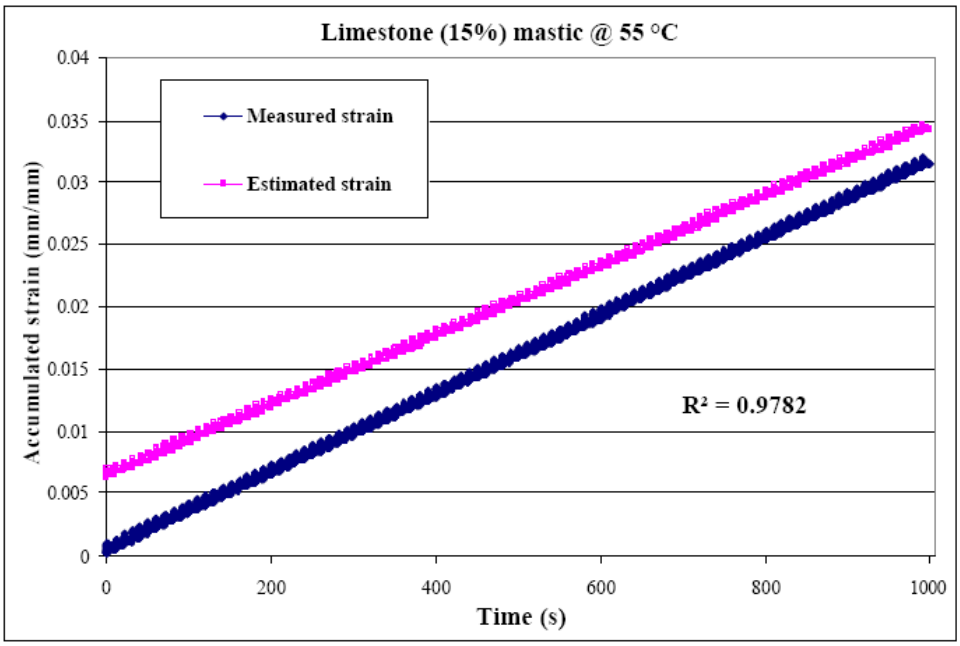

Figure 4.26 Predicted and measured accumulated strain values after 100 cycles.

4.4 Estimation of Complex Shear Modulus G* Using the Hirsch Model

One of the purposes of this research was to employ the Hirsch new micromechanical model (Christensen et al., 2003) used for estimating the complex shear modulus G* of asphalt concrete, in order to evaluate the complex shear modulus of mastics by using the binder complex modulus and volumetric composition of the mineral fillers. The new model is based upon an existing version of the law of mixtures for composite behavior (Hirsch model, see fig. 4.18), which combines series and parallel elements of phases (composite materials, in this case asphalt binder and mineral aggregate) and was developed as part of NCHRP Projects 9-25 and 9-31, the objectives of which were to evaluate existing Superpave requirements for volumetric composition and modify them if warranted. The model was developed during the initial stages of

these NCHRP projects to be used as a tool for analyzing the effect of changes in air voids (AV), voids in mineral aggregate (VMA) and other volumetric mix factors on the modulus of asphalt concrete and related mechanical properties.

Figure 4.18 presents the old Hirsch model, in which the two phases are a combination of series and parallel arrangement. In this arrangement, V_{1S} and V_{2S} are phases in series, and V_{1P} and V_{2P} are phases in parallel.

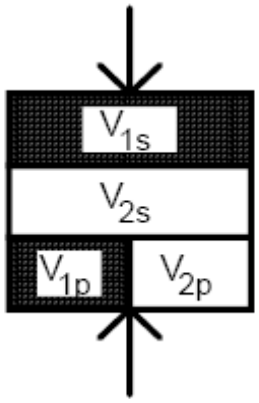

Figure 4.27 Hirsch arrangement of phases for asphalt concrete (Christensen et al., 2003).

Due to the fact that asphalt concrete tends to behave like a series composite at high temperature, but more like a parallel composite at low temperature, the Hirsch model was considered to be appropriate for estimating the shear modulus of asphalt concrete. The aggregate phase in the parallel portion of the model (V_{1P}) is important in characterizing the behavior and performance of HMA, as it represents that portion of the aggregate particles in intimate contact with each other, this portion of the aggregate therefore being called the aggregate ***contact volume***, P_C. In general, as the aggregate contact volume increases, so will the modulus, strength, and resistance to permanent deformation (Yongqi and Metcalf, 2005). High values of P_C indicate a very effective structure producing good strengths and stiffness, typical at low temperature,

while low values of P_C tend to occur at high temperatures, and indicate mixtures with low strength and stiffness.

Various modifications of the Hirsch model were devised and evaluated in developing the final version, but the version of the model that was found to exhibit consistently good accuracy is shown in Figure 4.19, this alternate formulation of the Hirsch model being very similar to the original model.

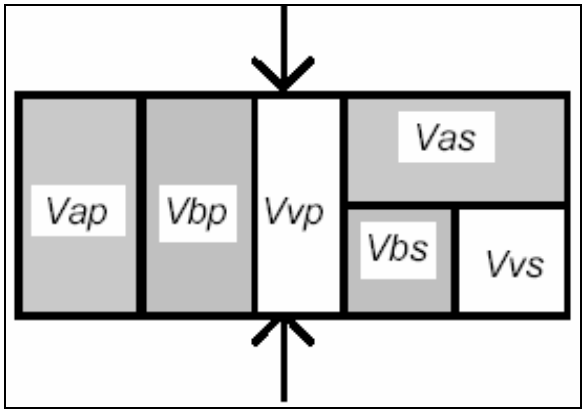

Figure 4.28 Alternate version of the modified Hirsch model (Christensen et al., 2003).

In the figure above, subscripts p and s stand for parallel and series phases, V_a refers to the aggregate volume (without the contact volume), V_b effective binder volume, and V_v is the air voids volume. The only difference in this version is that the series and parallel sub-units of the model are combined in parallel, rather than in series, placing more emphasis on the parallel sub-units of the model. This version of the Hirsch model produced the best results, and has the additional advantages of being relatively simple and very similar to the original version of the model as formulated by Hirsch. Mathematically, the modulus can be expressed using the following equation:

$$E_c = V_{ap}E_a + V_{bp}E_b + (V_{as} + V_{bs} + V_{vs})^2 \left(\frac{V_{as}}{E_a} + \frac{(V_{bs} + V_{vs})^2}{V_{bs}E_b} \right)^{-1} \quad (4.16)$$

where:

E_c = composite (asphalt concrete) modulus [Pa]

E_a = aggregate modulus [Pa]

V_a = aggregate volume [%]

V_b = binder volume [%]

In applying the Hirsch model to asphalt concrete, the relative proportion of material in parallel arrangement, called the contact volume, P_C, is not constant but varies with time and temperature, thus another expression for E_c function of contact volume looks like:

$$E_c = P_C(V_aE_a + V_bE_b) + (1 - P_C) \left(\frac{V_a}{E_a} + \frac{(V_b + V_v)^2}{V_bE_b} \right)^{-1} \quad (4.17)$$

Hence, the most effective model, in which the shear modulus of the asphalt concrete is directly estimated from binder shear complex modulus G*, VMA (Voids in Mineral Aggregate), and VFA (Voids Filled with Asphalt) has the following expression (Christensen et al., 2003):

$$G^*_{mix} = P_C \left[E_b \left(1 - \frac{VMA}{100} \right) + G^*_b \left(\frac{VFA \cdot VMA}{10000} \right) \right] + (1 - P_C) \left[\frac{1 - \frac{VMA}{100}}{E_b} + \frac{VMA}{VFA \cdot G^*_b} \right]^{-1} \quad \text{[Pa]} \quad (4.18)$$

where:

P_C = contact volume factor representing the proportion of parallel to total phase volume

G^*_{mix} = complex shear modulus of the mixture, in this case mastic [Pa]

G^*_b = binder complex shear modulus obtained from the DSR testing [Pa]

E_a = back-calculated aggregate modulus [Pa]

VFA = number of voids filled with asphalt [%]

VMA = number of voids in the mineral aggregate [%]

Also, the expression of P_C is given in the following (Christensen et al., 2003):

$$P_C = \frac{\left(3 + \frac{VFA \cdot G^*_b}{VMA}\right)^{0.678}}{396 + \left(\frac{VFA \cdot G^*_b}{VMA}\right)^{0.678}} \quad (4.19)$$

Values for G^*_b were determined experimentally from oscillation at constant strain (see 4.1) by using the Dynamic Shear Rheometer (DSR). Figures 4.27 through 4.29 show the G* values estimated using equations 4.17 and 4.18 versus the measured values using a dynamic rheometer. From these figures it can be seen that there is a generally good correlation between the values, with R^2 values being all above 0.95. Calculations have been made for all types of mastics at the three temperatures - 46°, 55°, and 64 °C. Below are presented the graphs for the donna fill mastics. Figures containing estimated values of shear modulus for limestone and granite mastics are showed in **Appendix F**. Calculated values of E_b, VFA, and VMA (using Excel software) are also presented in the above appendix.

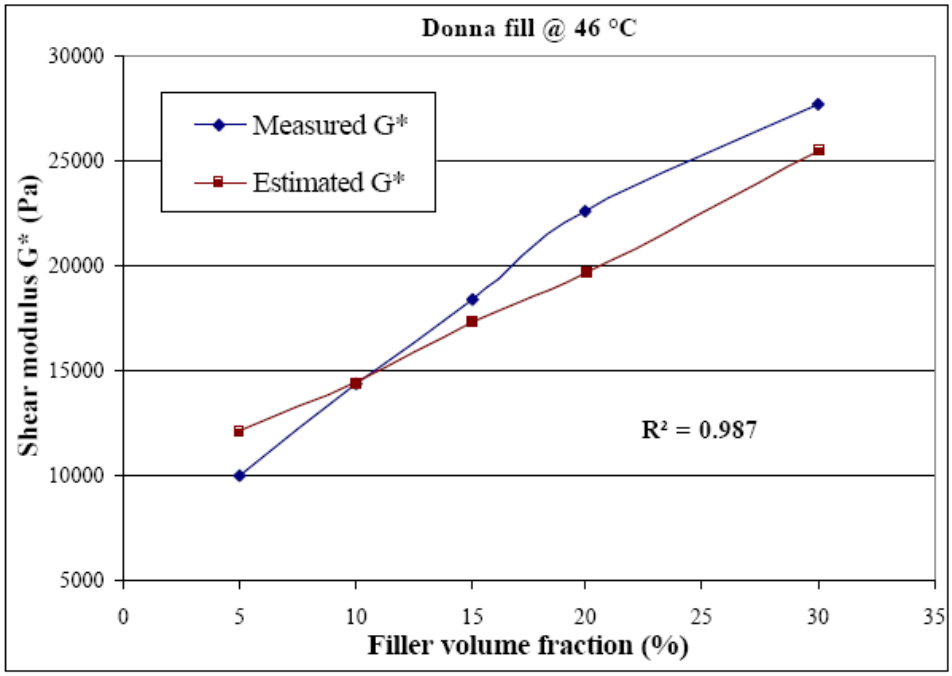

Figure 4.29 Estimated versus measured complex shear modulus for donna fill mastics at 46 °C.

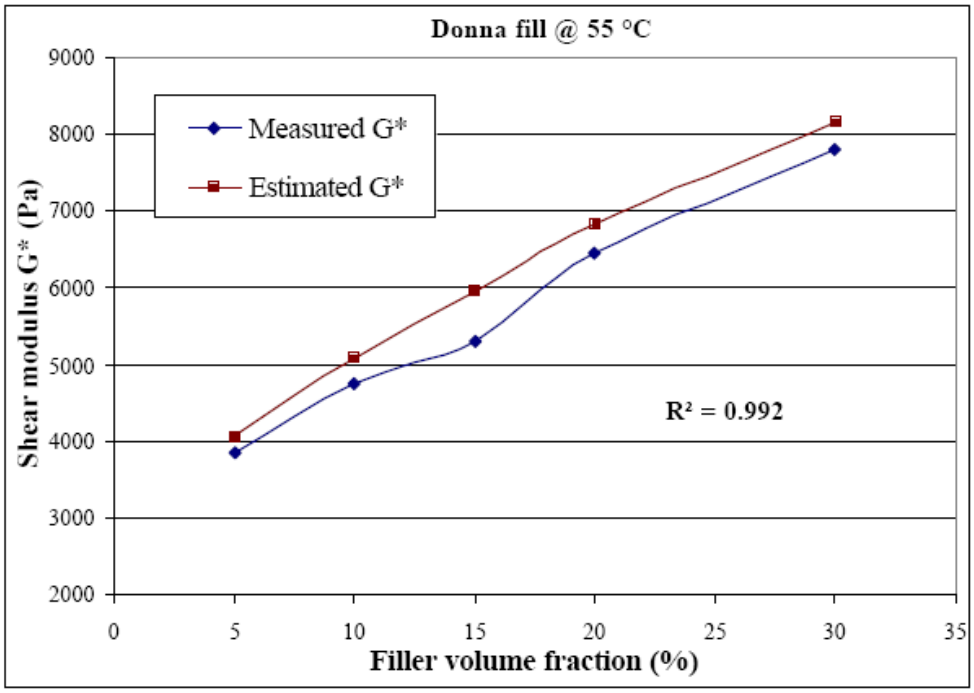

Figure 4.30 Estimated versus measured complex shear modulus for donna fill mastics at 55 °C.

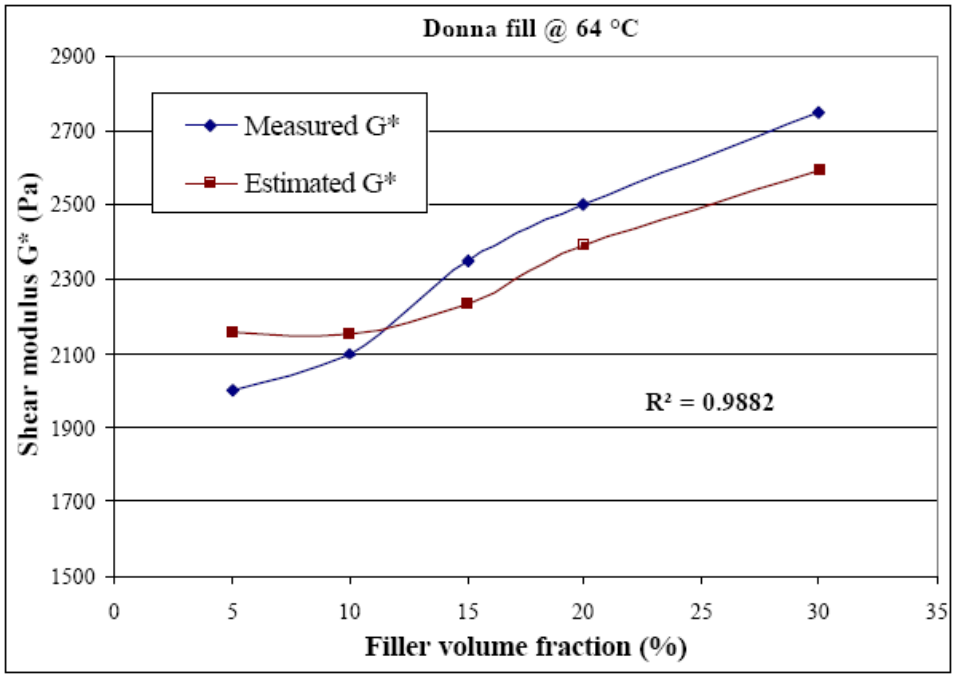

Figure 4.31 Estimated versus measured complex shear modulus for donna fill mastics at 64 °C.

CHAPTER 5. LABORATORY SUPERPAVE ASPHALT MIXTURES DESIGN

This chapter provides information on the materials and procedures that have been employed in order to acquire a desired design for asphalt mixtures or hot mix asphalt (HMA) in the laboratory, by using some of the Superpave system (see Chapter 1 & 3) requirements. It also contains information about the asphalt binder and aggregate influence on the hot mix asphalts, as well as information about aggregate gradation and asphalt mixture volumetrics.

5.1 Asphalt Mixture or Hot Mix Asphalt (HMA)

Asphalt mixture, also known as asphalt concrete (AC) or hot mix asphalt (HMA) is essentially a two part (composite) material consisting of both the asphalt binder and the mineral aggregate skeleton, plus a percent of air voids controlled by the specific mix design, as shown in Figure 5.1 (see also Fig. 1.2, Chapter 1).

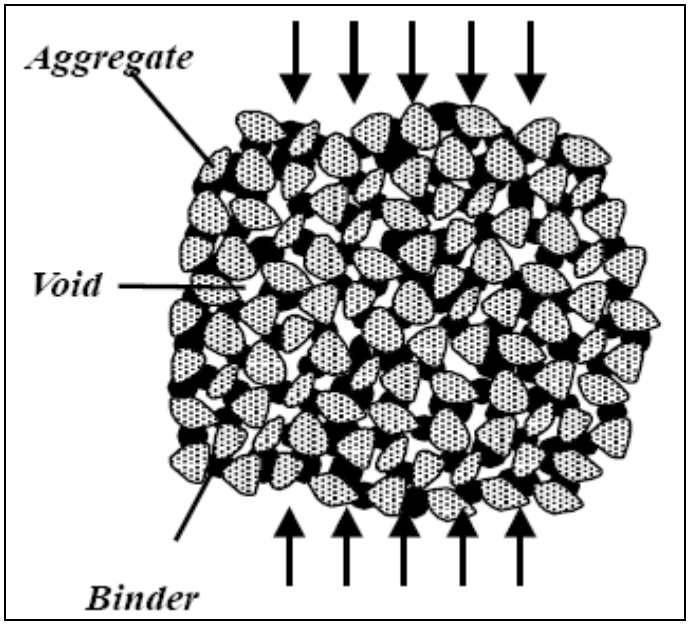

Figure 5.1 Schematic of asphalt mixture material (Atkins, 2003).

Each part, as well as the asphalt binder-aggregate interface, contributes to the asphalt mixture's resistance to permanent deformation (rutting) (Jiang et al., 1996). However, each part influences differently, and the asphalt binder's influence also changes with time. It is well understood that the HMA is affected by both temperature and the rate of loading and rutting is usually greatest when temperatures are at its highest and traffic is moving its slowest. However, by modifying the high temperature end binder grade, the effects on rutting can be minimized, or greatly reduced.

5.2 Asphalt Binder

Performance graded (PG) asphalt binders are selected based on the climate in which the pavement will serve. The distinction among the various binder grades is the specified minimum and maximum pavement temperatures at which the requirements must be met.

Taking into account that almost eight months a year the temperatures in Louisiana are around or higher than 30 °C, fact which gives a temperature of approximately 60 °C at the pavement surface, a PG64-22 asphalt binder was also selected for the mixtures design, for a reliability of at least 60 percent. The binder is produced by CITGO Asphalt Refining Company and its properties and characteristics are presented in Chapter 3 and **Appendix A**. It was used in five percentages from 3% through 7% (1% step increase) at a constant air voids content of 6%. More details will be given in Chapter 6 regarding the samples preparation.

5.3 Mineral Aggregate

A wide variety of mineral aggregates have been used to produce asphalt concrete mixtures. Some materials are referred to as natural aggregate because they are simply mined from river or glacial deposits and are used without further processing to manufacture the asphalt concrete (Waltham, 2002). These are often called "bank-run" or "pit-run" materials. On the other

hand, processed aggregate can include natural aggregate that has been separated into distinct size fractions, washed, crushed, or otherwise treated to enhance certain performance characteristics of the finished HMA. In most of the cases, the main processing consists of crushing and sizing.

Regardless of the source, processing method, or mineralogy, aggregate is expected to provide a strong, stone skeleton to resist repeated load applications. Cubical, rough-textured aggregates provide more strength than rounded, smooth-textured aggregates Even though a cubical piece and rounded piece of aggregate may possess the same inherent strength, cubical aggregate particles tend to lock together resulting in a stronger mass of material. Instead of locking together, rounded aggregate particles tend to slide by each other.

The aggregate selected for this study was granite, an igneous rock, also used by Louisiana Transportation Research Center. Granite is a coarse-grained igneous rock that forms from slow cooling of molten material and can be found in deposits composed of many different types of mineral particles - such as limestone, sandstone, and granite - depending on the original bedrock source of the particles. Selected coarse and fine aggregates were crushed granite and were supplied in two size numbers #78 and #9, according to ASTM D 448,"Standard Classification for Sizes of Aggregate for Road and Bridge Construction". Properties of granite aggregate are provided in Table 5.1. This type of aggregate has irregular shapes and presents a rough-textured structure providing a very good locking in asphalt concrete mixes (HMAs).

Table 5.1 Properties of granite (Waltham, 2002)

Aggregate type	Dry density (kg/m^3)	Porosity (%)	Dry UCS mean (MPa)	Elasticity modulus (GPa)	Tensile strength (MPa)	Shear strength (MPa)	Friction angle $\phi°$	FAA value
Granite	2.72	1	200	75	15	35	55	49.8

5.4 Aggregate Gradation

To specify the aggregate gradation, Superpave uses a modification of an approach already used by some agencies. It uses a standard set of ASTM sieves and the following definitions with respect to aggregate size:

- Maximum Size: One sieve size larger than the nominal maximum size
- Nominal Maximum Size: One sieve size larger than the first sieve to retain more than 10 percent

To specify an aggregate gradation, two additional features are added to the 0.45 power chart: control points and a restricted zone, as shown in Figure 5.2.

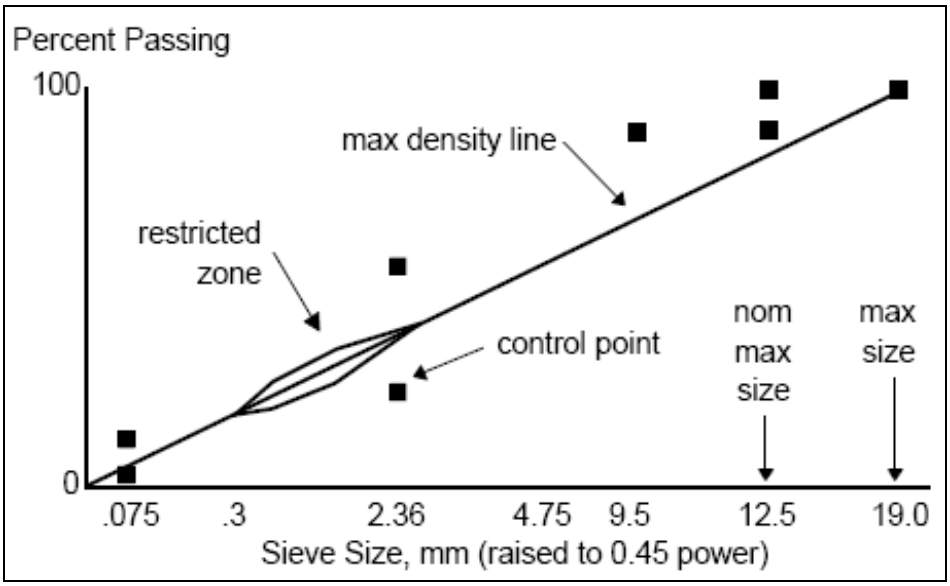

Figure 5.2 Example of Superpave aggregate gradation (FHWA Superpave, 1995).

Control points function as master ranges through which gradations must pass (Kandhal and Mallick, 2001). They are placed on the nominal maximum size, an intermediate size (2.36 mm), and the dust size (0.075 mm). Illustrated in Figure 5.2 are the control points and restricted zone for a 12.5 mm Superpave mixture. The restricted zone resides along the maximum density gradation between the intermediate size (either 4.75 or 2.36 mm) and the 0.3 mm size and it

forms a band through which gradations should not pass. It was adopted by the Superpave system to reduce premature rutting. Control points also ensure a certain filler (0.075 mm material) content which gives a higher stability to the asphalt mixture (Tayebali et al., 1998). Gradations that violate the restricted zone may possess weak aggregate skeletons that depend too much on asphalt binder stiffness to achieve mixture shear strength. These mixtures are also very sensitive to asphalt content and can easily become plastic.

The term used to describe the cumulative frequency distribution of aggregate particle sizes is the **design aggregate structure**. A design aggregate structure that lies between the control points and avoids the restricted zone meets the requirements of Superpave with respect to gradation. Gradation of the aggregate used in this research study is presented in Table 5.2 and Figure 5.3. The nominal maximum aggregate size for this study was 12.5 mm, while the maximum aggregate size was 19 mm.

Table 5.2 Granite aggregate gradation for HMA (6% air voids) mix design

Sieve Size (mm)	Passing (%)
19	100
12.5	95
9.5	85
4.75	50
2.36	31
1.18	20
0.60	15
0.30	11
0.15	9
0.075	5.5

In order to meet the gradation requirements for Superpave asphalt concrete the aggregates that came in two size numbers (#78 and #9) were blended using the trial-and-error method. This method is quite simple and just about as fast as any other more complex method.

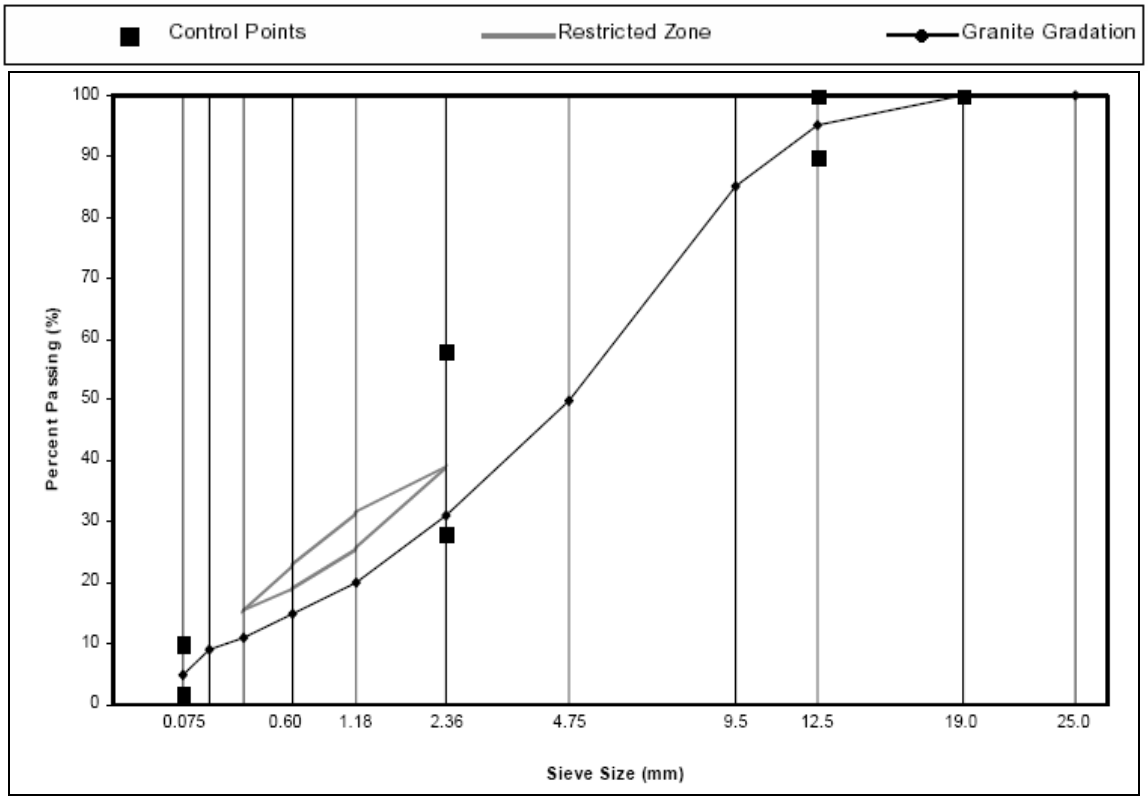

Figure 5.3 Granite gradation used in the study.

To properly develop the aggregate blends, the aggregates were sieved and separated into bins and then recombined for preparing asphalt mixtures. This separation was very important in order to obtain accurate mixture gradations, because the differences between the two gradations for the different aggregates size numbers were fairly small. During the development of these aggregate blends, several trial blends were tested in order to select viable blends.

5.5 Asphalt Mixture Behavior

While the individual properties of asphalt concrete (or HMA) components are important, asphalt mixture behavior is best explained by considering asphalt cement (binder) and mineral aggregate acting together (Daniel and Kim, 1998). One way to understand asphalt mixture behavior is to consider one of the primary asphalt pavement distress types that engineers try to avoid: permanent deformation, a type of distress analyzed in Superpave system.

When a wheel load is applied to a flexible pavement (see Figure 1.1), two stresses are transmitted to the HMA layer: vertical compressive stress within the asphalt layer or HMA surface, and horizontal tensile stress at the bottom of the asphalt layer, as shown in Figure 5.4. Compressive stresses are labeled with (1), (3), and (4), whilst tensile stresses with (2).

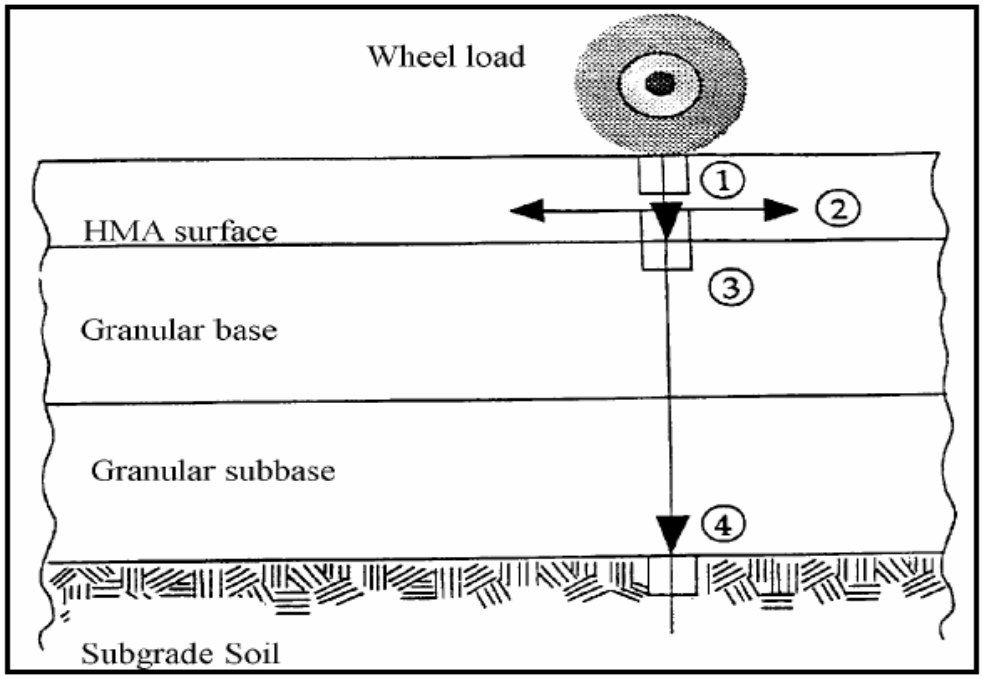

Figure 5.4 Critical stresses transmitted in flexible pavement (Hyung et al., 2003).

The HMA must be internally strong and resilient to resist the compressive stresses and prevent permanent deformation within the mixture. In the same manner, the material must also have enough tensile strength to withstand the tensile stresses at the base of the asphalt layer, and also be resilient to withstand many load applications without fatigue cracking. The asphalt mixture must also resist the stresses imparted by rapidly decreasing temperatures and extremely cold temperatures, attributes acquired through a good mixture design.

5.6 Wheel Path Rutting

Wheel path rutting (see also §1.3) is a permanent deformation that is characterized by a surface cross section that is no longer in its design position. It is called "permanent" deformation because it represents an accumulation of small amounts of deformation (strain) that occurs each time a load is applied (a vehicle passes) (Anderson et al., 2003). This deformation cannot be recovered and it is considered the most common form of permanent deformation. Some researchers consider that rutting is mainly caused by deformation flow rather than volume change. While rutting can have many sources (e.g., underlying HMA weakened by moisture damage, abrasion, and traffic densification), it has two principal causes.

In one case, the rutting is caused by too much repeated stress being applied to the subgrade (or subbase or base) below the asphalt concrete layer. Although stiffer paving materials will partially reduce this type of rutting, it is normally considered more of a structural problem rather than a materials problem (see Fig. 5.5). Essentially, there is not enough pavement strength or thickness to reduce the applied stresses to a tolerable level. A pavement layer that has been unexpectedly weakened by the intrusion of moisture may also cause it. The deformation occurs in the underlying layers rather than in the asphalt concrete layers.

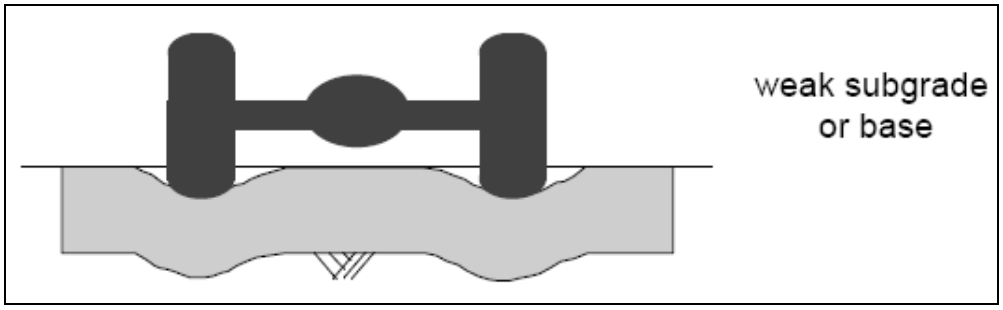

Figure 5.5 Deformation of the flexible pavement due to weak structure (FHWA Superpave, 1995).

The second type of rutting of most concern to asphalt designers is deformation in the asphalt concrete layers, as shown in Figure 5.6. This rutting results from an asphalt mixture without enough shear strength to resist the repeated heavy loads. A weak mixture will accumulate small, but permanent, deformations with each vehicle pass, eventually forming a rut characterized by a downward and lateral movement of the mixture. The rutting may occur in the asphalt surface course, or the rutting that shows on the surface may be caused by a weak underlying asphalt base course.

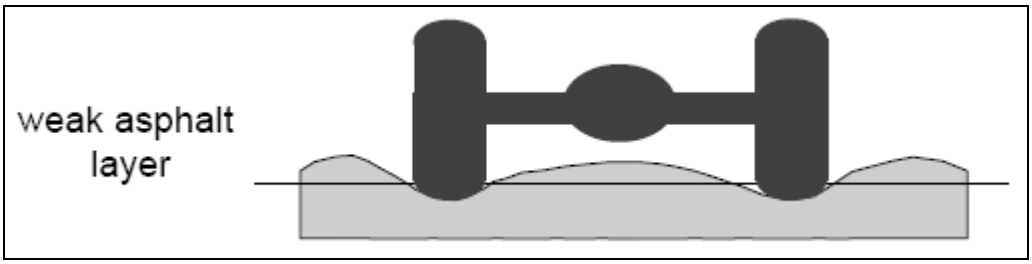

Figure 5.6 Deformation of the flexible pavement due to poor HMA design (FHWA, 1995).

5.7 Asphalt Mixture Volumetrics

This section describes volumetric analysis of asphalt mixtures (HMA), which plays a significant role in most mixture design procedures, including the Superpave system. It reviews the component relationships (mass and volume, aggregate and asphalt), presents the calculation formulas for conducting a volumetric analysis, and describes the Superpave volumetric requirements. The information here applies to both paving mixtures that have been compacted in the laboratory and to undisturbed samples that have been cut from a pavement in the field.

A factor that must be taken into account when considering asphalt mixture behavior is the *volumetric proportions* of asphalt binder and aggregate components, or more simply, *asphalt mixture volumetrics*. The volumetric properties of a compacted paving mixture provide some indication of the mixture's probable pavement service performance.

A tool that can assist in analyzing the properties of HMA is the component diagram - Figure 5.7 - a diagram that illustrates the individual components that make up the HMA: asphalt, aggregate and air. The simplified layout of the component diagram helps visualize the volumetric and mass relationships that are used in the analysis of HMA.

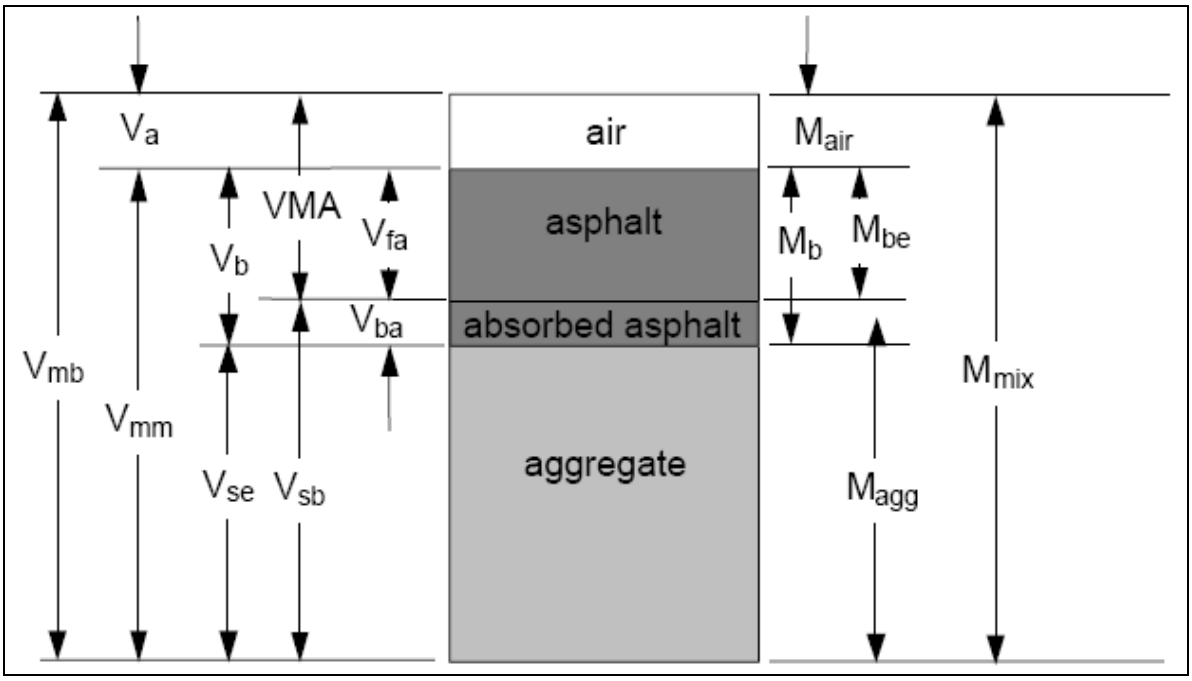

Figure 5.7 Mass and volume relationships in asphalt mixtures (FHWA Superpave, 1995).

All the components are defined in the following:

VMA = Volume of voids in mineral aggregate

V_{mb} = Bulk volume of compacted mix

V_{mm} = Voidless volume of paving mix

V_{fa} (VFA) = Volume of voids filled with asphalt

V_a = Volume of air voids

V_b = Volume of asphalt binder

V_{ba} = Volume of absorbed asphalt binder

V_{sb} = Volume of mineral aggregate (by bulk specific gravity)

V_{se} = Volume of mineral aggregate (by effective specific gravity)

M = Total mass of asphalt mixture

M_{be} = Mass of effective asphalt binder

M_{agg} = Mass of aggregate

M_{air} = Mass of air = 0

M_b = Mass of asphalt binder

The most important parameters of the diagram are called primary volumetric parameters and secondary volumetric parameters. The primary volumetric parameters are those relating directly to the relative volumes (or masses) of the individual components, and they are:

• Total air voids volume (V_v),

• Asphalt binder volume (V_b),

• Volume of mineral aggregate (V_{se}) (by effective specific gravity)

For many years, three other volumetric parameters - V_a, VMA, and VFA - have been widely used and at various times have formed critical design thresholds (Christensen and Bonaquist, 2005). They are:

• V_a - the volume of the air voids (V_v) expressed as a percentage of the total volume of the mixture,

• VMA - Voids in the mineral aggregate,

• VFA - Voids filled with asphalt

In practice, two of these parameters - V_a and VMA - are obtained from measurements of various specific gravities, like $\mathbf{G_{mb}}$, the bulk specific gravity of the compacted mixture; $\mathbf{G_{mm}}$, the maximum theoretical (void-free) specific gravity of the mixture; and $\mathbf{G_{sb}}$, the bulk specific

gravity of the blended aggregate and a knowledge of the mass percentage of bituminous binder in the mixture, V_b. The above parameters and some other parameters involved in the asphalt mixtures design will be presented in the next chapter related to the asphalt mixture specimen preparation. Also, complete definitions of other components are presented in **Appendix H**. Taking into account that all specimens were prepared with an air voids content of 6%, based on previous work done by several Department of Transportation (DOTs), the Superpave asphalt mix design was chosen as shown in Table 5.3. The design was based on ESAL's (see Figure 5.8) of 0.3 to 3 million also chosen from previous research work performed by DOTs.

Table 5.3 Superpave asphalt mix design requirements

ESAL's (millions)	Asphalt binder content (%)	Air voids content (%) V_a	Nom. Max. Agg. Size (mm)	Voids in Min. Agg. (VMA) (%)	Voids Filled with Asphalt (VFA)	Dust to binder Ratio
0.3 - 3	3 - 7	6	12.5	14 - 16	65 - 78	0.6 - 1.2

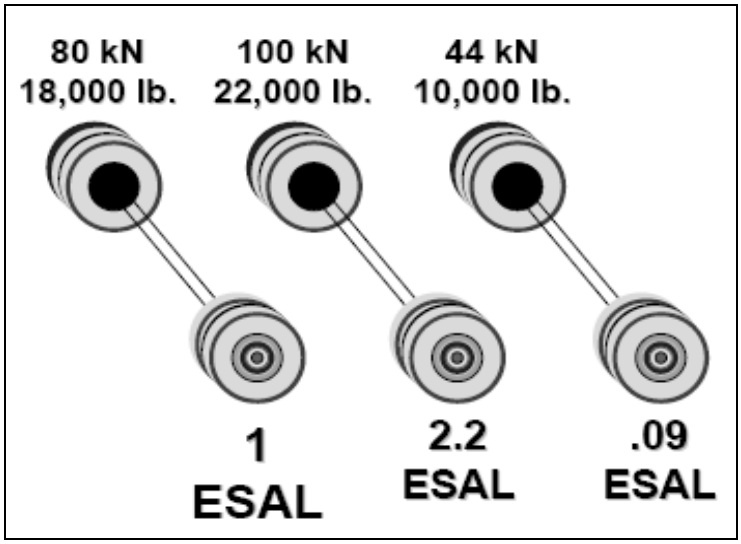

Figure 5.8 Types of ESALs used by the Superpave system (FHWA, 1995).

An ESAL is defined as one 18,000-pound (80-kN) four-tired dual axle, as shown in Figure 5.8, and is the unit used by most pavement thickness design procedures to quantify the

various types of axle loadings into a single design traffic number. If an axle contains more or less weight, it is related to the ESAL using a **load equivalency factor**.

The relationship between axle load and ESAL is not a one to one equivalency, but a fourth power relationship. If you double an 18,000 lb load, the ESAL is not 2, but almost the fourth power of two, (2^4) or about 14. As well, if axles are grouped together, such as in tandem or tridem axle arrangements, the total weight carried by the axle configuration determines its load equivalency factor.

CHAPTER 6. ASPHALT CONCRETE (HMA) SPECIMEN PREPARATION

This chapter contains information about the procedures and the equipment that have been used in order to obtain desired asphalt mixtures (HMA) specimens in the laboratory, by using some of the Superpave system (see Chapter 1 & 3) requirements. It also contains information about the asphalt binder percentages, maximum specific gravity (G_{mm}) and bulk specific gravity (G_{mb}) of compacted mixtures with different asphalt contents, as well as information about percent of air voids in the compacted mixture. Only ten specimens were fabricated in order to see if the results could be used to verify the Hirsch model and Shenoy's empirical equation.

6.1 Procedure Overview

Once the aggregate blends were selected and the initial trial asphalt binder content was calculated, the HMA mixtures were prepared. This phase consists of the following main steps:

• Heating the aggregates and asphalt binder to the mixing temperature (159° ± 3 °C).

• Mix both components and short-term age the mixture for 2 hours at 135 °C.

• Compact the mixture at a temperature of at least 145° ± 3 °C.

All asphalt mixes in this study were prepared at the Louisiana Transportation Research Center (LTRC) using the gradation from Table 5.2 and five asphalt binder contents, from 3% through 7% (by mass) with 1% step increase. Filler content was kept constant around 20% by mass of total asphalt content. Samples were produced in duplicates for each asphalt content, resulting in a total number of ten (10), after they were cut in order to fit in the shear testing machine (SST). The process of cutting and preparing the samples for testing with the Superpave Shear Tester (SST) will be described in more details later in this chapter.

Before being mixed with the asphalt binder, the aggregates were heated at 160 °C for one hour in order to have the same temperature with the binder and thus, to not contain any moisture

that could impede a good adherence of the binder on the aggregate surface. Once the aggregates reached the mix temperature, the appropriate amount of asphalt binder was added and the batch was then mixed using a heated mechanical mixer as shown in Figures 6.1 and 6.2.

Figure 6.1 Adding the appropriate quantity of asphalt binder to the aggregate.

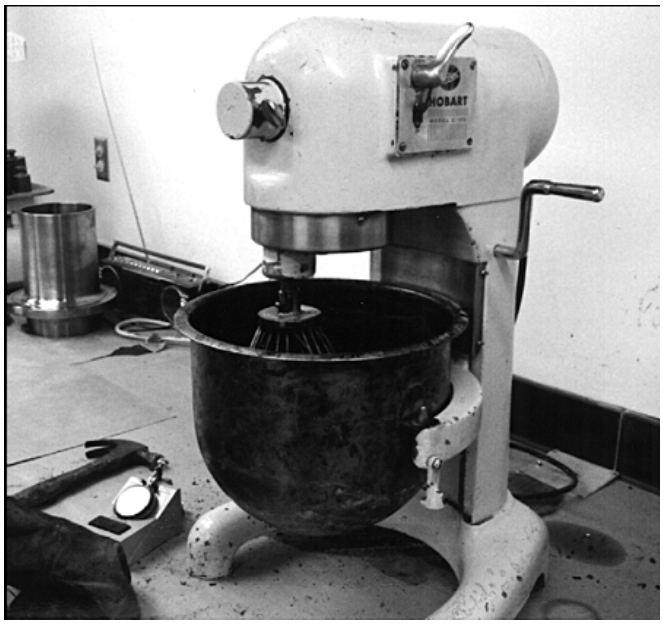

Figure 6.2 Mechanical mixer used for preparing the batch.

The mixing was done until the aggregate was completely covered by the binder and immediately after mixing, the batch was transferred to a pan and cured for 2 hours in the oven at the compaction temperature of 155 °C. This is said to model the aging of the mix that occurs at the mixing plant and in the truck in route from the asphalt plant to the construction site. After the samples had been 'short termed aged', the mix was transferred to the corresponding compaction mold and then compacted, as presented in Figure 6.3.

Figure 6.3 Pouring the asphalt mixture in the mold in order to be compacted.

All samples were compacted at the same height (120 mm) using a Superpave Gyratory Compactor, which will be presented in the following section.

6.2 Superpave Gyratory Compactor

SHRP researchers had several goals in selecting a method of laboratory compaction. Most important, they desired a device that would realistically compact trial mix specimens to densities achieved under actual pavement climate and loading conditions. The device needed to

be capable of accommodating large aggregates, and furthermore, it was desired that the device afford a measure of compactability so that potential tender mixture behavior and similar compaction problems could be identified. A high priority for SHRP researchers was a device that was well suited to mixing facility quality control and quality assurance operations. Because no compactor in current use achieved all these goals, consequently, a new compactor was developed, called the Superpave Gyratory Compactor (SGC).

The basis for the SGC was a large Texas gyratory compactor modified to use the compaction principles of a French gyratory compactor (Brown et al., 2001). The Texas device accomplished the goals of achieving realistic specimen densification and it was reasonably portable. Its 6-inch sample diameter (ultimately 150 mm on an SGC) could accommodate mixtures containing aggregate up to 50 mm maximum (37.5 nominal) size. SHRP researchers modified the Texas device by lowering its angle and speed of gyration and adding real time specimen height recording.

As shown in Figure 6.4, the SGC is a mechanical device comprised of the following system of components:

- Reaction frame, rotating base, and motor
- Loading system, loading ram, and pressure gauge
- Height measuring and recording system
- Mold and base plate.

The reaction frame provides a stiff structure against which the loading ram can push when compacting specimens, while the base of the SGC rotates and is affixed to the loading frame. It supports the mold while compaction occurs.

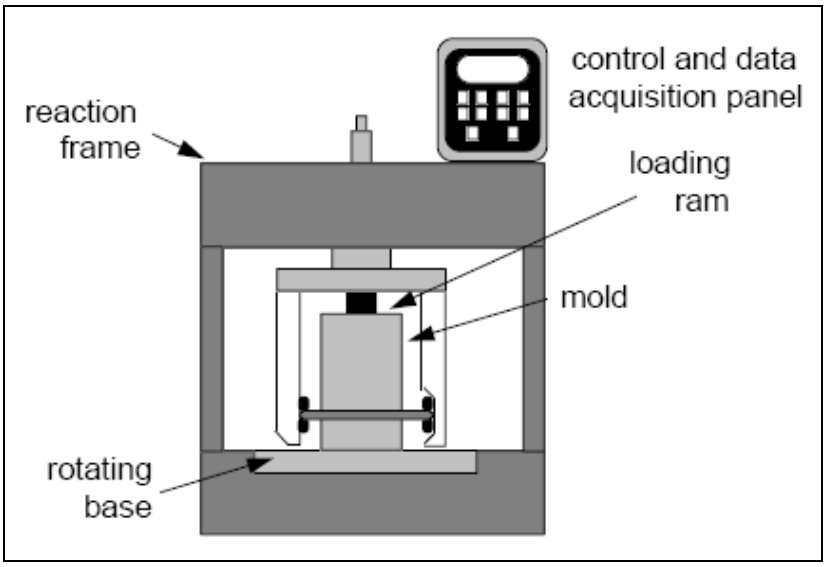

Figure 6.4 Schematic of a gyratory compactor proposed by Superpave (FHWA Superpave, 1995).

Reaction bearings are used to position the mold at a compaction angle of 1.25 degrees, as shown in Figure 6.5, which is the compaction angle of the SGC. An electric motor drives the rotating base at a constant speed of 30 revolutions per minute.

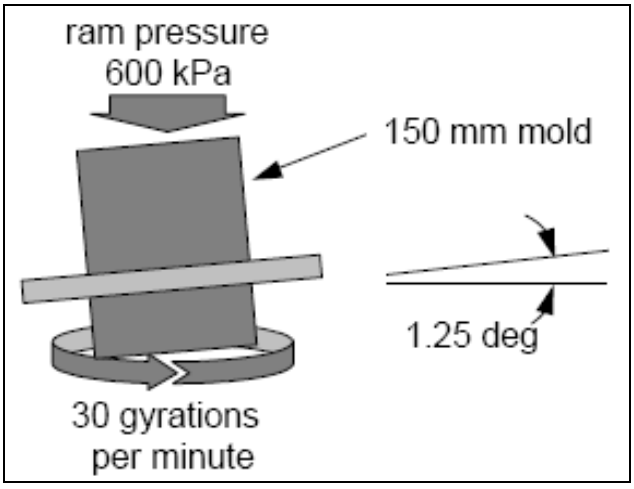

Figure 6.5 Schematic of the compaction process in the SGC (FHWA Superpave, 1995).

The SGC uses a mold with an inside diameter of 150 mm and a nominal height of at least 250 mm. A base plate fits in the bottom of the mold to afford specimen confinement during compaction. A hydraulic or mechanical system applies a load to the loading ram, which imparts 600 kPa (see Fig. 6.5) compaction pressure to the specimen. The loading ram diameter nominally matches the inside diameter of the mold, which is 150 mm. A pressure gauge measures the ram pressure during compaction. As the specimen densifies during compaction, the pressure gauge and loading ram maintain compaction pressure. Figure 6.6 presents a gyratory compactor used by most U.S. Departments of Transportation (DOTs).

Figure 6.6 Actual Superpave Gyratory Compactor (FHWA Superpave, 1995).

Specimen height measurement is also an important function of the SGC. Using the mass of material placed in the mold (see Section 6.3), the diameter of the mold, and the specimen height, an estimate of specimen density can be made at any time throughout the compaction process. The specimen volume is calculated as the volume of a smooth sided cylinder with a diameter of 150 mm and the measured height. Height is recorded by measuring the position of the ram before and during the test. The vertical change in ram position equals the change in specimen height. The specimen height signal is connected to a personal computer, printer, or other device to record height (i.e., density) measurements throughout the compaction process. By this method, a compaction characteristic is developed as the specimen is compacted.

6.3 Specimens Compaction and Cutting

In order for the specimens to be tested in the laboratory they are obtained from loose material (asphalt mixture batch) by compaction in the SGC, after being scoop poured in the molds (see Fig. 6.3). Figure 6.7 shows how the mold is inserted into the gyratory compactor in order for the asphalt mixture to be compacted.

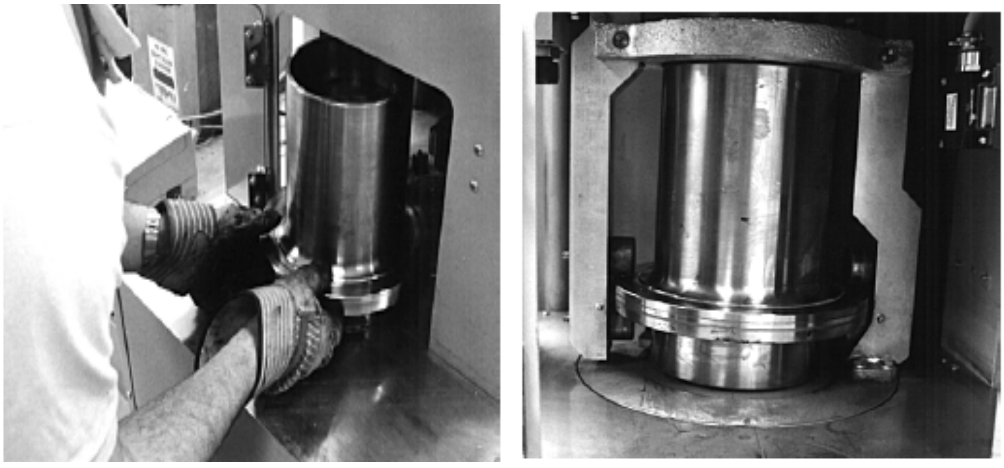

Figure 6.7 Compacting asphalt mixture in the gyratory compactor.

After compaction the specimen is demolded and let to cool off for at least two hours before being prepared for testing. Figure 6.8 shows several specimens that have just been demolded and placed on a grate for cooling.

Figure 6.8 Demolding and cooling of asphalt concrete specimens.

The specimens produced for this study needed approximately 4500 grams of mixture each in order to fabricate one specimen that is 150 mm in diameter by approximately 120 mm in height. In this case, specimens had to be cut and trimmed to a height 50 mm before testing with the Superpave Shear Tester (SST) or Indirect Tensile Tester (IDT), as shown in Figure 6.9.

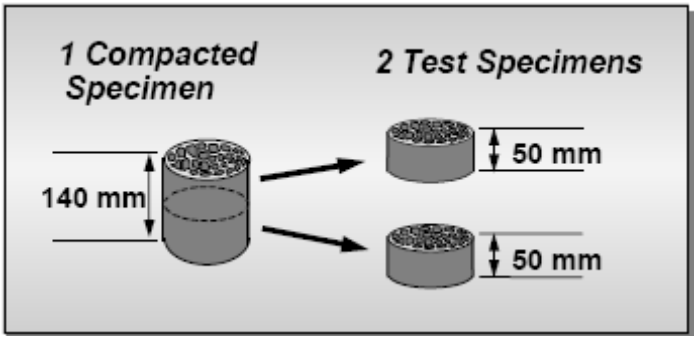

Figure 6.9 Cutting compacted specimen at required dimensions for testing (FHWA Superpave, 1995).

For this study 5 specimens 150 mm in diameter by 120 mm in height were compacted using the gyratory compactor. A total number of 10 specimens, two for each asphalt content, 150 mm in diameter by 50 mm in height, were obtained after being cut and ground for the SST testing. **Appendix H** (Table H1) contains all the information on compacted samples at each asphalt content.

6.4 Analyzing Compacted Paving Mixtures

The method employed for calculating asphalt mixtures parameters uses the specific gravity measurements with mathematical formulas to directly determine the mixture properties. This method, because of the mathematical formulas, can easily be placed into spreadsheet calculations and is more often used in laboratory mix design and analysis. During compaction three gyration levels are of interest:

- Design number of gyrations (N_{design} or N_{des}).
- Initial number of gyrations ($N_{initial}$ or N_{ini}), and
- Maximum number of gyrations ($N_{maximum}$ or N_{max}).

Test specimens are compacted using N_{des} gyrations, design number that ranges from 50 to 125 and is a function of the traffic level. The range of values for N_{des}, N_{max}, and N_{ini} are illustrated in Table 6.1 below. For this study the design ESALs (see § 5.7) has been chosen between 0.3 and 3 millions.

Table 6.1 Number of gyrations function of design ESALs (FHWA Superpave, 1995)

Superpave Design Gyratory Compactive Effort			
Design ESALs (millions)	Compaction Parameters		
	$N_{initial}$	N_{design}	$N_{maximum}$
< 0.3	6	50	75
0.3 to < 3	7	75	115
3 to < 10	8	100	160
≥ 30	9	125	205

6.4.1 Maximum Specific Gravity of Compacted Mixtures G_{mm}

In designing a paving mixture with a given aggregate, the maximum specific gravity, G_{mm}, at each asphalt content is needed to calculate the percentage of air voids for each asphalt content. Maximum specific gravity (G_{mm}) is defined as the ratio of the weight in air of a unit volume of an uncompacted bituminous paving mixture at a stated temperature to the weight of an equal volume of gas-free distilled water at a stated temperature. G_{mm} is required to calculate air voids of the compacted specimens. The Rice Method, as specified in the ASTM D2041 "Standard Test Method for Theoretical Maximum Specific Gravity and Density of Bituminous Paving materials", was used in this study. In the procedure, approximately 2000 grams of oven dried mix was used in the process. The oven-dried mix was first weighed in the air (A). A glass pycnometer or a metal flask, as specified in the ASTM D2041, was then filled with water and weighed (B). A vacuum was gradually applied on the pycnometer after filling in with the mix and water to release any air that might be trapped in the mix. The vacuum was then released and the weight of the container filled with water and sample mix was taken (C). Theoretical maximum density was computed using the following formula:

$$G_{mm} = \frac{A}{A + B - C} \tag{6.1}$$

where:

A = weight of mix [g]

B = weight of pycnometer filled with water [g]

C = weight of pycnometer, water, and mix [g]

6.4.2 Bulk Specific Gravity of Compacted Mixtures G_{mb}

This test was conducted according to AASHTO T-166 "Standard Specification for Bulk Specific Gravity of Compacted Bituminous Mixtures Using Saturated Surface Dry Specimens". The specimen was placed in an oven at a temperature of 52°C overnight and then weighed every two hours. The sample was considered dry when the change in weights obtained (in any consecutive two hours) was less than 0.05% of the sample weight. Then the sample was removed from the oven for five hours to cool to room temperature. The weight of the specimen in the air (W_{air}) was recorded. Then, the specimen was soaked in water bath at 25°C for 4 minutes and weighted in water (W_{sub}). The specimen was removed from the water and blotted with a towel as quickly as possible to achieve Saturated Surface Dry (SSD) condition. The weight in this condition (W_{ssd}) was then measured. The bulk specific gravity (G_{mb}) of the specimen was calculated as follows:

$$G_{mb} = \frac{W_{air}}{W_{ssd} - W_{sub}} \tag{6.2}$$

6.4.3 Percent VMA in Compacted Mixtures

The voids in the mineral aggregate, VMA, are defined as the intergranular void space between the aggregate particles in a compacted paving mixture that includes the air voids and the effective asphalt content, expressed as a percent of the total volume. The VMA is calculated on the basis of the bulk specific gravity (G_{sb}) of the aggregate and is expressed as a percentage of the bulk volume of the compacted paving mixture (G_{mb}). Therefore, the VMA can be calculated by subtracting the volume of the aggregate determined by its bulk specific gravity from the bulk volume of the compacted paving mixture. If the mix composition is determined as percent by mass of total mixture, then VMA is calculated using the following formula:

$$VMA = 100 - \frac{G_{mb} \cdot P_s}{G_{sb}} \quad (6.3)$$

where: VMA = voids in mineral aggregate (% of bulk volume)

G_{sb} = bulk specific gravity of total aggregate

G_{mb} = bulk specific gravity of compacted mixture (from § 6.4.2)

P_s = aggregate content (% by total mass of mixture)

6.4.4 Bulk Specific Gravity of Aggregate (G_{sb})

When the total aggregate consists of separate fractions of coarse aggregate, fine aggregate, and mineral filler, all having different specific gravities, the bulk specific gravity for the total aggregate is calculated using the following formula:

$$G_{sb} = \frac{P_1 + P_2 + \ldots + P_N}{\frac{P_1}{G_1} + \frac{P_2}{G_2} + \ldots + \frac{P_N}{G_N}} \quad (6.4)$$

where: G_{sb} = bulk specific gravity for the total aggregate

P_1, P_2, P_N = individual percentages by mass of aggregate

G_1, G_2, G_N = individual bulk specific gravities of aggregate

The bulk specific gravity of mineral filler is difficult to determine accurately. However, if the apparent specific gravity of the filler is substituted, the error is usually negligible. Table 6.2 shows an example of the data for one sample of paving mixture (3% asphalt content).

Table 6.2 Data for sample of asphalt mixture

Mixture components				
Material	Specific gravity		Mix composition	
		Bulk	Percent by mass of total mix	Percent by mass of total aggregate
Asphalt binder	1.030 (G_b)		3 (P_b)	3.3 (P_b)
Coarse aggregate	---	2.716 (G_1)	49.4 (P_1)	55.2 (P_1)
Fine aggregate	---	2.689 (G_2)	47.6 (P_2)	41.5 (P_2)
Filler	---	---	---	---

6.4.5 Percent Air Voids in Compacted Mixture (V_a)

The air voids, V_a, in the total compacted paving mixture consist of the small air spaces between the coated aggregate particles. The volume percentage of air voids in a compacted mixture can be determined using the formula:

$$V_a = 100\left(1 - \frac{G_{mb}}{G_{mm}}\right) \quad (6.5)$$

where:

V_a = air voids in compacted mixture (% of total volume of asphalt mixture)

G_{mm} = maximum specific gravity of paving mixture (see § 6.4.1)

G_{mb} = bulk specific gravity of compacted mixture

In order to obtain the same air voids content (6%) for 6% and 7% asphalt content the filler percentage was decreased from 20% to 19% (by mass of total asphalt content).

6.4.6 Percent VFA in Compacted Mixtures

The percentage of the voids in the mineral aggregate that are filled with asphalt, VFA, not including the absorbed asphalt, is determined using the formula:

$$VFA = 100\left(1 - \frac{V_a}{VMA}\right) \quad (6.6)$$

where:

VFA = voids filled with asphalt (% of VMA)

VMA = voids in mineral aggregate (% of bulk volume)

V_a = air voids in compacted mixture (% of total volume of asphalt mixture)

Complete Superpave gyratory compaction data and volumetric parameters regarding the asphalt mixtures analyses are presented in **Appendix G**.

CHAPTER 7. ASPHALT MIXTURES TESTING METHODOLOGY

This chapter provides information on specimen preparation and instrumentation used for testing the compacted samples obtained previously from the gyratory compactor. Testing procedures and types of tests performed on these samples are also presented.

7.1 Specimen Preparation

The first step in specimen preparation is to trim test specimens to a thickness of 50 mm and make sure that both faces of the specimen are smooth and plane. For the two tests performed with the SST, that require no confining pressure, the specimen is glued between two platens, as shown in figure 7.1.

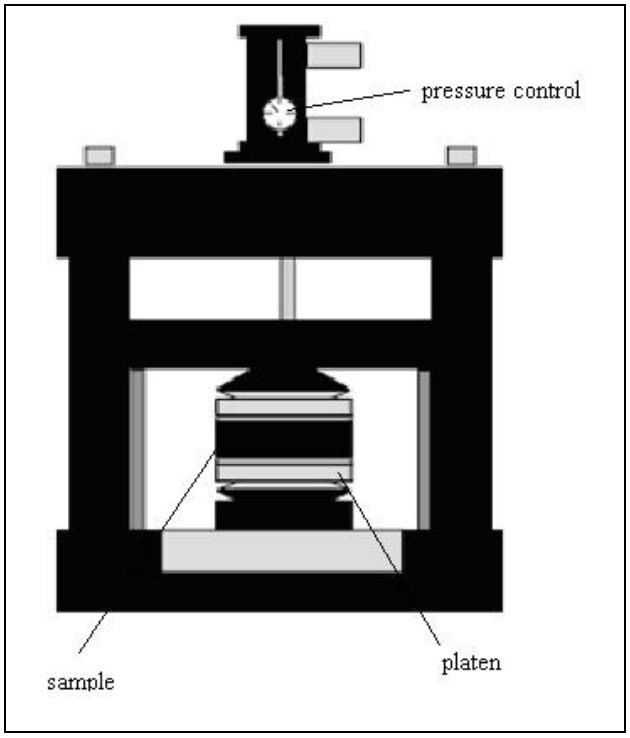

Figure 7.1 Compression device used for gluing asphalt specimens and platens together (FHWA Superpave, 1995).

A compression device is used to squeeze the specimen between the platens while the glue cures. Epoxy glue such as Devcon Plastic Steel is used. The compression device rigidly holds the

platens and specimen to ensure that the platen faces are parallel. After the glue has cured the specimen with the two platens attached to it is ready for being installed inside the shear tester where LVDTs are also attached to the platens like in Figure 7.2.

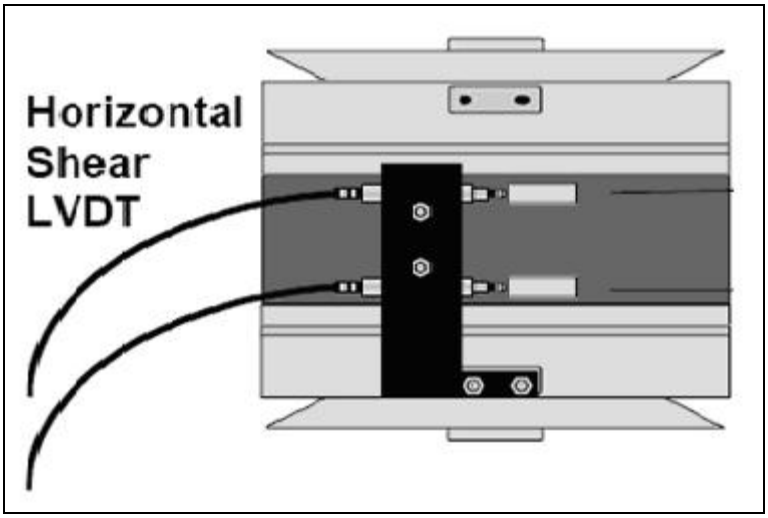

Figure 7.2 Asphalt mixture specimen with two platens and horizontal LVDT attached to it (SST Manual).

Before gluing, the platens are thoroughly cleaned to ensure that the surfaces are free of dust and prior specimen debris. With the compression device, the specimen is bonded to the platens under a pressure of approximately 35 kPa for the period of time recommended by the epoxy cement manufacturer. For the 5-minute Devcon Plastic Steel Epoxy, five minutes is used and quick action is required. Any excess epoxy is trimmed from the specimen and platens. The glue set-up times will also vary with the "thickness" of the application and the ambient temperature.

7.2 Superpave Shear Tester (SST)

Two mechanical test devices were developed under SHRP: the Superpave Shear Tester (SST) and the Indirect Tensile Tester (IDT). The original Superpave mix analysis procedures used the results from tests in these equipment to determine the extent of permanent deformation, fatigue cracking, and low temperature cracking that would develop under the project conditions.

Depending on the traffic level, either an intermediate or complete analysis of the design mixture would be performed. An intermediate analysis could be used for traffic levels up to ten million ESALs.

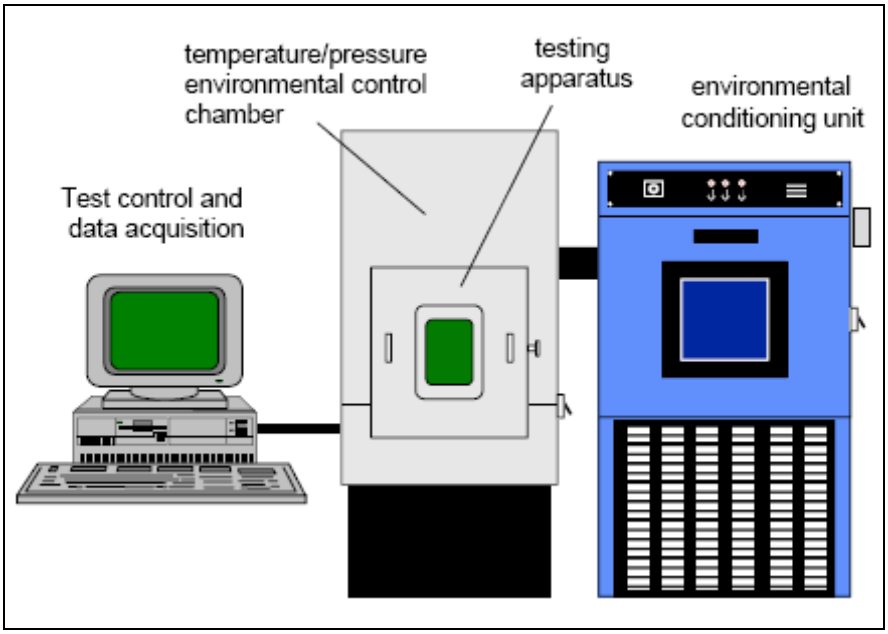

Figure 7.3 Schematic of the Superpave Shear Tester Equipment (FHWA Superpave, 1995).

The testing apparatus includes a reaction frame and shear table. It also serves to house the various components that are driven by other system components such as temperature/pressure control, hydraulic actuators, and input and output transducers. The reaction frame is extremely rigid so that precise specimen displacement measurements can be achieved without worrying about displacements from frame compliance. The shear table holds specimens during testing and can be actuated to impart shear loads. Picture of an actual shear tester used by Louisiana Transportation Research Center (LTRC) is presented in Figure 7.4.

Figure 7.4 COX 7000 Superpave Shear Tester (LTRC Laboratory).

The test control unit consists of the system hardware and software. The hardware interfaces with the testing apparatus through input and output transducers, and it consists of controllers, signal conditioners, and a computer and its peripherals. The software consists of the algorithms required to control the testing apparatus and to acquire data during a test.

Linear Variable Differential Transducers (LVDTs) are affixed to platens and measure the response of specimens to applied testing loads. The LVDTs make it possible for the system to also operate in a closed loop feedback mode, which means that LVDT signals are used to control applied testing loads. The environmental control unit is required to control the temperature and air pressure inside the testing chamber at a constant level. The unit is capable of maintaining temperatures within a wide range from -20° to 80 °C. Air pressure and the rate of pressure change within the chamber is precisely controlled. Air pressure is normally applied at a rate of 70 kPa per second, up to a maximum value of 840 kPa. This is achieved by storing compressed

air in separate storage tanks that can be emptied into the testing chamber at the required rate. Air pressure provides specimen confinement for two of the six tests that can be performed with the SST. Also, the hydraulic system provides the force required to load specimens in different testing conditions. A hydraulic motor powers two actuators, each with a capacity of approximately 32 kN. The vertical actuator applies an axial force to test specimens, while the horizontal actuator drives the shear table, which imparts shear loads to the specimen.

7.3 Tests Performed with the Superpave Shear Tester (SST)

According to the traffic levels (ESALs) selected for this study, an intermediate analysis is required for the asphalt mixtures made in the laboratory. This analysis prediction of permanent deformation requires:

- Frequency sweep at constant height (FSCH)
- Repeated shear loading at constant height (RSCH)

7.3.1 SST Frequency Sweep at Constant Height (FSCH)

For performing this type of test the assembled test specimen is placed in the environmental control chamber and/or an auxiliary chamber, set at the specified test temperature (55° and 64 °C for this study), to condition for 2 to 4 hours prior to initiating the test. The time will vary with test temperature and operator experience. For mixes of known resistance, the tests are usually conducted in ascending order of test temperature from coolest to warmest. For unknown mix specimens, it is safer to start the testing at 20°C, to evaluate whether adjustments in electronic gain settings would be necessary to avoid specimen damage at the other test temperatures. In addition, the environmental chamber requires a minimum amount of time to achieve a new test temperature (usually overnight) prior to installing the assembled test specimen. The most effective manner of testing is to perform various types of testing using one

temperature per testing day and to change the temperature of the testing chamber overnight. Also, a horizontal LVDT and an axial LVDT are attached directly to the top and bottom platens as shown in Figure 7.5.

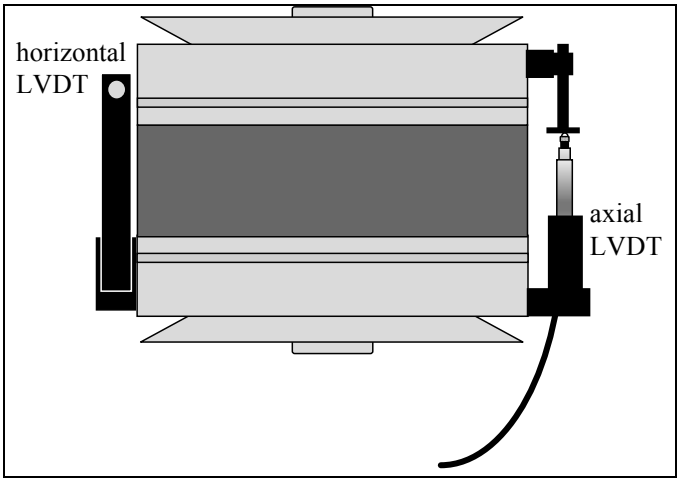

Figure 7.5 Asphalt mixture specimen prepared for SST testing (SST Manual).

All LVDTs are checked for proper alignment and mechanically zeroed, usually to the extreme low end of the range to maximize the capacity for measurement. For the frequency sweep test at constant height the SST is programmed to record the axial deformation, the shear deformation, the axial load, and the shear load on the specimen at a constant rate of 50 data points per dynamic strain cycle. The actual sampling rates per second and the number of cycles sampled are shown in Table 7.1. The cycles that are sampled are the last group in the total number of cycles applied.

For example, for the 0.5 Hz frequency, the last four (for CS 7000) of the seven applied cycles are recorded by the SST. The frequency sweep test at constant height takes up to 135 minutes to complete for each one of up to three required temperatures (if necessary). This time includes set-up, placing the specimen in the test equipment, temperature stabilization in the chamber, running the test, and removing the specimen from the apparatus.

Table 7.1 Testing schedule for frequency sweep at constant height

Frequency (Hz)	Number of cycles
10	50
5	50
2	20
1	20
0.5	7
0.2	7
0.1	7
0.05	4
0.02	4
0.01	4

However, it does not include bringing the environmental control chamber to proper test temperature. The frequency sweep test at constant height (FSCH) is the only SST test in a Superpave mix analysis that uses a *dynamic* type of loading, where the shear modulus characteristics of the asphalt mixture are measured. In this test, a sinusoidal horizontal shear strain and axial stress are applied as shown in Figure 7.6.

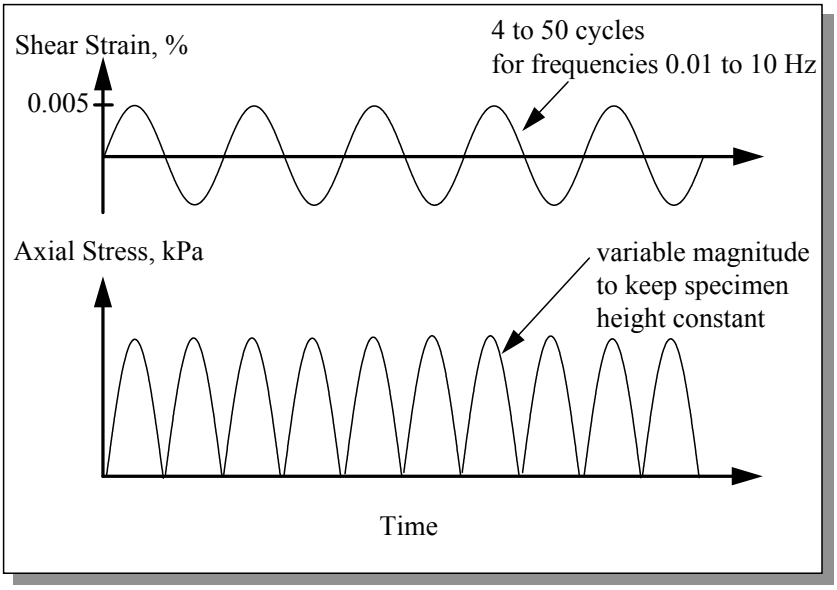

Figure 7.6 Shear strain and axial stress applications in frequency sweep test at constant height (FSCH) (SST Manual).

A repeated sinusoidal shearing strain of ± 0.005 percent (maximum peak-to-peak amplitude of 0.0001 mm/mm) is created in the specimen to achieve a sinusoidal shear stress. Like the simple shear test, as the specimen is sheared, it seeks to increase in volume or dilate, which increases its height. The vertical actuator uses the signal from the axial LVDT to apply sufficient axial stress to keep the specimen height constant.

Since the deformation or strain is the controlling feature for the SST, the wave form should appear uniform (as depicted in Fig. 7.6) and the resulting measured load or stress curve may appear slightly misshapen compared to an ideal wave form. The axial deformation is a measured response used to signal the application of an axial load to maintain constant height. Therefore, these axial recordings will not exhibit a cyclical wave form. Figures 7.7 and 7.8 provide an example of a portion (5 Hz frequency) of an acceptable data file. The traces for the shear load, axial load, and the two LVDTs are reasonable. The load cell readings were properly zeroed prior to test and the shear strain is applied as programmed, as shown in the shear LVDT trace.

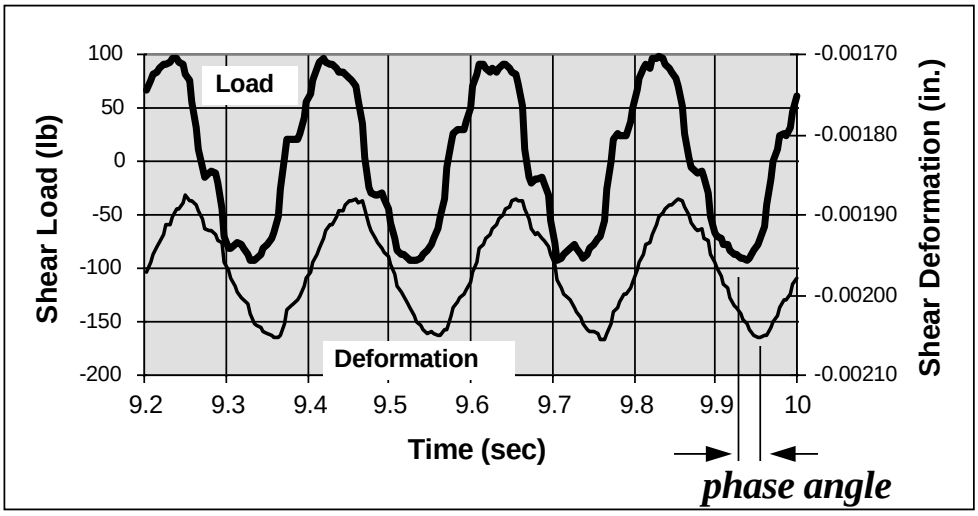

Figure 7.7 Example frequency sweep shear load and deformation curves (5 Hz) (SST Manual).

There is a slight time delay between the measured peak load and the programmed peak shear deformation. This time delay is related to the phase angle, δ, of the mix, which is a typical viscoelastic material response (see § 3.6.7). Very little measured axial load (mostly 4 to 8 lb in compression) is apparently necessary for this test frequency and temperature (54 °C) to maintain a constant specimen height, as can be seen from Figure 7.8. Generally, the amount of axial load that is necessary is dependent on temperature and frequency. At low temperatures when the specimen is relatively hard, axial loads can be considerably higher (1000 to 1500 lb) and it is possible to break the specimen or fail the glue. As shown by the apparent output from the axial LVDT, there is very little, if any, vertical deformation for this case (5 Hz and 54 °C).

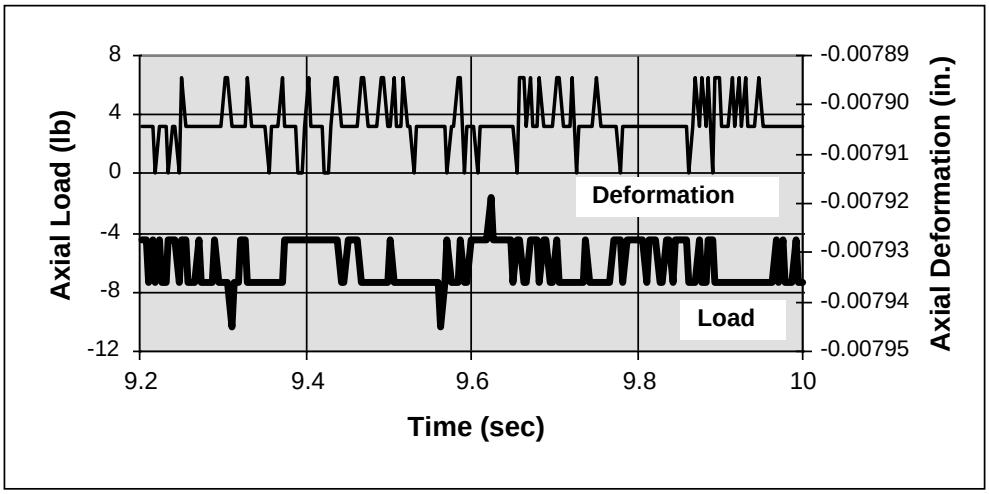

Figure 7.8 Example frequency sweep axial load and deformation curves (5 Hz) (SST Manual).

Although this level of precision is not to be taken as an absolute measurement, the data fluctuates between 0.007915 in. and 0.007895 in. which indicates a total axial deformation of about 0.00002 in. (0.0005 mm). This is judged to be well within the required definition for constant height, ± 0.0013 mm (± 0.00005 in.).

Figures 7.9 and 7.10 below, show poorly-formed wave forms for the resulting shear load and the programmed shear deformation, also for the 5 Hz, portion of an unacceptable frequency sweep test. The deformation curve, again on expanded scale, appears to indicate a problem with the LVDT (possibly loosely-connected or the reference points are moving). This kind of data file should not be used and the specimen should be remounted and retested after the problem is resolved. Figure 7.9 shows very ununiform axial and shear load curves at a frequency of 5 Hz and a temperature of 54 °C.

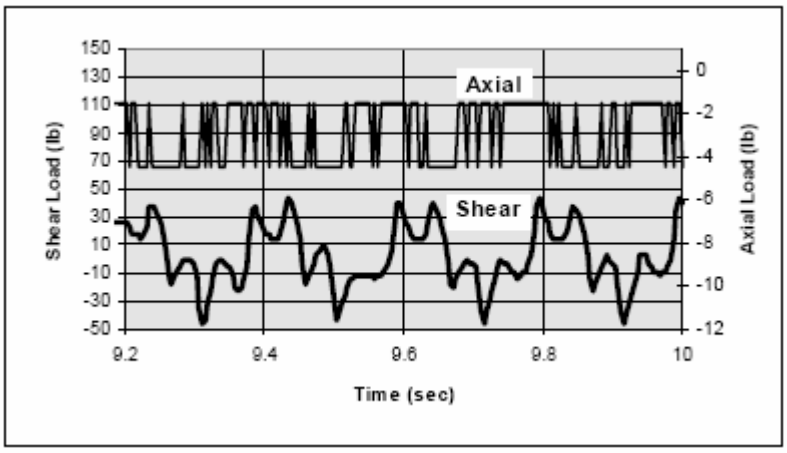

Figure 7.9 Poor example of frequency sweep axial and shear load curves (5 Hz) (SST Manual).

Also, figure 7.10 shows defective deformation curves at the same testing parameters.

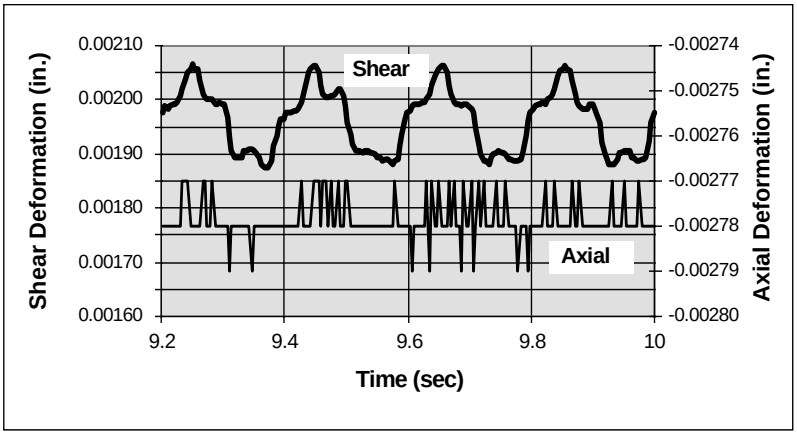

Figure 7.10 Poor example of frequency sweep axial and shear deformation curves (5 Hz) (SST Manual).

A frequency sweep test may be unacceptable if the gain settings of the SST are not adequate and the shear stress is too low at the high frequencies. This improper "tuning" can cause a significant error (up to 100,000 psi) in the complex shear modulus at 10 Hz and the poorly-formed wave forms. However at high frequencies, "perfect" sinusoidal waves (load and deformation) remain an extremely difficult goal to achieve.

7.3.2 SST Repeated Shear at Constant Height (RSCH)

This test is an initial screening tool for either an intermediate or a complete mix analysis using the SST and is included in AASHTO TP7 as an optional test procedure used to estimate the relative rut depth (permanent deformation). It is used for evaluating the potential of a tertiary flow portion of the permanent deformation curve plotted on logarithmic scale, as shown in Figure 7.11.

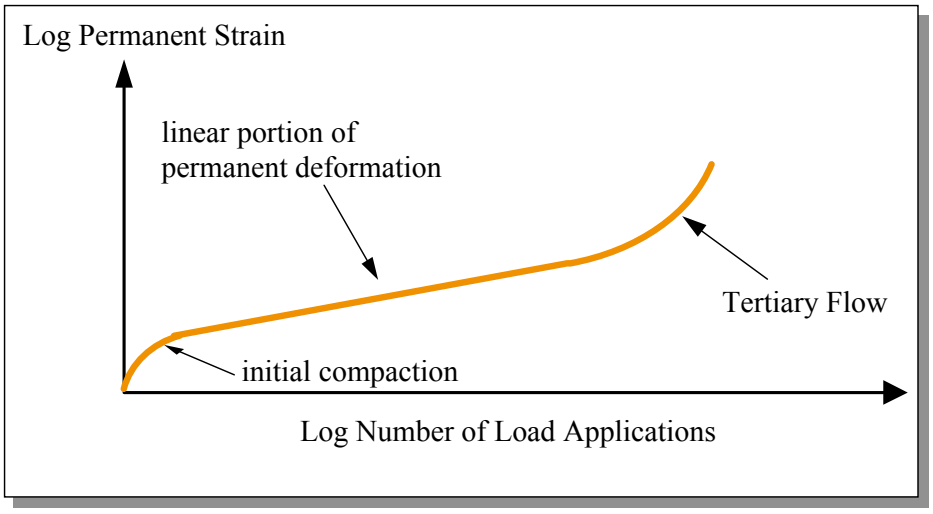

Figure 7.11 Plot of permanent deformation vs. load applications showing three parts (SST Manual).

Stage 3 of permanent deformation (rutting), also known as tertiary flow, represents a condition of the asphalt mixture when the air voids (V_a) content decreases approximately below 3% and the binder starts to act as a lubricant between the aggregates, reducing the contact pressures. At this

point, the HMA has ultimately failed and the rutting will occur at a much quicker rate. Therefore, once compaction has finished in the pavement under the wheel loads, shear strains, caused primarily by large shear stresses in the upper portion of the HMA, are dominant (Brown et al., 2001). Since the compaction of the HMA is a natural phenomenon that is inevitable in most HMAs, it is the shear strains that a properly designed HMA must withstand.

In the repeated shear test at constant height (RSCH), the stresses are applied as shown in Figure 7.12. A controlled cyclical haversian shearing stress is applied to the test specimen. At the same time, the specimen is subjected to synchronized haversian axial or vertical stress pulses. A haversian wave form is a special type of load pulse [(1-cosθ)/2] which approximates the effect of a wheel load in the field; the load magnitude does not change sign as opposed to the sinusoidal loading in the frequency sweep test which continually cycles from positive to negative. The ratio of the axial stress to the shear stress is held within a constant range of 1.2 to 1.5. Both axial and horizontal load actuators are adjusted by closed-loop feedback control from the axial and shear load measurements, respectively.

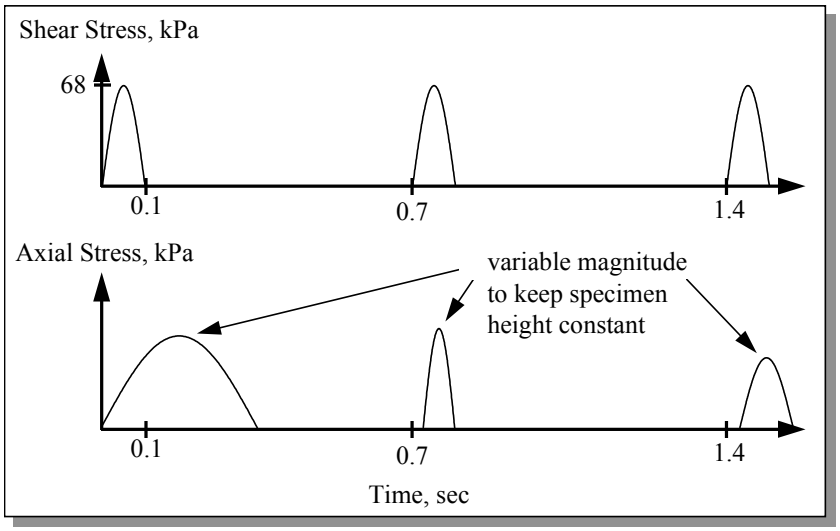

Figure 7.12 Haversian stress applications in the repeated shear test at constant height (SST Manual).

Ideally, the curve shown in Figure 7.11 should not turn up after a large amount of load repetitions; instead, it should remain nearly at a constant slope. As the third distinct part of the curve, it has been described as *tertiary flow*. Mixes that exhibit this tertiary flow behavior are susceptible to gross instability, especially at high binder contents. Therefore, prior to performing any performance-related tests, a mix should be examined for this kind of instability.

The repeated shear test at constant height is also stress-controlled and for the one required temperature takes up to 210 minutes to complete 5,000 cycles, but the actual test time depends on the final number of cycles, test temperature, and equipment. In some cases the test stops automatically if the permanent strain reaches 5%, while the shear stress amplitude is maintained at 68 ± 5 kPa. The test time includes set-up, placing the specimen in the testing equipment, temperature stabilization in the chamber, running the test, and removing the specimen from the apparatus. However, it does not include bringing the environmental control chamber to proper test temperature. The system is allowed to stabilize for 25 ± 5 minutes, after securing the environmental chamber, prior to initiating the test. If a significant amount of time is taken in mounting the specimen, this stabilization time may need to be increased.

The SST is programmed to record the axial deformation, the shear deformation, the axial load, the shear load, and the phase angle (ϕ) of the specimen during specific loading cycles at a sampling rate of 60 data points per second. The following intervals of cycles (Table 7.2) are recommended for sampling during the first 5000 cycles.

Figure 7.13 shows two load pulses of actual data from a repeated shear test at constant stress ratio. The pulse has a 0.1 second duration with a 0.6 second rest period between pulses, as programmed. The axial load has a peak of approximately 500 lb and the shear load has a peak of about 330 lb, resulting in a 72 kPa shear stress and 104.4 kPa axial stress.

Table 7.2 Data collection during an RSCH test

Data Collection During Cycle Ranges :	
1 through 10	1747 through 1750
20 through 22	2000 through 2002
30 through 32	2247 through 2250
50 through 52	2500 through 2502
80 through 82	2748 through 2750
100 through 102	2997 through 3000
200 through 202	3200 through 3202
300 through 302	3400 through 3402
400 through 402	3600 through 3602
500 through 502	3800 through 3802
600 through 602	3997 through 4000
800 through 802	4200 through 4202
1000 through 1002	4500 through 4502
1247 through 1250	4998 through 5000
1500 through 1502	

In this example, the axial to shear stress ratio (104.4/72) is about 1.45, as recommended by the manual.

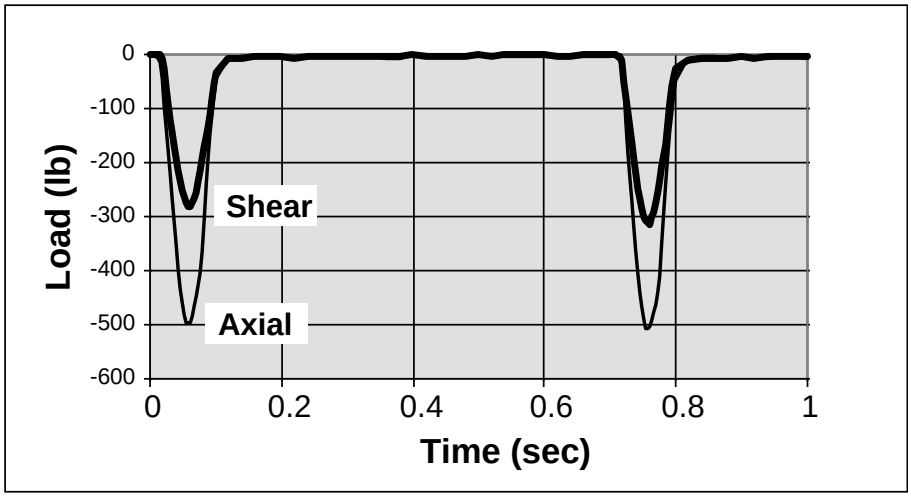

Figure 7.13 Example of axial and shear load curves of RSCH test (SST Manual).

Also, an example plot of the cumulative plastic shear strain versus the number of load repetitions, on logarithmic scale, is shown in Figure 7.14.

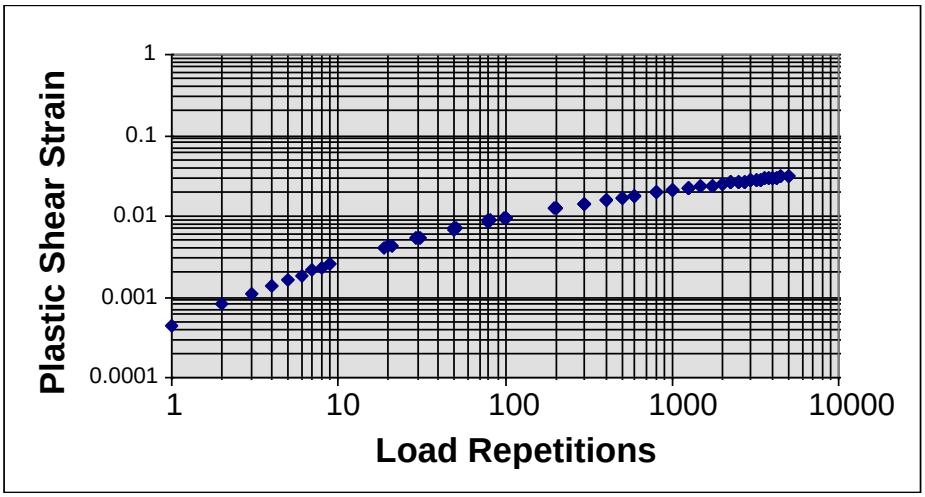

Figure 7.14 Plot of cumulative shear strain vs. number of shear load cycles (SST Manual).

If the rate of plastic shear strain appears to be increasing or accelerating as shown in Figure 7.11 (i.e. exhibiting tertiary flow) within the specified number of load pulses (5,000), the test is terminated and the asphalt concrete mix is considered undesirable. In the example shown in Figure 7.14, the plastic strain was about three percent (0.03) after the specified 5000 repetitions for the selected test temperature, and there was no indication of an increasing slope. Therefore, this mix would then be evaluated with the performance-related tests and modeling in the Superpave mix analysis.

In its present form, RSCH test may offer a possible alternative design step to evaluate a mix for possible permanent deformation problems. In addition, in the future it may be beneficial to examine the use of other more severe stress applications and/or more repetitions with this test. Since this repeated shear tests produce a resulting plot of permanent strain vs. number of load applications like Figure 7.14, they provide a technique for examining the relative rutting performance of various mixes. Similar to the Georgia Loaded Wheel Tester or the Hamburg Wheel Tracking Device, all of these "cycling" type tests can be used to empirically rate or rank different mixes in comparison to established criteria.

CHAPTER 8. SUMMARY AND ANALISYS OF SST TEST RESULTS

This chapter presents a discussion on the asphalt mixtures tests results obtained in the laboratory by using a Superpave Shear Tester (SST). The tests results are used to draw conclusions on the performance of the asphaltic materials and their ability to meet the SHRP specifications. It also presents comparisons with the test results obtained from the DSR testing of asphalt mastics (see Chapter 6). Only ten asphalt mixture samples (150 mm in diameter by 50 mm in height) were tested at 55° and 64 °C in order for the results to be used in predicting the shear stiffness and permanent strain.

8.1 Shear Frequency Sweep at Constant Height (FSCH) Tests Results

The shear frequency sweep or shear dynamic modulus G* test conducted with the Superpave Shear Tester (SST) was developed under the SHRP research program to measure mixture properties that can be used to predict mixture performance. As stated in chapter 7, during the loading cycles the specimen height is maintained constant by applying sufficient axial stress. This is accomplished by controlling the vertical actuator using close-loop feedback from an axial LVDT. The data (deformation and load) obtained from the FSCH test is used to automatically calculate two material properties: dynamic shear modulus G* and phase angle δ. During this test, the load is applied to the asphalt concrete specimen until a shear stress of 0.01% is obtained. This ensures that the sample is solely tested in the linear elastic range.

Figure 8.1 shows the dependencies of shear complex modulus on frequency loading and testing temperatures. As for the asphalt mastics, the curves for the mixtures exhibited the same trend, with larger G* values at higher frequencies and smaller values at lower frequencies, compared to the curve at 25 °C. Also, larger values were obtained for the lower temperature (55 °C) compared to the higher temperature (64 °C) this fact showing again that the binder behaves

more elastically at lower temperatures. Compared to the mastics shear moduli, the shear moduli for asphalt concrete mixtures increased by three orders of magnitude, from 85 kPa to 192.67 MPa at 55 °C and from 27 kPa to 121.5 MPa at 64 °C. These values were obtained at 10 Hz frequency loading which is considered as a typical highway speed (Anderson et al., 2002).

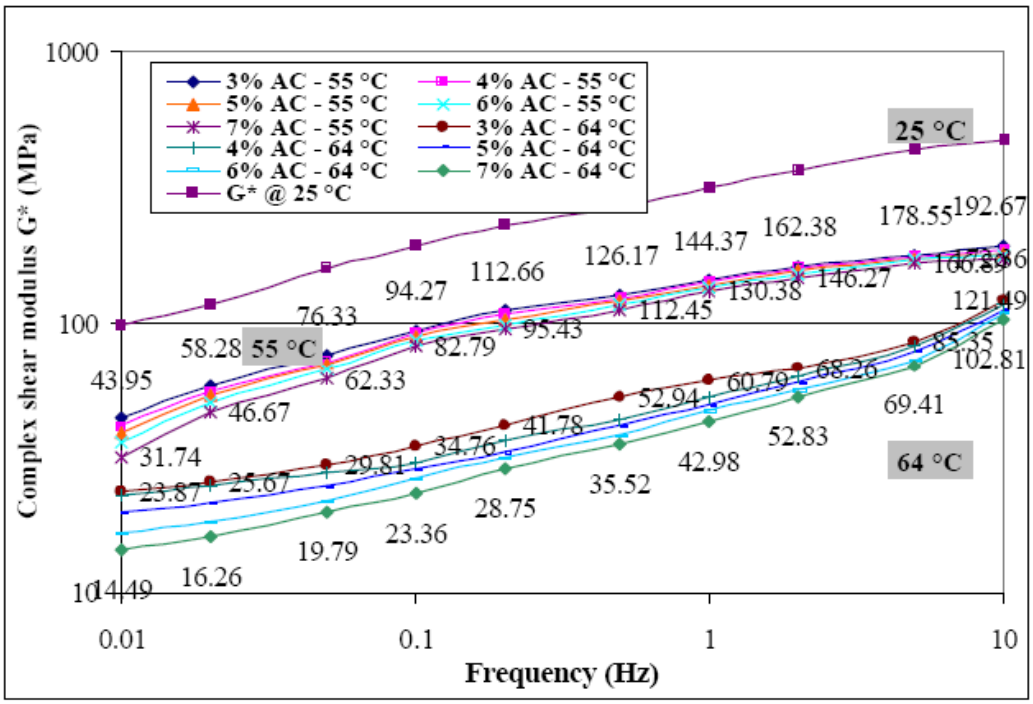

Figure 8.1 Shear complex modulus dependency on temperature and loading frequency of asphalt mixtures.

Figure 8.1 shows that the shear complex modulus depends not only on temperature, but also on the asphalt binder content. As it can be seen from the above figure, the shear modulus has decreased with the increase in asphalt content, for both temperatures - 55° and 64 °C. The decrease was of about 20 MPa at the 10 Hz frequency and 10 MPa at 0.01 Hz. This means that the shear modulus is more affected by the aggregate interaction while sheared, more asphalt content resulting in less friction between the aggregate particles due to the increased asphalt film thickness between the particles.

Another important parameter that defines the behavior of the asphalt mixture, and is recorded by the SST, is represented by the phase angle, defined as the lag time between the application of a stress and the corresponding strain (see Fig. 7.7). Figure 8.2 shows the phase angle versus the frequency for all the asphalt mixture specimens that were tested at 55° and 64 °C. The values ranged from 22 to 60 degrees at 55 °C, while at 64 °C they were slightly higher ranging from 44 to almost 70 degrees. Compared to the asphalt mastics there was a decrease of 20 degrees at 55 °C and 14 degrees at 64 °C, again, due to the mineral aggregate effect, which impedes the binder to regain its elasticity quicker than in the case of mastics. Curves at 3% asphalt content were not as smooth as those at higher contents due to lack of bondage between coarse aggregate particles.

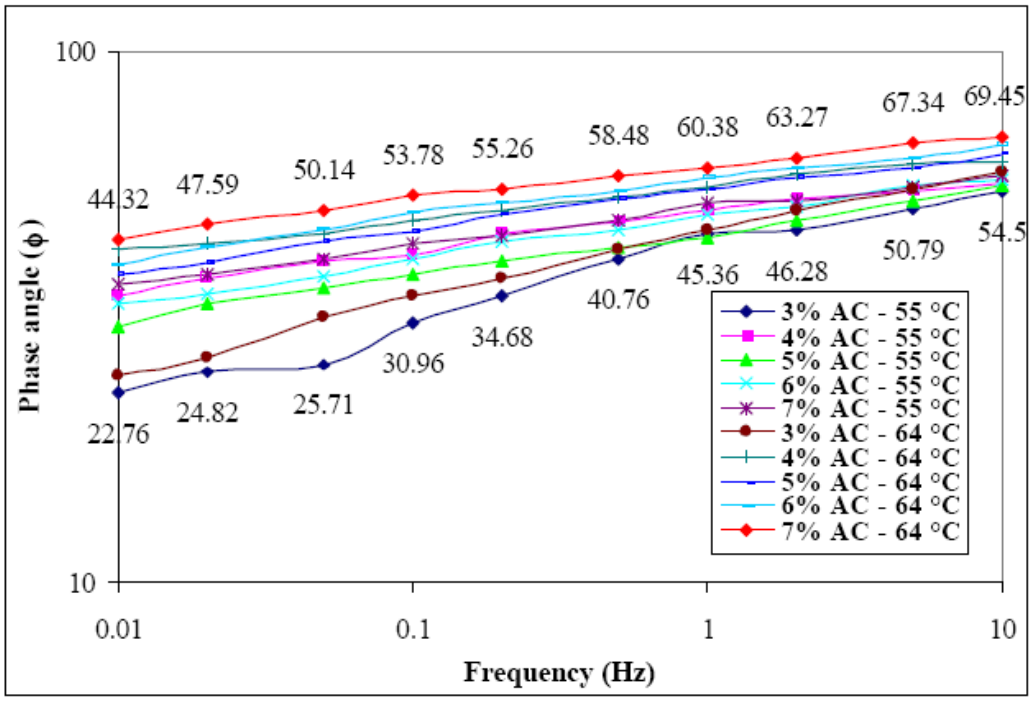

Figure 8.2 Phase angle dependency on frequency and temperature of asphalt mixture.

Same reason (aggregate effect) was the cause of the fact, in the case of the asphalt mixtures, that the phase angles have increased with the increase of the frequency, opposite to the asphalt mastics, where the phase angle have decreased with the increase in frequency (see Fig. 4.11).

Therefore, at higher temperatures and frequencies (usually over 1 Hz) the asphalt mixtures exhibit more viscous behavior than at lower temperatures and frequencies. This behavior is also shown by the G* components, G' (storage modulus) and G" (loss modulus) in Figure 8.3. It can be seen that the viscous component (G") is larger than the elastic component (G') for frequencies higher than 0.1 Hz. All samples exhibited the same behavior for larger asphalt contents at the same frequencies. Test results for frequency sweep at 4, 5, 6, and 7% asphalt contents are presented in **Appendix H**.

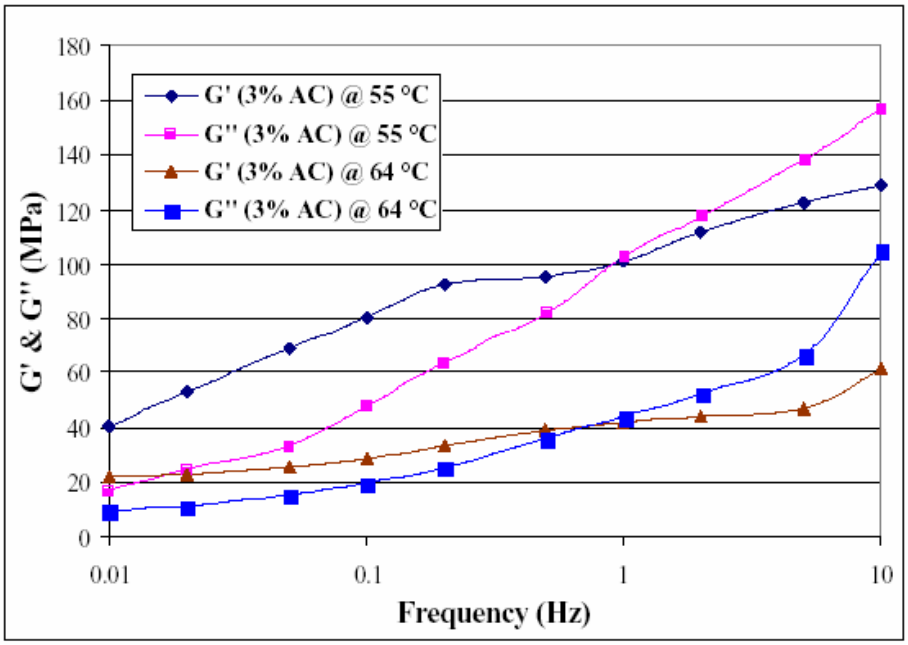

Figure 8.3 Variation of G* components with the loading frequency at 3% asphalt content.

Lower phase angles indicate more resistance to permanent deformation (rutting) of the asphalt mixtures, thus it can be inferred that mixtures with lower asphalt content are less prone to permanent deformation than those having higher asphalt contents.

For rutting resistance to be contributed by asphalt cement, a high complex modulus, G*, and low phase angle, ϕ, are both desirable. The ratio used in Superpave system to determine the resistance to permanent deformation by asphalt cements is the rutting parameter - $G^*/\sin\delta$ at

different temperatures. For asphalt mastics and mixtures, the greater this ratio, the more resistant to permanent deformation the asphalt cement will be. A comparison of the G*/sinδ values for the different asphalt mixtures is presented in Figure 8.4, showing G*/sinδ as a function of test loading frequency.

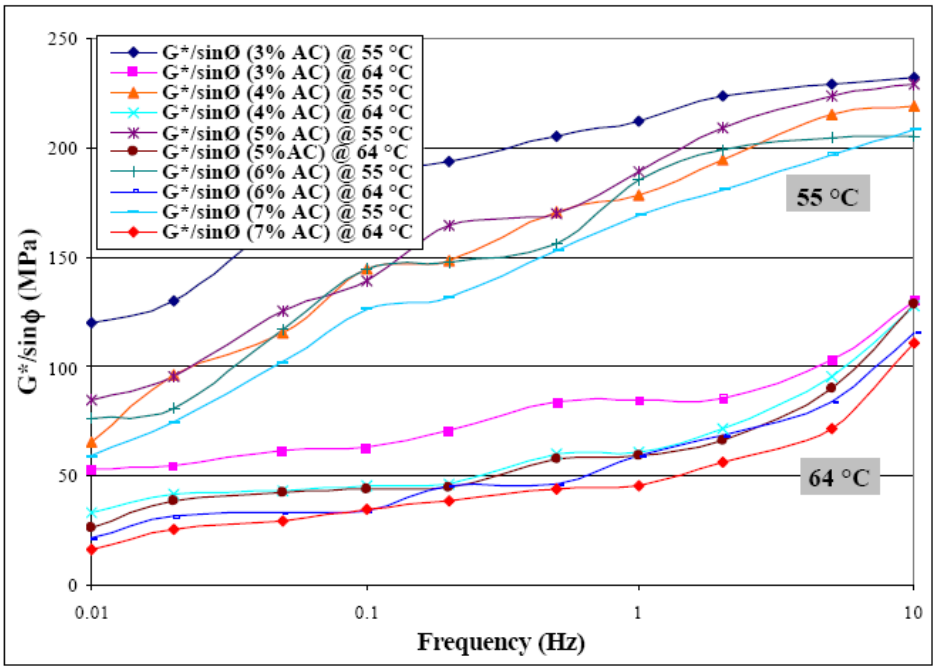

Figure 8.4 G*/sinϕ versus frequency for different asphalt mixtures at 6% air voids.

In this case, also lower asphalt contents indicate more resistance to permanent deformation of the HMA mixtures. The graph, indicate that low asphalt contents give higher G*/sinδ values than higher asphalt contents. For constant air voids content (VA), 6% in this study in all the blends, higher asphalt contents generally yield higher susceptibility to permanent deformation. As for the asphalt mastics, there was an increase in the rutting parameter for the lower temperature (55 °C) as well as for higher frequencies.

Also, by using the same procedures on Chapter 4, § 4.2, combining all the test data from one material at the two temperatures (55° and 64°C) and translating the individual curves along

the time axis (using the shift factor a_T), single master curves are obtained as shown in Figure 8.5 below. Table containing the shift factors (a_T) and constants (C_1 and C_2) for all the asphalt mixtures, along with the single master curves for the rest of the asphalt contents are presented in **Appendix H**.

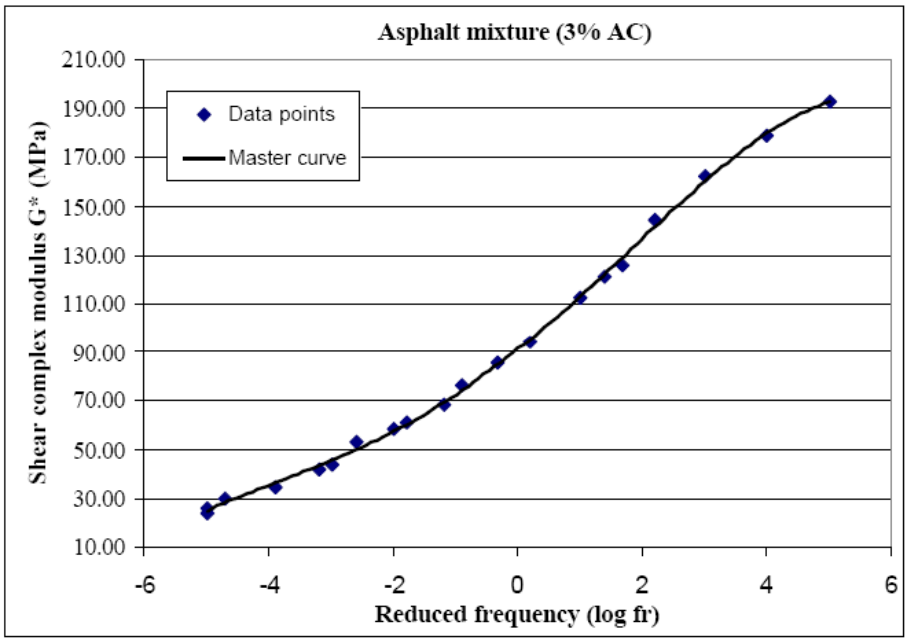

Figure 8.5 Single master curve at 3% asphalt content mixture.

8.2 Repeated Shear Loading at Constant Height (RSCH) Tests Results

As mentioned in the previous chapter, RSCH test was developed as a simplified method used to estimate relative rut depth and permanent deformation by recording the accumulated strain in the specimen. In the RSCH test, repeated haversine shear load pulses (68 ± 5 kPa) are applied to the specimen for 5,000 cycles or until the permanent strain reaches 5%. When the repeated shear load is applied, the test specimen tends to dilate. To prevent vertical dilation, a controlled axial load is applied to keep the specimen at a constant height. The load cycle requires 0.7 seconds, wherein a 0.1-second load is followed by 0.6-second rest period. This test was

performed at the design asphalt content (corresponding to six percent air voids at N_{des}) using only granite as the mineral aggregate. Before testing, the specimens were preconditioned by applying 100 cycles of a haversine shear load with a peak magnitude of 7 ± 1 kPa. After preconditioning, the specimens were subjected to 5,000 load cycles at two temperatures - 55° and 64 °C in accordance with ATS Manual and AASHTO TP7.

The accumulated permanent shear strains versus the number of loading cycles for the RSCH tests at 55° and 64 °C are shown in Figure 8.6. As shown in the figure, the mixture samples having the lowest asphalt content (3%) achieved the lowest permanent shear strain (2.06%), while the mixtures with the largest asphalt content (7%) achieved the highest (4.31%). There was an increase of 36% in permanent shear strain from 3% asphalt content through 7% asphalt content at 55 °C and about 25% at 64 °C for the same range. Also, no tertiary zones appeared during the testing, meaning that there was no permanent damage in the specimens.

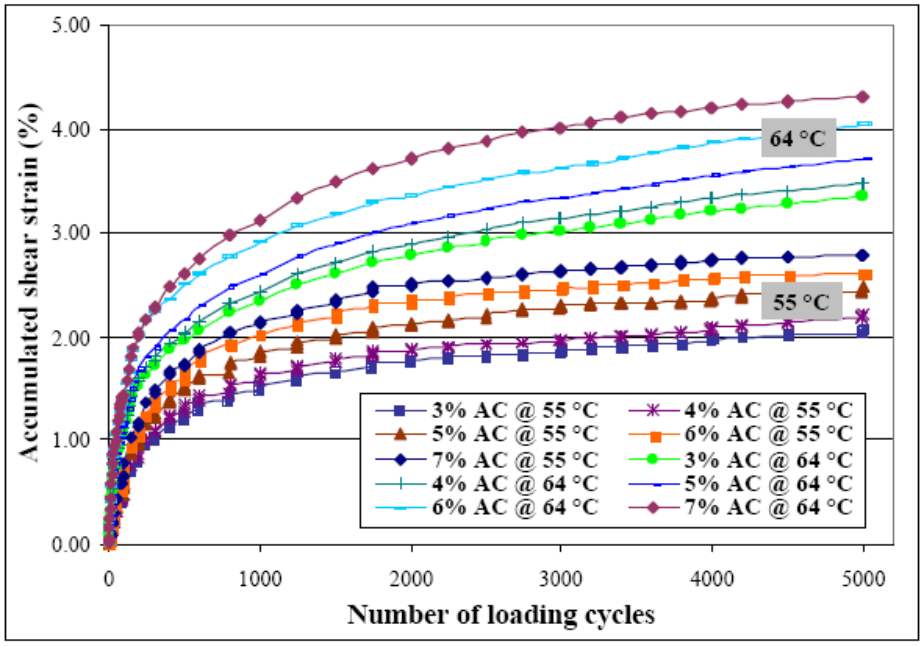

Figure 8.6 SST RSCH test results for asphalt mixtures at 55° and 64 °C.

Compared to the strains obtained for 15% limestone mastics, strains for asphalt mixtures (20% granite filler) are almost similar at 64 °C (around 4%), but approximately 30% lower (around 2.5%) than those of mastic (3.3%) at 55 °C. Maximum accumulated shear strains values for asphalt mixtures are presented in Table 8.1. Selected permanent shear strain values from tests at both temperatures are presented in **Appendix J**.

Table 8.1 Maximum accumulated shear strain (γ_{acc}) values for asphalt mixtures

Material	Maximum accumulated shear strain (γ_{acc})	
	55 °C	**64 °C**
3% Asphalt content mixture	0.0206	0.0335
4% Asphalt content mixture	0.0221	0.0348
5% Asphalt content mixture	0.0248	0.0371
6% Asphalt content mixture	0.0261	0.0404
7% Asphalt content mixture	0.0279	0.0431

8.3 Estimation of Complex Shear Modulus G* Using the Hirsch Model

By using the Hirsch model presented in section 4.4, the complex shear moduli G* of asphalt concrete specimens were estimated. Figure 8.7 presents the results of the measured shear complex moduli (FSCH at 10 Hz) versus estimated moduli of asphalt samples for five binder contents (3% through 7%) at two testing temperatures - 55° and 64°C.

Values for G^*_b were determined experimentally from oscillation at constant strain (see § 4.1) by using the Dynamic Shear Rheometer (DSR). Figure 8.7 shows the G* values estimated using equations 4.17 and 4.18 versus the measured values using a dynamic rheometer. From the above figure it can also be seen that there is a generally good correlation between the measured and predicted values, with R^2 numbers being all above 0.95. This fact indicates that the Hirsch model can be used as in the case for the asphalt mastics. Calculations have been made for all 5 asphalt contents at the two temperatures - 55° and 64 °C. Calculated values of E_a, VFA, and VMA (using Excel software) are presented in **Appendix H**.

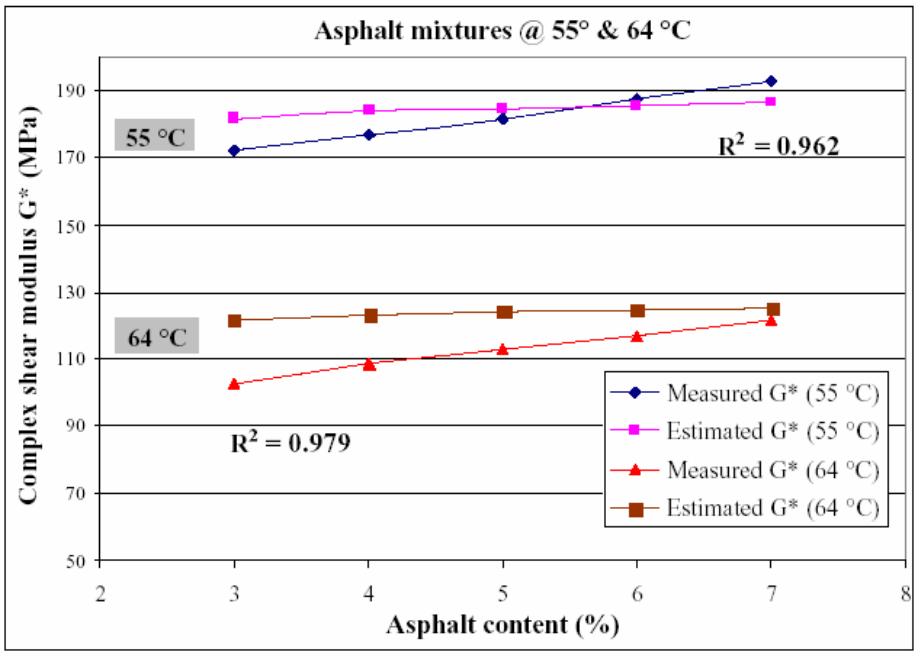

Figure 8.7 Estimated versus measured complex shear modulus for asphalt mixtures.

8.4 Estimation of Accumulated Shear Strain in Asphalt Mixtures using Shenoy Equation

By using the Shenoy equation from section 4.3 the accumulated permanent strain was estimated for all the asphalt concrete samples. Due to the fact that the load applied during the SST testing (68 kPa) was two orders of magnitude larger than the load applied when testing the mastics, ($100\tau_0$) term from eq. 4.16 was replaced by ($10\tau_0$). By doing this replacement, values obtained by applying eq. (4.16) were much closer to the values determined from the testing, indicating that it is applicable also to asphalt mixtures. The binder shear modulus G* used in the formula was taken from the granite (20% filler) mastic sweep frequency test at 10 Hz and it was 85 kPa. Figures 8.8 and 8.9 show the measured accumulated unrecovered (permanent) shear strain of the mixtures containing 3% asphalt against the accumulated shear strain obtained by using Shenoy's equation 4.16. Figures showing measured accumulated shear strains versus estimated strains for the remaining asphalt contents are presented in **Appendix J**. The graphs in

this appendix show a good correlation between the estimated shear strain values and the measured strain values, taking into account that all the R^2 values are around 0.90.

The best estimation was obtained for 6% asphalt content (0.9732) at 55°, while the poorest was for 7% asphalt content (0.8967) also at 55°C. An example of SST repeated shear test data file is also presented in **Appendix J**.

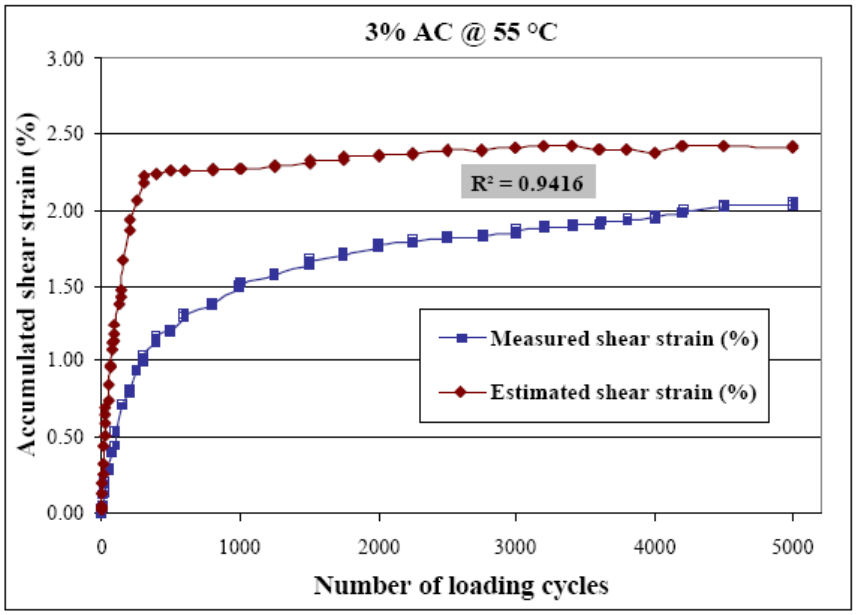

Figure 8.8 Estimated versus measured accumulated shear strain values for 3% asphalt content mixture at 55 °C.

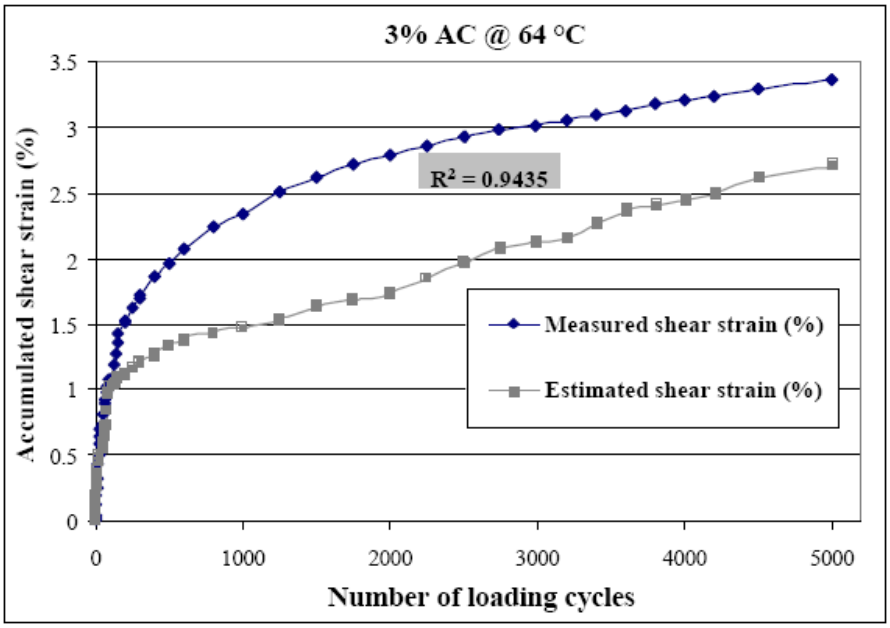

Figure 8.9 Estimated versus measured accumulated shear strain values for 3% asphalt content mixture at 64 °C.

CHAPTER 9. CONCLUSIONS AND RECOMMENDATIONS

Predicting the performance of hot mix asphalt (HMA) concrete is very difficult due to the complexity of HMA, the complexity of the underlying unbound layers and varying environmental conditions. In the present, there are no specific methods being used nationally to design and control HMA in order to prevent rutting, fatigue cracking, and other flexible pavement distresses. Hence, some additional research and more standardization are needed to minimize the occurrence of these distresses. Finally, this study intended to simply perform mastics and mixtures laboratory tests and use some of the results to predict performance parameters.

9.1 Research Summary

This study included two laboratory testing phases regarding the asphalt pavements: a first phase in which asphalt binder (PG64-22) and mastics were tested using a dynamic shear rheometer (DSR) and a second phase in which asphalt mixtures were tested using a Superpave Shear Tester (SST). Both pieces of equipment are currently used by US Departments of Transportation (DOTs) in order to assess rheological properties of asphalts and mixtures. In each phase, both types of material (mastics and mixtures) were tested under frequency sweep shear loading and repeated shear creep loading. Asphalt binder and mastics obtained from three types of filler - donna fill, limestone, and granite were tested at three temperatures (46°, 55°, and 64 °C), while the mixtures at five asphalt contents (3% through 7%), 6% air voids content, and 20% granite filler were tested only at 55° and 64°C.

Parameters like rut-controlling ($G^*/\sin\delta$), complex shear modulus (G^*), phase angle (δ), and accumulated permanent shear strain (γ_{acc}) were the main quantities that have been measured, among others, in order to be used for future predictions.

9.2 Conclusions

The main goals of this research study were to estimate (1) the shear complex moduli and (2) the accumulated shear strains of asphalt mastics and mixtures using the binder complex moduli through testing by Dynamic Shear Rheometer (DSR) and Superpave Shear Tester (SST). This study tries to link the shear complex moduli of the binder with those of mastics and asphalt mixtures using the "master curve" technique and micromechanical Hirsch and Shenoy models based on volumetric composition of asphalt mastics and mixtures.

In doing so, a number of different performance tests, testing configurations, and test parameters were evaluated. Based on the results obtained from this study, the following conclusions can be made:

1. Mineral fillers used in the study had different stiffening effects on asphalt binder regarding the type and amount used. The highest values for the shear modulus values and rut parameter ($G^*/\sin\delta$) were obtained for granite and the lowest values were recorded for donna fill, due to the fact that granite has the largest modulus of elasticity (75 GPa) among the three fillers used. Also, the highest values for the above parameters were obtained for 30% filler type, meaning that the largest percentage of filler type used showed the highest stiffness values for the mastics at the same test temperature.

2. Asphalt mastics and mixtures behave the same regarding the testing temperatures. At high temperatures both materials have low shear moduli G^* and rut parameters $G^*/\sin\delta$, as for lower temperatures there is an increase for the two parameters. This is due to the viscoelastic behavior of the asphalt binder, which is more elastic at lower temperatures, usually under 40 °C, and becomes more viscous at temperatures above 40 °C.

3. Shear phase angles in asphalt mastics and mixtures have showed same tendencies at different testing temperatures, but they behave quite opposite regarding the loading frequencies. Phase

angles in asphalt binder and mastics have increased with the temperature, by approximately 5%, same as the asphalt mixtures, but they decreased with the increase in loading frequencies from (88 ÷ 80) deg to (47 ÷ 52) deg. Opposite to the binder and mastics, shear phase angles in asphalt mixtures have increased with the increase in loading frequencies, for both temperatures (55° and 64 °C), from around 22 deg to near 62 deg. This behavior in asphalt mixtures was due to the effect of mineral aggregate on the asphalt binder, making it behave more elastically.

4. Dynamic shear stiffness or shear modulus (G*) was estimated very accurate, for both mastics and mixtures, with the help of the master curves. Both materials showed same behavior, in that, their stiffness moduli G* increased with the decrease in temperature and increase in loading frequency.

5. Accumulated permanent shear strains from repeated shear loading has been in the same ranges for asphalt mastics and mixtures at both temperatures (55° and 64 °C). Permanent shear strain values for limestone (15% filler) mastic were 3.3% at 55 °C and 4.2% at 64 °C, while for asphalt mixtures were in the range of 2.06 ÷ 2.8% at 55 °C and 3.35 ÷ 4.31% at 64 °C.

6. Shenoy's equation for predicting asphalt binder accumulated shear strain has been successfully employed for predicting also shear strains in mastics and mixtures. Results in both cases, mastics and mixtures, have correlated in a proportion of 95% and over for mastics and 90% or better for asphalt mixtures.

7. Hirsch model for estimating the modulus of asphalt concrete using binder shear modulus and volumetric composition was also used, with very good correlation parameter values of 0.95 or over, to estimate the shear complex modulus of asphalt mastics. For both materials, mastics and mixtures, estimated shear modulus values were in good agreement with those obtained by measurement with dynamic shear rheometer (DSR) and Superpave shear tester (SST).

9.3 Recommendations

There is always the opportunity for future research in the area of asphalt binders, mastics and mixtures characterization. For this reason, future research work may include:

1. Refinement of the laboratory testing and analysis methods, with additional binders, mastics - using different mineral fillers, and mixtures - with different designs, being tested.
2. It would also be desirable to correlate more the binders and mixtures tests in the laboratory with the mixture performance in the field.
3. Modifying the Hirsch model by adding a few micro structural features that include aggregate size, shape, texture and packing geometry.
4. Modify the Shenoy equation for permanent strain predictions by using a calibrated constant.
5. Microstructure effects on asphalt concrete permanent deformation evaluation using x-ray computed tomography (XCT) (Figure 9.1).

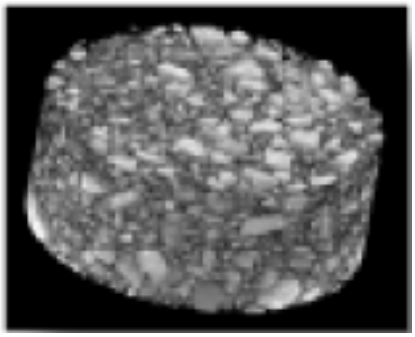

Figure 9.1 Asphalt concrete 3-D X-ray tomography image.

REFERENCES

AASHTO TP5-98, "*Standard Test Method for Determining the Rheological Properties of Asphalt Binder Using a Dynamic Shear Rheometer (DSR)*" (1998).

ASTM D 2041-00, "*Standard Test Method for Theoretical Maximum Specific Gravity and Density of Bituminous Paving Mixtures*" (2000).

AASHTO 320-03, "*Determining the Permanent Shear Strain and Stiffness of Asphalt Mixtures using the Superpave Shear Tester (SST)*" (2003).

Anderson, Richard M., D. E. Walker, and P. Turner, "Low Temperature Evaluation of Kentucky PG 70-22 Asphalt Binders" Transportation Research Board, 78th Annual Meeting, Washington, D.C. (1999).

Anderson, David A. and M. O. Marasteanu, "Physical Hardening of Asphalt Binders Relative to Their Glass Transition Temperatures", Transportation Research Record 1661, Paper No. 1547, National Research Council, Washington, D.C., pp.27-35 (1999).

Anderson, David A., M. O. Marasteanu, J. M. Mahoney, and J. E. Stephens, "Factors Affecting Variability in Strategic Highway Research Program Binder Tests" Transportation Research Record 1728, Paper No. 1360, National Research Council, Washington, D.C. pp. 28-36 (2000).

Anderson, David A., Y. M. Le Hir, J-P Planche, and D. Martin, "Zero Shear Viscosity of Asphalt Binders", Transportation Research Board, 80th Annual Meeting, Washington, D.C. (2001).

Anderson, Richard M., R. K. Steger, G. A. Huber, and P. Romero, "Precision of Shear Tests Used for Evaluating Asphalt Mixtures", Transportation Research Board, 82nd Annual Meeting, Washington, D.C. (2003).

Antes, Paul W., A. E. van Dommelen, L. J. M. Houben, A. A. Molenaar, and U. Parajuli, "Stress Dependent Behavior of Asphalt Mixtures at High Temperatures", Association of Asphalt Paving Technologists (AAPT), Vol. 72, pp. 84-101 (2003).

Atkins, Harold N., "Highway Materials, Soils, and Concretes", Prentice Hall, pp.204-241 (2003).

Bahia, Hussain, E. Masad, A. Stakston, S. Dessouky, and F. Bayomy, "Simplistic Mixture Design using SGC and the DSR" *Journal Association of Asphalt Paving Technologists* (AAPT), Vol. 72, pp. 196-225 (2003).

Basu, Arindam, M. O. Marasteanu, and S. M. Hesp, "Time-Temperature Superposition and Physical Hardening Effects in Low-Temperature Asphalt Binder Grading", Transportation Research Board, 82nd Annual Meeting, Washington, D.C. (2003).

Bennert, Thomas, A. Maher, and N. Gucunski, "Evaluation of Modified Binders", NJDOT Report (2003).

Brown, Ray E., P. S. Kandhal, and J. Zhang, "Performance Testing for hot Mix Asphalt" NCAT Report 01-05 (2001).

Buttlar, William G., D. Bozkurt, G. G. Al-Khateeb, and A. S. Waldhoff, "Understanding Asphalt Mastic Behavior through Micromechanics" Transportation Research Board, 77th Annual Meeting, Washington, D.C. (1998).

Chang, G.K. and J. N. Meegoda, "Micromechanic Model for Temperature Effects of Hot Mix Asphalt Concrete" Transportation Research Board, 78th Annual Meeting, Washington, D.C. (1999).

Chen, Jian-Shiuh, "Rheological Properties of Asphalt-Mineral Filler Mastics" Transportation Research Board, 75th Annual Meeting, Washington, D.C. (1996).

Chowdhury, Arif, J. W. Button, and J. D. Grau, "Effects of Superpave Restricted Zone on Permanent Deformation" Report No. 201-2, Texas Transportation Institute (2001).

Christensen, Donald W., T. Pellinen, and R.F. Bonaquist, "Hirsch Model for Estimating the Modulus of Asphalt Concrete", Association of Asphalt Paving Technologists (AAPT), Vol. 72, pp. 184-204 (2003).

Christensen, Donald W. and R. F. Bonaquist, "VMA: One Key to Mixture Performance", National Superpave Newsletter (2005).

Coree, Brian J., "Hot-Mix Asphalt Volumetrics Revisited - A New Paradigm" Transportation Research Record 1681, Paper No. 0513, National Research Council, Washington, D.C., pp.50-59 (1999).

Daniel, Jo Sias and Y. R. Kim, "Relationships Among Rate-Dependent Stiffnesses of Asphalt Concrete using Laboratory and Field Test Methods", Transportation Research Board, 77th Annual Meeting, Washington, D.C. (1998).

Daniel, Jo Sias, Y. R. Kim and H. J. Lee, "Effects of Aging on Viscoelastic Properties of Asphalt-Aggregate Mixtures" Transportation Research Record, Paper No. 0334, National Research Council, Washington, D.C., pp. 21-28 (1998).

Delgadillo, Rodrigo, K. Nam, and H. Bahia, "Why do we need to change G*/sinδ and how?" Transportation Research Board, 83rd Annual Meeting, Washington, D.C. (2004).

Derucher, Kenneth N., G. P. Korfiatis, and A. S. Ezeldin, "Materials for Civil and Highway Engineers", Prentice Hall, 4th Ed., pp.51-62, 202-216 (1998).

Deshpande, Vikram S. and D. Cebon, "Uniaxial experiments on idealized asphalt mixes" Transportation Research Board, 77th Annual Meeting, Washington, D.C. (1998).

Dongre, Raj and J. D'Angelo, "Evaluation of Different Parameters for Superpave High Temperature Binder Specification Based on Rutting Performance in the Accelerated Loading Facility at FHWA", Transportation Research Board, 81st Annual Meeting, Washington, D.C. (2002).

Dongre, Raj, J. D'Angelo, and M.G. Bouldin, "Effect of Sample Preparation Protocol on Binder Tensile Strength and the MP1A Critical Cracking Temperature", Transportation Research Board, 82nd Annual Meeting, Washington, D.C. (2003).

Dongre, Raj, J. D'Angelo, and G. Reinke, "A New Criterion for Superpave High Temperature Binder Specification", Transportation Research Board, 83rd Annual Meeting, Washington, D.C. (2004).

Gubler, R., Y. Liu, D.A. Anderson, and M.N. Partl, "Investigation of the System Filler and Asphalt Binders by Rheological Means" Association of Asphalt Paving Technologists (AAPT), Vol. 68, pp. 284-304 (1999).

Hand, A. J., J.L. Stiady, T.D. White, A.S. Noureldin, and K. Galal, "Gradation Effects on Hot-Mix Asphalt Performance", Transportation Research Record 1767, National Research Council, Washington, D.C., pp.152-158 (2001).

Huang, Yang H., "Pavement Analysis and Design", Prentice Hall, pp. 1-48, (1993).

Ishai, Ilan and J. Craus, "Effects of Some Aggregate and Filler Characteristics on Behavior and Durability of Asphalt Paving Mixtures" Transportation Research Record 1530, National Research Council, Washington, D.C., pp. 75-86 (1996).

Jiang, Rong-Bin, J. D. Lin, and D. F. Lin "Rheology of Asphaltic Binders and Their Effects on Asphalt Concrete" Transportation Research Record 1535, National Research Council, Washington, D.C., pp. 74-81 (1996).

Jo, D. and R. Kim, "Relationships among rate-dependent stiffnesses of asphalt concrete using laboratory and field test methods" Transportation Research Board, 77th Annual Meeting, Washington, D.C. (1998)

Kandhal, Prithvi S., C. Y. Lynn, and F. Parker Jr., "Characterization Tests for Mineral Fillers Related to Performance of Asphalt Paving Mixtures" NCAT Report No. 98-2 (1998).

Kandhal, Prithvi S. and R. B. Mallick, "Effect of Mix Gradation on Rutting Potential of Dense-Graded Asphalt Mixtures", Transportation Research Record 1767, National Research Council, Washington, D.C., pp.146-152 (2001).

Kern, Jeffrey S. and S. H. Carpenter, "Performance-Graded High-Temperature Selection Criterion - Can We Do It Better", Transportation Research Record 1661, Paper No. 1337, National Research Council, Washington, D.C., pp.122-131 (1999).

Kim, Yong-Rak, D.N. Little, and I. Song, "Mechanistic Evaluation of Mineral Fillers on Fatigue Resistance and Fundamental Material Characteristics", Transportation Research Board, 82nd Annual Meeting, Washington, D.C. (2003).

Kim, Yong-Rak and D.N. Little, "Linear Viscoelastic Analysis of Asphalt Mastics", ASCE *Journal of Materials in Civil Engineering*, Vol. 16, No. 2, pp. 122-132 (2004).

Kose, Sadi, M. Guler, H. U. Bahia, and E. Masad, "Distribution of Strains Within Hot-Mix Asphalt Binders", Transportation Research Record 1728, Paper No. 1391, National Research Council, Washington, D.C., pp.21-28 (2000).

Lay, Maxwell G., "Handbook of Road Technology", Gordon and Breach Science Publishers, 2nd Ed., pp. 193-208, 235-256 (1990).

Medani, T. O. and M. Huurman, "Constructing the Stiffness Master Curves for Asphalt Mixes", Report 7-10-127-3, Faculty of Civil Engineering and Geosciences, Delft University of Technology (2003).

Meegoda, Jay N. and G. K. Chang, "Micro-mechanic Model For Temperature Effects of Hot Mix Asphalt Concrete" *Journal of Engineering Mechanics*, Vol. 123, No. 5, pp. 495-516 (1997).

Neubauer, Oskar and M. N. Partl, "Impact of Binder Content on Selected Properties of Stone Mastic Asphalt", 3rd Eurasphalt & Eurobitume Congress, Vienna, Paper No. 093, pp. 1614-1621 (2004).

Pellinen, Terhi K., D. W. Christensen, G. M. Rowe, and M. Sharrock, "Fatigue Transfer Functions - How Do They Compare?", Transportation Research Board, 83rd Annual Meeting, Washington, D.C. (2004).

Peterson, Robert L., H. R. Soleymani, R. M. Anderson, R. S. McDaniel, "Recovery and Testing of RAP Binders from Recycled Asphalt Pavements", Transportation Research Board, 78th Annual Meeting, Washington, D.C (1999).

Roberts, Freddy L., P.T. Kandhal, E.R. Brown, D-Y Lee, and T.W. Kennedy, "Hot-Mix Asphalt Materials, Mixture Design, and Construction", NAPA Research and Education Foundation, Second Ed. (1996).

Roberts, Freddy L., L. N. Mohammad, and L. Wang, "History of Hot Mix Asphalt Mixture Design in the United States", *Journal of Materials in Civil Engineering*, Vol. 14, No. 4, pp. 279-293 (2002).

Romero, Pedro and R. M. Anderson, "Variability of Asphalt Mixture Tests using Superpave Shear Tester Repeated shear at Constant Height Test", Transportation Research Record 1767, National Research Council, Washington, D.C., pp.95-102 (2001).

Roque, Reynaldo, B. Birgisson, J. Kim, and L. V. Pham, "Use of Complex Modulus to Characterize the Performance of Asphalt Mixtures and Pavements in Florida" Report No. 4910-784-12 University of Florida (2004).

Rowe, Geoffrey M., J. A. D'Angelo, and M. J. Sharrock, "Use Of The Zero Shear Viscosity AS A Parameter For The High Temperature Binder Specification Parameter", 2nd International Symposium On Binder Rheology and Pavement Performance", San Antonio, Texas (2004).

Schramm, Gebhard, "A Practical Approach to Rheology and Rheometry" ThermoHaake Rheology, 2nd Ed., pp. 15-28, 101-114, 120-128 (2000).

Schwartz, C.W., N.H. Gibson, R.A. Schapery, M.W. Witczak, "Viscoplasticity Modeling of Asphalt Concrete Behavior" 15th ASCE Engineering Mechanics Conference (2002).

Shashidhar, Naga and P. Romero, "Factors Affecting the Stiffening Potential of Mineral Fillers" Transportation Research Record 1638, Paper No. 0989, National Research Council, Washington, D.C., pp. 94-101 (1998).

Shenoy, Aroon and P. Romero, "Superpave Shear Tester as a Simple Standardized Measure to Evaluate Aggregate-Asphalt Mixture Performance", *Journal of Testing and Evaluation*, Vol. 29, No. 5, pp. 472-484 (2001).

Shenoy, Aroon, "Refinement of the Superpave Specification Parameter for Performance Grading of Asphalt" Journal of Transportation Engineering, Vol. 127, pp. 357-362 (2001).

Shenoy, Aroon, "Model-fitting the Master Curves of the Dynamic Shear Rheometer Data to Extract a Rut-Controlling Term for Asphalt Pavements", ASTM *Journal of Testing and Evaluation*, Vol. 30, No. 2 (2002).

Shenoy, Aroon, K. Stuart, and W. Mogawer, "Do Asphalt Mixtures Correlate Better with Mastics or Binders in Evaluating Permanent Deformation?" Transportation Research Board, 82nd Annual Meeting, Washington, D.C. (2003).

Smith, B.J. and A.M. Hesp, "Crack Pinning in Asphalt Mastic and Concrete: effect of rest periods and polymer modifiers on the fatigue life" Transportation Research Board, 77th Annual Meeting, Washington, D.C. (1998)

Smith, Benjamin J. and A.M. Hesp, "Crack Pinning in Asphalt Mastic and Concrete - Regular Fatigue Studies" Transportation Research Record 1728, No. 1233, National Research Council, Washington, D.C., pp.75-81 (2000).

Smith, Benjamin J. and S. Hesp, "Crack Pinning in Asphalt Mastic and Concrete: Effect of Rest Periods and Polymer Modifiers on the Fatigue Life", 2nd Eurasphalt & Eurobitume Congress, Barcelona, pp. 539-545 (2000).

Tayebali, Akhtarhusein, G. A. Malpass, and N. Paul Khosla, "Effect of Mineral Filler Type and Amount on the Design and Performance of Asphalt Concrete Mixtures", Transportation Research Board, 77th Annual Meeting, Washington, D.C. (1998).

Uddin, Waheed, "A Micromechanical Model for Prediction of Creep Compliance and Viscoelastic Analysis of Asphalt Pavements" Transportation Research Board, 78th Annual Meeting, Washington, D.C. (1999).

Uddin, Waheed, "Viscoelastic Characterization of Polymer-Modified Asphalt Binders of Pavement Applications" Applied Rheology, Vol. 13, Issue 4, pp. 191-199 (2003).

Vacin, Ota J., J. Stastna, and L. Zanzotto, "Creep Compliance of Polymer Modified Asphalt, Asphalt Mastic and Hot Mix Asphalt", Transportation Research Board, 82nd Annual Meeting, Washington, D.C. (2003).

Vacin, Ota, "Investigation of Polymer Modified Asphalt by Shear and Tensile Compliances", Annual Conference of the Transportation Association of Canada, Quebec (2004).

Waltham, Tony, "Foundations of Engineering Geology" SPON PRESS, 2nd Ed., pp. 45-52 (2002).

Weissman, Shmuel L., J. L. Sackman, J. Harvey, and F. Long, "Selection of Laboratory Test Specimen Dimension for Permanent Deformation of Asphalt Concrete Pavements", Transportation Research Board, 78th Annual Meeting, Washington, D.C. (1999).

Wright, Paul H. and K. Dixon, "Highway Engineering", 7th Ed., Wiley & Sons, Inc. pp. 433-458 (2004).

Yongqi, Li and J.B. Metcalf, "Two-Step Approach to Prediction of Asphalt Concrete Modulus from Two-Phase Micromechanical Models" *Journal of Materials in Civil Engineering*, Vol. 17, No. 4 (2005)

Zaniewski, John P. and M. E. Pumphrey, "Evaluation of Performance Graded Asphalt Binder Equipment and Testing Protocol" Asphalt Technology Program, West Virginia (2004).

Zhang, Jingna, L.A. Cooley, and P.S. Kandhal, "Comparison of Fundamental and Simulative Test Methods for Evaluating Permanent Deformation of HMA", NCAT Report, No. 07 (2002).

Zhao, Yanqing and Y. R. Kim, "The Time-Temperature Superposition for Asphalt Mixtures with Growing Damage and Permanent Deformation in Compression", Transportation Research Board, 82nd Annual Meeting, Washington, D.C. (2003).

APPENDIX A

ASPHALT BINDER PG64-22 CHARACTERISTICS

The asphalt cement (binder) used in this study, in mastics, as well as in mixtures was tested according to the Superpave asphalt binder specification - AASHTO MP1, "Standard Specification for Performance Graded Asphalt Binder" by the Louisiana Transportation Research Center (LTRC). The mixing and compaction temperatures and complex shear moduli at different frequencies and temperatures were also determined. A summary of the results is provided in Table A1. These results confirm that the grade of the asphalt cement is PG 64-22.

Table A1. Asphalt binder PG64-22 requirements (LTRC, 2001)

Binder Property	Binder Aging Condition	Test Result	Superpave Requirement
Flash Point (°C)	Unaged	299	>230
Viscosity at 135°C (Pa-second)	Unaged	0.41	<3.00
Dynamic Shear, G*/sin δ at 64°C (kPa)	Unaged	1.045	>1.00
Mass Loss (%)	RTFO aged	0.55	<1.00
Dynamic Shear, G*/sin δ at 64°C (kPa)	RTFO aged	2.91	>2.20
Dynamic Shear, G*sin δ at 25°C (kPa)	PAV aged	2842	<5000
Creep Stiffness, S at – 12°C (MPa)	PAV aged	176	<300
m-value at – 12°C	PAV aged	0.301	>0.300

RTFO - Rolling Thin Film Oven Test
PAV - Pressure Aging Vessel Test

The rheological properties of the asphalt cement were determined according to AASHTO TP5, "Determining the Rheological Properties of Asphalt Binder Using a Dynamic Shear Rheometer". The test apparatus used was a Bohlin Automated Dynamic Shear Rheometer. In the following tables different test conditions and test results obtained using the Dynamic Shear Rheometer (DSR) are presented.

DSR Single Frequency Oscillation Test Results

Table A2. DSR single frequency oscillation results for pure binder (PG64-22)

Type of Filler	**Asphalt binder**		
Filler Volume Fraction (%)	0	0	0
Temperature T(°C)	46	55	64
Frequency f (Hz)	1.596	1.596	1.596
Phase Angle δ (°)	76 / 76.2	80.1 / 80	83.4 / 84.3
Complex Modulus **G*** (Pa)	**6.584e+03 / 6.593e+03**	**3.324e+03 / 3.331e+03**	**1.926e+03 / 1.875e+03**
Elastic Modulus **G'** (Pa)	1.593e+03 / 1.572e+02	5.715e+02 / 5.784e+02	2.214e+02 / 1.862e+02
Viscous Modulus **G"** (Pa)	6.388e+03 / 6.403e+03	3.274e+03 / 3.280e+03	1.913e+03 / 1.866e+03
Complex Viscosity η* (Pas)	6.571e+02 / 6.588e+02	3.312e+02 / 3.325e+02	1.921e+02 / 1.972e+02
Shear Stress σ (Pa)	7.887e+02 / 7.918e+02	4.015e+02 / 4.007e+02	2.315e+02 / 2.233e+02
Strain γ(%)	1.198e-01 / 1.201e-01	1.208e-01 / 1.203e-01	1.202e-01 / 1.191e-01
G*/sin(δ) (kPa)	**6.786 / 6.789**	**3.374 / 3.382**	**1.939 / 1.887**

Table A3. DSR single frequency oscillation results for Donna Fill Mastic (46°C)

Type of Filler	**Donna Fill Mastic - 46°C**				
Filler Volume Fraction (%)	5	10	15	20	30
Temperature T(°C)	46	46	46	46	46
Frequency f (Hz)	1.596	1.596	1.596	1.596	1.596
Phase Angle δ (°)	76.1 / 76.3	76.2 / 75.8	75.9 / 76	76 / 76.1	76.3 / 76.2
Complex Modulus **G*** (Pa)	**1.021e+04 / 9.977e+03**	**1.417e+04 / 1.432e+04**	**1.837e+04 / 1.841e+04**	**2.266e+04 / 2.263e+04**	**2.762e+04 / 2.777e+04**
Elastic Modulus **G'** (Pa)	2.453e+03 / 2.363e+03	3.380e+03 / 3.513e+03	4.475e+03 / 4.454e+03	5.482e+03 / 5.436e+03	6.541e+03 / 6.624e+03
Viscous Modulus **G"** (Pa)	9.911e+03 / 9.693e+03	1.376e+04 / 1.388e+04	1.782e+04 / 1.786e+04	2.199e+04 / 2.197e+04	2.683e+04 / 2.696e+04
Complex Viscosity η* (Pas)	1.024e+03 / 9.965e+02	1.422e+03 / 1.426e+03	1.829e+03 / 1.846e+03	2.255e+03 / 2.251e+03	2.763e+03 / 2.762e+003
Shear Stress σ (Pa)	1.221e+03 / 11.972e+02	1.710e+03 / 1.734e+03	2.232e+03 / 2.228e+03	2.712e+03 / 2.720e+03	3.323e+03 / 3.349e+03
Strain γ (%)	1.196e-01 / 1.200e-01	1.207e-01 / 1.211e-01	1.215e-01 / 1.210e-01	1.197e-01 / 1.202e-01	1.203e-01 / 1.206e-01
G*/sin(δ) (kPa)	**10.518 / 10.269**	**14.591 / 14.771**	**18.941 / 18.973**	**23.354 / 23.313**	**28.429 / 28.595**

Table A4. DSR single frequency oscillation results for Donna Fill Mastic (55°C)

Type of Filler	**Donna Fill Mastic - 55°C**				
Filler Volume Fraction (%)	5	10	15	20	30
Temperature T(°C)	55	55	55	55	55
Frequency f (Hz)	1.596	1.596	1.596	1.596	1.596
Phase Angle δ (°)	79.8 / 80.2	80.1 / 80.1	80.2 / 80.1	80 / 79.8	80.2 / 79.9
Complex Modulus **G*** (Pa)	**3.845e+03 / 3.854e+03**	**4.726e+03 / 4.733e+03**	**5.227e+03 / 5.234e+03**	**6.463e+03 / 6.472e+03**	**7.738e+03 / 7.795e+03**
Elastic Modulus **G'** (Pa)	6.809e+02 / 6.560e+02	8.125e+02 / 8.137e+02	8.897e+02 / 8.998e+02	11.223e+02 / 11.461e+02	13.171e+02 / 13.670e+02
Viscous Modulus **G"** (Pa)	3.784e+03 / 3.798e+03	4.656e+03 / 4.663e+03	5.151e+03 / 5.156e+03	6.365e+03 / 6.369e+03	7.625e+03 / 7.674e+03
Complex Viscosity η* (Pas)	3.847e+02 / 3.843e+02	4.715e+02 / 4.726e+02	5.214e+02 / 5.243e+02	6.451e+02 / 6.466e+02	7.727e+02 / 7.788e+02
Shear Stress σ (Pa)	4.568e+02 / 4.605e+02	5.643e+02 / 5.694e+02	6.256e+02 / 6.249e+02	7.801e+02 / 7.850e+02	9.270e+02 / 9.362e+02
Strain γ (%)	1.188e-01 / 1.195e-01	1.194e-01 / 1.203e-01	1.197e-01 / 1.194e-01	1.207e-01 / 1.213e-01	1.198e-01 / 1.201e-01
G*/sin(δ) (kPa)	**3.907 / 3.911**	**4.797 / 4.804**	**5.304 / 5.313**	**6.563 / 6.576**	**7.853 / 7.918**

Table A5. DSR single frequency oscillation results for Donna Fill Mastic (64°C)

Type of Filler	**Donna Fill Mastic - 64°C**				
Filler Volume Fraction (%)	5	10	15	20	30
Temperature T(°C)	64.0	64.0	64.0	64.0	64.0
Frequency f (Hz)	1.596	1.596	1.596	1.596	1.596
Phase Angle δ (°)	84.2 / 84.2	83.8 / 84.2	83.8 / 83.5	83.7 / 83.7	83.7 / 83.6
Complex Modulus **G*** (Pa)	**1.980e+03/ 2.012e+03**	**2.074e+03/ 2.132e+03**	**2.366e+03/ 2.385e+03**	**2.556e+03/ 2.576e+03**	**2.769e+03/ 2.827e+03**
Elastic Modulus **G'** (Pa)	2.001e+02/ 2.033e+02	2.240e+02/ 2.154e+02	2.555e+02/ 2.700e+02	2.805e+02/ 2.827e+02	3.038e+02/ 3.151e+02
Viscous Modulus **G"** (Pa)	1.969e+03/ 2.011e+03	2.062e+03/ 2.121e+03	2.352e+03/ 2.370e+03	2.541e+03/ 2.560e+03	2.752e+03/ 2.809e+03
Complex Viscosity η* (Pas)	1.974e+02/ 2.016e+02	2.088e+02/ 2.145e+02	2.358e+02/ 2.377e+02	2.552e+02/ 2.564e+02	2.753e+02/ 2.818e+02
Shear Stress σ (Pa)	2.366e+02/ 2.422e+02	2.493e+02/ 2.556e+02	2.853e+02/ 2.891e+02	3.077e+02/ 3.094e+02	3.389e+02/ 3.452e+02
Strain γ (%)	1.195e-01/ 1.204e-01	1.202e-01/ 1.199e-01	1.206e-01/ 1.212e-01	1.204e-01/ 1.201e-01	1.224e-01/ 1.221e-01
G*/sin(δ) (kPa)	**1.991 / 2.022**	**2.086 / 2.143**	**2.380 / 2.400**	**2.571 / 2.592**	**2.786 / 2.845**

Table A6. DSR single frequency oscillation results for Limestone Mastic (46°C)

Type of Filler	**Limestone Mastic - 46°C**				
Filler Volume Fraction (%)	5	10	15	20	30
Temperature T(°C)	46	46	46	46	46
Frequency f (Hz)	1.596	1.596	1.596	1.596	1.596
Phase Angle δ (°)	76.2 / 76.1	76.1 / 76.1	76.1 / 76.2	75.9 / 76	76.4 / 76.1
Complex Modulus **G*** (Pa)	**2.049e+04 / 2.064e+04**	**2.322e+04 / 2.329e+04**	**2.568e+04 / 2.571e+04**	**2.945e+04 / 2.936e+04**	**3.207e+04 / 3.209e+04**
Elastic Modulus **G'** (Pa)	4.887e+03 / 4.958e+03	5.578e+03 / 5.595e+03	6.169e+03 / 6.133e+03	7.174e+03 / 7.103e+03	7.541e+03 / 7.709e+03
Viscous Modulus **G"** (Pa)	1.990e+04 / 2.004e+04	2.254e+04 / 2.261e+04	2.493e+04 / 2.497e+04	2.856e+04 / 2.849e+04	3.117e+04 / 3.024e+04
Complex Viscosity η* (Pas)	2.051e+03 / 2.055e+03	2.318e+03 / 2.322e+03	2.559e+03 / 2.562e+03	2.944e+03 / 2.934e+03	3.216e+03 / 3.198e+03
Shear Stress σ (Pa)	2.483e+03 / 2.493e+03	2.784e+03 / 2.802e+03	3.120e+03 / 3.129e+03	3.510e+03 / 3.544e+03	3.893e+03 / 3.870e+03
Strain γ (%)	1.212e-01 / 1.208e-01	1.199e-01 / 1.203e-01	1.215e-01 / 1.217e-01	1.192e-01 / 1.207e-01	1.214e-01 / 1.206e-01
G*/sin(δ) (kPa)	**21.099 / 21.263**	**23.920 / 23.993**	**26.455 / 26.474**	**30.365 / 30.259**	**32.995 / 33.058**

Table A7. DSR single frequency oscillation results for Limestone Mastic (55°C)

Type of Filler	**Limestone Mastic - 55°C**				
Filler Volume Fraction (%)	5	10	15	20	30
Temperature T(°C)	55	55	55	55	55
Frequency f (Hz)	1.596	1.596	1.596	1.596	1.596
Phase Angle δ(°)	80 / 80.1	80.2 / 80.3	80.1 / 79.7	80 / 79.8	80.2 / 79.9
Complex Modulus **G*** (Pa)	**4.711e+03 / 4.703e+03**	**5.885e+03 / 5.872e+03**	**7.244e+03 / 7.253e+03**	**8.686e+03 / 8.698e+03**	**9.629e+03 / 9.622e+03**
Elastic Modulus **G'** (Pa)	8.181e+02 / 8.086e+02	10.017e+02 / 9.894e+02	12.454e+02 / 12.968e+02	15.083e+02 / 15.403e+02	16.389e+02 / 16.874e+02
Viscous Modulus **G"** (Pa)	4.639e+03 / 4.633e+03	5.799e+03 / 5.788e+03	7.136e+03 / 7.136e+03	8.554e+03 / 8.560e+03	9.488e+03 / 9.473e+03
Complex Viscosity η* (Pas)	4.715e+02 / 4.712e+02	5.874e+02 / 5.867e+02	7.256e+02 / 7.249e+02	8.671e+02 / 8.706e+02	9.624e+02 / 9.628e+02
Shear Stress σ (Pa)	5.615e+02 / 5.634e+02	7.103e+02 / 7.099e+02	8.693e+02 / 8.732e+02	10.510e+02 / 10.559e+02	11.535e+02 / 11.594e+02
Strain γ (%)	1.192e-01 / 1.198e-01	1.207e-01 / 1.209e-01	1.200e-01 / 1.204e-01	1.210e-01 / 1.214e-01	1.198e-01 / 1.205e-01
G*/sin(δ) (kPa)	**4.784 / 4.774**	**5.972 / 5.957**	**7.353 / 7.372**	**8.820 / 8.838**	**9.771 / 9.773**

Table A8. DSR single frequency oscillation results for Limestone Mastic (64°C)

Type of Filler	**Limestone Mastic - 64°C**				
Filler Volume Fraction (%)	5	10	15	20	30
Temperature T(°C)	64.0	64.0	64.0	64.0	64.0
Frequency f (Hz)	1.596	1.596	1.596	1.596	1.596
Phase Angle δ (°)	84.2 / 84.2	84 / 84.2	83.8 / 83.5	83.7 / 83.7	83.7 / 83.6
Complex Modulus **G*** (Pa)	**2.130e+03/ 2.152e+03**	**2.584e+03 / 2.612e+03**	**2.967e+03/ 2.975e+03**	**3.176e+03/ 3.146e+03**	**3.819e+03/ 3.767e+03**
Elastic Modulus **G'** (Pa)	2.152e+02/ 2.175e+02	2.701e+02 / 2.639e+02	3.204e+02/ 3.368e+02	3.485e+02/ 3.452e+02	4.191e+02/ 4.200e+02
Viscous Modulus **G"** (Pa)	2.119e+03/ 2.141e+03	2.570e+03 / 2.598e+03	2.951e+03/ 2.956e+03	3.157e+03/ 3.127e+03	3.796e+03/ 3.743e+03
Complex Viscosity η* (Pas)	2.121e+02/ 2.136e+02	2.577e+02 / 2.605e+02	2.960e+02/ 2.964e+02	3.165e+02/ 3.134e+02	3.811e+02/ 3.761e+02
Shear Stress σ (Pa)	2.547e+02/ 2.591e+02	3.106e+02 / 3.129e+02	3.578e+02/ 3.603e+02	3.811e+02/ 3.791e+02	4.636e+02/ 4.600e+02
Strain γ (%)	1.196e-01/ 1.204e-01	1.202e-01 / 1.198e-01	1.206e-01 / 1.211e-01	1.200e-01 / 1.205e-01	1.214e-01/ 1.221e-01
G*/sin(δ) (kPa)	**2.141 / 2.163**	**2.598 / 2.625**	**2.984 / 2.994**	**3.195 / 3.165**	**3.842/ 3.791**

Table A9. DSR single frequency oscillation results for Granite Mastic (46°C)

Type of Filler	**Granite Mastic - 46°C**				
Filler Volume Fraction (%)	5	10	15	20	30
Temperature T(°C)	46	46	46	46	46
Frequency f (Hz)	1.596	1.596	1.596	1.596	1.596
Phase Angle δ (°)	75.8 / 76.3	76.2 / 76.1	76 / 76.1	75.9 / 76	76.3 / 76
Dynamic Complex **G*** (Pa) Modulus	**2.664e+04 / 2.702e+04**	**3.018e+04 / 3.085e+04**	**3.494e+04 / 3.486e+04**	**3.981e+04 / 3.937e+04**	**4.505e+04 / 4.463e+04**
Elastic Modulus **G'** (Pa)	6.535e+03 / 6.399e+03	7.199e+03 / 7.411e+03	8.453e+03 / 8.374e+03	9.698e+03 / 9.524e+03	10.670e+03 / 10.797e+03
Viscous Modulus **G"** (Pa)	2.582e+04 / 2.625e+04	2.931e+04 / 2.995e+04	3.390e+04 / 3.384e+04	3.861e+04 / 3.820e+04	4.377e+04 / 4.330e+04
Complex Viscosity η* (Pas)	2.665e+03 / 2.708e+03	3.022e+03 / 3.076e+03	3.492e+03 / 3.488e+03	3.978e+03 / 3.934e+03	4.495e+03 / 4.464e+03
Shear Stress σ (Pa)	3.226e+03 / 3.264e+03	3.582e+03 / 3.702e+03	4.168e+03 / 4.228e+03	4.801e+03 / 4.772e+03	5.478e+03 / 5.396e+03
Strain γ (%)	1.211e-01 / 1.208e-01	1.187e-01 / 1.200e-01	1.193e-01 / 1.213e-01	1.206e-001 / 1.212e-01	1.216e-01 / 1.209e-01
G*/sin(δ) (kPa)	**27.480 / 27.811**	**31.077 / 31.781**	**36.009 / 35.912**	**41.047 / 40.575**	**46.369 / 45.996**

Table A10. DSR single frequency oscillation results for Granite Mastic (55°C)

Type of Filler	**Granite Mastic - 55°C**				
Filler Volume Fraction (%)	5	10	15	20	30
Temperature T(°C)	55	55	55	55	55
Frequency f (Hz)	1.596	1.596	1.596	1.596	1.596
Phase Angle δ (°)	80.2 / 79.8	79.9 / 80.2	80.1 / 79.8	80 / 80.1	80.2 / 79.9
Dynamic Complex **G*** (Pa) Modulus	**6.387e+03 / 6.446e+03**	**7.102e+03 / 7.144e+03**	**8.028e+03 / 8.134e+03**	**9.807e+03 / 9.877e+03**	**1.118e+04 / 1.123e+04**
Elastic Modulus **G'** (Pa)	1.087e+03 / 1.141e+03	1.245e+03 1.216e+03	1.380e+03 1.440e+03	1.703e+03 1.698e+03	1.903e+03 1.969e+03
Viscous Modulus **G"** (Pa)	6.294e+03 / 6.344e+03	6.992e+03 / 7.040e+03	7.908e+03 / 8.006e+03	9.658e+03 / 9.730e+03	11.017e+03 / 11.056e+03
Complex Viscosity η* (Pas)	6.382e+02 / 6.438e+02	7.094e+02 / 7.139e+02	8.031e+02 / 8.136e+02	9.812e+02 / 9.877e+02	1.122e+03 / 1.117e+03
Shear Stress σ (Pa)	7.556e+02 / 7.645e+02	8.515e+02 / 8.594e+02	9.690e+02 / 9.801e+02	11.739e+02 / 11.783e+02	1.348e+03 / 1.341e+03
Strain γ (%)	1.183e-01 / 1.186e-01	1.199e-01 / 1.203e-01	1.207e-01 / 1.205e-01	1.197e-01 / 1.193e-01	1.206e-01 / 1.194e-01
G*/sin(δ) (kPa)	**6.482 / 6.550**	**7.214 / 7.250**	**8.149 / 8.264**	**9.958 / 10.026**	**11.345 / 11.407**

Table A11. DSR single frequency oscillation results for Granite Mastic (64°C)

Type of Filler	**Granite Mastic - 64°C**				
Filler Volume Fraction (%)	5	10	15	20	30
Temperature T(°C)	64.0	64.0	64.0	64.0	64.0
Frequency f (Hz)	1.596	1.596	1.596	1.596	1.596
Phase Angle δ (°)	84.1 / 84.2	83.9 / 84	83.8 / 83.7	83.8 / 84.1	83.7 / 83.9
Dynamic Complex **G*** (Pa) Modulus	**2.487e+03 / 2.552e+03**	**2.964e+03 / 2.892e+03**	**3.405e+03 / 3.367e+03**	**3.882e+03 / 3.796e+03**	**4.313e+03 / 4.247e+03**
Elastic Modulus **G'** (Pa)	2.556e+02 / 2.579e+02	3.150e+02 / 3.023e+02	3.677e+02 / 3.695e+02	4.192e+02 / 3.902e+02	4.733e+02 / 4.513e+02
Viscous Modulus **G"** (Pa)	2.474e+03 / 2.538e+03	2.947e+03 / 2.876e+03	3.385e+03 / 3.347e+03	3.859e+03 / 3.776e+03	4.287e+03 / 4.223e+03
Complex Viscosity η* (Pas)	2.483e+02 / 2.536e+02	2.958e+02 / 2.785e+02	3.396e+02 / 3.362e+02	3.875e+02 / 3.791e+02	4.311e+02 / 4.240e+02
Shear Stress σ (Pa)	3.022e+02 / 3.073e+02	3.563e+02 / 3.522e+02	4.106e+02 / 4.077e+02	4.713e+02 / 4.570e+02	5.120e+02 / 5.062e+02
Strain γ (%)	1.215e-01 / 1.204e-01	1.202e-01 / 1.218e-01	1.206e-01/ 1.211e-01	1.214e-01/ 1.204e-01	1.187e-01/ 1.192e-01
G*/sin(δ) (kPa)	**2.500 / 2.565**	**2.981 / 2.908**	**3.425 / 3.387**	**3.905 / 3.816**	**4.339 / 4.271**

APPENDIX B

DSR FREQUENCY SWEEP OSCILLATION AT CONSTANT SHEAR STRESS TEST RESULTS

Table B1. DSR frequency sweep oscillation results for pure binder (PG64-22)

Pure Binder (PG64-22)

T(°C)	**f** (Hz)	δ (°)	**G*** (Pa)	**G'** (Pa)	**G"** (Pa)	η (Pa·s)	γ (%)
	0.1	80.0	4.245e+03	7.377e+02	4.164e+03	6.344e+03	3.813e-01
	1	79.9	3.026e+04	5.306e+03	2.979e+04	5.225e+03	6.609e-02
46	10	67.6	1.479e+05	5.636e+04	1.368e+05	3.468e+03	1.352e-02
	50	71	2.586e+05	8.419e+04	2.445e+05	2.346e+03	7.734e-03
	100	48.7	3.114e+05	2.058e+05	2.348e+05	6.776e+02	6.423e-03
	0.1	85.8	8.825e+02	6.463e+01	8.806e+02	1.390e+03	2.266e+00
	1	80.4	6.826e+03	1.138e+03	6.756e+03	1.096e+03	2.934e-01
55	10	73.5	4.872e+04	1.384e+03	4.672e+04	6.979e+02	4.265e-02
	50	62.1	8.653e+04	4.048e+04	7.647e+04	3.458e+02	2.326e-02
	100	46.9	9.621e+04	6.574e+04	7.225e+04	1.194e+02	2.078e-02
	01	89	2.028e+02	3.539e+00	2.028e+02	4.754e+02	9.862e+00
	1	82.9	1.435e+03	1.774e+02	1.424e+03	3.668e+02	1.394e+00
64	10	77.8	9.782e+03	2.067e+03	9.561e+03	3.352e+02	2.044e-01
	50	72.6	4.184e+04	1.251e+04	3.892e+04	9.836e+02	4.780e-02
	100	47	5.208e+04	3.552e+04	3.969e+04	6.875e+01	3.842e-02

Table B2. DSR frequency sweep oscillation results for Donna Fill (5%) Mastic

Donna Fill (5%)

T(°C)	**f** (Hz)	δ (°)	**G*** (Pa)	**G'** (Pa)	**G"** (Pa)	η (Pa·s)	γ (%)
	0.1	81	4.957e+03	7.548e+02	4.896e+03	9.673e+03	4.034e-01
	1	74.1	3.255e+04	8.927e+03	3.148e+04	9.324e+03	6.239e-02
46	10	67	1.712e+05	6.689e+04	1.576e+05	4.219e+03	1.168e-02
	50	65.2	2.964e+05	1.247e+05	2.698e+05	3.823e+03	6.746e-03
	100	45	3.528e+05	2.495e+05	2.495e+05	7.366e+02	5.669e-03
	0.1	86.8	9.962e+02	5.561e+01	9.948e+02	1.464e+03	2.007e+00
	1	79.9	7.342e+03	1.288e+03	7.228e+03	1.133e+03	2.724e-01
55	10	74	5.471e+04	1.508e+04	5.266e+04	9.612e+02	3.655e-02
	50	69	9.506e+04	3.408e+04	8.875e+04	7.116e+02	2.104e-02
	100	47.1	1.108e+05	7.542e+04	8.118e+04	2.689e+02	1.805e-02
	0.1	89.1	2.170e+02	3.408e+00	2.169e+02	5.120e+02	9.216e+00
	1	84	1.713e+03	2.154e+02	1.759e+03	4.011e+02	1.167e+00
64	10	78.2	1.112e+04	2.274e+03	1.088e+04	3.832e+02	1.826e-01
	50	74	4.471e+04	1.238e+04	4.329e+04	1.217e+02	4.478e-02
	100	47.9	6.087e+04	4.266e+04	4.576e+04	7.968e+01	3.285e-02

Table B3. DSR frequency sweep oscillation results for Donna Fill (10%) Mastic

Donna Fill (10%)

T(°C)	**f** (Hz)	δ (°)	**G*** (Pa)	**G'** (Pa)	**G"** (Pa)	η (Pa·s)	γ (%)
	0.1	80.8	5.289e+03	8.456e+02	5.221e+03	9.702e+03	3.781e-01
	1	74.1	3.674e+04	1.006e+04	3.533e+04	9.476e+03	5.443e-02
46	10	67.8	2.009e+05	7.598e+04	1.861e+05	4.356e+03	9.955e-03
	50	71	3.711e+05	1.208e+05	3.528e+05	3.977e+03	5.394e-03
	100	48.4	4.626e+05	3.072e+05	3.466e+05	9.861e+02	4.323e-03
	0.1	86.2	1.197e+03	7.933e+01	1.194e+03	1.605e+03	1.671e+00
	1	79	8.671e+03	1.655e+03	8.512e+03	1.287e+03	2.306e-01
55	10	74	6.597e+04	1.818e+04	6.341e+04	9.743e+02	3.032e-02
	50	68.2	1.082e+05	4.218e+04	1.064e+05	7.239e+02	1.848e-02
	100	47.4	1.293e+05	8.752e+04	9.518e+04	2.811e+02	1.547e-02
	0.1	89	2.518e+02	4.395e+00	2.517e+02	5.268e+02	7.943e+00
	1	84.2	2.194e+03	2.217e+02	2.182e+03	4.325e+02	9.115e-01
64	10	78	1.605e+04	3.336e+03	1.569e+04	3.988e+02	1.246e-01
	50	73.7	5.192e+04	1.457e+04	4.983e+04	1.348e+02	3.852e-02
	100	47.8	6.883e+04	4.623e+04	5.098e+04	8.246e+01	2.916e-02

Table B4. DSR frequency sweep oscillation results for Donna Fill (15%) Mastic

Donna Fill (15%)

T(°C)	**f** (Hz)	δ (°)	**G*** (Pa)	**G'** (Pa)	**G"** (Pa)	η (Pa·s)	γ (%)
	0.1	81.3	5413e+03	7.133e+02	4.658e+03	9.833e+03	4.243e-01
	1	79.1	3.938e+04	7.446e+03	3.867e+04	9.567e+03	5.078e-02
46	10	69	2.166e+05	7.761e+04	2.022e+05	4.503e+03	9.261e-03
	50	62.5	4.587e+05	2.128e+05	4.068e+05	4.109e+03	4.365e-03
	100	47.8	5.565e+05	3.735e+05	4.825e+05	1.048e+03	2.932e-03
	0.1	86.5	1.354e+03	8.266e+01	1.351e+03	1.726e+03	1.477e+00
	1	79	9.124e+03	1.741e+03	8.956e+03	1.464e+03	2.192e-01
55	10	74.5	7.038e+04	1.881e+04	6.782e+04	9.878e+02	2.842e-02
	50	67.9	1.175e+05	4.421e+04	1.088e+05	7.388e+02	1.732e-02
	100	46.1	1.489e+05	1.032e+05	1.073e+05	2.907e+02	1.343e-02
	0.1	89.2	2.878e+02	4.212e+00	2.877e+02	5.403e+02	6.951e+00
	1	83.1	2.619e+03	3.146e+02	2.600e+03	4.478e+02	7.636e-01
64	10	78.5	2.017e+04	4.071e+03	2.006e+04	4.115e+02	9.898e-02
	50	72.8	5.677e+04	1.678e+04	5.423e+04	1.498e+02	3.523e-02
	100	48.4	7.202e+04	4.382e+04	5.316e+04	8.396e+01	1.564e-02

Table B5. DSR frequency sweep oscillation results for Donna Fill (20%) Mastic

Donna Fill (20%)

T(°C)	**f** (Hz)	δ (°)	**G*** (Pa)	**G'** (Pa)	**G"** (Pa)	η (Pa·s)	γ (%)
	0.1	80.8	6.872e+03	1.098e+03	6.783e+03	1.008e+04	2.911e-01
	1	74.1	5.645e+04	1.546e+04	5.429e+04	9.715e+03	3.542e-02
46	10	67.8	2.883e+05	1.089e+05	2.669e+05	4.651e+03	6.937e-03
	50	63.7	5.362e+05	2.376e+05	4.807e+05	4.224e+03	3.734e-03
	100	48.3	6.786e+05	4.514e+05	5.066e+05	1.218e+03	2.947e-03
	0.1	86.1	1.527e+03	1.038e+01	1.523e+03	1.883e+03	1.319e+00
	1	80.2	1.087e+04	1.857e+03	1.071e+04	1.612e+03	1.842e-01
55	10	73.8	7.462e+04	2.086e+04	7.166e+04	1.009e+03	2.684e-02
	50	67.7	1.451e+05	5.506e+04	1.342e+05	7.528e+02	1.378e-02
	100	47.9	1.659e+05	1.122e+05	1.234e+05	3.027e+02	1.206e-02
	0.1	89.2	3.479e+02	4.857e+00	3.478e+02	5.546e+02	5.748e+00
	1	84.1	3.047e+03	3.142e+02	3.041e+03	4.621e+02	6.542e-01
64	10	78.2	2.256e+04	4.613e+03	2.208e+04	4.236e+02	8.865e-02
	50	76	6.443e+04	1.563e+04	6.271e+04	1.659e+02	3.147e-02
	100	47.6	7.973e+04	5.376e+04	5.887e+04	8.549e+02	2.548e-02

Table B6. DSR frequency sweep oscillation results for Donna Fill (30%) Mastic

Donna Fill (30%)

T(°C)	**f** (Hz)	δ (°)	**G*** (Pa)	**G'** (Pa)	**G"** (Pa)	η (Pa·s)	γ (%)
	0.1	81.1	7.896e+03	1.221e+03	7.110e+03	1.145e+04	2.539e-01
	1	73.8	6.044e+04	1.686e+04	5.804e+04	9.962e+03	3.309e-02
46	10	67.4	3.078e+05	1.182e+05	2.842e+05	4.899e+03	6.512e-03
	50	62.9	6.125e+05	2.794e+05	5.455e+05	4.574e+03	3.265e-03
	100	57.5	8.066e+05	4.387e+05	6.887e+05	1.421e+03	2.489e-03
	0.1	86	1.836e+03	1.282e+02	1.832e+03	2.125e+03	1.089e+00
	1	79.9	1.384e+04	2.427e+03	1.363e+04	1.846e+03	1.446e-01
55	10	74.1	8.543e+04	2.344e+04	8.216e+04	1.188e+03	2.346e-02
	50	68.1	1.646e+05	6.139e+04	1.528e+05	7.769e+02	1.226e-02
	100	49.6	1.968e+05	1.276e+05	1.499e+05	3.217e+02	1.085e-02
	0.1	88.8	3.785e+02	7.926e+00	3.784e+02	5.846e+02	5.284e+00
	1	83.9	3.469e+03	3.686e+02	3.449e+03	4.871e+02	5.765e-01
64	10	78.7	2.731e+04	5.347e+03	2.678e+04	4.346e+02	7.401e-02
	50	74.1	6.874e+04	1.883e+04	6.621e+04	1.858e+02	2.915e-02
	100	48.2	8.367e+04	5.577e+04	6.237e+04	8.765e+01	2.393e-02

Table B7. DSR frequency sweep oscillation results for Limestone (5%) Mastic

Limestone (5%)							
T(°C)	**f** (Hz)	δ (°)	**G*** (Pa)	**G'** (Pa)	**G"** (Pa)	η (Pa·s)	γ (%)
	0.1	81.1	5.148e+03	7.964e+02	5.086e+03	9.672e+03	3.885e-01
	1	74.1	3.477e+04	9.525e+03	3.343e+04	9.338e+03	5.752e-02
46	10	68	1.926e+05	7.214e+04	1.785e+05	5.109e+03	1.038e-02
	50	64.1	3.304e+05	1.446e+05	2.972e+05	4.725e+03	6.153e-03
	100	47.9	3.913e+05	2.623e+05	2.916e+05	1.021e+03	5.226e-03
	0.1	85.8	1.079e+03	7.912e+01	1.076e+03	2.016e+03	1.854e+00
	1	80	8.126e+03	1.411e+03	8.135e+03	1.497e+03	2.462e-01
55	10	73.9	6.107e+04	1.694e+04	5.867e+04	9.586e+02	3.275e-02
	50	67.9	9.896e+04	3.728e+04	9.173e+04	7.524e+02	2.022e-02
	100	48.2	1.189e+05	7.925e+04	8.864e+04	3.177e+02	1.682e-02
	0.1	89	2.349e+02	4.099e+00	2.348e+02	7.114e+02	8.514e+00
	1	83.9	1.931e+03	2.051e+02	1.921e+03	5.722e+02	1.035e+00
64	10	79	1.314e+04	2.507e+03	1.289e+04	4.391e+02	1.522e-01
	50	74.1	4.896e+04	1.341e+04	4.708e+04	1.511e+02	4.084e-02
	100	47.5	6.482e+04	4.379e+04	4.779e+04	9.165e+01	3.085e-02

Table B8. DSR frequency sweep oscillation results for Limestone (10%) Mastic

Limestone (10%)							
T(°C)	**f** (Hz)	δ (°)	**G*** (Pa)	**G'** (Pa)	**G"** (Pa)	η (Pa·s)	γ (%)
	0.1	81	5.362e+03	8.388e+02	5.295e+03	9.802e+03	3.729e-01
	1	73.9	3.795e+04	1.052e+04	3.646e+04	9.587e+03	5.271e-02
46	10	67.1	2.121e+05	8.253e+04	1.953e+05	5.294e+03	9.429e-03
	50	63	4.123e+05	1.876e+05	3.674e+05	4.867e+03	4.852e-03
	100	47.4	5.497e+05	3.727e+05	4.046e+05	1.198e+03	3.638e-03
	0.1	86.1	1.284e+03	8.733e+01	1.281e+03	2.128e+03	1.558e+00
	1	79.8	8.874e+03	1.572e+03	8.733e+03	1.632e+03	2.254e-01
55	10	73.9	6.749e+04	1.872e+04	6.487e+04	9.745e+02	2.964e-02
	50	68.1	1.152e+05	4.296e+04	1.068e+05	7.674e+02	1.736e-02
	100	48.5	1.361e+05	9.058e+04	1.039e+05	3.217e+02	1.468e-02
	0.1	88.9	2.768e+02	5.313e+01	2.767e+02	7.226e+02	7.225e+00
	1	84	2.336e+03	2.441e+02	2.323e+03	5.851e+02	8.561e-01
64	10	79.1	1.724e+04	3.261e+03	1.692e+04	4.518e+02	1.161e-01
	50	74.3	5.487e+04	1.564e+04	5.292e+04	1.662e+02	3.642e-02
	100	47.9	7.104e+04	4.763e+04	5.276e+04	9.298e+01	2.815e-02

Table B9. DSR frequency sweep oscillation results for Limestone (15%) Mastic

Limestone (15%)							
T(°C)	**f** (Hz)	δ (°)	**G*** (Pa)	**G'** (Pa)	**G"** (Pa)	η (Pa·s)	γ (%)
	0.1	80.8	5.983e+03	9.578e+02	5.906e+03	9.924e+03	3.343e-01
	1	74.1	4.734e+04	1.297e+04	4.553e+04	9.731e+03	4.234e-02
46	10	68.2	2.605e+05	9.675e+04	2.419e+05	5.492e+03	7.694e-03
	50	61.7	4.993e+05	2.367e+05	4.396e+05	5.101e+03	4.115e-03
	100	48.3	6.322e+05	4.225e+05	4.727e+05	1.305e+03	3.164e-03
	0.1	86.2	1.442e+03	9.557e+01	1.438e+03	2.261e+03	1.387e+00
	1	79.4	9.579e+03	1.762e+03	9.416e+03	1.874e+03	2.088e-01
55	10	74	7.263e+04	2.084e+04	6.982e+04	9.988e+02	2.754e-02
	50	67.9	1.267e+05	4.766e+04	1.174e+05	7.883e+02	1.578e-02
	100	47.8	1.563e+05	1.058e+05	1.167e+05	3.389e+02	1.283e-02
	0.1	89	3.298e+02	5.756e+00	3.297e+02	7.308e+02	6.064e+00
	1	83.9	2.843e+03	3.021e+02	2.826e+03	6.002e+02	7.034e-01
64	10	78.3	2.112e+04	4.283e+03	2.068e+04	4.711e+02	9.476e-02
	50	77.1	5.963e+04	1.331e+04	5.813e+04	1.894e+02	3.354e-02
	100	52.7	7.536e+04	4.568e+04	5.995e+04	9.487e+01	2.654e-02

Table B10. DSR frequency sweep oscillation results for Limestone (20%) Mastic

Limestone (20%)							
T(°C)	**f** (Hz)	δ (°)	**G*** (Pa)	**G'** (Pa)	**G"** (Pa)	η (Pa·s)	γ (%)
	0.1	80.9	7.132e+03	1.127e+03	7.042e+03	1.029e+04	2.804e-01
	1	74	5.955e+04	1.641e+04	5.724e+04	9.886e+03	3.358e-02
46	10	67.8	3.023e+05	1.142e+05	2.798e+05	5.513e+03	6.615e-03
	50	63	5.721e+05	2.618e+05	5.096e+05	5.221e+03	3.528e-03
	100	58.2	7.864e+05	4.143e+05	6.683e+05	1.435e+03	2.543e-03
	0.1	86.1	1.642e+03	1.118e+02	1.638e+03	2.407e+03	1.218e+00
	1	80	1.176e+04	2.052e+03	1.158e+04	2.012e+03	1.726e-01
55	10	74	7.926e+04	2.185e+04	7.806e+04	1.122e+03	2.529e-02
	50	67.9	1.491e+05	5.629e+04	1.382e+05	8.031e+02	1.342e-02
	100	51.6	1.816e+05	1.328e+05	1.443e+05	3.534e+02	1.125e-02
	0.1	89	3.641e+02	6.354e+00	3.647e+02	7.451e+02	5.493e+00
	1	84.1	3.217e+03	3.318e+02	3.224e+03	6.223e+02	6.217e-01
64	10	79	2.476e+04	4.724e+03	2.431e+04	4.844e+02	8.077e-02
	50	74.2	6.619e+04	1.802e+04	6.368e+04	2.016e+02	3.021e-02
	100	49.7	8.162e+04	6.913e+04	6.845e+04	9.628e+01	2.048e-02

Table B11. DSR frequency sweep oscillation results for Limestone (30%) Mastic

Limestone (30%)							
T(°C)	**f** (Hz)	δ (°)	**G*** (Pa)	**G'** (Pa)	**G"** (Pa)	η (Pa·s)	γ (%)
	0.1	80.7	8.323e+03	1.345e+03	8.214e+03	1.311e+04	2.403e-01
	1	74.2	6.441e+04	1.754e+04	6.197e+04	1.056e+04	3.105e-02
46	10	68	3.227e+05	1.209e+05	2.992e+05	5.712e+03	6.202e-03
	50	63.1	6.482e+05	2.932e+05	5.814e+05	5.438e+03	3.345e-03
	100	58.3	8.874e+05	4.663e+05	7.551e+05	1.622e+03	2.254e-03
	0.1	85.9	2.036e+03	1.456e+02	2.032e+03	2.653e+03	9.823e-01
	1	80	1.725e+04	2.995e+03	1.706e+04	2.124e+03	1.159e-01
55	10	74.1	9.214e+04	2.524e+04	8.862e+04	1.346e+03	2.172e-02
	50	58.2	2.032e+05	7.546e+04	1.886e+05	8.282e+02	9.846e-03
	100	50.1	2.413e+05	1.548e+05	1.852e+05	3.773e+02	8.288e-03
	0.1	88.7	4.466e+02	1.013e+01	4.465e+02	7.655e+02	4.478e+00
	1	84	3.853e+03	4.027e+02	3.832e+03	6.473e+02	5.191e-01
64	10	78.1	3.095e+04	6.382e+03	3.028e+04	5.027e+02	6.462e-02
	50	76	7.243e+04	1.752e+04	7.028e+04	2.196e+02	2.761e-02
	100	48.3	8.742e+04	5.836e+04	6.527e+04	9.822e+01	2.288e-02

Table B12. DSR frequency sweep oscillation results for Granite (5%) Mastic

Granite (5%)							
T(°C)	**f** (Hz)	δ (°)	**G*** (Pa)	**G'** (Pa)	**G"** (Pa)	η (Pa·s)	γ (%)
	0.1	80.9	5.273e+03	8.339e+02	5.206e+03	1.037e+04	3.792e-01
	1	74	3.612e+04	9.956e+03	3.472e+04	9.511e+03	5.537e-02
46	10	67.2	2.002e+05	7.758e+04	1.845e+05	6.174e+03	9.992e-03
	50	63.1	3.691e+05	1.676e+05	3.292e+05	5.998e+03	5.419e-03
	100	48.6	4.347e+05	2.885e+05	3.267e+05	1.226e+03	4.638e-03
	0.1	85.8	1.184e+03	8.674e+01	1.188e+03	2.446e+03	1.689e+00
	1	80	8.496e+03	1.475e+03	8.366e+03	1.872e+03	2.354e-01
55	10	74	6.473e+04	1.784e+04	6.224e+04	1.134e+03	3.089e-02
	50	67.9	1.069e+05	4.028e+04	9.905e+04	8.266e+02	1.879e-02
	100	47.9	1.227e+05	8.226e+04	9.948e+04	3.538e+02	1.636e-02
	0.1	89	2.498e+02	4.534e+00	2.597e+02	7.659e+02	7.698e+00
	1	84	2.086e+03	2.184e+02	2.074e+03	6.604e+02	9.587e-01
64	10	78.8	1.543e+04	2.997e+03	1.513e+04	4.816e+02	1.296e-01
	50	74	5.124e+04	1.412e+04	4.925e+04	2.141e+02	3.903e-02
	100	47.8	6.851e+04	4.601e+04	5.075e+04	9.723e+01	2.919e-02

Table B13. DSR frequency sweep oscillation results for Granite (10%) Mastic

			Granite (10%)				
T(°C)	**f** (Hz)	δ (°)	**G*** (Pa)	**G'** (Pa)	**G"** (Pa)	η (Pa·s)	γ (%)
	0.1	80.8	5.391e+03	8.619e+02	5.321e+03	1.186e+04	3.709e-01
	1	73.9	3.884e+04	1.077e+04	3.731e+04	9.635e+03	5.149e-02
46	10	68	2.158e+05	8.084e+04	2.008e+05	6.308e+03	9.267e-03
	50	71.1	4.517e+05	2.146e+05	4.178e+05	6.193e+03	4.428e-03
	100	49.7	5.528e+05	3.575e+05	4.216e+05	1.334e+03	3.617e-03
	0.1	86	1.338e+03	9.344e+01	1.345e+03	2.576e+03	1.495e+00
	1	79	9.085e+03	1.732e+03	8.918e+03	2.004e+03	2.204e-01
55	10	74.3	6.924e+04	1.874e+04	6.667e+04	1.252e+03	2.878e-02
	50	68.9	1.165e+05	4.194e+04	1.187e+05	8.397e+02	1.717e-02
	100	48.7	1.452e+05	9.583e+04	1.098e+05	3.688e+02	1.377e-02
	0.1	88.9	2.866e+02	5.544e+00	2.865e+02	7.789e+02	7.052e+00
	1	84	2.584e+03	2.701e+02	2.569e+03	6.746e+02	7.739e-01
64	10	78	1.932e+04	4.016e+03	1.889e+04	4.942e+02	1.035e-01
	50	74.2	5.668e+04	1.543e+04	5.458e+04	2.278e+02	3.568e-02
	100	57.6	7.197e+04	3.856e+04	6.076e+04	9.854e+01	2.764e-02

Table B14. DSR frequency sweep oscillation results for Granite (15%) Mastic

			Granite (15%)				
T(°C)	**f** (Hz)	δ (°)	**G*** (Pa)	**G'** (Pa)	**G"** (Pa)	η (Pa·s)	γ (%)
	0.1	80.3	6.745e+03	1.136e+03	6.648e+03	1.229e+04	3.466e-01
	1	73.9	4.882e+04	1.354e+04	4.691e+04	9.785e+03	4.196e-02
46	10	67.9	2.646e+05	9.896e+04	2.442e+05	6.457e+03	7.606e-03
	50	70.8	5.349e+05	1.762e+04	5.151e+05	6.339e+03	3.739e-03
	100	49.6	6.548e+05	4.334e+05	5.124e+05	1.484e+03	3.065e-03
	0.1	86	1.518e+03	1.068e+02	1.514e+03	2.711e+03	1.318e+00
	1	79.1	9.971e+03	1.886e+03	9.793e+03	2.122e+03	2.156e-01
55	10	73.9	7.432e+04	2.165e+04	7.146e+04	1.406e+03	2.692e-02
	50	68.7	1.397e+05	5.174e+04	1.312e+05	8.541e+02	1.432e-02
	100	48.3	1.624e+05	1.086e+05	1.218e+05	3.847e+02	1.231e-02
	0.1	89	3.468e+02	6.052e+00	3.467e+02	7.914e+02	5.767e+00
	1	83.7	3.023e+03	3.317e+02	3.018e+03	6.895e+02	6.616e-01
64	10	78.2	2.249e+04	4.596e+03	2.214e+04	5.096e+02	8.892e-02
	50	73.6	6.385e+04	1.827e+04	6.126e+04	2.420e+02	3.134e-02
	100	58.5	7.875e+04	4.346e+04	7.226e+04	1.007e+02	2.546e-02

Table B15. DSR frequency sweep oscillation results for Granite (20%) Mastic

			Granite (20%)				
T(°C)	**f** (Hz)	δ (°)	**G*** (Pa)	**G'** (Pa)	**G"** (Pa)	η (Pa·s)	γ (%)
	0.1	81	7.439e+03	1.163e+03	7.347e+03	1.316e+04	2.688e-01
	1	74.3	5.984e+04	1.619e+04	5.767e+04	9.875e+03	3.342e-02
46	10	67.1	3.056e+05	1.189e+05	2.815e+05	6.597e+03	6.544e-03
	50	65.7	6.119e+05	2.518e+05	5.578e+05	6.493e+03	3.272e-03
	100	55.2	7.898e+05	4.507e+05	6.485e+05	1.603e+03	2.532e-03
	0.1	86.1	1.755e+03	1.194e+02	1.752e+03	2.854e+03	1.146e+00
	1	79.9	1.327e+04	2.348e+03	1.336e+04	2.265e+03	1.527e-01
55	10	74	8.496e+04	2.342e+04	8.167e+04	1.538e+03	2.354e-02
	50	69	1.614e+05	5.784e+04	1.508e+05	8.696e+02	1.239e-02
	100	55.4	1.943e+05	1.104e+05	1.598e+05	4.035e+02	1.046e-02
	0.1	88.9	3.765e+02	7.228e+00	3.764e+02	8.043e+02	5.312e+00
	1	84.2	3.456e+03	3.493e+02	3.438e+03	7.033e+02	5.787e-01
64	10	78.2	2.707e+04	5.535e+03	2.649e+04	5.227e+02	7.388e-02
	50	74.1	6.851e+04	1.876e+04	6.589e+04	2.569e+02	2.927e-02
	100	51.6	8.349e+04	5.186e+04	6.543e+04	1.118e+02	2.396e-02

Table B16. DSR frequency sweep oscillation results for Granite (30%) Mastic

			Granite (30%)				
T(°C)	**f** (Hz)	δ (°)	**G*** (Pa)	**G'** (Pa)	**G"** (Pa)	η (Pa·s)	γ (%)
	0.1	80.9	9.734e+03	1.537e+03	9.612e+03	1.549e+04	2.055e-01
	1	74.2	7.034e+04	1.922e+04	6.784e+04	1.115e+04	2.855e-02
46	10	66.9	3.824e+05	1.503e+05	3.527e+05	6.818e+03	5.236e-03
	50	66.8	7.263e+05	3.432e+05	6.468e+05	6.793e+03	2.756e-03
	100	56.9	9.128e+05	4.985e+05	7.642e+05	1.858e+03	2.196e-03
	0.1	86.3	2.437e+03	1.573e+02	2.432e+03	3.093e+03	8.206e-01
	1	79.7	2.078e+04	3.732e+03	2.056e+04	2.511e+03	9.583e-02
55	10	74	1.075e+05	2.963e+04	1.035e+05	1.788e+03	1.864e-02
	50	68.9	2.329e+05	8.384e+04	2.173e+05	8.938e+02	8.587e-03
	100	52.3	2.763e+05	1.689e+05	2.186e+05	4.278e+02	7.238e-03
	0.1	88.1	5.209e+02	1.721e+01	5.206e+02	8.288e+02	3.839e+00
	1	84.1	4.574e+03	4.691e+02	4.551e+03	7.281e+02	4.374e-01
64	10	78.3	3.418e+04	6.927e+03	3.347e+04	5.441e+02	5.903e-02
	50	74.4	7.865e+04	2.115e+04	7.576e+04	2.805e+02	2.544e-02
	100	48.6	9.276e+04	6.134e+03	6.958e+04	1.319e+02	2.156e-02

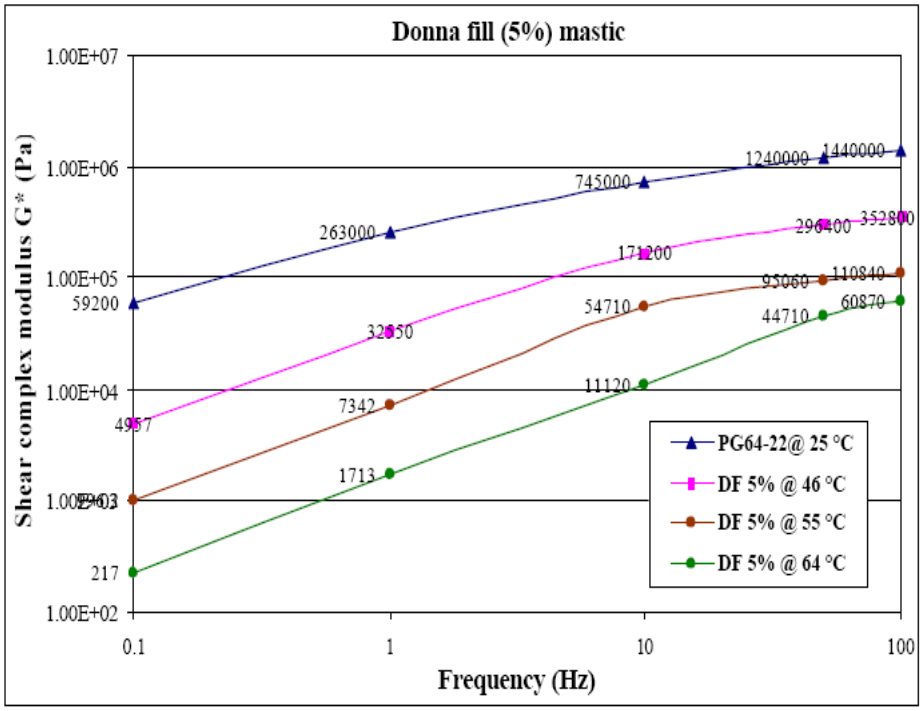

Figure B1 Shear complex moduli for donna fill (5%) mastic.

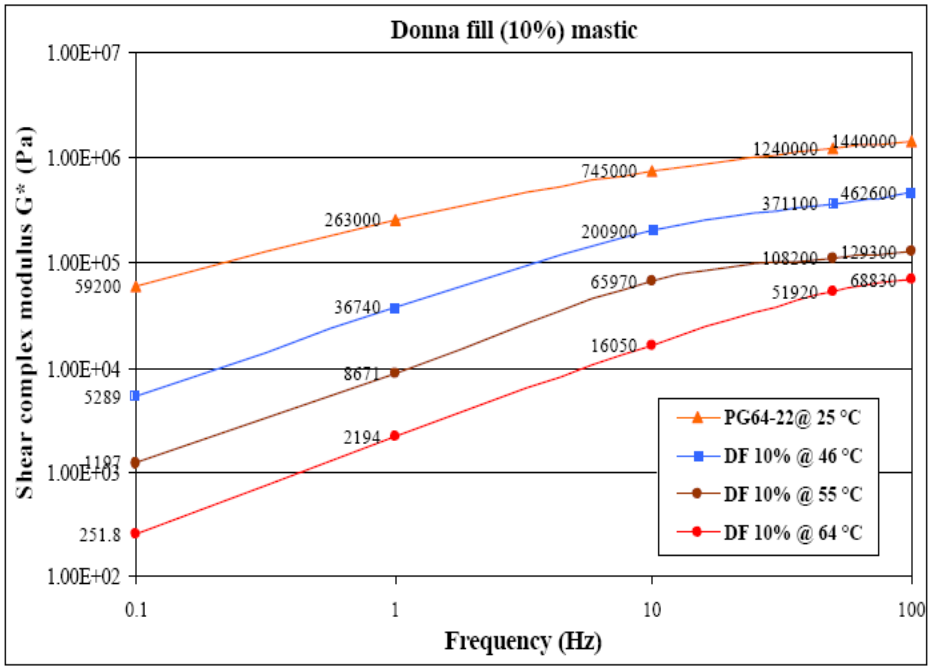

Figure B2 Shear complex moduli for donna fill (10%) mastic.

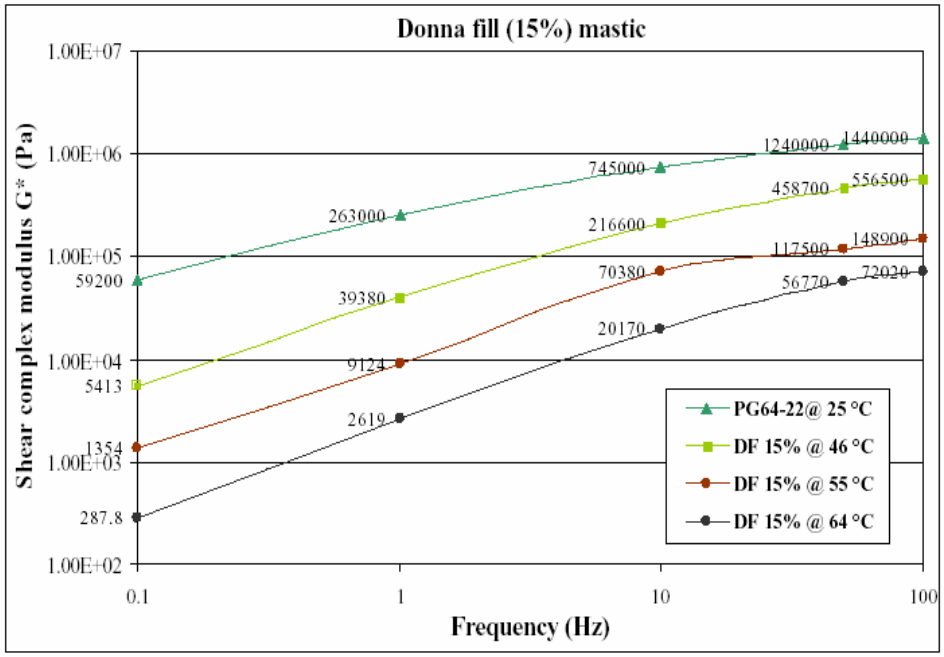

Figure B3 Shear complex moduli for donna fill (15%) mastic.

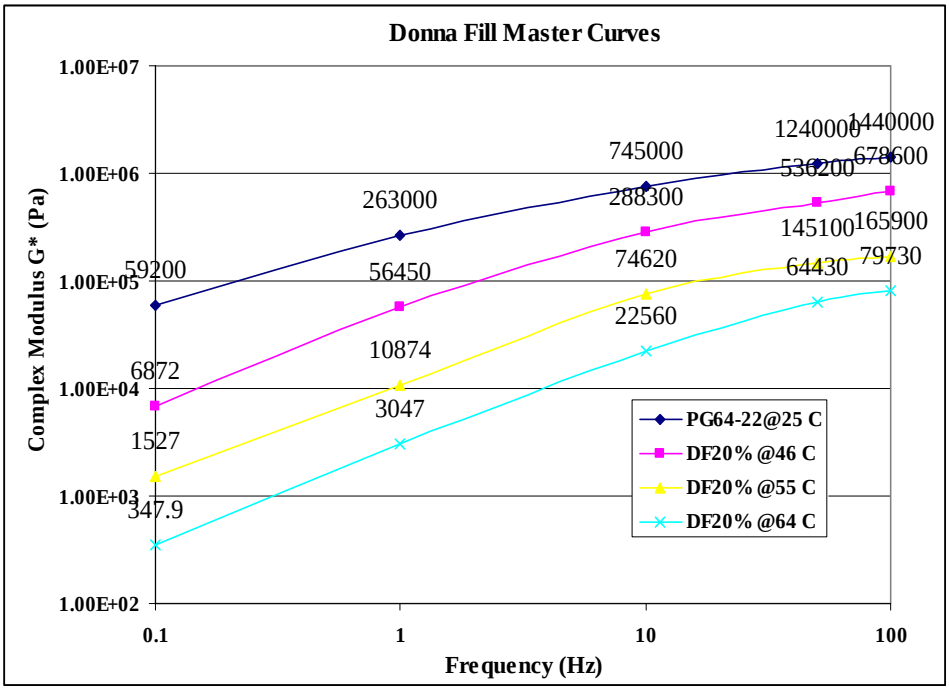

Figure B4 Shear complex moduli for donna fill (20%) mastic.

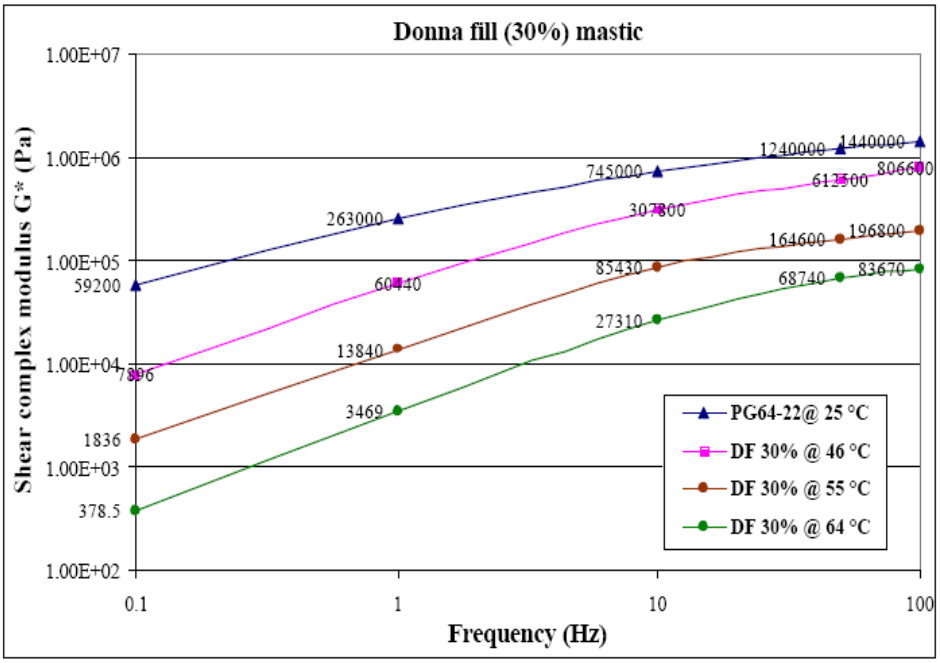

Figure B5 Shear complex moduli for donna fill (30%) mastic.

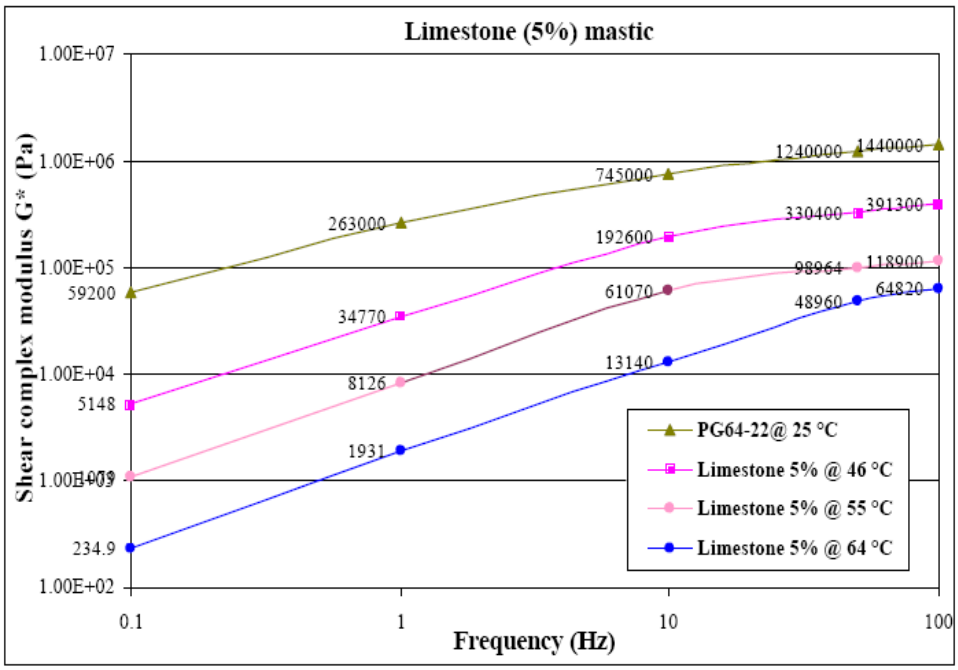

Figure B6 Shear complex moduli for limestone (5%) mastics.

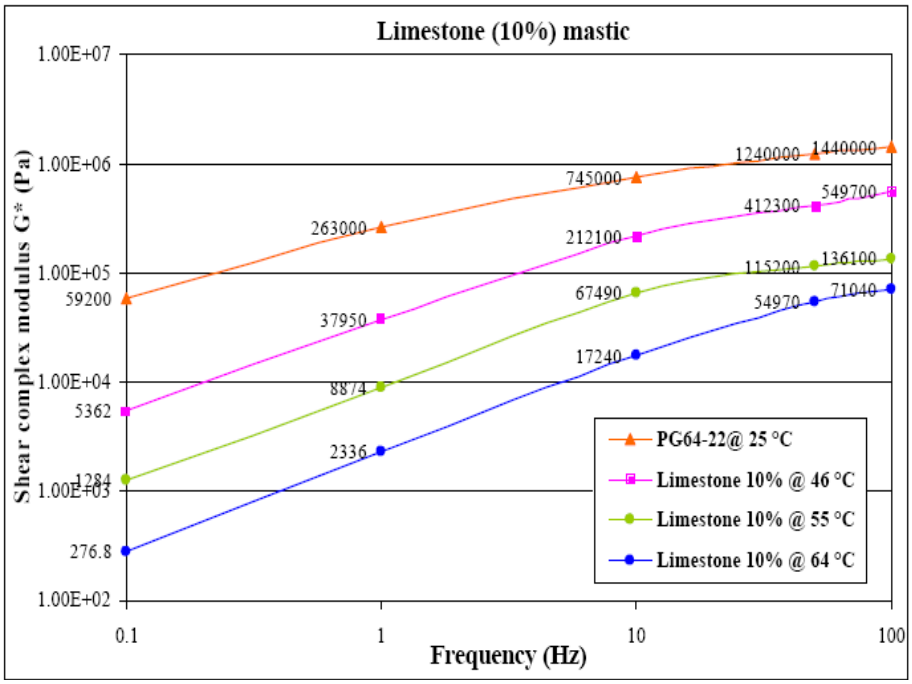

Figure B7 Shear complex moduli for limestone (10%) mastics.

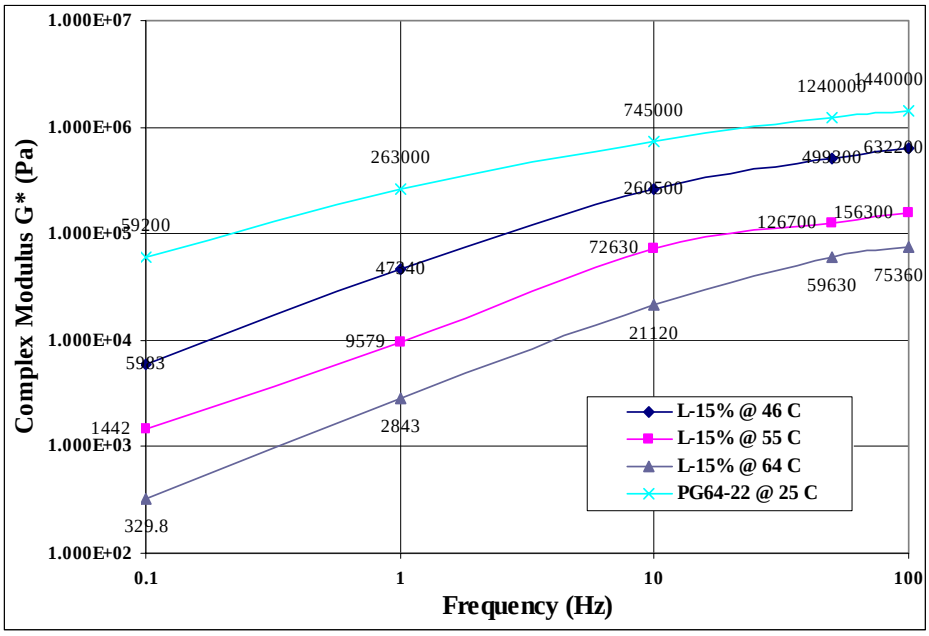

Figure B8 Shear complex moduli for limestone (15%) mastics.

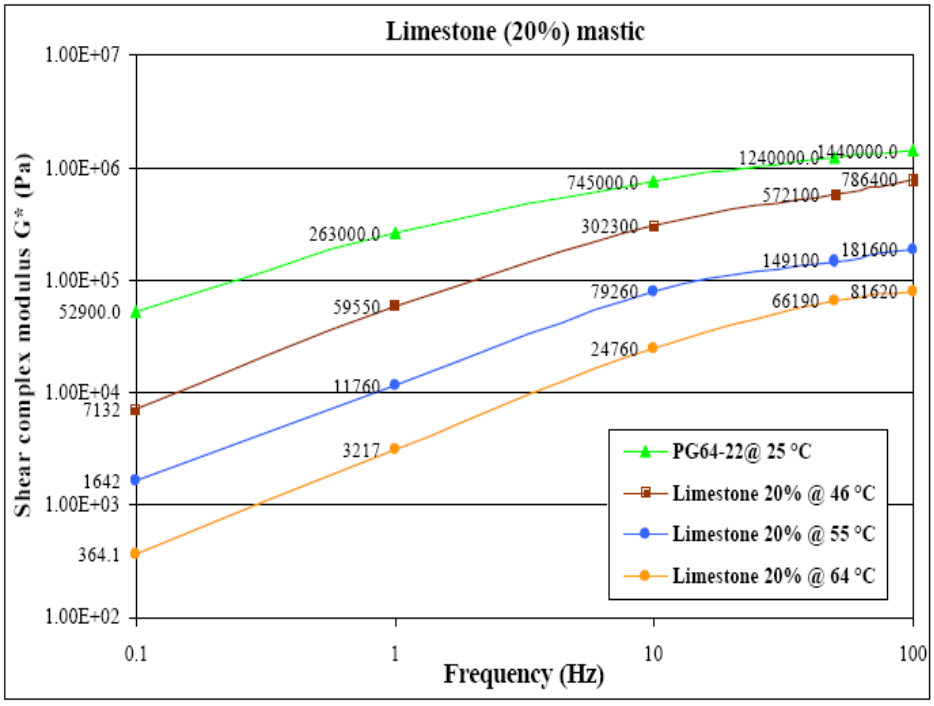

Figure B9 Shear complex moduli for limestone (20%) mastics.

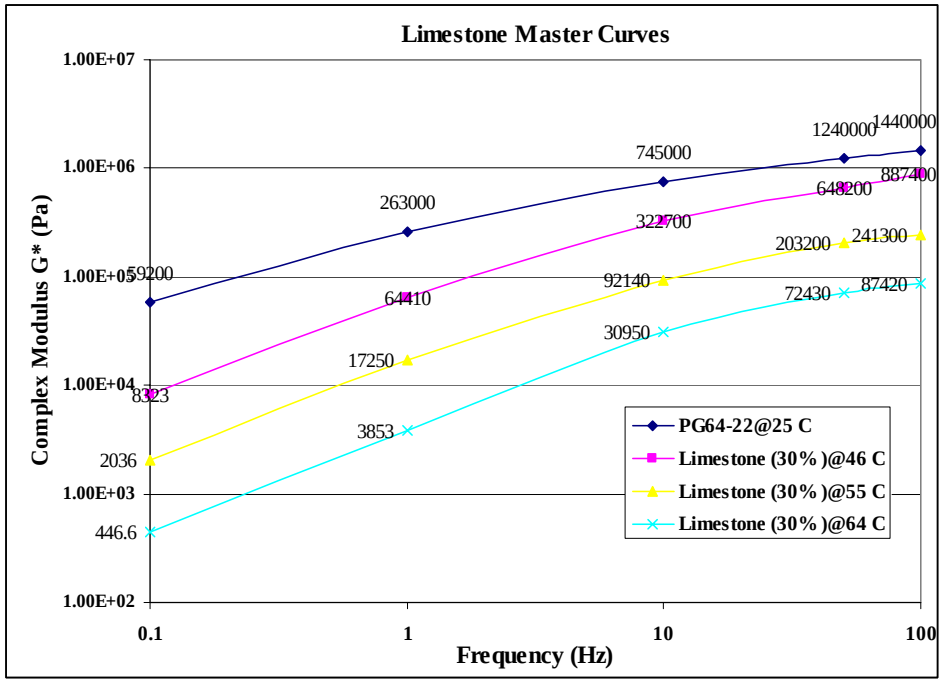

Figure B10 Shear complex moduli for limestone (30%) mastics.

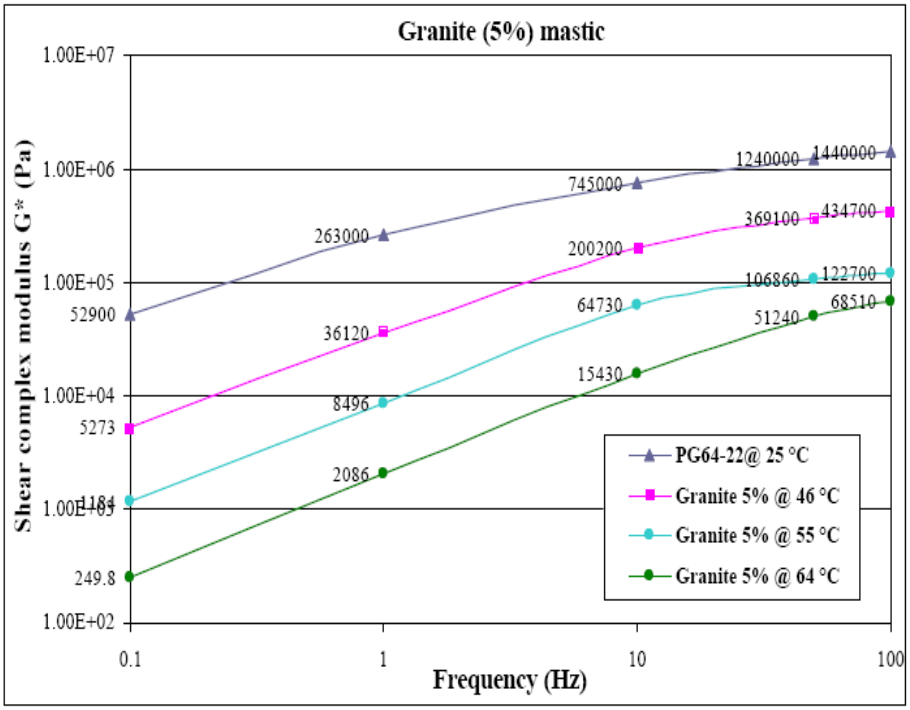

Figure B11 Shear complex moduli for granite (5%) mastics.

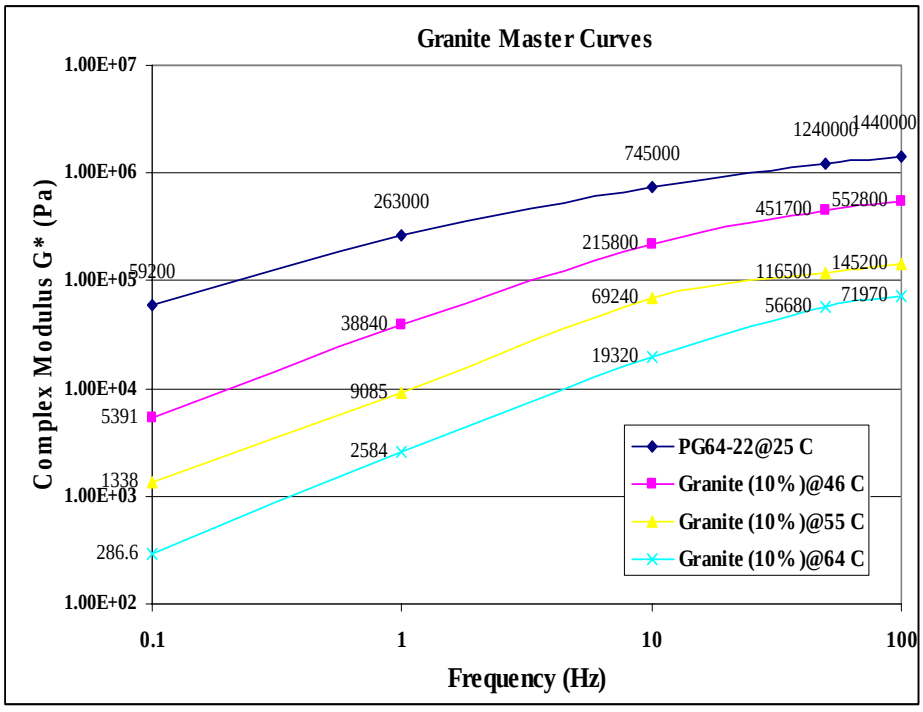

Figure B12 Shear complex moduli for granite (10%) mastics.

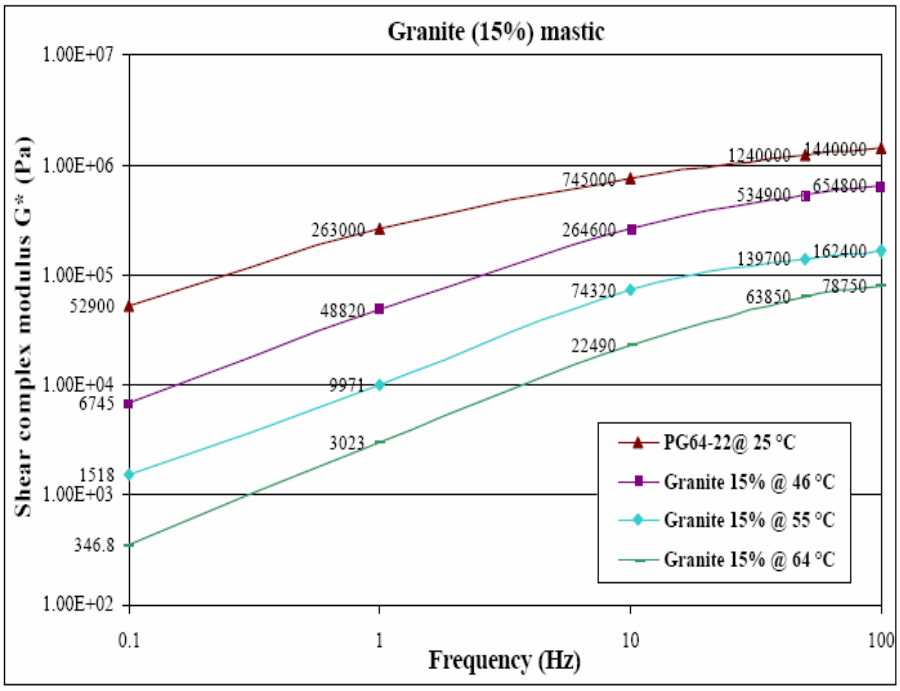

Figure B13 Shear complex moduli for granite (15%) mastics.

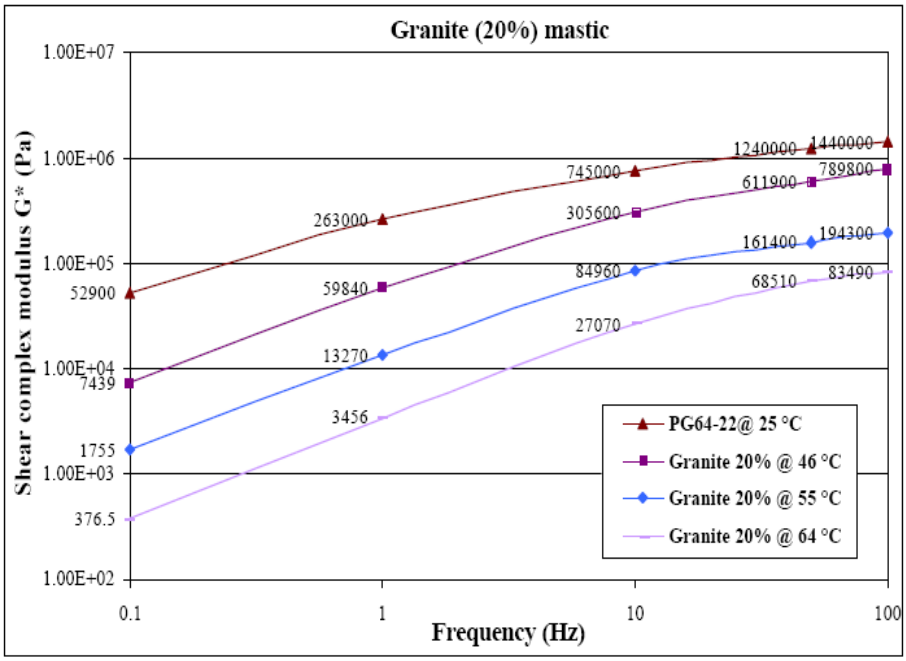

Figure B14 Shear complex moduli for granite (20%) mastics.

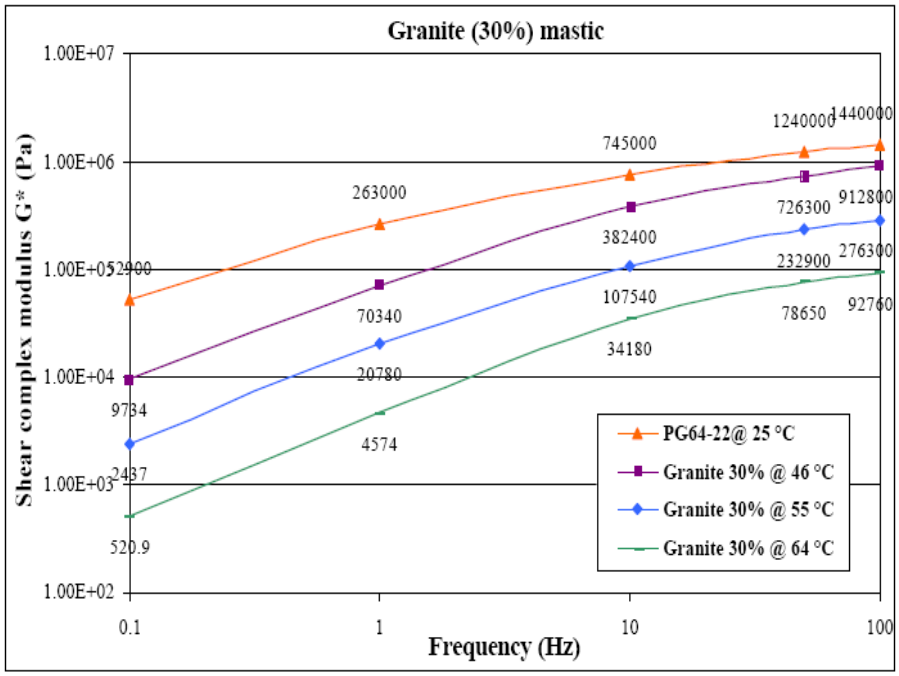

Figure B15 Shear complex moduli for granite (30%) mastics.

APPENDIX C

PHASE ANGLE DEPENDENCY ON LOADING FREQUENCY

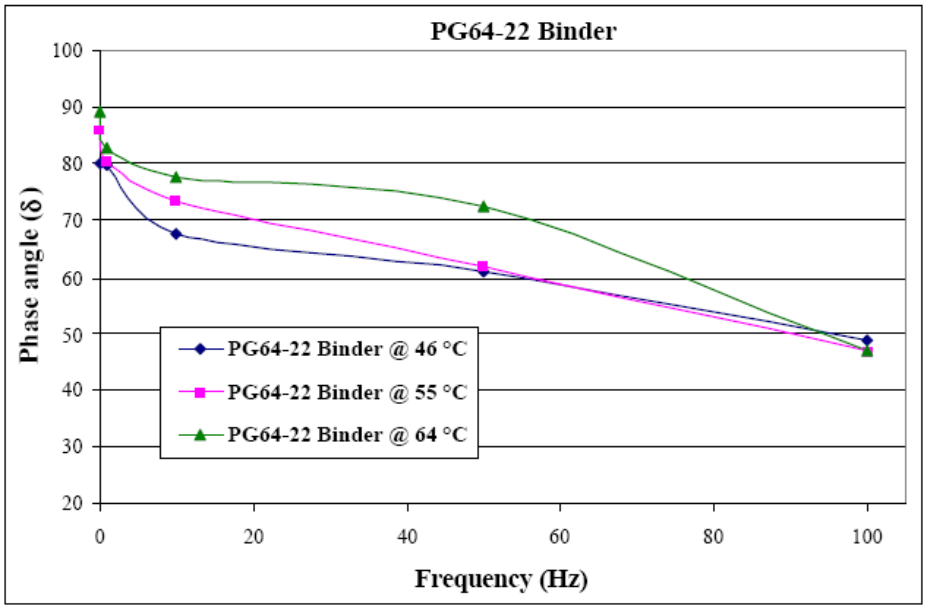

Figure C1 Phase Angle Dependency on Loading Frequency for Pure Binder.

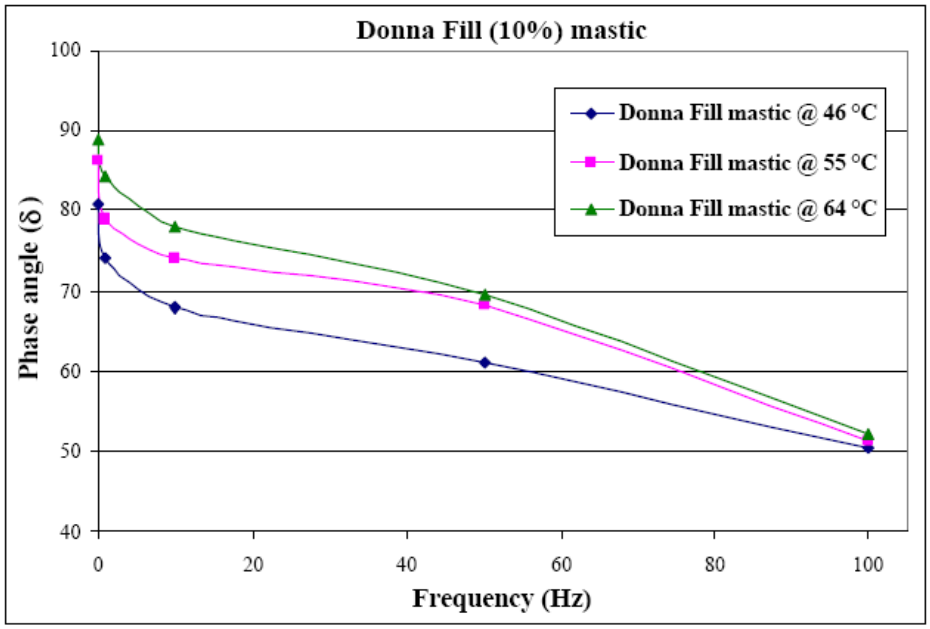

Figure C2 Phase Angle Dependency on Loading Frequency for 10% Filler Mastic.

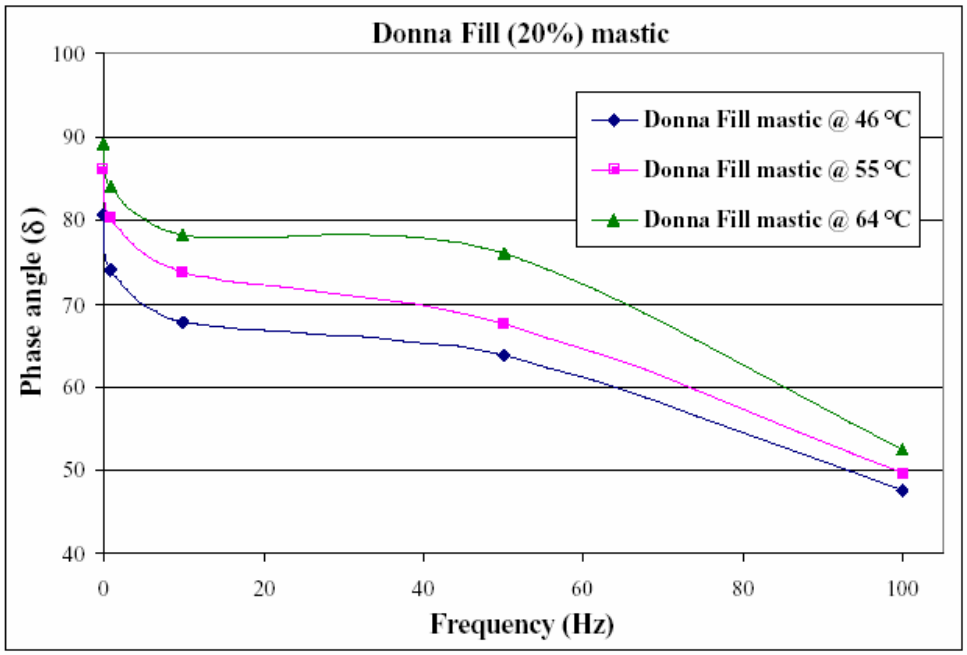

Figure C3 Phase Angle Dependency on Loading Frequency for 20% Filler Mastic.

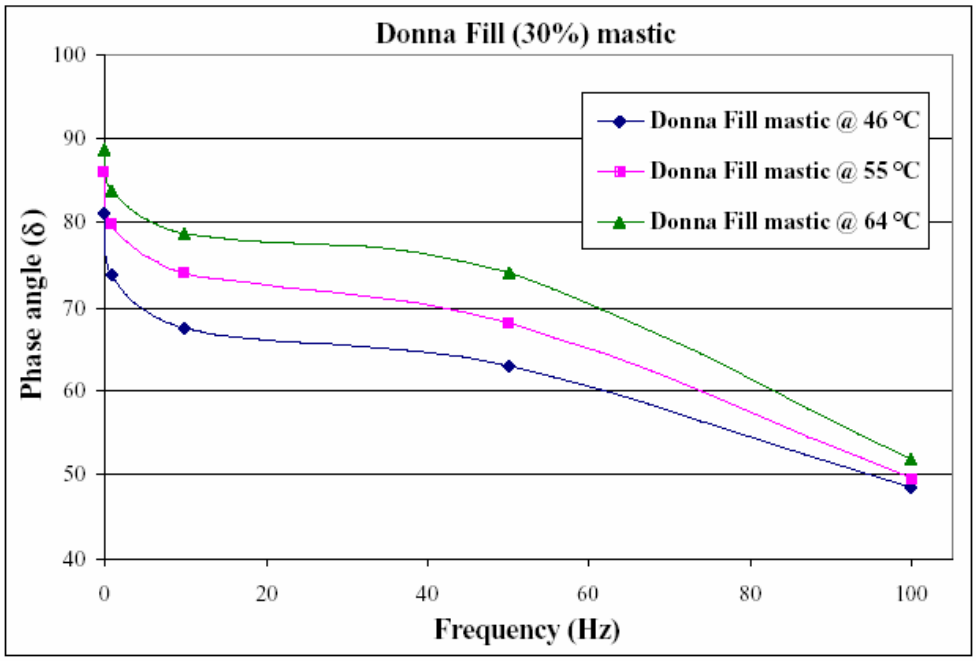

Figure C4 Phase Angle Dependency on Loading Frequency for 30% Filler Mastic.

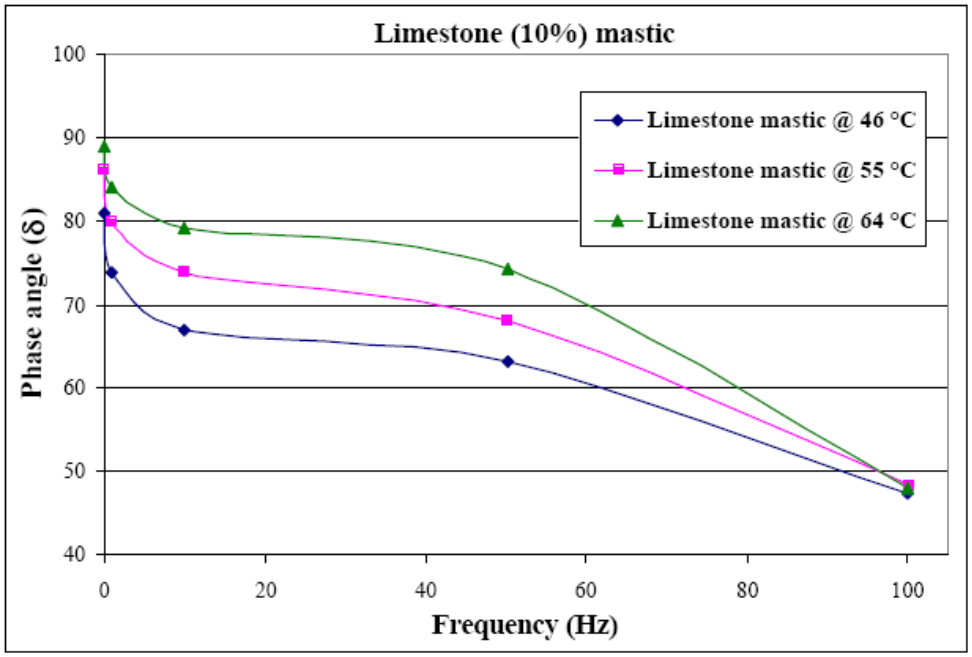

Figure C5 Phase Angle Dependency on Loading Frequency for 10% Filler Mastic.

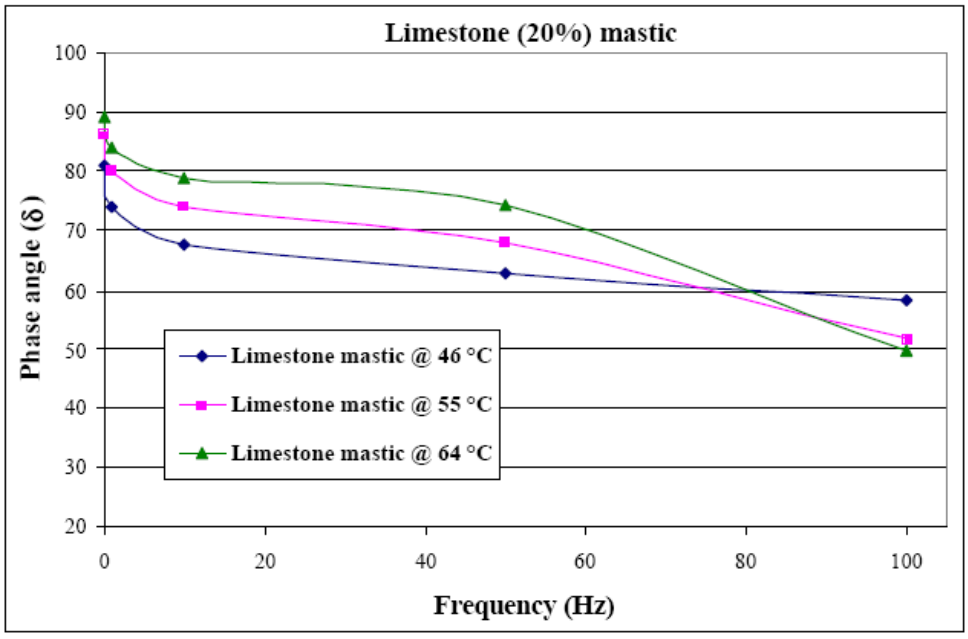

Figure C6 Phase Angle Dependency on Loading Frequency for 20% Filler Mastic.

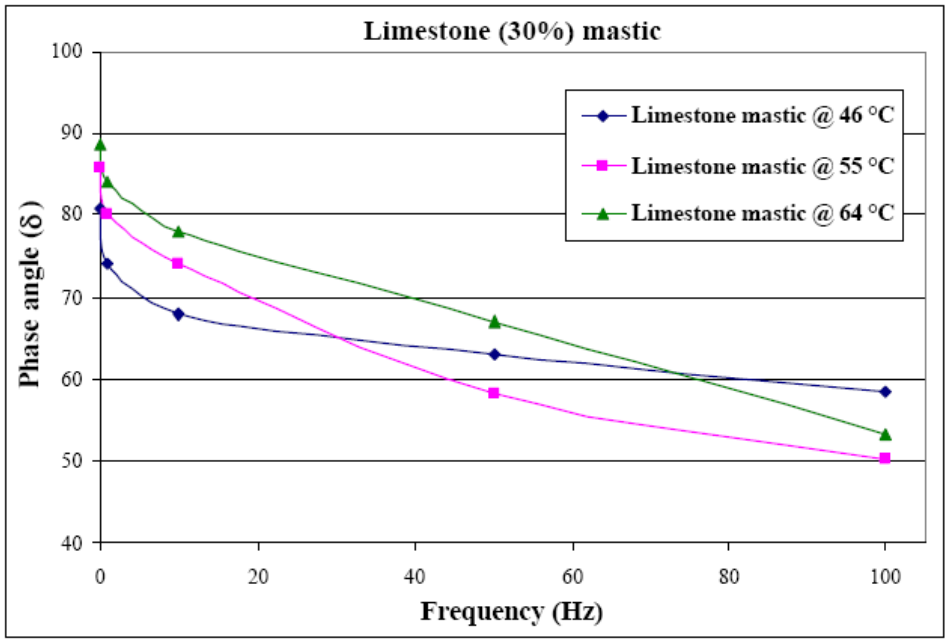

Figure C7 Phase Angle Dependency on Loading Frequency for 30% Filler Mastic.

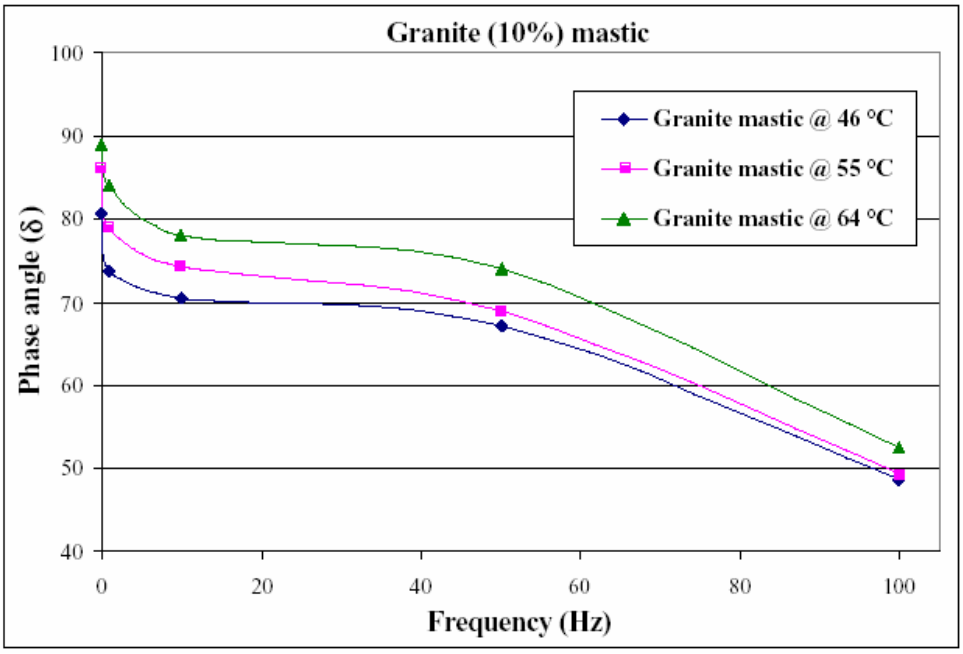

Figure C8 Phase Angle Dependency on Loading Frequency for 10% Filler Mastic.

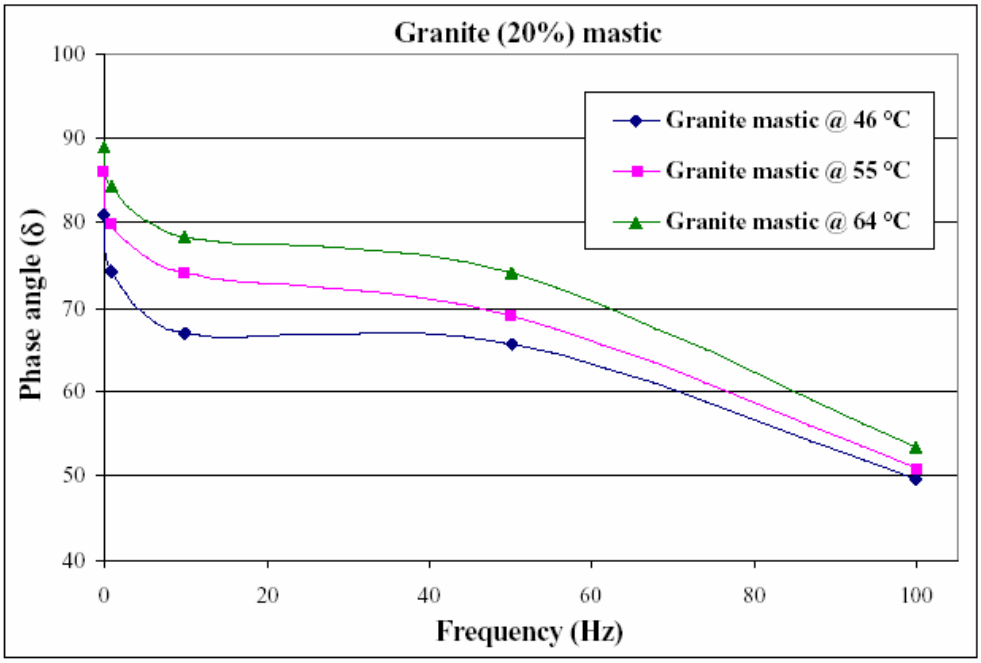

Figure C9 Phase Angle Dependency on Loading Frequency for 20% Filler Mastic.

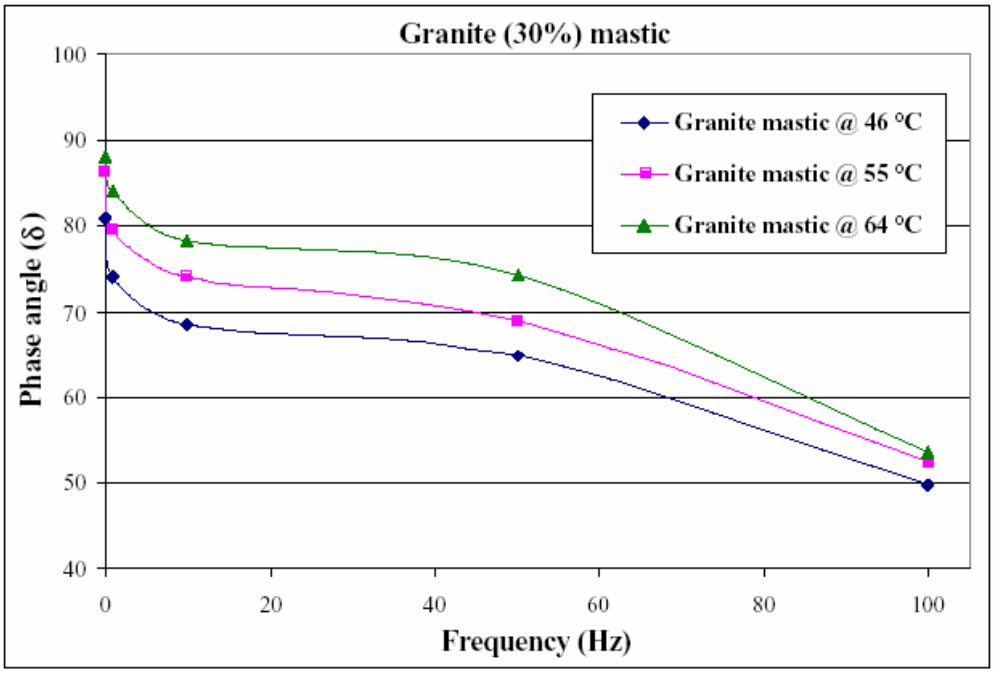

Figure C10 Phase Angle Dependency on Loading Frequency for 30% Filler Mastic.

APPENDIX D

DSR MASTER CURVES

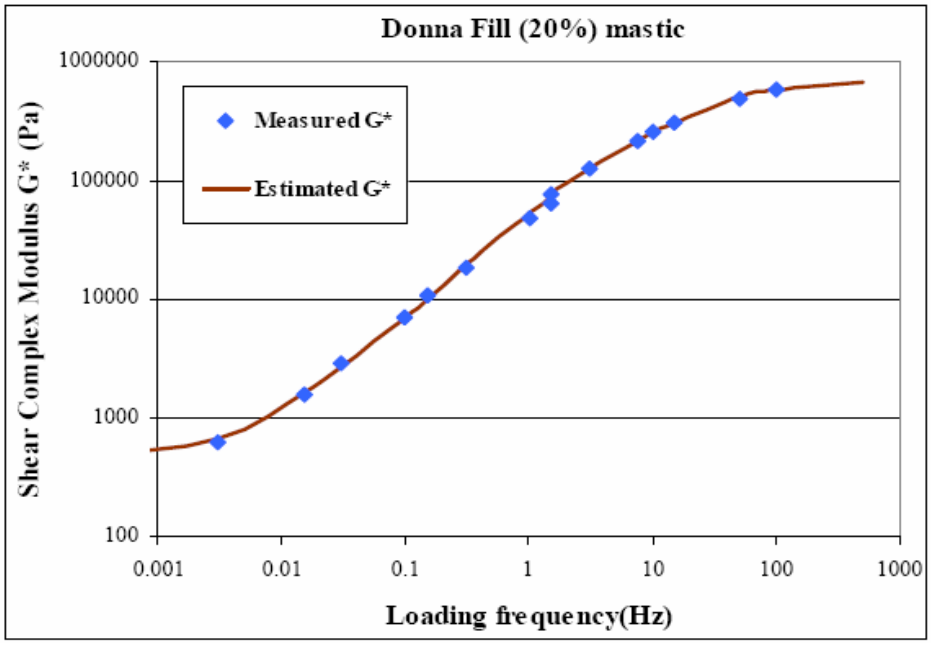

Figure D1 Master curve for mastic containing 20% donna fill.

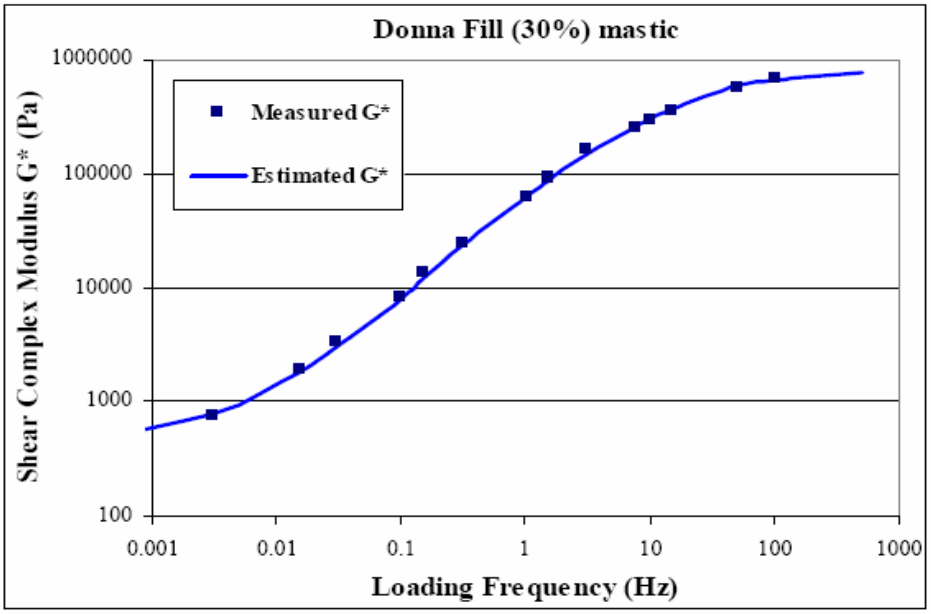

Figure D2 Master curve for mastic containing 30% donna fill.

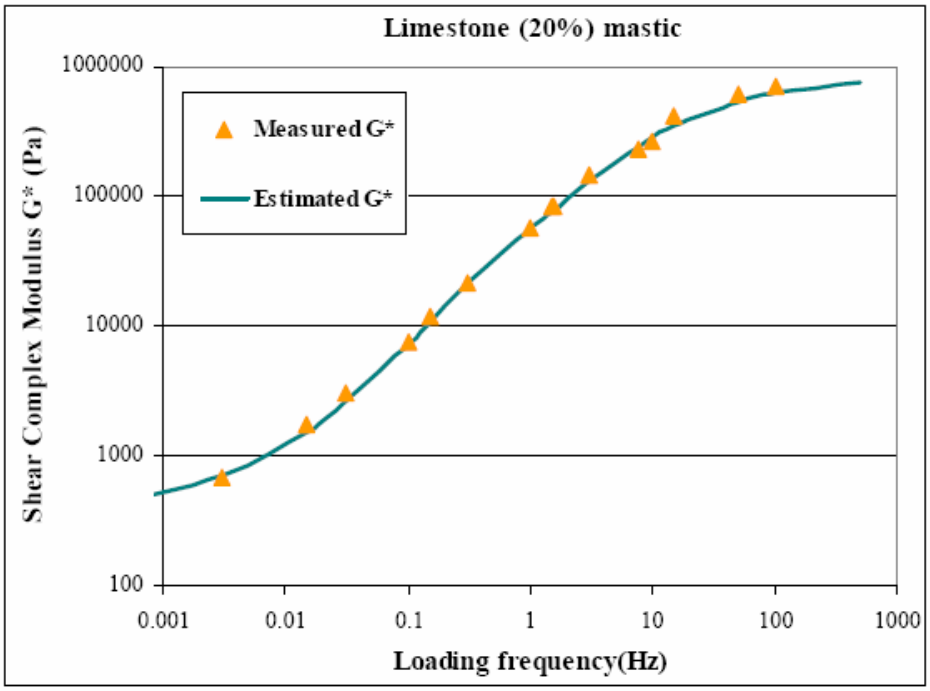

Figure D3 Master curve for mastic containing 20% limestone.

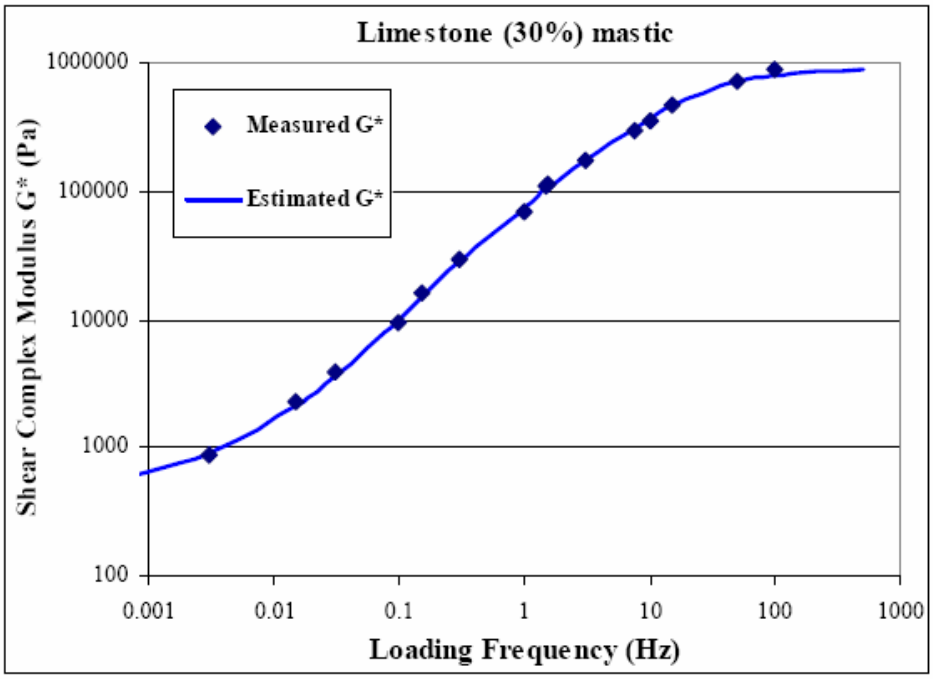

Figure D4 Master curve for mastic containing 30% limestone.

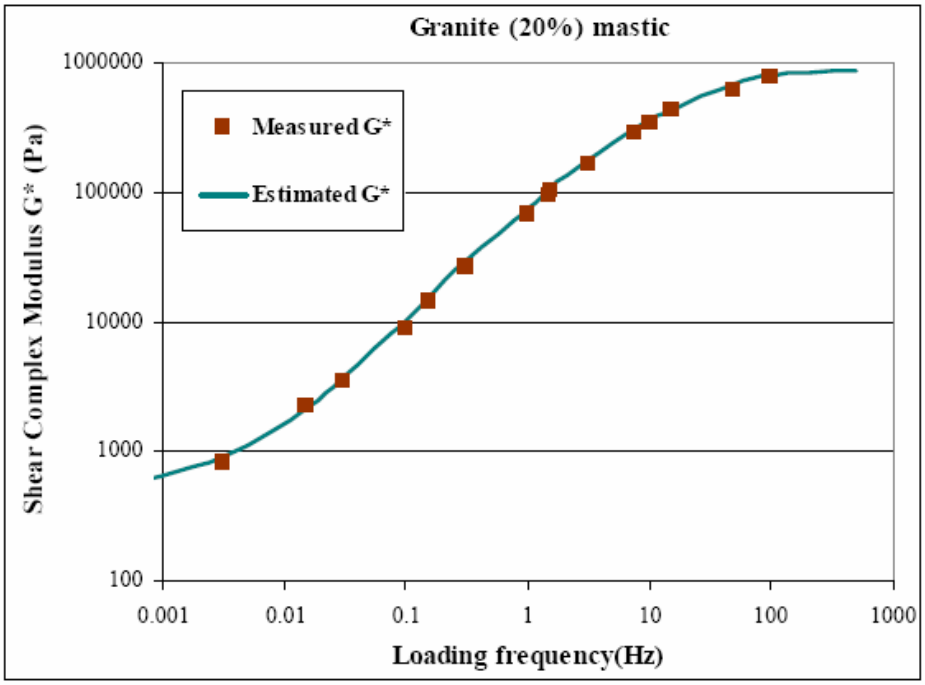

Figure D5 Master curve for mastic containing 20% granite.

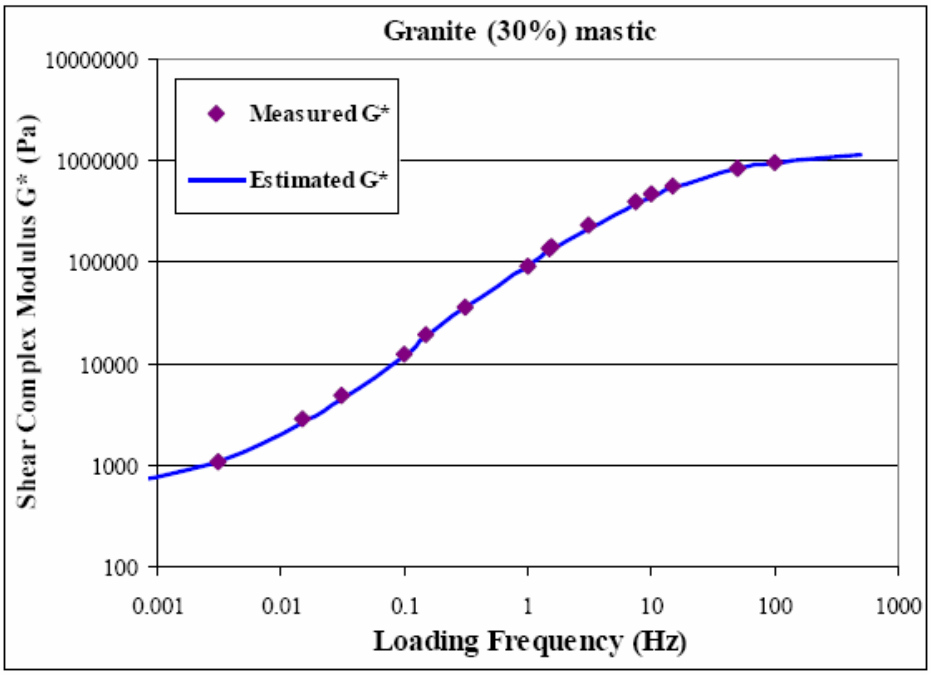

Figure D6 Master curve for mastic containing 30% granite.

Table D1. Shift factors for asphalt binder and mastics

Material	Shift factor a(T)		
	46 °C	55 °C	64 °C
Pure binder PG64-22	1.0037	0.822	1.517
Donna fill (20%) mastic	1.0039	0.789	1.531
Limestone (20%) mastic	1.0035	0.827	1.516
Granite (20%) mastic	1.0028	0.817	1.509

Table D2. Shift factors for asphalt binder and mastics

Material	Shift factor a(T)		
	46 °C	55 °C	64 °C
Pure binder PG64-22	1.0037	0.822	1.517
Donna fill (30%) mastic	1.0041	0.798	1.522
Limestone (30%) mastic	1.0026	0.826	1.508
Granite (30%) mastic	1.0024	0.823	1.496

APPENDIX E

DSR REPEATED SHEAR CREEP LOADING AND RECOVERY TEST RESULTS

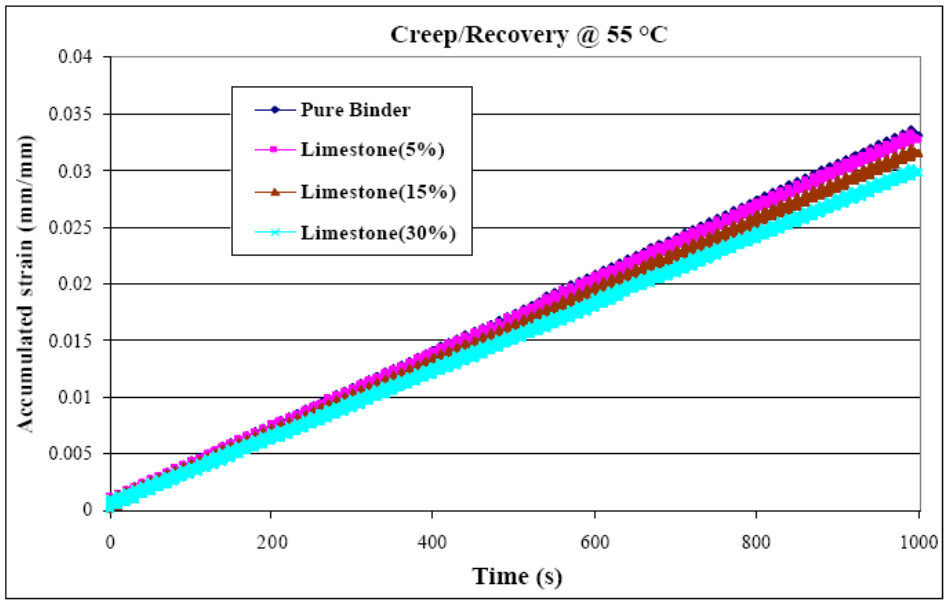

Figure E1 Repeated Creep and Recovery for Limestone Mastics @ 55 °C.

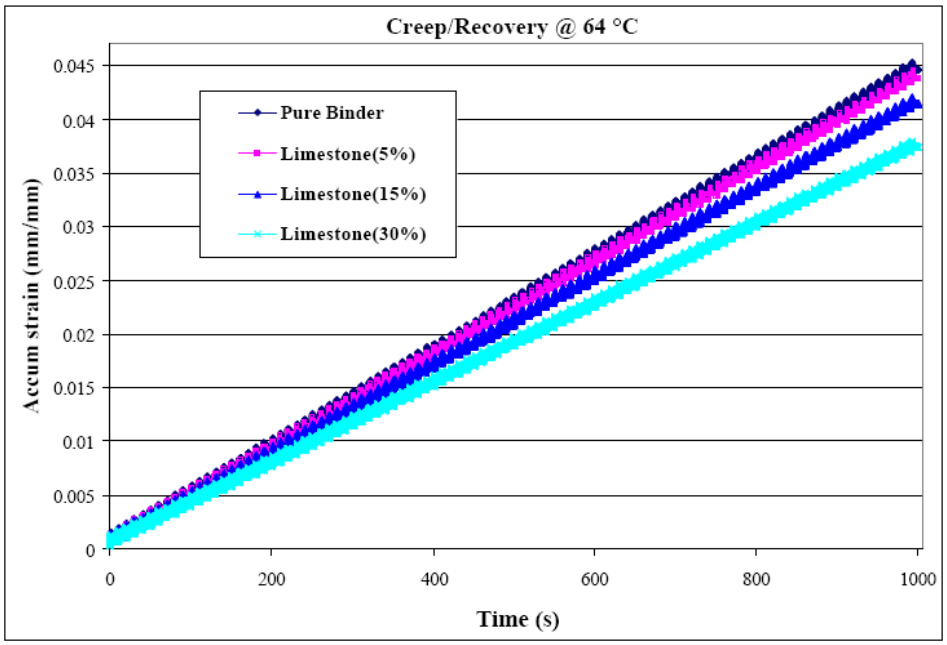

Figure E2 Repeated Creep and Recovery for Limestone Mastics @ 64 °C.

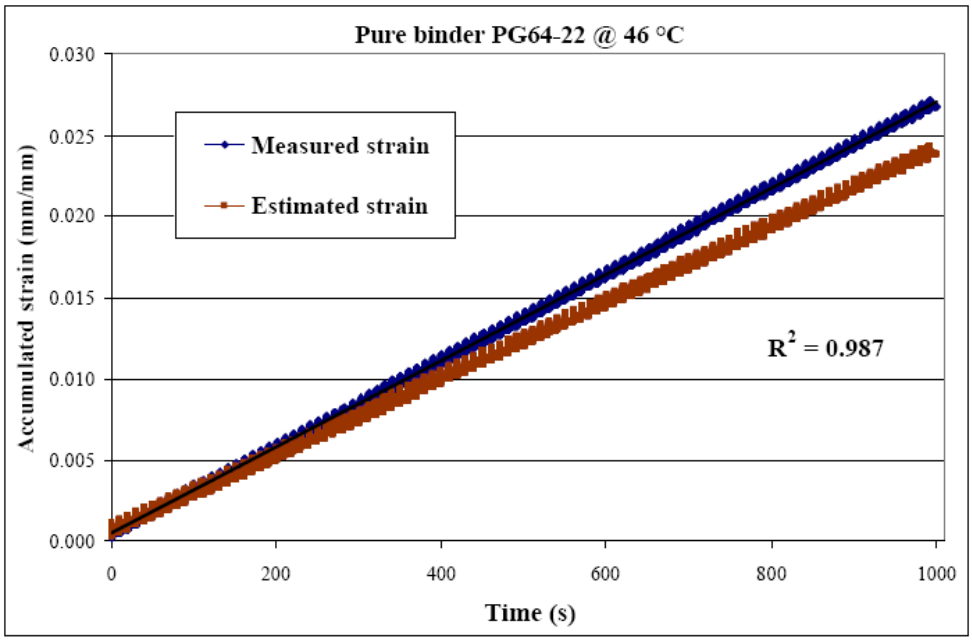

Figure E3 Measured versus Estimated Shear Strain for Pure Binder @ 46 °C.

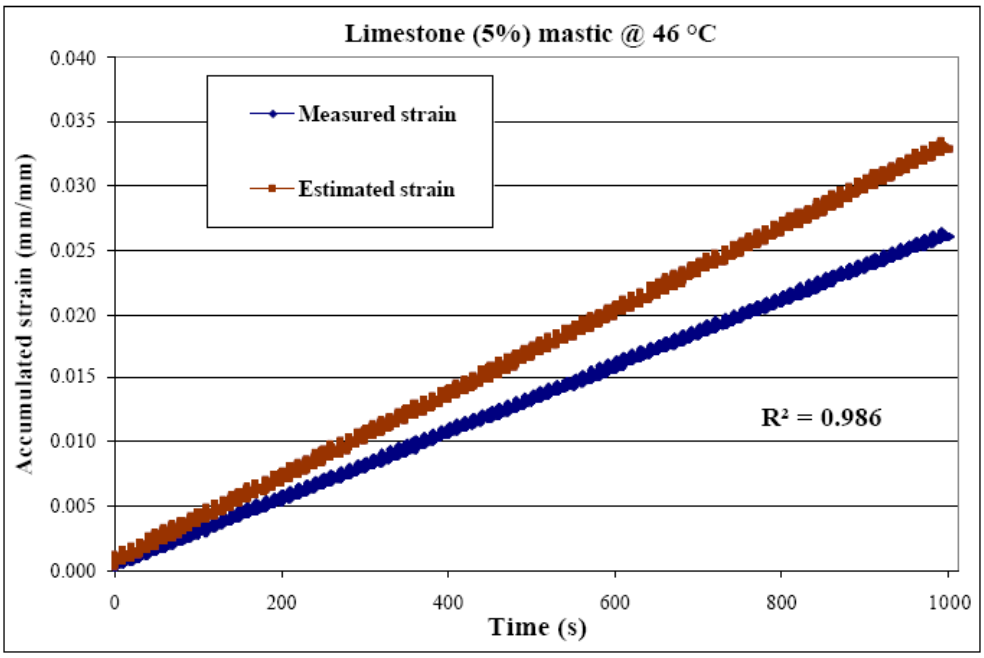

Figure E4 Measured versus Estimated Shear Strain for 5% Filler Mastic @ 46 °C.

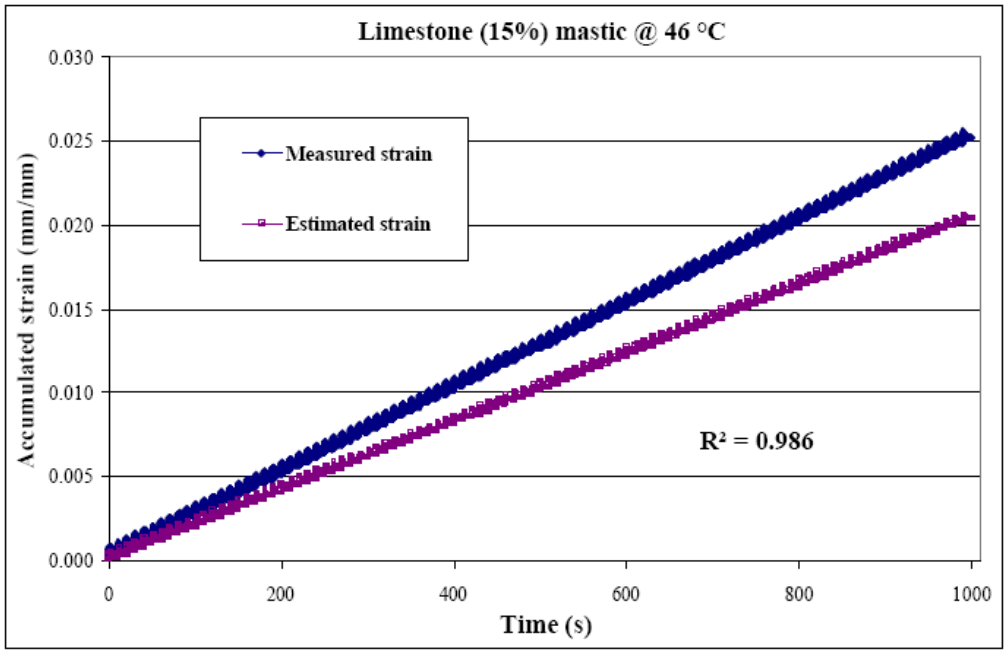

Figure E5 Measured versus Estimated Shear Strain for 15% Filler Mastic @ 46 °C.

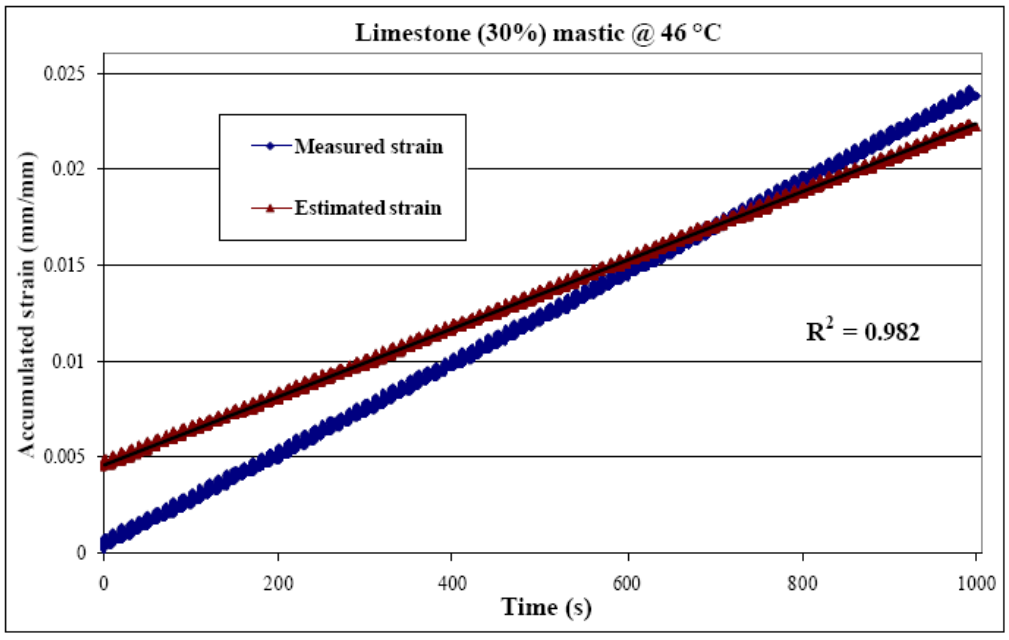

Figure E6 Measured versus Estimated Shear Strain for Mastic @ 46 °C.

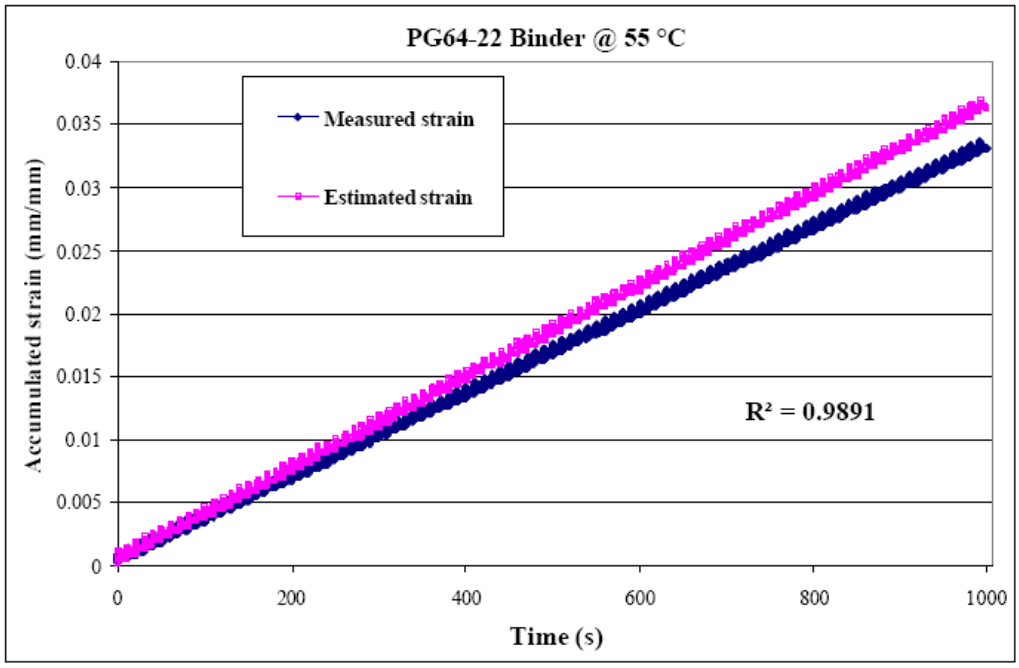

Figure E7 Measured versus Estimated Shear Strain for Pure Binder @ 55 °C.

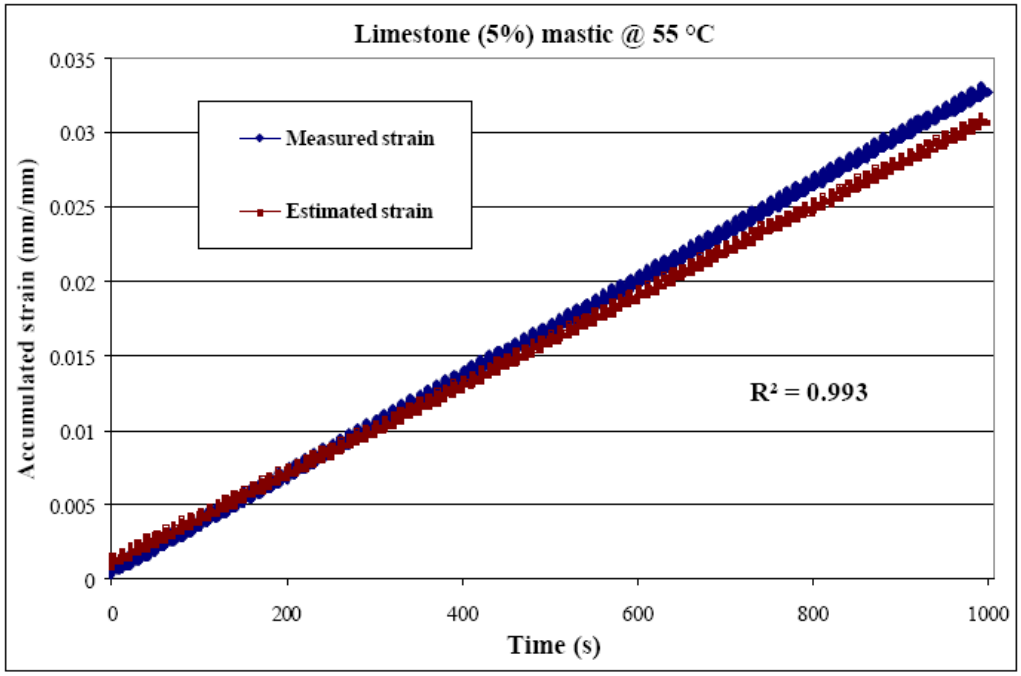

Figure E8 Measured versus Estimated Shear Strain for Limestone Mastic @ 55 °C.

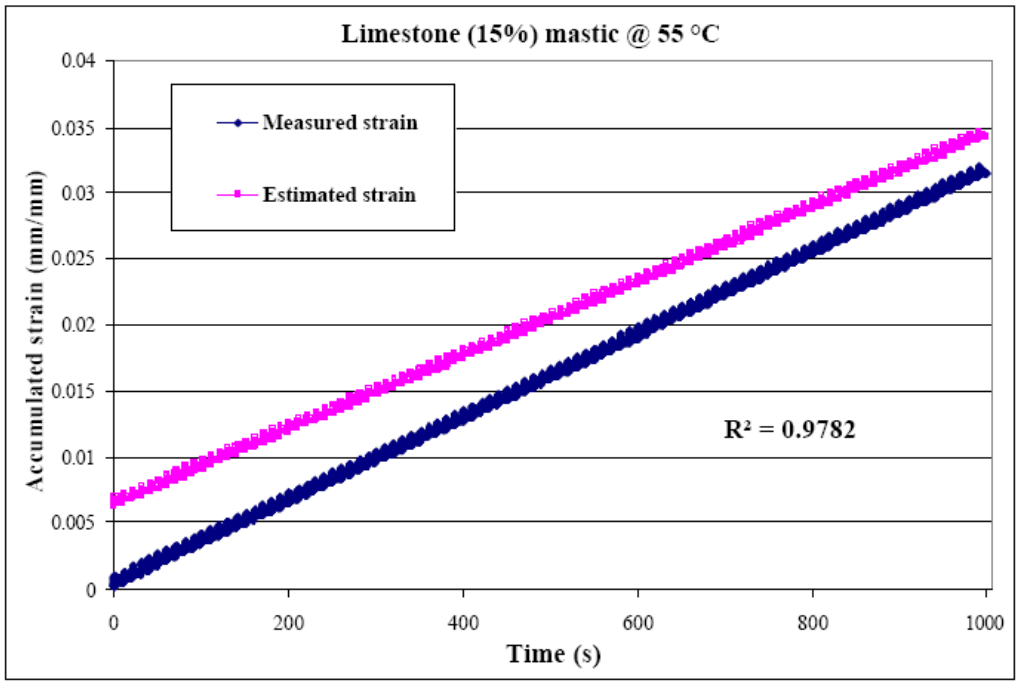

Figure E9 Measured versus Estimated Shear Strain for 15% Filler Mastic @ 55 °C.

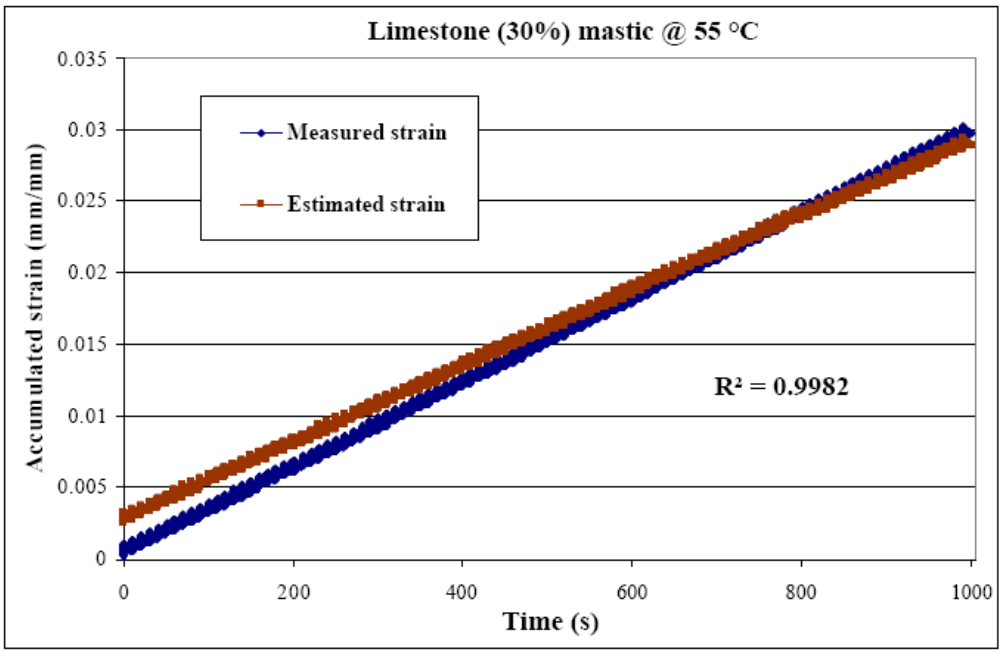

Figure E10 Measured versus Estimated Shear Strain for 30% Filler Mastic @ 55 °C.

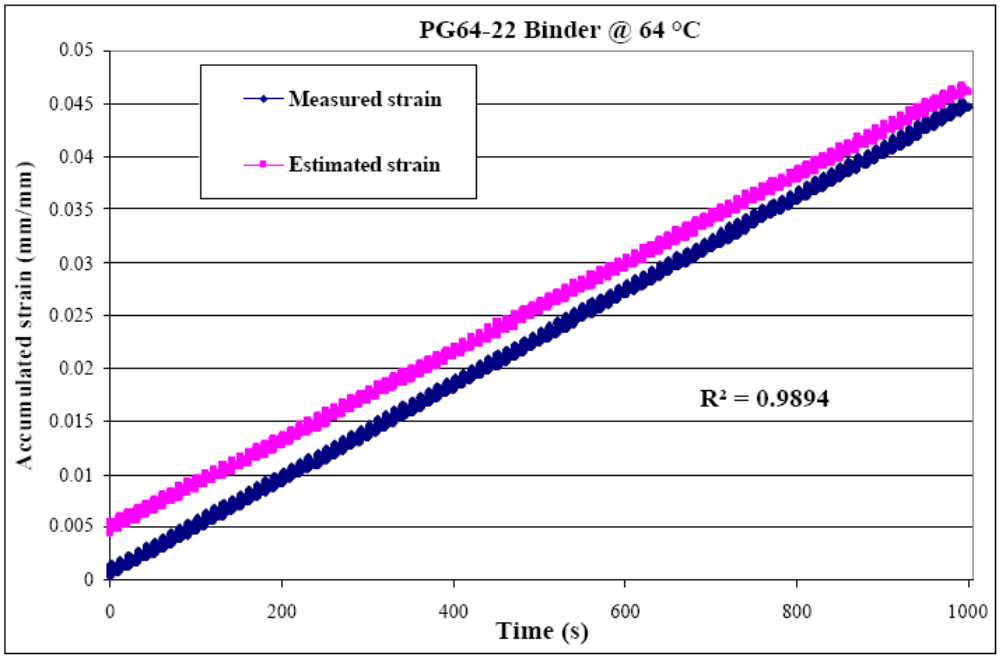

Figure E11 Measured versus Estimated Shear Strain for Pure Binder @ 64 °C.

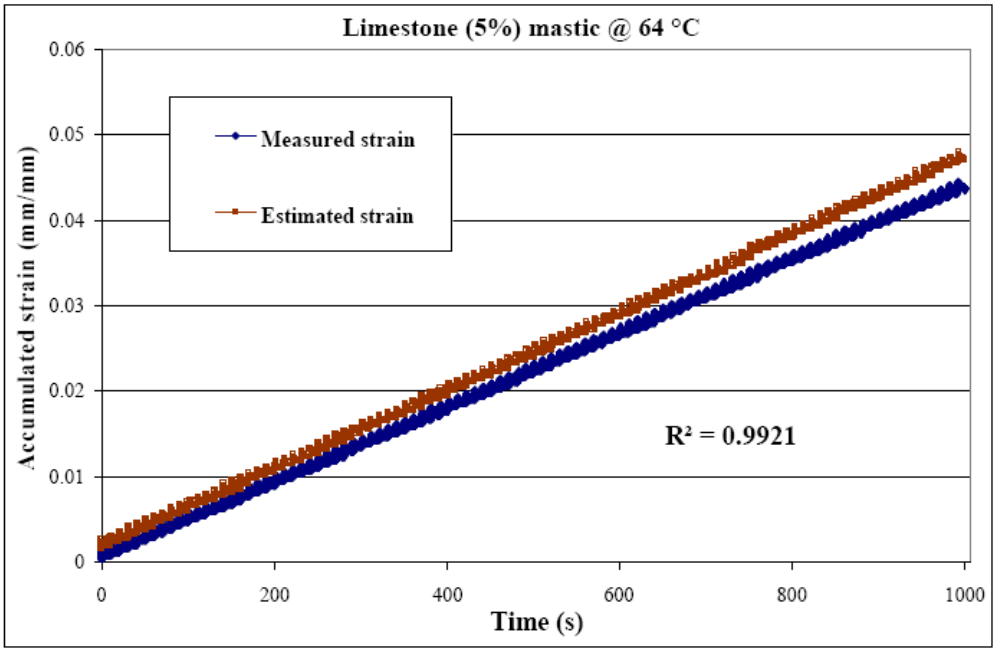

Figure E12 Measured versus Estimated Shear Strain for 5% Filler Mastic @ 64 °C.

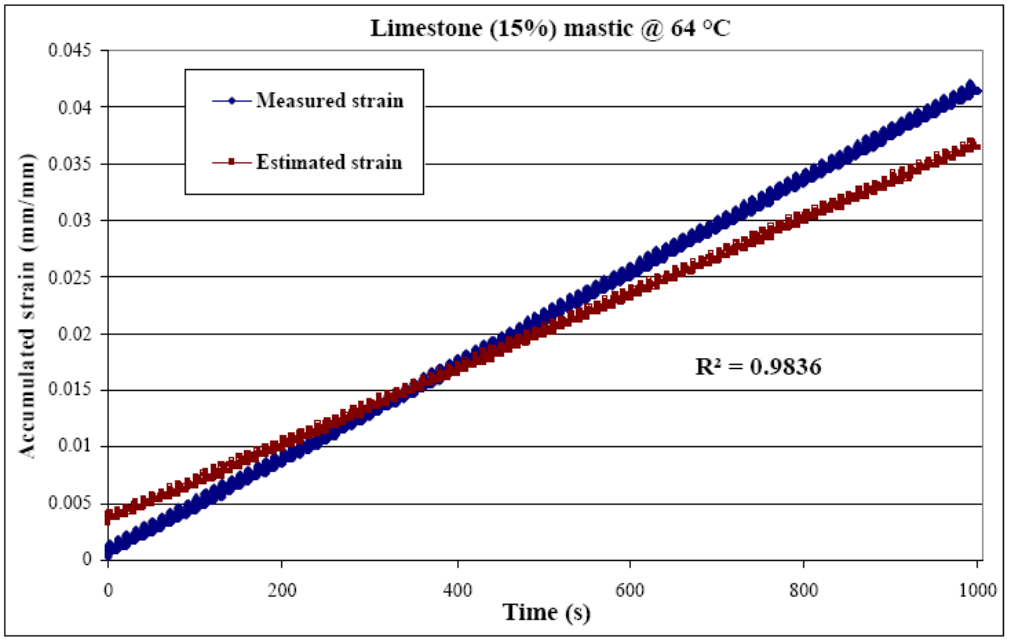

Figure E13 Measured versus Estimated Shear Strain for 15% Filler Mastic @ 64 °C.

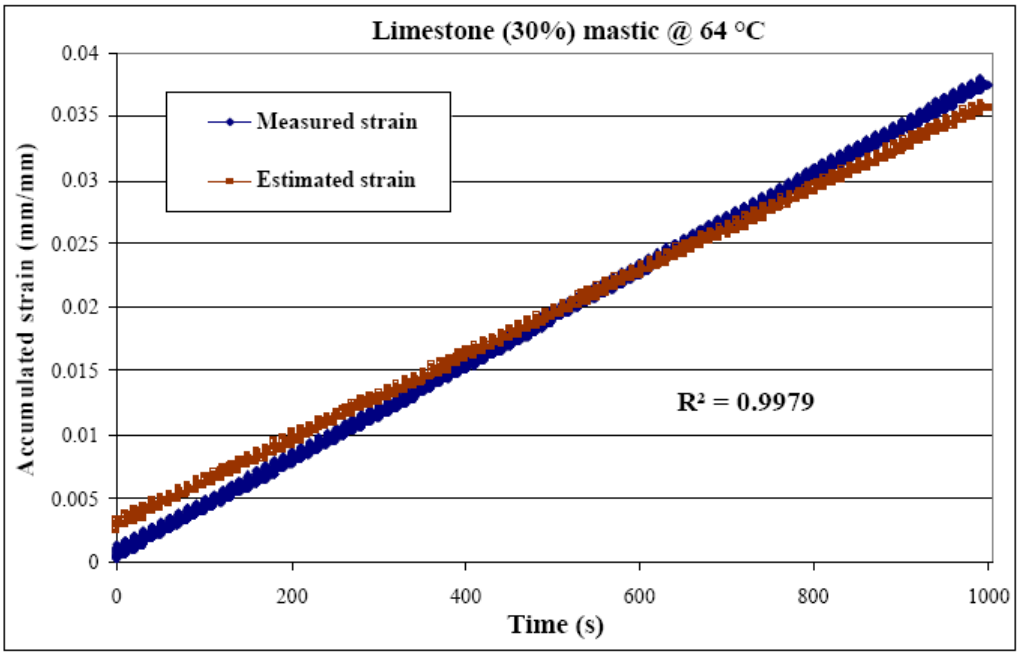

Figure E14 Measured versus Estimated Shear Strain for 30% Filler Mastic @ 64 °C.

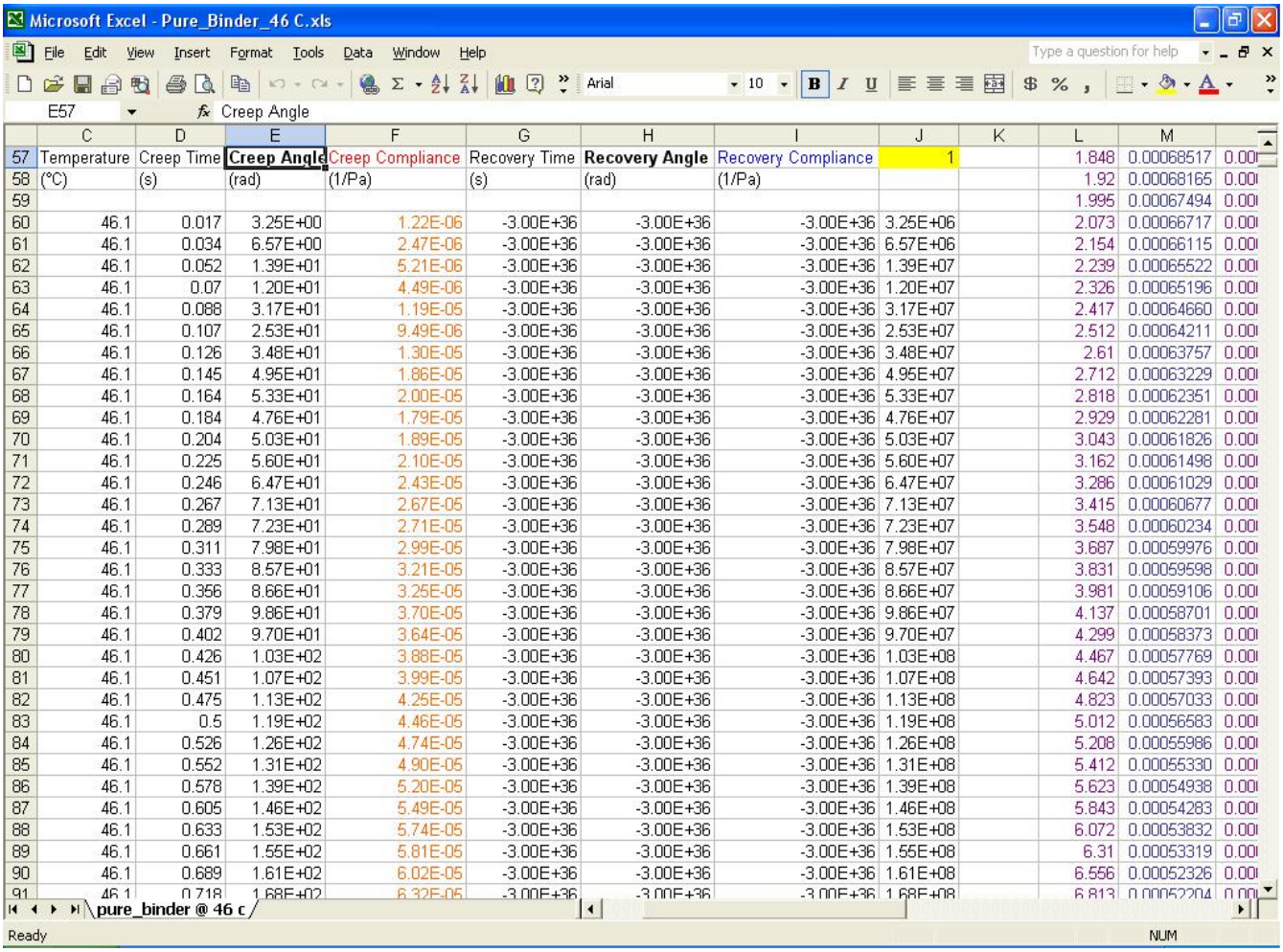

Microsoft Excel - Pure_Binder_46 C.xls

File Edit View Insert Format Tools Data Window Help

E57 Creep Angle

	C	D	E	F	G	H	I	J	K	L	M
57	Temperature	Creep Time	**Creep Angle**	Creep Compliance	Recovery Time	**Recovery Angle**	Recovery Compliance	1		1.848	0.00068517
58	(°C)	(s)	(rad)	(1/Pa)	(s)	(rad)	(1/Pa)			1.92	0.00068165
59										1.995	0.00067494
60	46.1	0.017	3.25E+00	1.22E-06	-3.00E+36	-3.00E+36	-3.00E+36	3.25E+06		2.073	0.00066717
61	46.1	0.034	6.57E+00	2.47E-06	-3.00E+36	-3.00E+36	-3.00E+36	6.57E+06		2.154	0.00066115
62	46.1	0.052	1.39E+01	5.21E-06	-3.00E+36	-3.00E+36	-3.00E+36	1.39E+07		2.239	0.00065522
63	46.1	0.07	1.20E+01	4.49E-06	-3.00E+36	-3.00E+36	-3.00E+36	1.20E+07		2.326	0.00065196
64	46.1	0.088	3.17E+01	1.19E-05	-3.00E+36	-3.00E+36	-3.00E+36	3.17E+07		2.417	0.00064660
65	46.1	0.107	2.53E+01	9.49E-06	-3.00E+36	-3.00E+36	-3.00E+36	2.53E+07		2.512	0.00064211
66	46.1	0.126	3.48E+01	1.30E-05	-3.00E+36	-3.00E+36	-3.00E+36	3.48E+07		2.61	0.00063757
67	46.1	0.145	4.95E+01	1.86E-05	-3.00E+36	-3.00E+36	-3.00E+36	4.95E+07		2.712	0.00063229
68	46.1	0.164	5.33E+01	2.00E-05	-3.00E+36	-3.00E+36	-3.00E+36	5.33E+07		2.818	0.00062351
69	46.1	0.184	4.76E+01	1.79E-05	-3.00E+36	-3.00E+36	-3.00E+36	4.76E+07		2.929	0.00062281
70	46.1	0.204	5.03E+01	1.89E-05	-3.00E+36	-3.00E+36	-3.00E+36	5.03E+07		3.043	0.00061826
71	46.1	0.225	5.60E+01	2.10E-05	-3.00E+36	-3.00E+36	-3.00E+36	5.60E+07		3.162	0.00061498
72	46.1	0.246	6.47E+01	2.43E-05	-3.00E+36	-3.00E+36	-3.00E+36	6.47E+07		3.286	0.00061029
73	46.1	0.267	7.13E+01	2.67E-05	-3.00E+36	-3.00E+36	-3.00E+36	7.13E+07		3.415	0.00060677
74	46.1	0.289	7.23E+01	2.71E-05	-3.00E+36	-3.00E+36	-3.00E+36	7.23E+07		3.548	0.00060234
75	46.1	0.311	7.98E+01	2.99E-05	-3.00E+36	-3.00E+36	-3.00E+36	7.98E+07		3.687	0.00059976
76	46.1	0.333	8.57E+01	3.21E-05	-3.00E+36	-3.00E+36	-3.00E+36	8.57E+07		3.831	0.00059598
77	46.1	0.356	8.66E+01	3.25E-05	-3.00E+36	-3.00E+36	-3.00E+36	8.66E+07		3.981	0.00059106
78	46.1	0.379	9.86E+01	3.70E-05	-3.00E+36	-3.00E+36	-3.00E+36	9.86E+07		4.137	0.00058701
79	46.1	0.402	9.70E+01	3.64E-05	-3.00E+36	-3.00E+36	-3.00E+36	9.70E+07		4.299	0.00058373
80	46.1	0.426	1.03E+02	3.88E-05	-3.00E+36	-3.00E+36	-3.00E+36	1.03E+08		4.467	0.00057769
81	46.1	0.451	1.07E+02	3.99E-05	-3.00E+36	-3.00E+36	-3.00E+36	1.07E+08		4.642	0.00057393
82	46.1	0.475	1.13E+02	4.25E-05	-3.00E+36	-3.00E+36	-3.00E+36	1.13E+08		4.823	0.00057033
83	46.1	0.5	1.19E+02	4.46E-05	-3.00E+36	-3.00E+36	-3.00E+36	1.19E+08		5.012	0.00056583
84	46.1	0.526	1.26E+02	4.74E-05	-3.00E+36	-3.00E+36	-3.00E+36	1.26E+08		5.208	0.00055986
85	46.1	0.552	1.31E+02	4.90E-05	-3.00E+36	-3.00E+36	-3.00E+36	1.31E+08		5.412	0.00055330
86	46.1	0.578	1.39E+02	5.20E-05	-3.00E+36	-3.00E+36	-3.00E+36	1.39E+08		5.623	0.00054938
87	46.1	0.605	1.46E+02	5.49E-05	-3.00E+36	-3.00E+36	-3.00E+36	1.46E+08		5.843	0.00054283
88	46.1	0.633	1.53E+02	5.74E-05	-3.00E+36	-3.00E+36	-3.00E+36	1.53E+08		6.072	0.00053832
89	46.1	0.661	1.55E+02	5.81E-05	-3.00E+36	-3.00E+36	-3.00E+36	1.55E+08		6.31	0.00053319
90	46.1	0.689	1.61E+02	6.02E-05	-3.00E+36	-3.00E+36	-3.00E+36	1.61E+08		6.556	0.00052326
91	46.1	0.718	1.68E+02	6.32E-05	-3.00E+36	-3.00E+36	-3.00E+36	1.68E+08		6.813	0.00052204

pure_binder @ 46 c

Ready NUM

Figure E15 Sample data from creep and recovery test of asphalt binder PG64-22.

APPENDIX F

PREDICTION OF COMPLEX SHEAR MODULUS G* USING THE HIRSCH MODEL

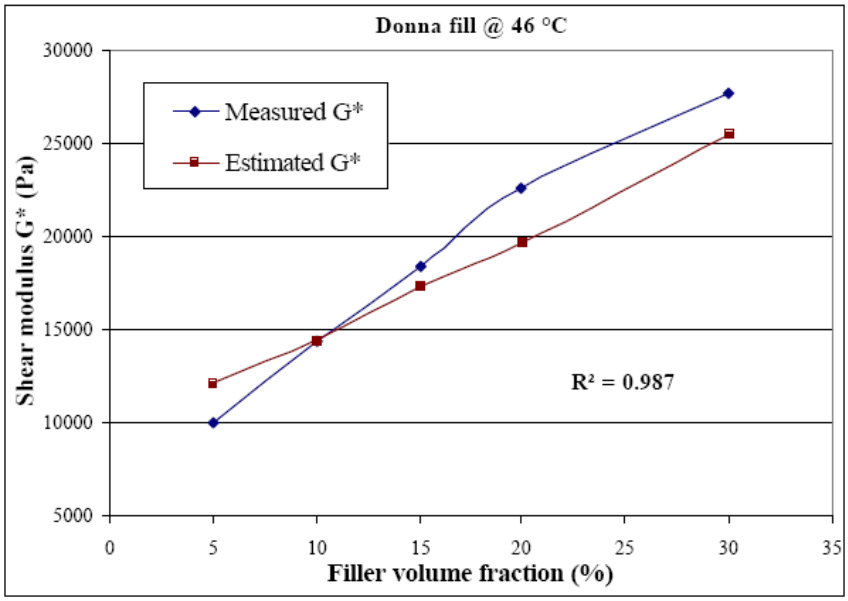

Figure F1 Estimated versus measured complex shear modulus for donna fill at 46 °C.

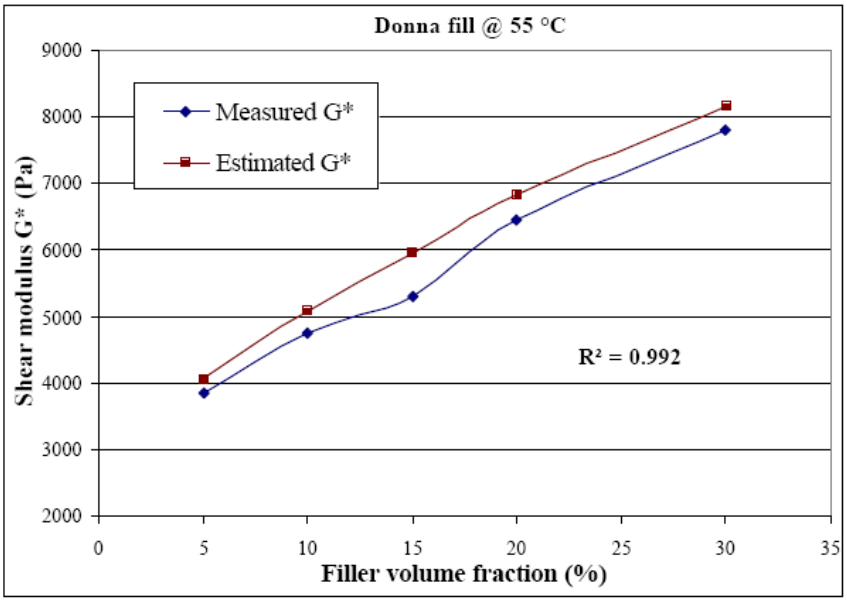

Figure F2 Estimated versus measured complex shear modulus for donna fill at 55 °C.

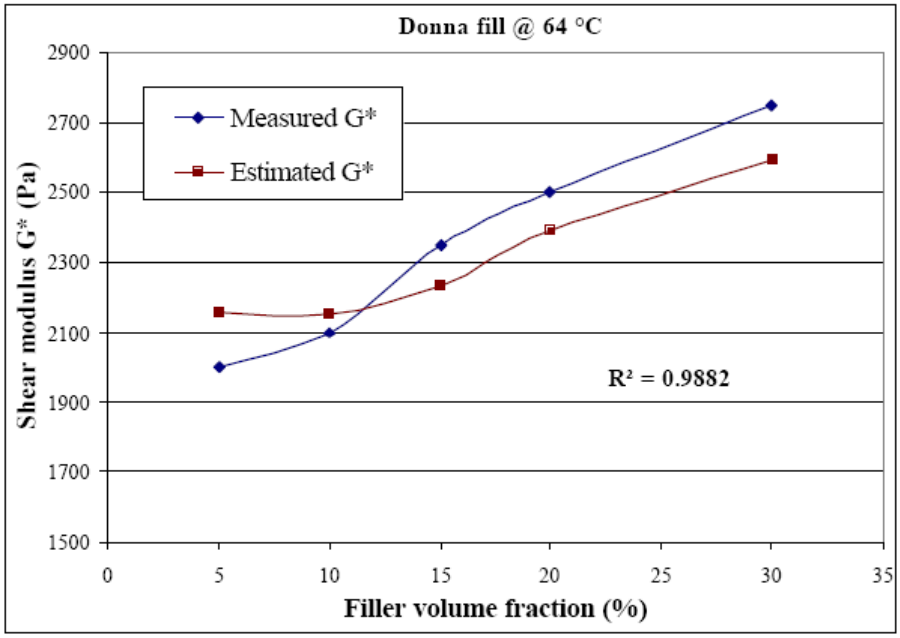

Figure F3 Estimated versus measured complex shear modulus for donna fill at 64 °C.

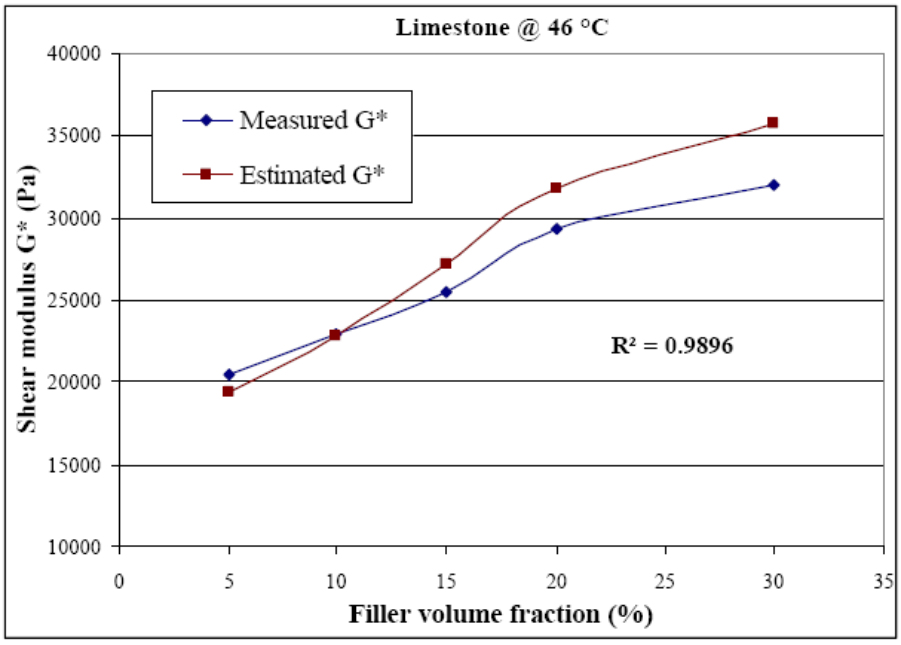

Figure F4 Estimated versus measured complex shear modulus for limestone at 46 °C.

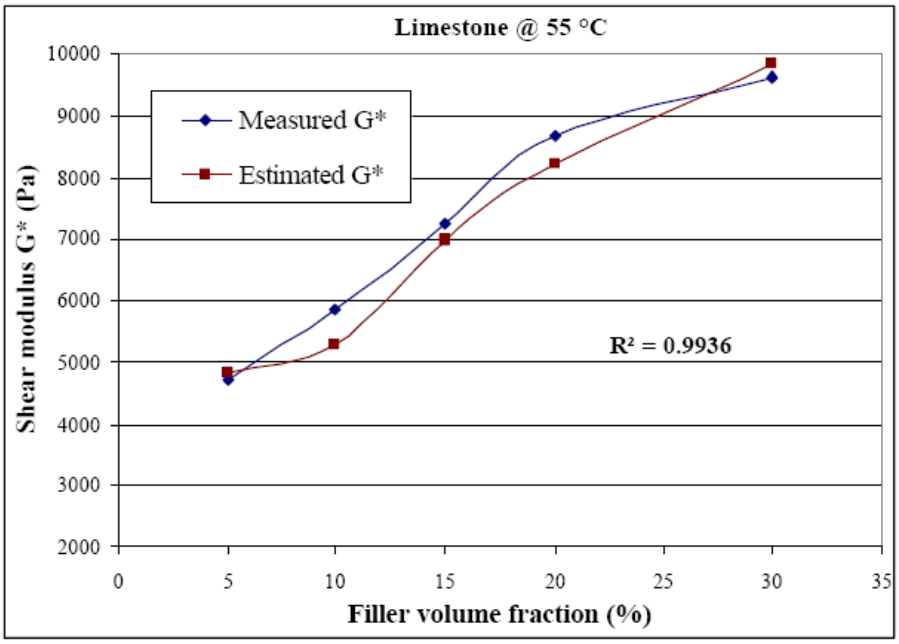

Figure F5 Estimated versus measured complex shear modulus for limestone at 55 °C.

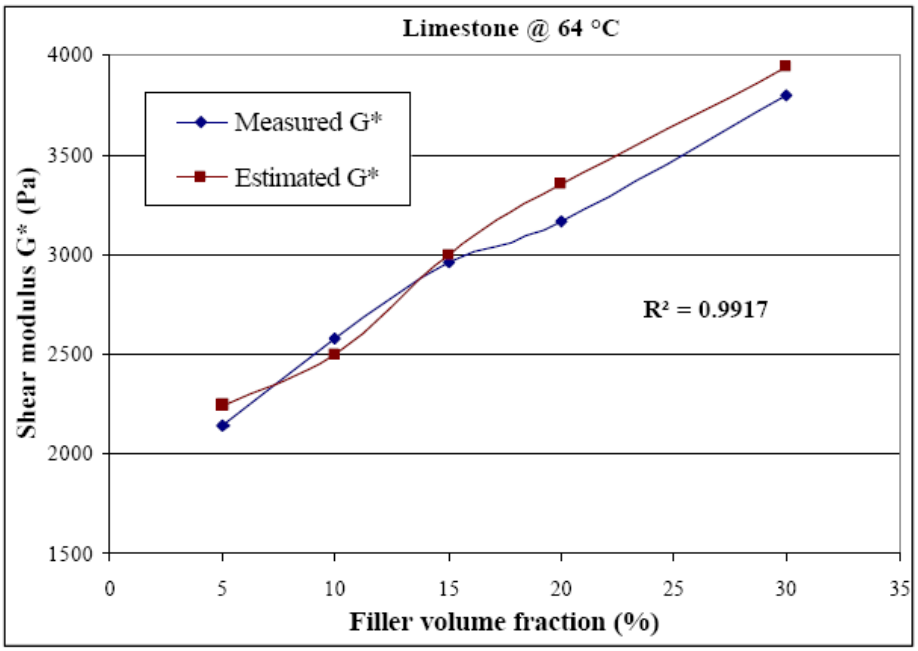

Figure F6 Estimated versus measured complex shear modulus for limestone at 64 °C.

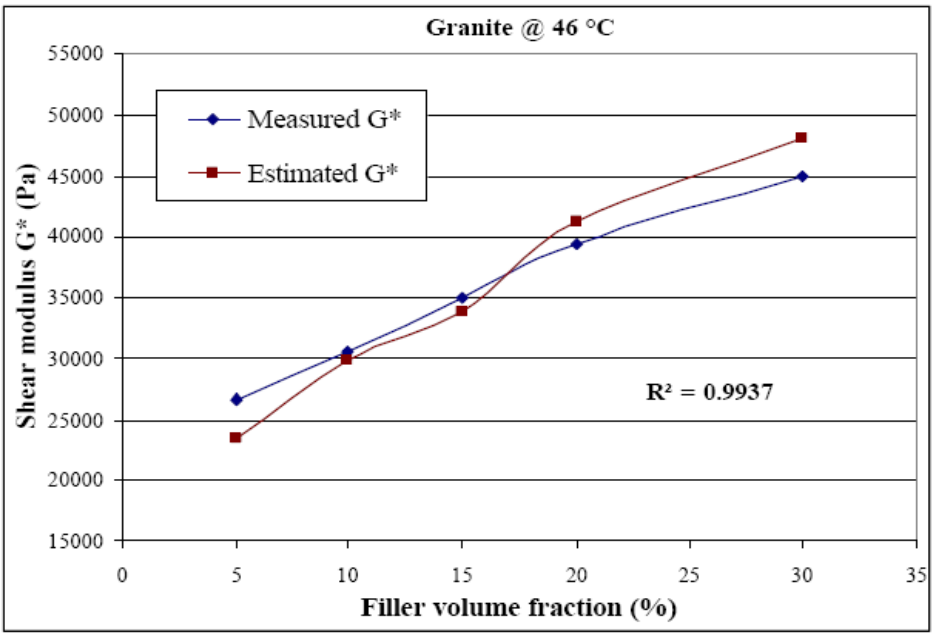

Figure F7 Estimated versus measured complex shear modulus for granite at 46 °C.

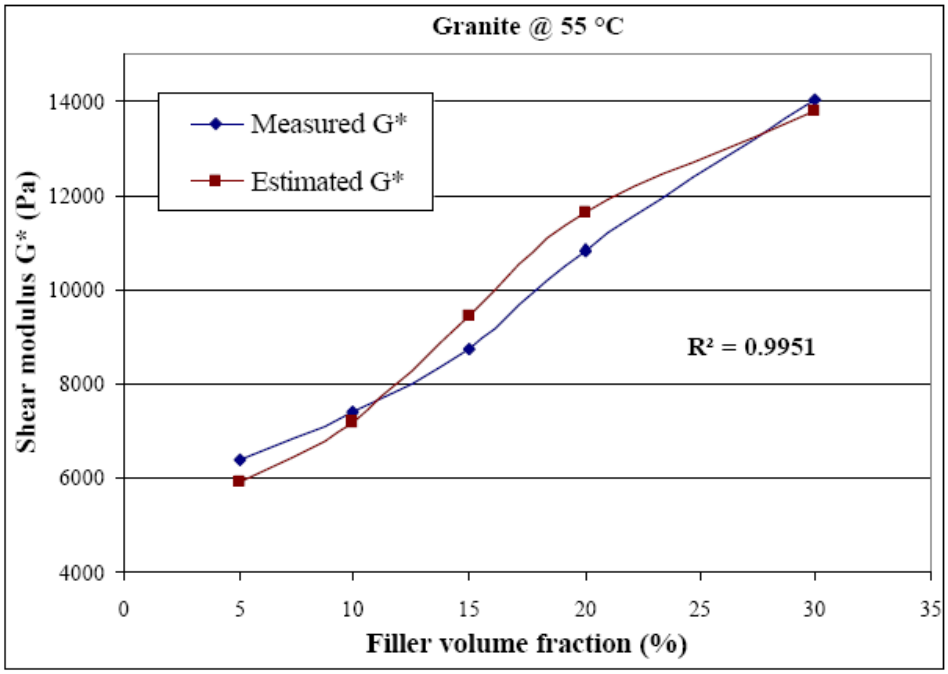

Figure F8 Estimated versus measured complex shear modulus for granite at 55 °C.

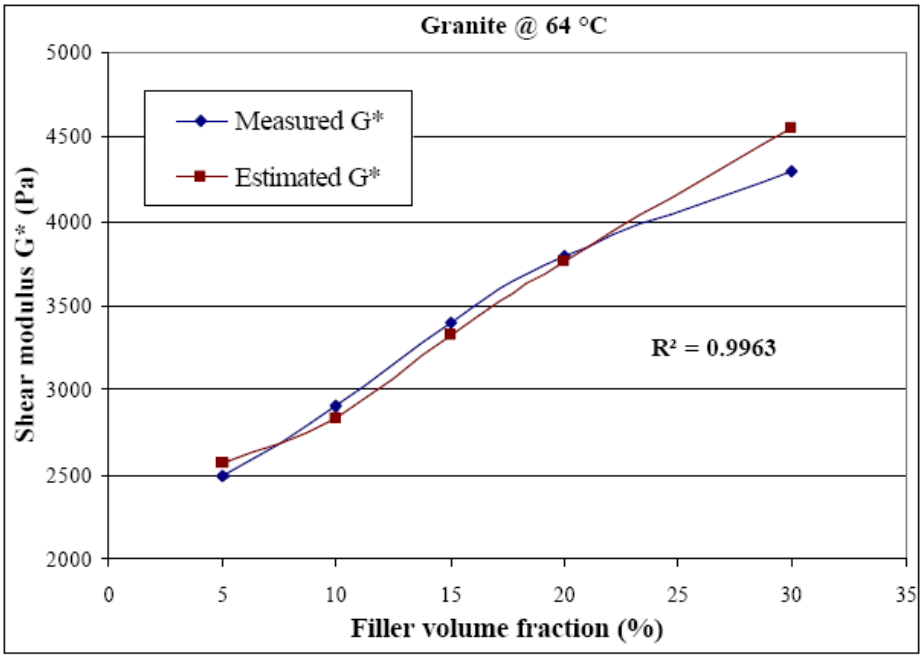

Figure F9 Estimated versus measured complex shear modulus for granite at 64 °C.

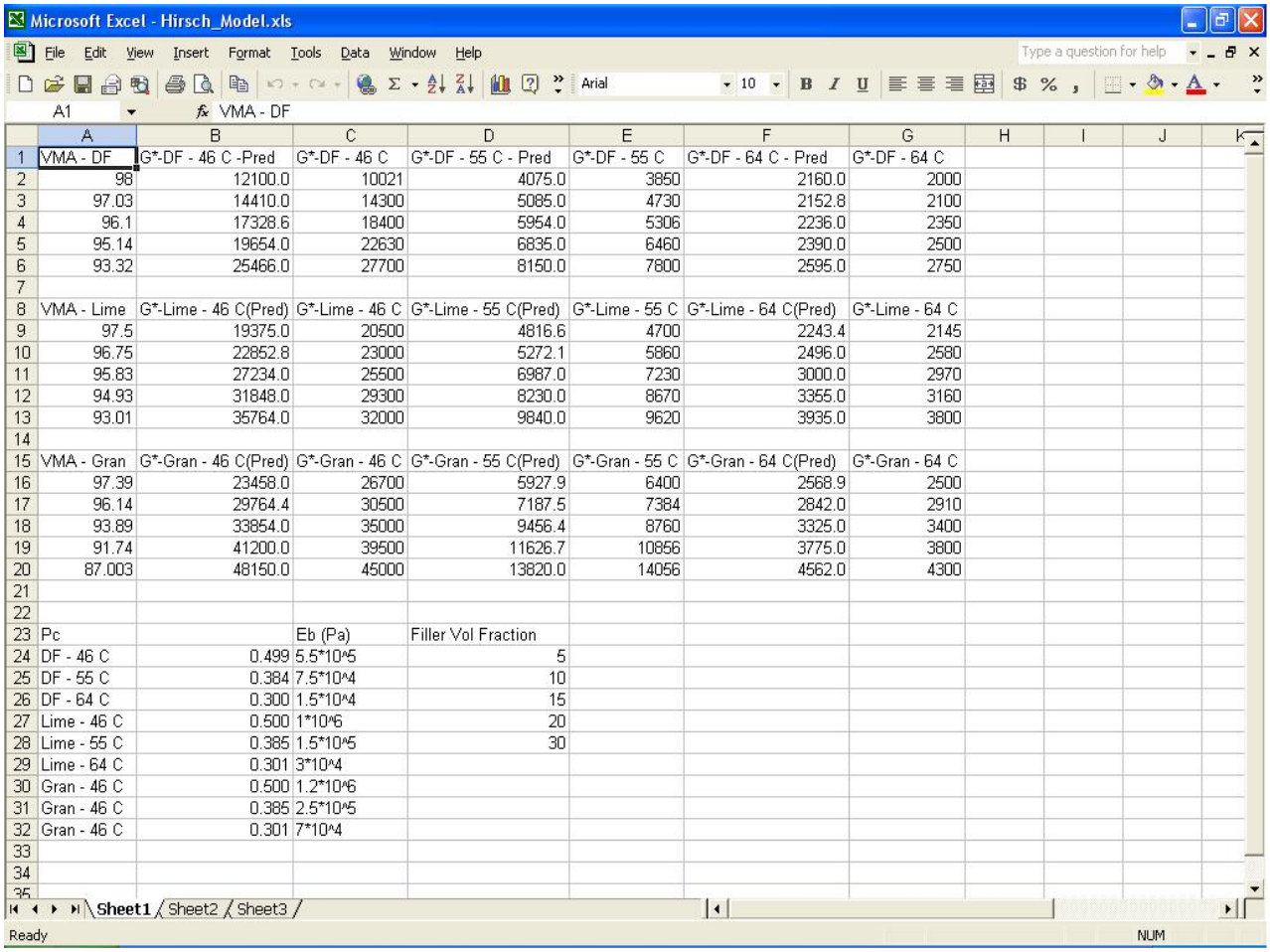

	A	B	C	D	E	F	G	H	I	J
1	VMA - DF	G*-DF - 46 C -Pred	G*-DF - 46 C	G*-DF - 55 C - Pred	G*-DF - 55 C	G*-DF - 64 C - Pred	G*-DF - 64 C			
2	98	12100.0	10021	4075.0	3850	2160.0	2000			
3	97.03	14410.0	14300	5085.0	4730	2152.8	2100			
4	96.1	17328.6	18400	5954.0	5306	2236.0	2350			
5	95.14	19654.0	22630	6835.0	6460	2390.0	2500			
6	93.32	25466.0	27700	8150.0	7800	2595.0	2750			
7										
8	VMA - Lime	G*-Lime - 46 C(Pred)	G*-Lime - 46 C	G*-Lime - 55 C(Pred)	G*-Lime - 55 C	G*-Lime - 64 C(Pred)	G*-Lime - 64 C			
9	97.5	19375.0	20500	4816.6	4700	2243.4	2145			
10	96.75	22852.8	23000	5272.1	5860	2496.0	2580			
11	95.83	27234.0	25500	6987.0	7230	3000.0	2970			
12	94.93	31848.0	29300	8230.0	8670	3355.0	3160			
13	93.01	35764.0	32000	9840.0	9620	3935.0	3800			
14										
15	VMA - Gran	G*-Gran - 46 C(Pred)	G*-Gran - 46 C	G*-Gran - 55 C(Pred)	G*-Gran - 55 C	G*-Gran - 64 C(Pred)	G*-Gran - 64 C			
16	97.39	23458.0	26700	5927.9	6400	2568.9	2500			
17	96.14	29764.4	30500	7187.5	7384	2842.0	2910			
18	93.89	33854.0	35000	9456.4	8760	3325.0	3400			
19	91.74	41200.0	39500	11626.7	10856	3775.0	3800			
20	87.003	48150.0	45000	13820.0	14056	4562.0	4300			
21										
22										
23	Pc		Eb (Pa)	Filler Vol Fraction						
24	DF - 46 C	0.499	5.5*10^5	5						
25	DF - 55 C	0.384	7.5*10^4	10						
26	DF - 64 C	0.300	1.5*10^4	15						
27	Lime - 46 C	0.500	1*10^6	20						
28	Lime - 55 C	0.385	1.5*10^5	30						
29	Lime - 64 C	0.301	3*10^4							
30	Gran - 46 C	0.500	1.2*10^6							
31	Gran - 46 C	0.385	2.5*10^5							
32	Gran - 46 C	0.301	7*10^4							
33										
34										
35										

Figure F10 Hirsch Model data for asphalt mastics.

APPENDIX G

DEFINITIONS OF VOLUMETRIC COMPONENTS OF ASPHALT MIXTURES

DEFINITIONS

Volumetric Properties of Asphalt Mixtures

Air Voids, V_a - the total volume of the small pockets of air between the coated aggregate particles throughout a compacted paving mixture, expressed as percent of the total volume of the compacted paving mixture.

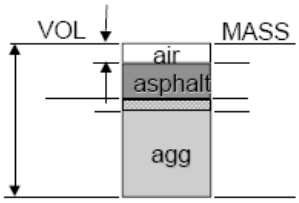

Voids in the Mineral Aggregate, VMA - the volume of intergranular void space between the aggregate particles of a compacted paving mixture that includes the air voids and the effective asphalt content, expressed as a percent of the total volume of the compacted paving mixture.

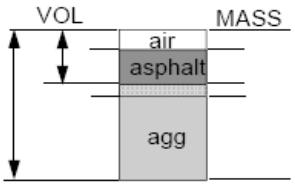

Voids Filled with Asphalt, VFA - the percentage portion of the volume of intergranular void space between the aggregate particles that is occupied by the effective asphalt. It is expressed as the ratio of (VMA - V_a) to VMA.

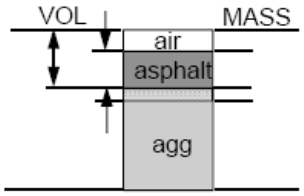

Asphalt Content, P_b - the total asphalt content of a paving mixture

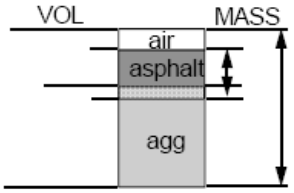

Effective Asphalt Content, P_{be} - the total asphalt content of a paving mixture minus the portion of asphalt absorbed into the aggregate particles.

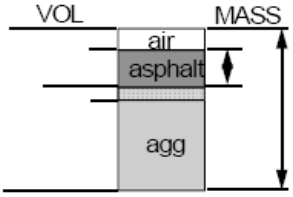

Absorbed Asphalt Content, P_{ba} - the portion of asphalt absorbed into the aggregate particles.

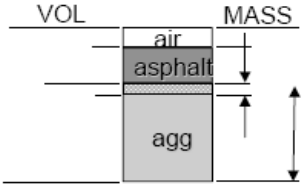

• Bulk aggregate volume, V_{sb} - the total volume of the aggregate, including the solid aggregate volume, the volume of the pore structure permeable to water but not to bituminous binder, and the volume of the pore structure permeable to the bituminous binder;

• Effective aggregate volume, V_{se} - the volume of the aggregate, including the solid aggregate volume and the volume of the pore structure permeable to water but not to bituminous binder); and

• Apparent aggregate volume, V_{sa} - the volume of the solid aggregate - i.e., that volume permeable to neither water nor bituminous binder.

Table G1. Superpave gyratory compaction data for uncut specimens

Asphalt content (%)	Specimen No. 1: Total mass = 4546 g	
3	Total number of gyrations (N_{max})	Specimen height (mm)
	78	120.16
4	Specimen No. 2: Total mass = 4552 g	
	Total number of gyrations (N_{max})	Specimen height (mm)
	77	120.08
5	Specimen No. 3: Total mass = 4558 g	
	Total number of gyrations (N_{max})	Specimen height (mm)
	80	120.11
6	Specimen No. 4: Total mass = 4562 g	
	Total number of gyrations (N_{max})	Specimen height (mm)
	78	120.09
7	Specimen No. 5: Total mass = 4549 g	
	Total number of gyrations (N_{max})	Specimen height (mm)
	76	120.15

* All specimens had the same diameter equal to 150 mm.

Table G2. Specific gravity - RICE Method for loose asphalt mixtures

Asphalt content (%)	Sample Number		
3	Sample No. 1: G_{mm} = 2.5286		
	Weight of mix (g)	Weight of pycnometer & water (g)	Weight of jar, water & mix (g)
	2010.5	7378.7	8593.1
4	Sample No. 2: G_{mm} = 2.4831		
	Weight of mix (g)	Weight of pycnometer & water (g)	Weight of jar, water & mix (g)
	2014.7	7378.7	8586.2
5	Sample No. 3: G_{mm} = 2.4642		
	Weight of mix (g)	Weight of pycnometer & water (g)	Weight of jar, water & mix (g)
	2023.2	7378.7	8584.8
6	Sample No. 4: G_{mm} = 2.4263		
	Weight of mix (g)	Weight of pycnometer & water (g)	Weight of jar, water & mix (g)
	2064.8	7378.7	8581.6
7	Sample No. 5: G_{mm} = 2.4047		
	Weight of mix (g)	Weight of pycnometer & water (g)	Weight of jar, water & mix (g)
	2055.3	7378.7	8579.3

Table G3. Bulk specific gravity of compacted mixtures (AASHTO T 166)

Asphalt content (%)	Specimen number			
3	Specimen # 1: G_{mb} = 2.375			
	W_{air} (g)	W_{ssd} (g)	W_{sub} (g)	Air voids (%)
	2149.5	2211.61	1306.55	6.052
3	Specimen # 2: G_{mb} = 2.372			
	W_{air} (g)	W_{ssd} (g)	W_{sub} (g)	Air voids (%)
	2161.4	2223.75	1312.54	6.171
4	Specimen # 3: G_{mb} = 2.331			
	W_{air} (g)	W_{ssd} (g)	W_{sub} (g)	Air voids (%)
	2148.7	2211.14	1289.35	6.122
4	Specimen # 4: G_{mb} = 2.3308			
	W_{air} (g)	W_{ssd} (g)	W_{sub} (g)	Air voids (%)
	2146.6	2209.18	1288.21	6.128
5	Specimen # 5: G_{mb} = 2.318			
	W_{air} (g)	W_{ssd} (g)	W_{sub} (g)	Air voids (%)
	2152.8	2215.94	1287.24	5.933
5	Specimen # 6: G_{mb} = 2.311			
	W_{air} (g)	W_{ssd} (g)	W_{sub} (g)	Air voids (%)
	2154.2	2216.79	1284.63	6.217
6	Specimen # 7: G_{mb} = 2.281			
	W_{air} (g)	W_{ssd} (g)	W_{sub} (g)	Air voids (%)
	2148.9	2212.13	1270.04	5.988
6	Specimen # 8: G_{mb} = 2.274			
	W_{air} (g)	W_{ssd} (g)	W_{sub} (g)	Air voids (%)
	2152.6	2215.05	1268.43	6.276
7	Specimen # 9: G_{mb} = 2.2541			
	W_{air} (g)	W_{ssd} (g)	W_{sub} (g)	Air voids (%)
	2151.3	2213.97	1259.57	6.268
7	Specimen # 10: G_{mb} = 2.263			
	W_{air} (g)	W_{ssd} (g)	W_{sub} (g)	Air voids (%)
	2150.5	2214.01	1263.72	5.893

Table G4. VMA and VFA for compacted asphalt mixture specimens

Specimen No.	Asphalt content (%)	G_{sb}	VMA (%)	VFA (%)	Averages (VMA & VFA)		Air voids (%)
1	3	2.786	13.877	65.045	14.331	64.802	6.052
2	3	2.786	14.783	64.558			6.171
3	4	2.786	15.763	68.889	15.612	68.879	6.122
4	4	2.786	15.461	68.869			6.128
5	5	2.786	16.058	71.691	16.178	71.182	5.933
6	5	2.786	16.197	70.670			6.217
7	6	2.786	16.238	74.008	16.756	73.522	5.988
8	6	2.786	16.875	73.035			6.276
9	7	2.786	17.155	74.679	17.195	75.293	6.268
10	7	2.786	17.234	75.906			5.893

APPENDIX H

SST FREQUENCY SWEEP AT CONSTANT HEIGHT (FSCH) TEST RESULTS

Table H1. FSCH at **55 °C** for **3%** AC* asphalt mixtures

SST Parameter	Frequency (Hz)									
	0.01	0.02	0.05	0.1	0.2	0.5	1	2	5	10
G* (S1*) MPa	46.57	54.72	72.39	96.74	105.53	134.27	137.04	166.85	177.51	188.91
G* (S2*) MPa	41.33	61.84	80.27	91.81	119.79	118.07	151.74	157.91	179.60	196.44
Average	**43.95**	**58.28**	**76.33**	**94.27**	**112.66**	**126.17**	**144.37**	**162.38**	**178.55**	**192.67**
Ph. angle ϕ_1(°) (S1)	22.76	24.82	25.71	30.96	34.68	40.76	45.36	46.28	50.79	54.5
Ph. angle ϕ_2(°) (S2)	23.78	24.44	26.18	31.22	35.49	42.75	45.58	48.23	53.34	55.25
G*/sin ϕ_1 (S1) MPa	120.37	130.36	166.86	188.05	153.83	205.65	192.59	230.86	229.09	232.04
G*/sin ϕ_2 (S2) MPa	102.49	149.46	181.94	177.13	206.33	173.93	212.45	211.72	223.88	239.08
G' (S1) MPa	40.53	52.90	68.77	80.84	92.65	95.57	101.44	112.23	122.87	128.88
G' (S2) MPa	40.22	53.06	68.50	80.62	91.73	92.65	101.05	108.17	106.61	109.82
G" (S1) MPa	17.00	24.46	33.11	48.50	64.10	82.38	102.72	117.36	138.35	156.86
G" (S2) MPa	17.72	24.11	33.68	48.86	65.41	85.64	103.11	121.11	143.23	158.31

* AC = Asphalt Content

Table H2. FSCH at **64 °C** for **3%** AC asphalt mixtures

SST Parameter	Frequency (Hz)									
	0.01	0.02	0.05	0.1	0.2	0.5	1	2	5	10
G* (S1) MPa	21.92	21.61	32.26	33.57	42.79	56.48	57.31	64.94	84.54	112.74
G* (S2) MPa	25.82	29.73	27.36	35.95	40.77	49.41	64.29	71.58	78.16	130.24
Average	**23.87**	**25.67**	**29.81**	**34.76**	**41.78**	**52.94**	**60.79**	**68.26**	**81.35**	**121.49**
Ph. angle ϕ(°) (S1)	24.47	26.64	31.72	34.89	37.45	42.67	46.36	50.29	55.17	59.65
Ph. angle ϕ(°) (S2)	23.32	24.21	29.88	32.71	36.14	41.92	45.57	52.81	56.16	60.12
G*/sin ϕ (S1) MPa	52.92	54.21	61.36	62.68	70.37	83.33	84.19	85.41	102.99	130.64
G*/sin ϕ (S2) MPa	65.22	72.49	74.92	76.52	79.13	83.96	90.03	91.85	94.11	150.22
G' (S1) MPa	21.73	22.94	25.36	28.51	33.17	38.93	41.95	43.61	46.46	61.39
G' (S2) MPa	21.92	23.41	25.85	29.25	33.74	39.39	42.56	41.26	45.30	60.52
G" (S1) MPa	9.89	11.51	15.67	19.88	25.41	35.88	43.99	52.51	66.78	104.84
G" (S2) MPa	9.45	10.53	14.85	18.78	24.64	35.37	43.41	54.38	67.57	105.34

Table H3. FSCH at **55 °C** for **4%** AC asphalt mixtures

SST Parameter	Frequency (Hz)									
	0.01	0.02	0.05	0.1	0.2	0.5	1	2	5	10
G* (S3) MPa	37.26	58.49	74.91	95.77	106.07	126.84	137.93	155.06	176.34	183.23
G* (S4) MPa	45.38	52.45	68.45	89.53	111.57	117.84	144.85	162.46	174.22	191.75
Average	**41.32**	**55.47**	**71.68**	**92.65**	**108.82**	**122.34**	**141.39**	**158.76**	**175.28**	**187.49**
Ph. angle ϕ(°) (S3)	34.76	37.68	40.46	41.37	45.62	47.81	50.39	52.74	54.89	56.63
Ph. angle ϕ(°) (S4)	35.64	36.75	39.61	42.85	46.34	51.92	52.68	54.21	55.73	56.59
G*/sin ϕ (S3) MPa	65.35	95.68	115.44	144.90	148.41	171.19	179.04	194.82	215.56	219.40
G*/sin ϕ (S4) MPa	77.88	87.65	107.36	131.65	154.22	155.71	182.14	200.28	210.82	229.71
G' (S3) MPa	33.95	43.90	54.54	69.53	76.11	82.16	90.14	96.12	110.81	123.13
G' (S4) MPa	33.58	44.45	55.22	67.93	75.13	75.45	85.72	92.85	98.70	103.24
G" (S3) MPa	23.56	33.91	46.51	61.23	77.78	90.64	108.93	126.36	143.39	156.58
G" (S4) MPa	24.08	33.19	45.70	63.01	78.73	96.30	112.44	128.78	144.85	156.51

Table H4. FSCH at **64 °C** for **4%** AC asphalt mixtures

SST Parameter	Frequency (Hz)									
	0.01	0.02	0.05	0.1	0.2	0.5	1	2	5	10
G* (S3) MPa	22.26	28.79	23.52	26.17	32.56	47.93	47.94	61.17	83.23	113.61
G* (S4) MPa	23.42	20.79	31.76	34.27	40.60	39.59	56.74	65.29	73.05	120.11
Average	**22.84**	**24.79**	**27.64**	**30.22**	**36.58**	**43.76**	**52.34**	**63.23**	**78.14**	**116.86**
Ph. angle ϕ(°) (S3)	42.72	43.57	45.61	48.32	50.48	53.22	55.46	58.87	61.44	62.27
Ph. angle ϕ(°) (S4)	38.77	40.62	41.38	45.84	47.36	51.41	53.82	56.97	58.31	60.84
G*/sin ϕ (S3) MPa	32.81	41.77	42.92	45.04	46.21	59.84	60.21	71.46	94.76	128.35
G*/sin ϕ (S4) MPa	37.41	38.94	48.04	49.77	55.19	57.65	70.29	77.87	85.84	137.54
G' (S3) MPa	16.78	17.96	19.34	20.10	23.28	26.20	29.68	32.69	43.36	54.38
G' (S4) MPa	17.81	18.82	20.74	21.05	24.78	27.30	30.90	34.47	41.05	56.94
G" (S3) MPa	15.50	17.09	19.75	22.57	28.22	35.05	43.11	54.12	68.63	93.44
G" (S4) MPa	14.30	16.14	18.27	21.68	26.91	34.20	42.25	53.01	66.49	92.05

Table H5. FSCH at **55 °C** for **5%** AC asphalt mixtures

SST Parameter	Frequency (Hz)									
	0.01	0.02	0.05	0.1	0.2	0.5	1	2	5	10
G* (S5) MPa	42.97	53.08	73.59	86.62	106.57	115.86	133.32	156.47	178.32	178.45
G* (S6) MPa	34.37	54.36	66.09	92.34	99.33	125.88	143.76	154.39	168.21	184.83
Average	**38.67**	**53.72**	**69.84**	**89.48**	**102.95**	**120.87**	**138.54**	**155.43**	**173.26**	**181.64**
Ph. angle ϕ(°) (S5)	30.56	33.78	35.86	38.25	40.34	42.91	44.69	48.35	52.67	55.89
Ph. angle ϕ(°) (S6)	32.57	34.91	35.74	39.95	43.19	47.83	50.66	52.97	53.37	56.28
G*/sin ϕ (S5) MPa	84.51	95.47	125.62	139.91	164.63	170.17	189.57	209.41	224.26	229.53
G*/sin ϕ (S6) MPa	63.85	94.98	113.15	143.81	145.16	169.84	185.88	193.39	209.61	222.21
G' (S5) MPa	33.30	44.65	56.60	70.27	78.47	88.53	98.49	103.30	105.07	114.86
G' (S6) MPa	32.59	44.05	56.69	68.60	75.06	81.14	87.82	93.61	103.37	109.83
G" (S5) MPa	19.66	29.87	40.91	55.40	66.64	82.29	97.43	116.14	137.77	150.39
G" (S6) MPa	20.82	30.74	40.79	57.46	70.46	89.58	107.15	124.08	139.04	151.08

Table H6. FSCH at **64 °C** for **5%** AC asphalt mixtures

SST Parameter	Frequency (Hz)									
	0.01	0.02	0.05	0.1	0.2	0.5	1	2	5	10
G* (S5) MPa	16.13	24.81	22.53	23.36	28.66	46.16	45.86	55.79	78.39	116.17
G* (S6) MPa	23.45	17.95	27.39	33.86	37.84	37.36	53.46	64.43	73.05	108.79
Average	**19.79**	**21.38**	**24.96**	**28.61**	**33.25**	**41.76**	**49.66**	**60.11**	**75.72**	**112.48**
Ph. angle ϕ(°) (S5)	38.23	40.26	43.97	45.91	49.37	52.88	55.35	57.96	60.48	64.21
Ph. angle ϕ(°) (S6)	37.84	40.71	42.89	45.36	48.62	51.97	54.64	58.39	61.21	65.72
G*/sin ϕ (S5) MPa	26.06	38.39	42.45	43.56	44.76	57.89	58.74	65.82	90.08	129.02
G*/sin ϕ (S6) MPa	38.23	39.52	40.24	47.58	50.43	51.45	65.55	75.66	83.34	119.36
G' (S5) MPa	15.55	16.32	17.96	19.91	21.65	25.20	28.23	31.89	37.31	48.94
G' (S6) MPa	15.63	16.21	18.29	20.10	21.98	25.73	28.74	31.51	36.47	46.25
G" (S5) MPa	12.25	13.82	17.33	20.55	25.23	33.30	40.85	50.95	68.89	101.28
G" (S6) MPa	12.14	13.94	16.99	20.36	24.95	32.89	40.50	51.19	66.36	102.53

Table H7. FSCH at **55 °C** for **6%** AC asphalt mixtures

SST Parameter	Frequency (Hz)									
	0.01	0.02	0.05	0.1	0.2	0.5	1	2	5	10
G* (S7) MPa	42.18	46.45	72.36	94.64	102.35	112.98	140.92	155.76	169.63	170.66
G* (S8) MPa	29.51	54.91	61.62	78.78	95.03	122.74	129.96	147.48	175.27	183.01
Average	**35.84**	**50.68**	**66.98**	**86.71**	**98.69**	**117.86**	**135.44**	**151.62**	**172.45**	**176.83**
Ph. angle ϕ(°) (S7)	33.68	35.16	37.95	40.76	43.85	46.27	49.42	51.32	55.93	57.44
Ph. angle ϕ(°) (S8)	31.56	34.43	36.46	39.99	41.84	45.85	48.76	50.17	54.38	56.92
G*/sin ϕ (S7) MPa	76.06	80.66	117.64	144.95	147.74	156.35	185.54	199.52	204.77	205.48
G*/sin ϕ (S8) MPa	31.56	34.43	36.46	39.99	41.84	45.85	48.76	50.17	54.38	56.92
G’ (S7) MPa	29.82	41.43	52.82	65.68	71.17	81.47	88.10	94.76	96.61	105.17
G’ (S8) MPa	30.54	41.80	53.87	66.43	73.53	82.09	89.28	97.11	100.44	106.52
G” (S7) MPa	19.88	29.18	41.19	56.61	68.37	85.17	102.87	118.36	142.85	149.04
G” (S8) MPa	18.76	28.65	39.80	55.72	65.83	84.57	101.84	116.44	140.18	148.17

Table H8. FSCH at **64 °C** for **6%** AC asphalt mixtures

SST Parameter	Frequency (Hz)									
	0.01	0.02	0.05	0.1	0.2	0.5	1	2	5	10
G* (S7) MPa	13.59	21.46	20.01	24.25	35.85	35.22	50.21	59.43	74.54	106.76
G* (S8) MPa	19.69	15.32	23.61	28.49	27.85	41.36	44.83	53.45	71.32	110.58
Average	**16.64**	**18.38**	**21.81**	**26.37**	**31.85**	**38.29**	**47.52**	**56.44**	**72.93**	**108.67**
Ph. angle ϕ(°) (S7)	39.81	42.94	46.38	49.74	52.18	54.65	57.82	60.73	63.24	66.78
Ph. angle ϕ(°) (S8)	38.62	41.19	45.97	48.76	52.21	55.73	58.74	61.22	64.96	67.41
G*/sin ϕ (S7) MPa	21.23	31.50	32.64	33.77	45.38	46.18	59.32	68.13	83.48	116.17
G*/sin ϕ (S8) MPa	31.55	32.26	33.83	37.88	38.24	50.05	52.44	60.98	78.72	119.77
G’ (S7) MPa	12.78	13.46	15.05	17.04	19.53	22.15	25.31	27.59	32.84	42.84
G’ (S8) MPa	13.00	13.83	15.16	17.38	19.52	21.56	24.66	27.17	30.87	41.74
G” (S7) MPa	10.65	12.52	15.79	20.12	25.16	31.23	40.22	49.23	65.12	99.87
G” (S8) MPa	10.39	12.10	15.68	19.83	25.17	31.64	40.62	49.47	66.08	100.33

Table H9. FSCH at **55 °C** for **7%** AC asphalt mixtures

SST Parameter	Frequency (Hz)									
	0.01	0.02	0.05	0.1	0.2	0.5	1	2	5	10
G* (S9) MPa	35.26	46.03	66.47	87.34	93.58	114.78	133.62	143.39	163.29	168.36
G* (S10) MPa	28.22	47.31	58.19	78.24	97.28	110.12	127.14	149.15	170.49	176.88
Average	**31.74**	**46.67**	**62.33**	**82.79**	**95.43**	**112.45**	**130.38**	**146.27**	**166.89**	**172.36**
Ph. angle ϕ(°) (S9)	36.65	38.26	40.68	43.54	45.25	48.39	51.92	52.33	55.79	58.48
Ph. angle ϕ(°) (S10)	38.81	40.42	43.78	45.51	49.79	52.92	54.28	57.73	59.84	60.11
G*/sin ϕ (S9) MPa	59.07	74.33	101.97	126.78	131.76	153.51	169.75	181.15	197.45	198.34
G*/sin ϕ (S10) MPa	45.03	72.96	84.11	109.67	127.38	138.03	156.59	176.39	197.18	204.02
G' (S9) MPa	25.46	36.65	47.27	60.01	67.18	74.67	80.41	89.39	93.83	98.11
G' (S10) MPa	24.73	35.53	45.00	58.02	61.61	67.80	76.12	78.09	83.85	93.89
G" (S9) MPa	18.95	28.90	40.63	57.03	67.77	84.08	102.63	115.78	138.02	146.93
G" (S10) MPa	19.89	30.26	43.13	59.06	72.88	89.71	105.85	123.68	144.30	149.43

Table H10. FSCH at **64 °C** for **7%** AC asphalt mixtures

SST Parameter	Frequency (Hz)									
	0.01	0.02	0.05	0.1	0.2	0.5	1	2	5	10
G* (S9) MPa	11.31	18.94	22.39	19.94	31.71	37.49	39.44	50.29	66.14	103.81
G* (S10) MPa	17.68	13.58	17.19	26.78	25.79	33.56	46.52	55.37	72.68	101.82
Average	**14.49**	**16.26**	**19.79**	**23.36**	**28.75**	**35.52**	**42.98**	**52.83**	**69.41**	**102.81**
Ph. angle ϕ(°) (S9)	44.32	47.59	50.14	53.78	55.26	58.48	60.38	63.27	67.34	69.45
Ph. angle ϕ(°) (S10)	42.64	44.93	46.31	47.28	50.49	54.83	57.72	61.86	64.45	70.21
G*/sin ϕ (S9) MPa	16.18	25.65	29.17	24.72	38.58	43.98	45.37	56.31	71.67	110.86
G*/sin ϕ (S10) MPa	26.11	27.22	28.77	36.45	37.42	41.05	55.02	62.79	80.55	108.21
G' (S9) MPa	10.66	11.51	13.67	15.85	18.29	20.46	22.95	24.92	29.94	34.81
G' (S10) MPa	13.06	14.61	15.87	18.17	19.41	20.33	24.84	26.15	31.34	36.47
G" (S9) MPa	10.12	12.01	15.19	18.85	23.63	30.28	37.36	47.18	58.05	76.27
G" (S10) MPa	9.82	11.48	14.31	17.16	22.18	29.04	36.34	46.59	62.62	74.74

Table H11. Shift factors and constants for asphalt mixtures

Material / Parameter	Asphalt content (%)									
	3		**4**		**5**		**6**		**7**	
	Temperature (°C)									
	55	**64**	**55**	**64**	**55**	**64**	**55**	**64**	**55**	**64**
Shift factor a_T	1.86	1.28	1.77	1.36	1.42	1.16	1.78	1.33	1.84	1.53
C_1	17.14	21.45	15.47	16.89	16.69	19.22	20.25	18.96	22.76	19.37
C_2	88.14	84.36	91.23	89.46	85.54	90.21	87.42	89.27	92.25	87.34

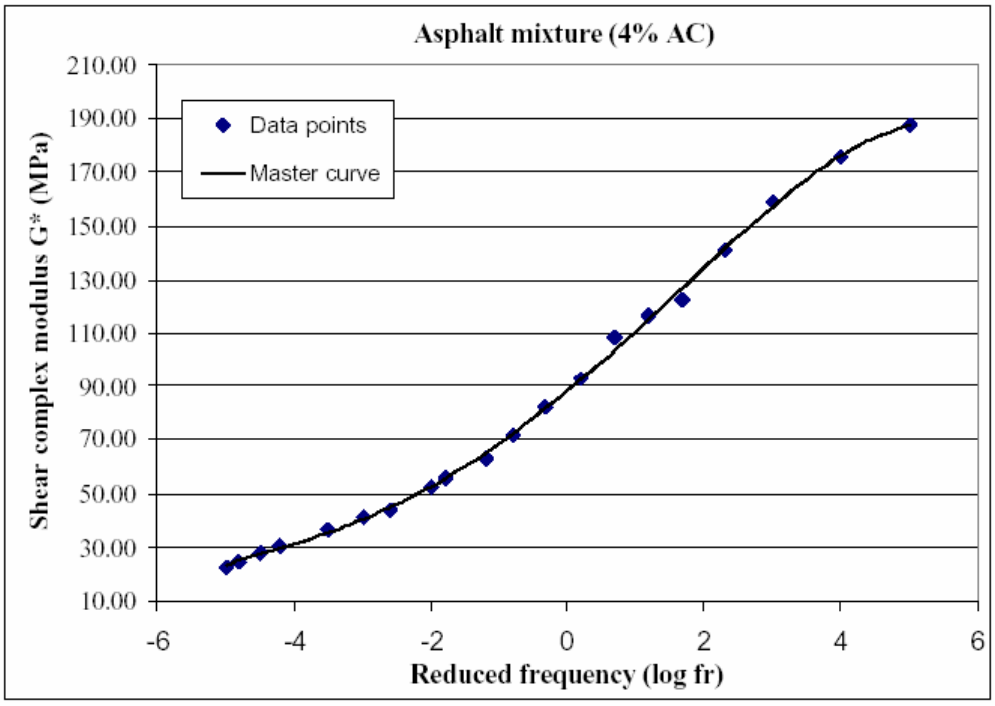

Figure H1 Single master curve at 4% asphalt content.

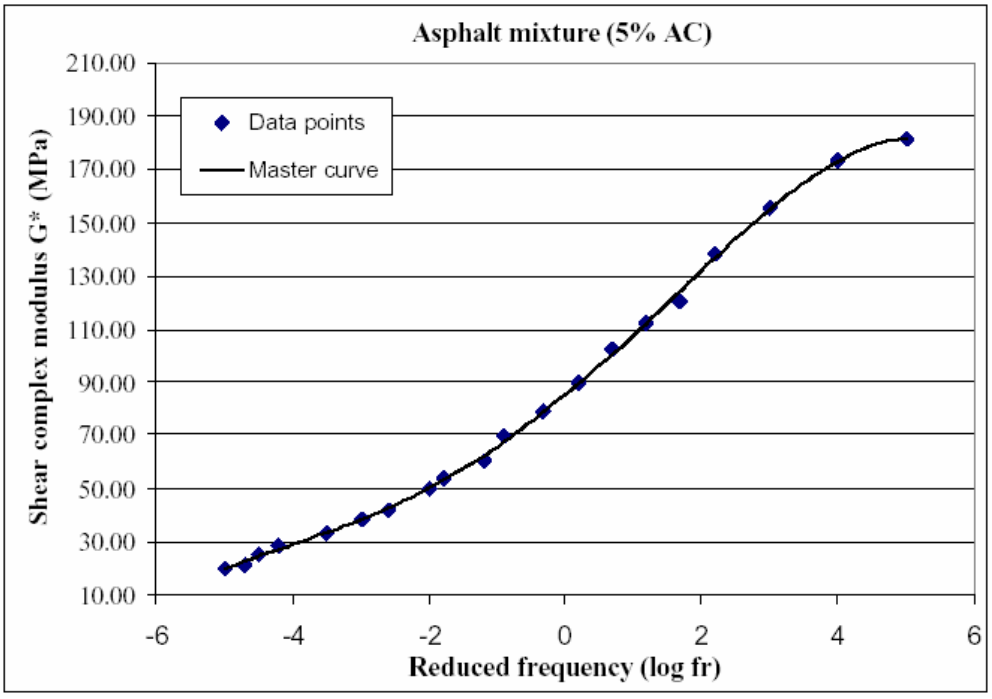

Figure H2 Single master curve at 5% asphalt content.

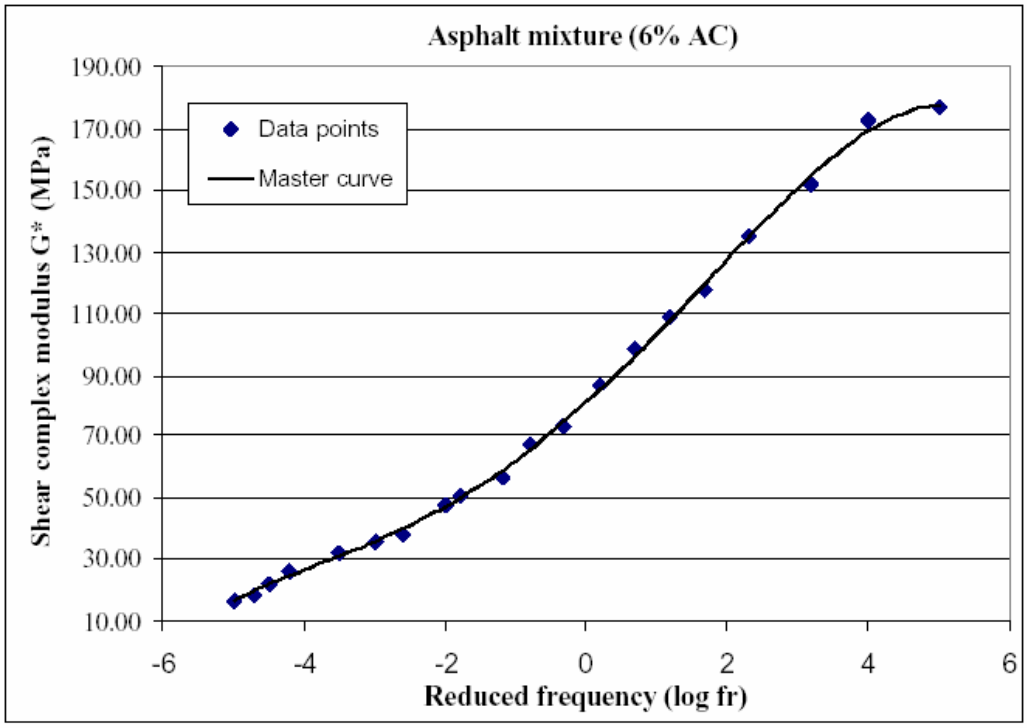

Figure H3 Single master curve at 6% asphalt content.

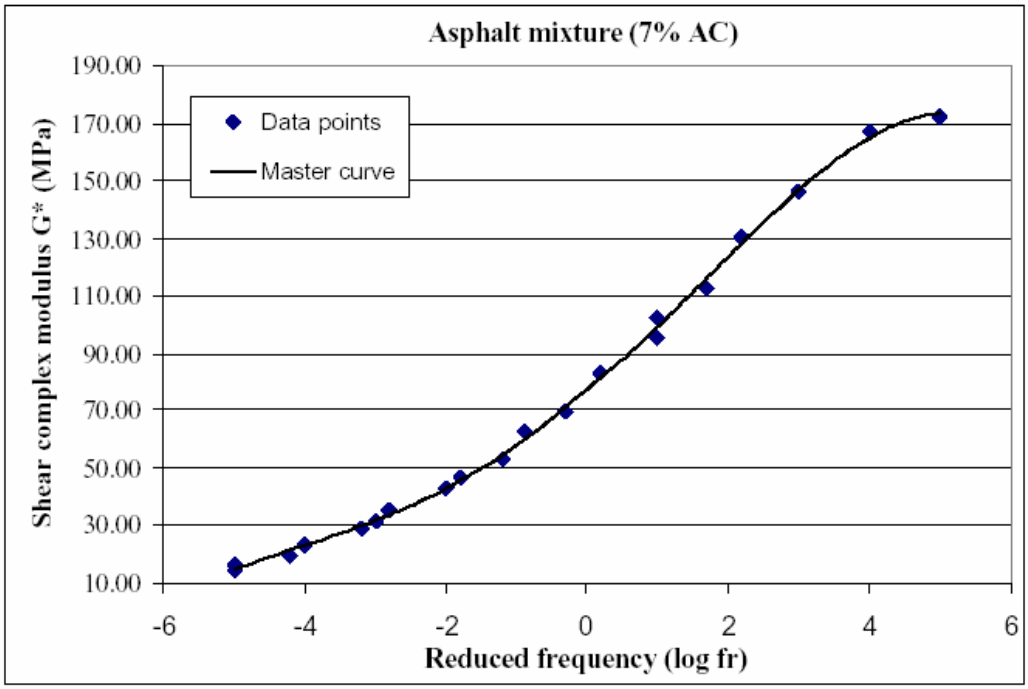

Figure H4 Single master curve at 7% asphalt content.

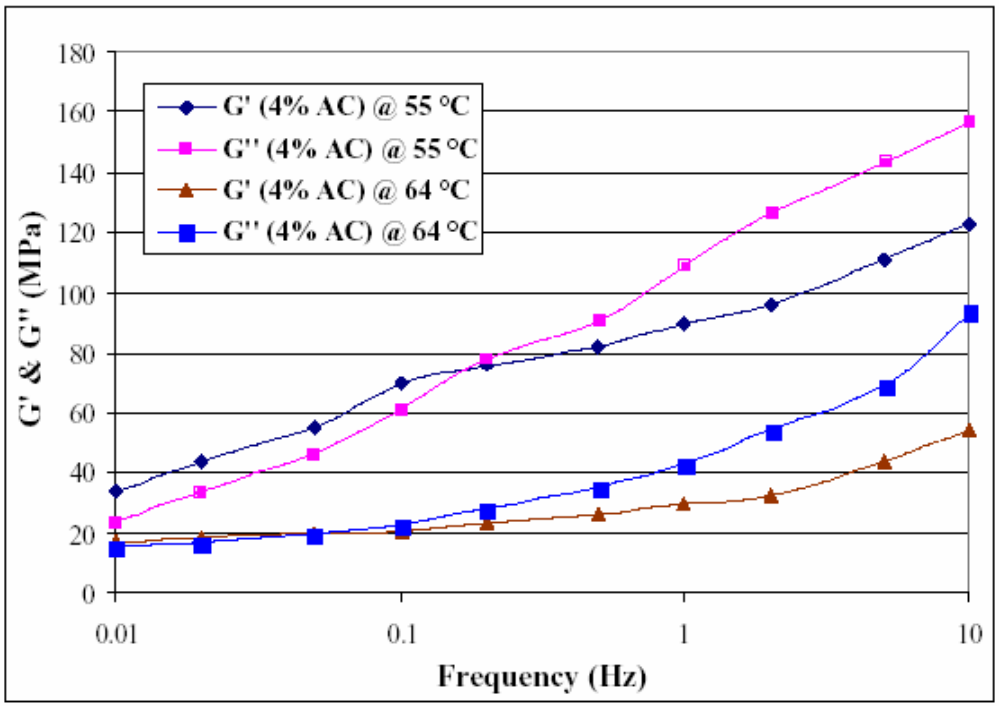

Figure H5 Variation of G* components with the loading frequency at 4% asphalt content.

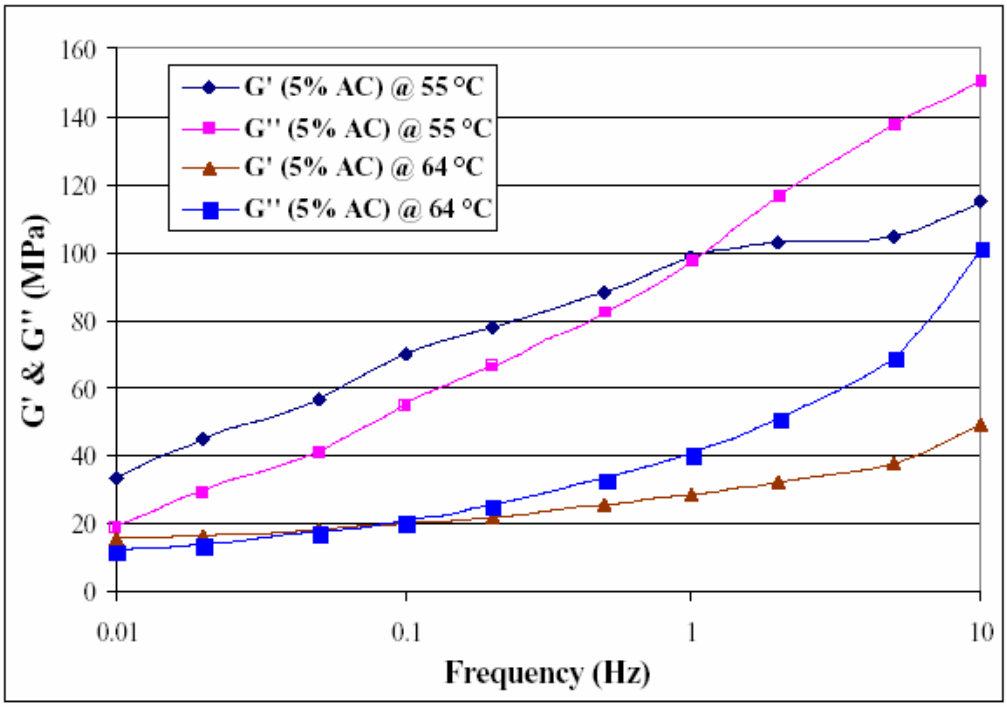

Figure H6 Variation of G* components with the loading frequency at 5% asphalt content.

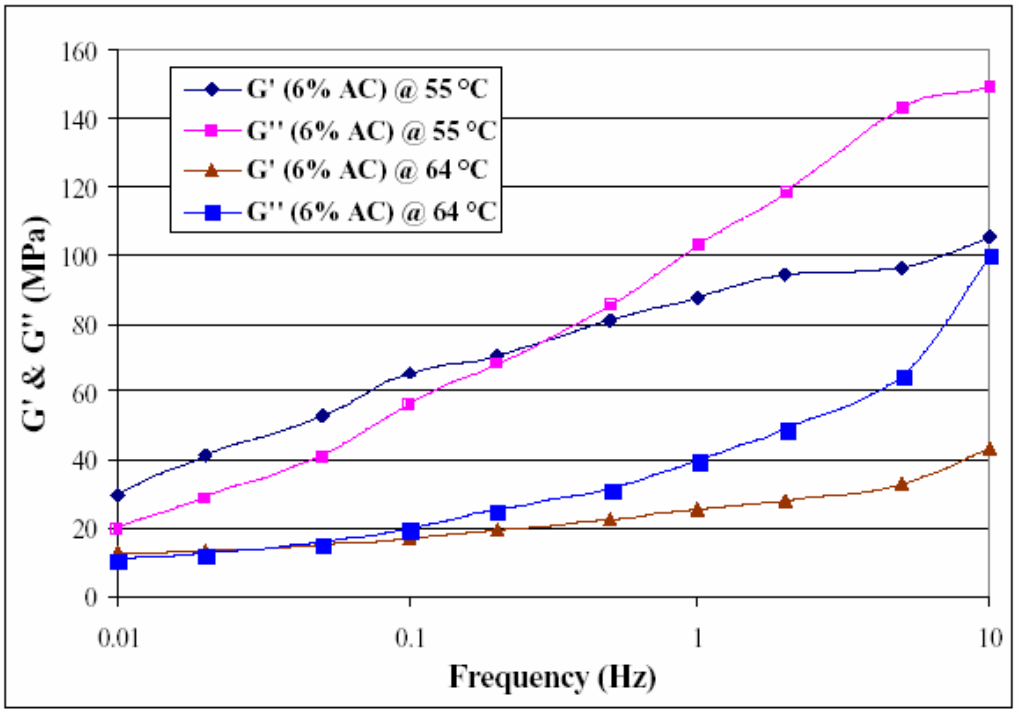

Figure H7 Variation of G* components with the loading frequency at 6% asphalt content.

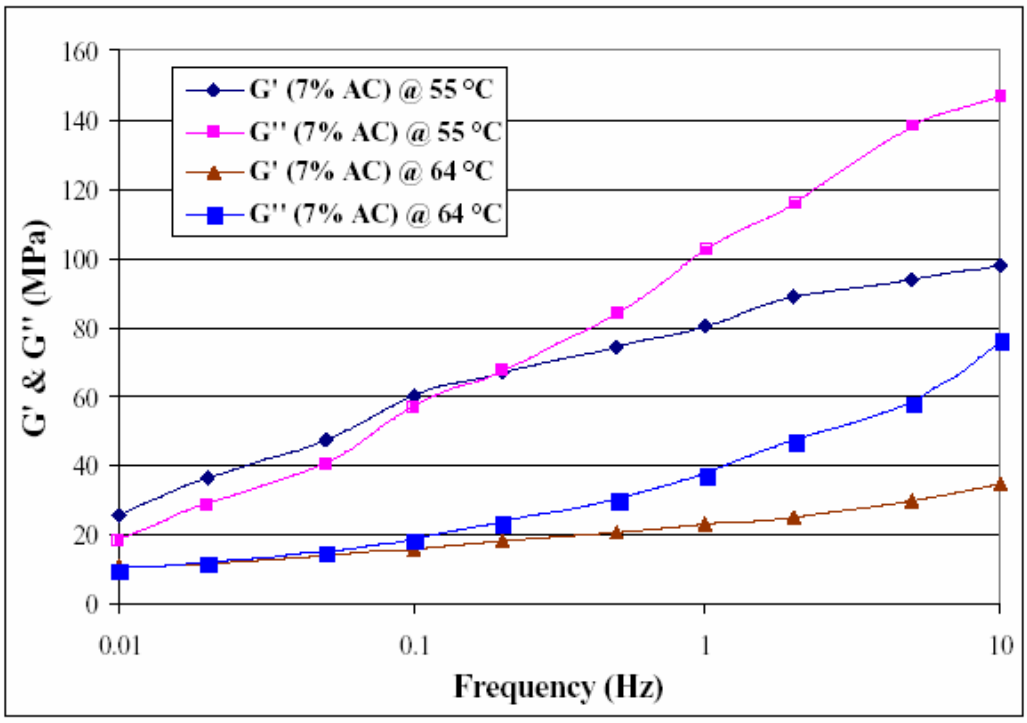

Figure H8 Variation of G* components with the loading frequency at 7% asphalt content.

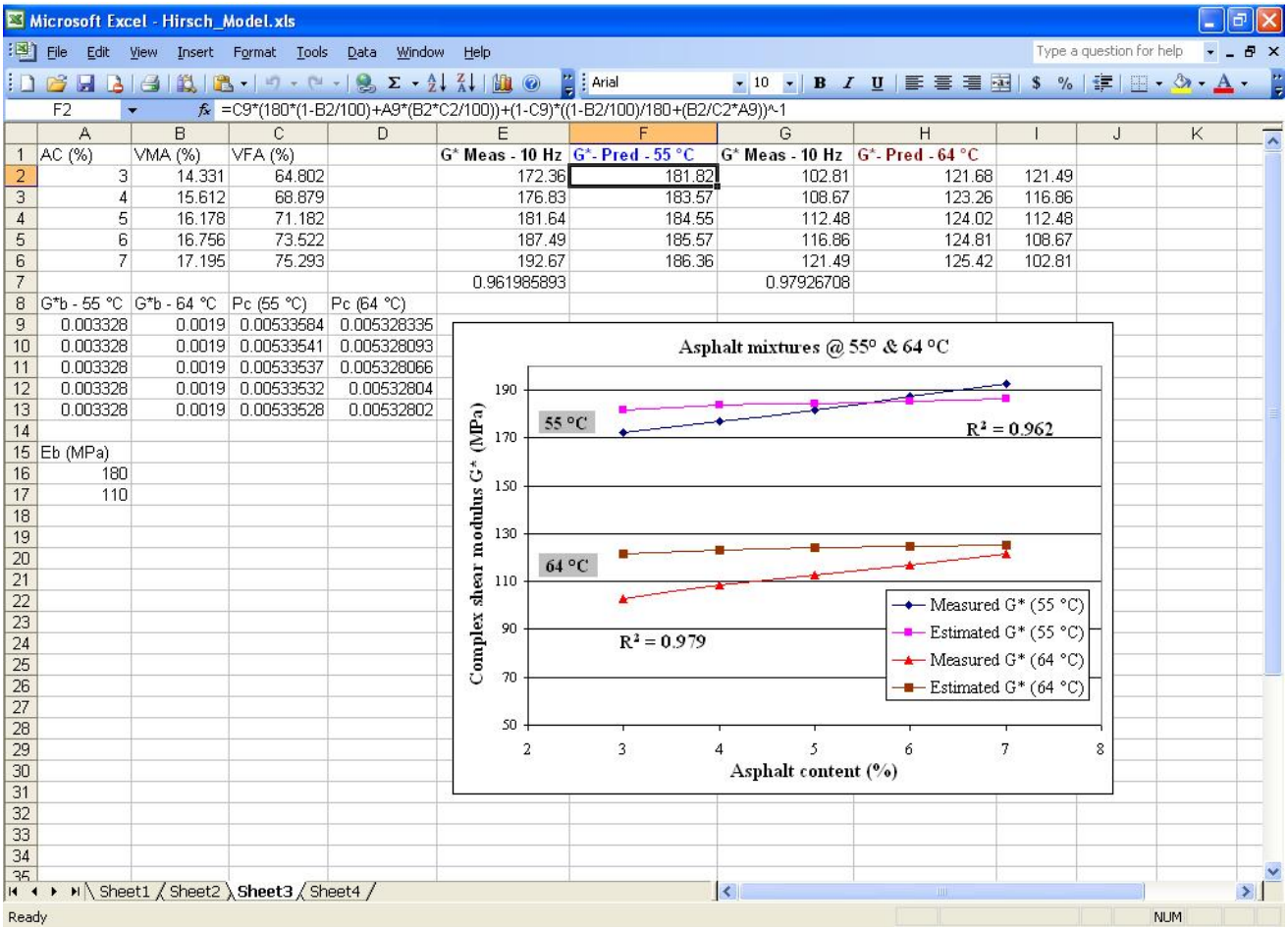

	A	B	C	D	E	F	G	H	I	J	K
1	AC (%)	VMA (%)	VFA (%)		G* Meas - 10 Hz	G*- Pred - 55 °C	G* Meas - 10 Hz	G*- Pred - 64 °C			
2	3	14.331	64.802		172.36	181.82	102.81	121.68	121.49		
3	4	15.612	68.879		176.83	183.57	108.67	123.26	116.86		
4	5	16.178	71.182		181.64	184.55	112.48	124.02	112.48		
5	6	16.756	73.522		187.49	185.57	116.86	124.81	108.67		
6	7	17.195	75.293		192.67	186.36	121.49	125.42	102.81		
7					0.961985893		0.97926708				
8	G*b - 55 °C	G*b - 64 °C	Pc (55 °C)	Pc (64 °C)							
9	0.003328	0.0019	0.00533584	0.005328335							
10	0.003328	0.0019	0.00533541	0.005328093							
11	0.003328	0.0019	0.00533537	0.005328066							
12	0.003328	0.0019	0.00533532	0.00532804							
13	0.003328	0.0019	0.00533528	0.00532802							
14											
15	Eb (MPa)										
16	180										
17	110										

Figure H9 Hirsch model data for asphalt mixtures.

APPENDIX J

SST REPEATED SHEAR AT CONSTANT HEIGHT (RSCH) TEST RESULTS

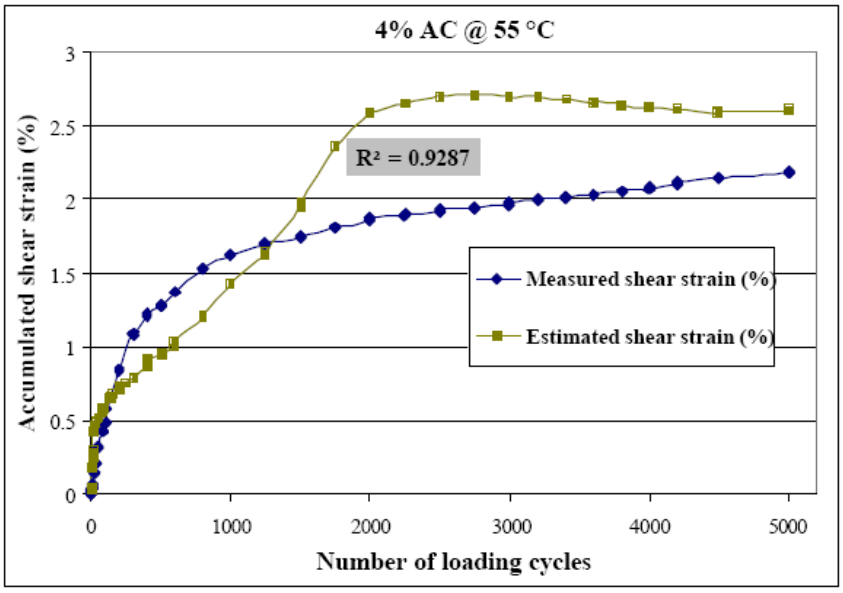

Figure J1 Estimated versus measured shear strain for HMA containing 4% asphalt @ 55 °C.

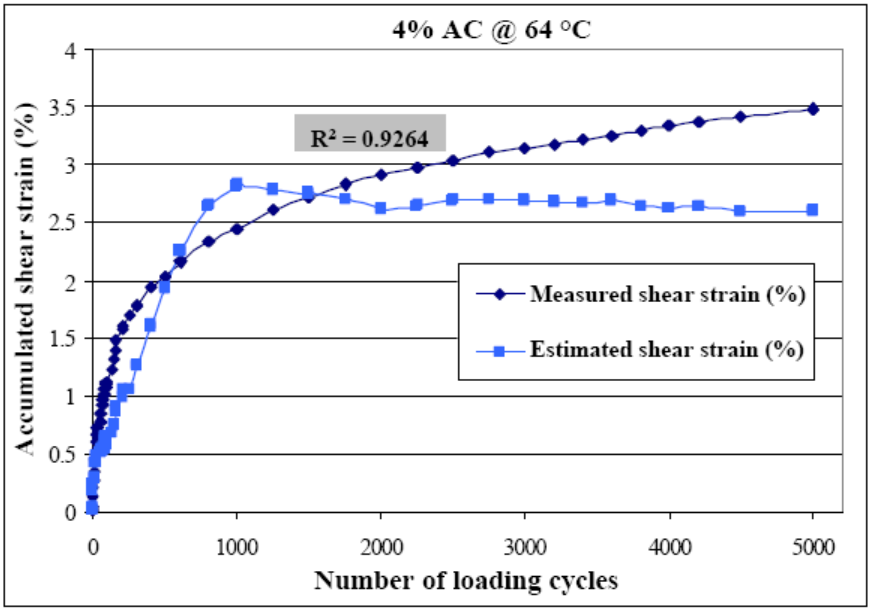

Figure J2 Estimated versus measured shear strain for HMA containing 4% asphalt @ 64 °C.

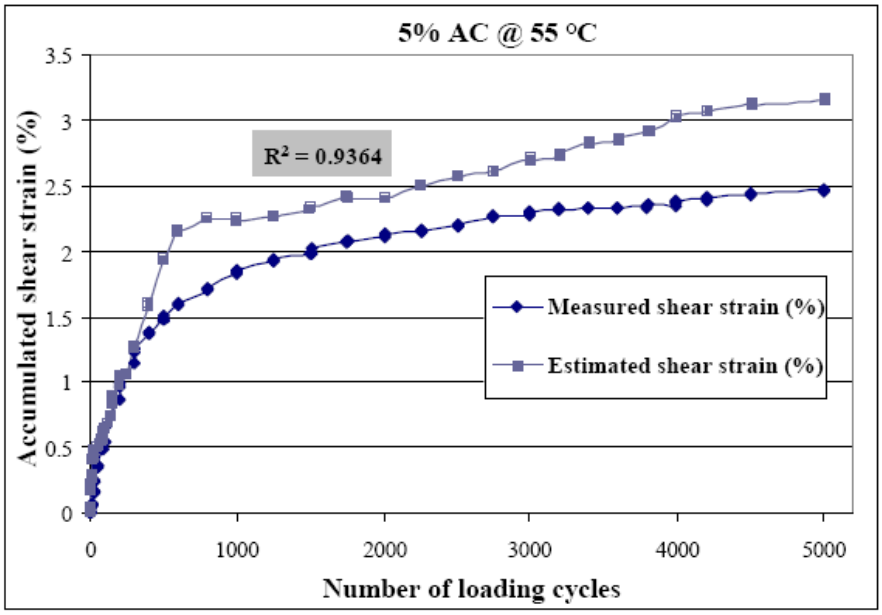

Figure J3 Estimated versus measured shear strain for HMA containing 5% asphalt @ 55 °C.

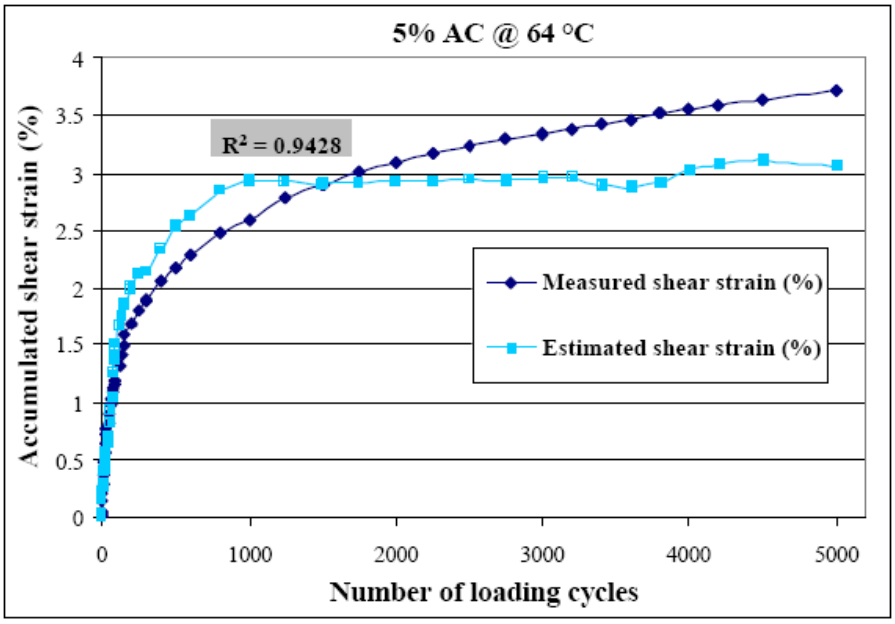

Figure J4 Estimated versus measured shear strain for HMA containing 5% asphalt @ 64 °C.

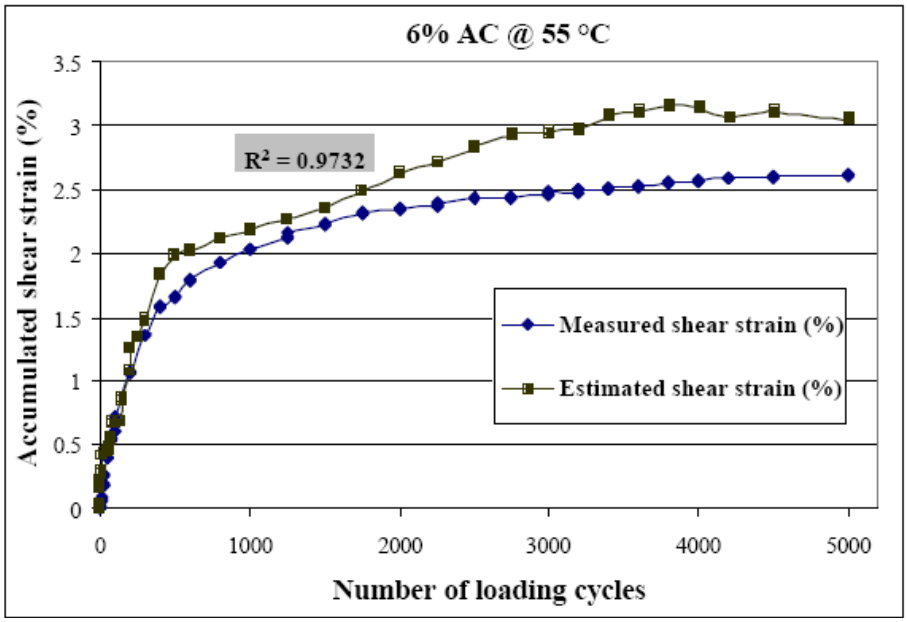

Figure J5 Estimated versus measured shear strain for HMA containing 6% asphalt @ 55 °C.

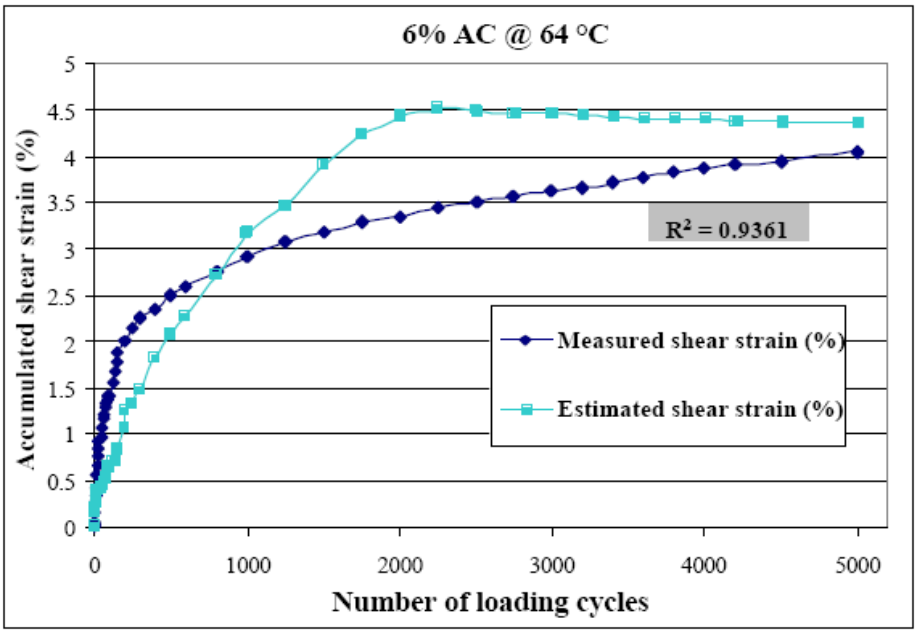

Figure J6 Estimated versus measured shear strain for HMA containing 6% asphalt @ 64 °C.

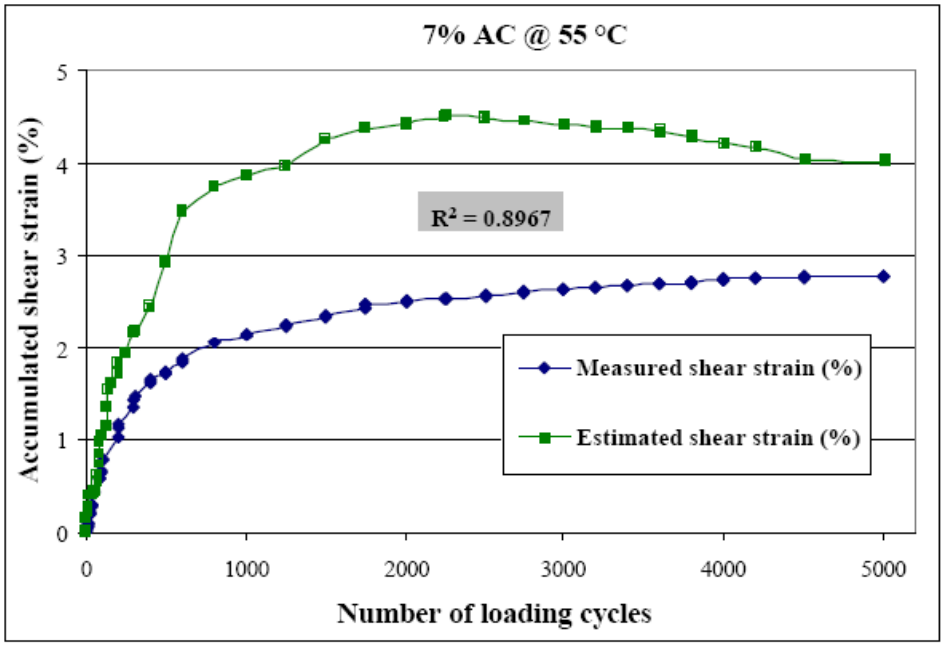

Figure J7 Estimated versus measured shear strain for HMA containing 7% asphalt @ 55 °C.

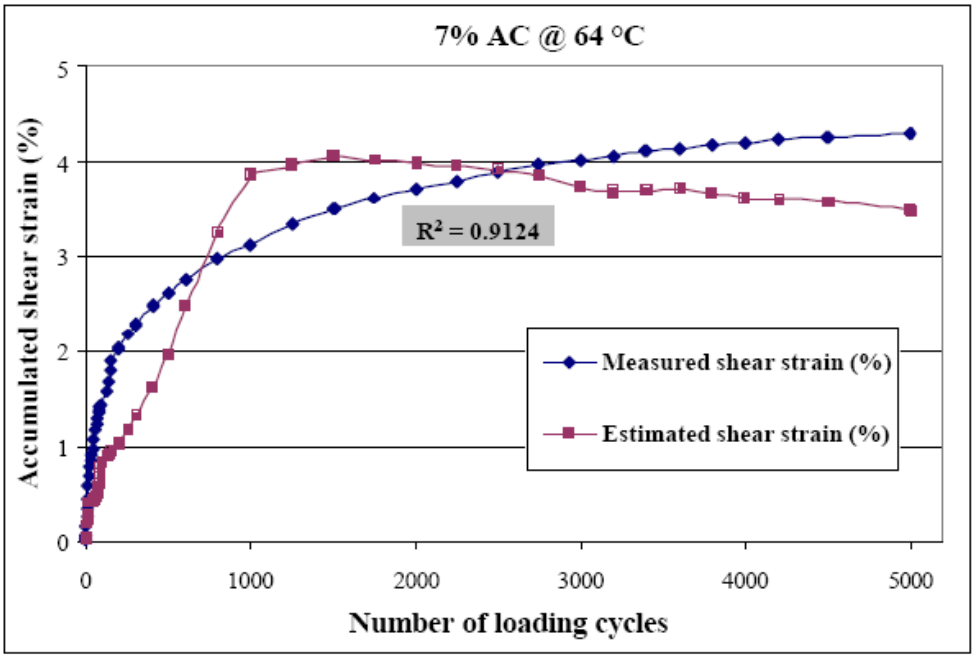

Figure J8 Estimated versus measured shear strain for HMA containing 7% asphalt @ 64 °C.

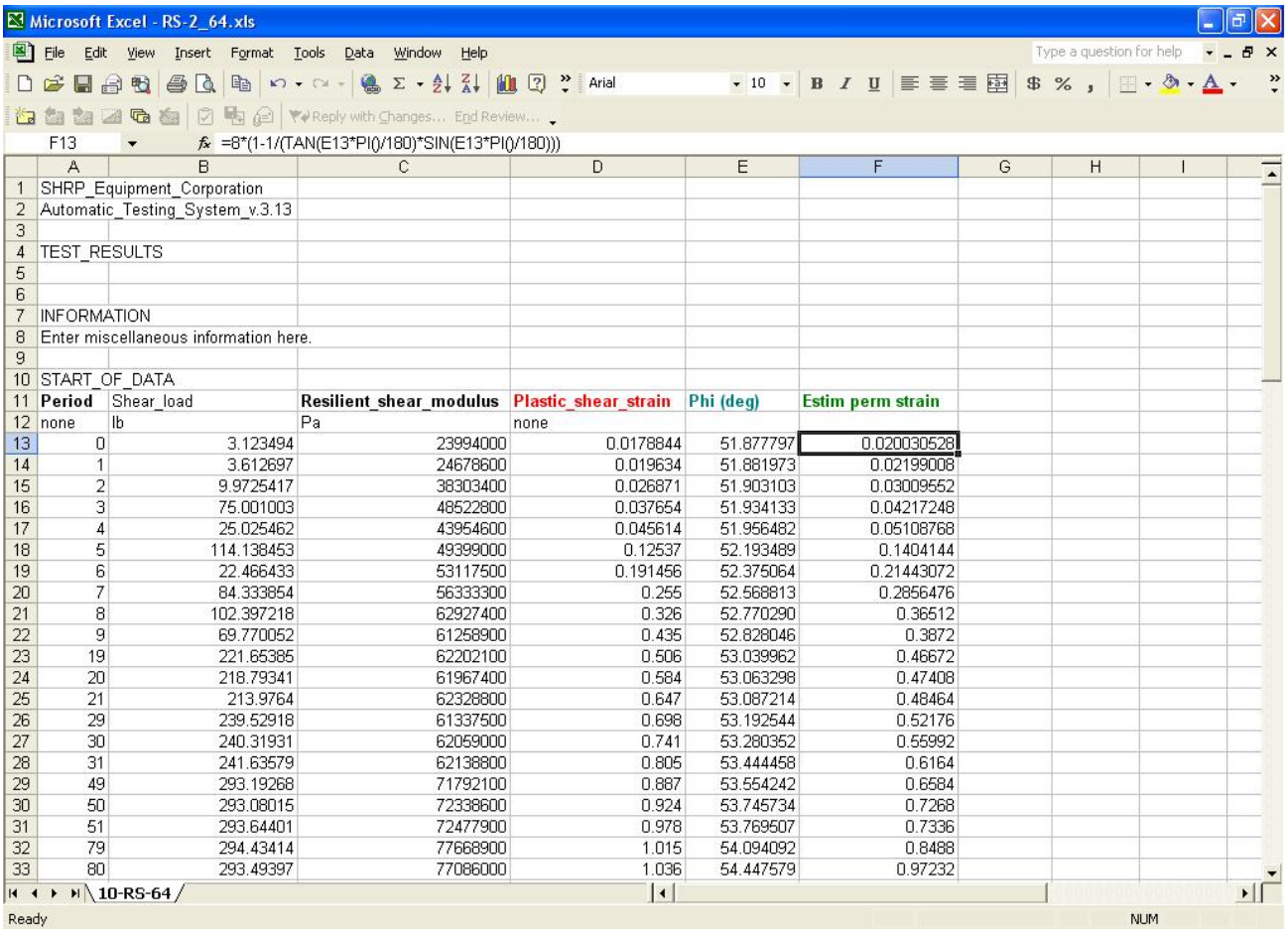

Figure J9 Estimation of permanent strain using Shenoy equation.

VITA

Cristian Druta received his bachelor of science degree in mechanical engineering from the Polytechnic University of Bucharest in June 1995 and his Master of Science in Engineering Science from Louisiana State University in May 2003. He started his doctoral program in August 2003, during which period he served as graduate assistant in research programs regarding asphalt and cement concrete pavements and image techniques. His research involves characterization and visualization of pavement materials and X-ray tomography of self-consolidating cement concrete. He is expected to receive the degree of Doctor of Philosophy at the August 2006 commencement.